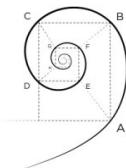




UNIVERSITÀ DEGLI STUDI
DI MILANO



DOTTORATO DI MEDICINA MOLECOLARE E TRASLAZIONALE

CICLO XXXIII

Anno Accademico 2019/2020

TESI DI DOTTORATO DI RICERCA

MED/07

Tackling biofilm-related opportunistic fungal infections

Dottorando: Emerenziana OTTAVIANO

Matricola N°: R11871

TUTORE: Prof.ssa Elisa BORGHI

COORDINATORE DEL DOTTORATO: Prof. Michele SAMAJA

RIASSUNTO

Ogni anno, oltre di 1 milione di persone muore a causa di infezioni fungine correlate alla produzione di biofilm. I biofilm sono comunità di microrganismi che si sviluppano adesi ad una superficie, biotica o abiotica, immerse in una matrice polimerica extracellulare autoprodotta. La capacità di organizzarsi in comunità microbiche è molto comune tra i microrganismi responsabili di infezione nell'uomo, tra questi vi sono anche i funghi. Tale organizzazione, rispetto alle forme planctoniche, è responsabile di una più difficile eliminazione del patogeno e predispone a frequenti fallimenti terapeutici legati alla maggiore refrattarietà alle terapie antimicrobiche. Alcune caratteristiche dell'ospite, quali alterazioni immunitarie o condizioni infiammatorie croniche, possono esacerbare la patogenesi dell'infezione e ritardarne la risoluzione. *Candida albicans*, tra i lieviti, e *Aspergillus fumigatus* tra le muffe, sono i patobionti più comuni tra gli agenti eziologici di infezioni nell'uomo.

Nel nostro studio abbiamo valutato diverse strategie per inibire la formazione di biofilm fungini e per contrastare le infezioni ad essi correlate, considerano sia i fattori di virulenza microbici sia la risposta immunitaria dell'ospite. Abbiamo studiato l'efficacia delle frazioni urinarie, raccolte da volontari sani dopo l'assunzione di un integratore a base di mirtillo rosso, nell'inibire il biofilm di *C. albicans*. Mediante analisi di spettrometria di massa, abbiamo identificato due metaboliti più concentrati nelle frazioni urinarie risultate più attive, il 5-(3', 4'-diidrossi fenil)- γ -valerolattone e l'acido 4-idrossibenzoico, che hanno mostrato avere un forte effetto

inibitorio sull'adesione di *C. albicans* e la sua filamentazione. Entrambi i composti sono stati anche in grado di ridurre l'espressione dei geni chiave delle prime fasi della formazione del biofilm.

A causa dell'alta diffusione dell'uso di cateteri o protesi in campo medico, lo sviluppo di biomateriali con attività inibitoria nei confronti della formazione di biofilm microbici potrebbe rappresentare una buona strategia per controllare le infezioni nosocomiali.

Abbiamo quindi testato matrici idro-gel di nuova sintesi e dimostrato la loro capacità di prevenire efficacemente la crescita di *C. albicans*. Al fine di valutare strategie che mirassero sia alla virulenza del patogeno sia alla risposta immunitaria dell'ospite, abbiamo condotto due diversi studi, il primo sulla candidosi sistemica da *C. albicans* e il secondo sull'infezione da *A. fumigatus* nei pazienti con CF. Abbiamo studiato l'attività, *in vitro* e *in vivo* nel modello di invertebrato *Galleria mellonella*, della pilocarpina, un agonista dei recettori muscarinici. La pilocarpina ha mostrato un effetto diretto nell'inibire la produzione di biomassa e l'attività metabolica del biofilm di *C. albicans* e la sua somministrazione alle larve precedentemente infettate ha aumentato la loro sopravvivenza. A causa del diverso comportamento della pilocarpina rispetto all'acetilcolina nella modulazione della risposta immunitaria della larva, abbiamo concluso che l'attività antifungina della pilocarpina potrebbe essere il risultato dell'attivazione in *C. albicans* di un recettore muscarinico-simile, mentre il forte effetto immunomodulante dell'acetilcolina (ma non di pilocarpina) potrebbe

derivare dal coinvolgimento dei recettori nicotinici, non ingaggiati da pilocarpina.

Un approccio simile, mirato pertanto a combattere simultaneamente infezione e infiammazione, è stato utilizzato per studiare la persistenza di *A. fumigatus* nei polmoni dei pazienti con CF. Infatti, i monociti CF sono caratterizzati da un anomalo accumulo di lipidi intracellulari, che promuove uno stato infiammatorio, a sua volta responsabile di una ridotta capacità di eliminare i patogeni e, di conseguenza, una tardiva risoluzione dell'infezione. Abbiamo dimostrato che il trattamento con miriocina dei monociti isolati da pazienti CF, inibendo la sintesi degli sfingolipidi e riducendo l'infiammazione intracellulare, migliora la fagocitosi e l'eliminazione dei conidi di *A. fumigatus*. Inoltre, la miriocina è risultata in grado di ridurre l'espressione dei geni che codificano per le citochine pro-infiammatorie e allo stesso tempo di aumentare l'espressione dei geni che codificano per i recettori coinvolti nel riconoscimento dei patogeni, cruciali per una corretta eliminazione di questi ultimi.

I nostri risultati indicano che, nonostante siamo ancora lontani dalla pratica clinica, esplorare strategie alternative anti-biofilm potrebbe aprire la strada alla scoperta di nuovi target e ad approcci integrati in grado di promuovere la risoluzione dell'infezione.

ABSTRACT

More than 1.5 million people/year die for a biofilm-related fungal infection. The ability to develop biofilms is widespread among human opportunistic pathogens, among them fungi. Biofilms are a community of microorganisms with the ability to attach to surfaces biotic or abiotic, surrounded by a self-produced extracellular polymeric matrix. The pathogen clearance and the general overcoming of the infection are complicated by biofilm presence as it confers tolerance to antimicrobial treatments. Compromised or altered immune response and an inflammatory milieu can exacerbate the pathogenesis and prolong the resolution of the infection. *Candida albicans*, between yeasts, and *Aspergillus fumigatus* between molds, are pathobionts considered the most common agents of opportunistic fungi mediated. In our study we assessed different strategies to eradicate biofilms and counteract biofilm-related infections, targeting both pathogens and host immune response. We investigated the efficacy of urinary fractions after cranberry extract intake by healthy volunteers against *C. albicans* biofilm. By mass spectrometry analyses, we identified two metabolites picking in the most active urine fractions, 5-(3',4'-dihydroxy phenyl)- γ -valerolactone and 4-hydroxybenzoic acid, which revealed a strong inhibitory effect on *C. albicans* adhesion and biofilm formation. Both compounds were also able to downregulate the expression of key genes involved in early phases of biofilm formation. Due to the spread of the use of catheters or prostheses in the medical field, the possibility to develop biomaterials with biofilm inhibitory activity could represent a good

strategy to control nosocomial infections. We thus investigated newly synthesized hydrogels and demonstrated their ability to prevent *C. albicans* growth.

To target both pathogen virulence and host immune response, we conducted two different studies, the first on *C. albicans* systemic candidiasis and the second on *A. fumigatus* infection in cystic fibrosis patients.

We investigated the possible dual action of pilocarpine, a muscarinic receptor agonist, *in vitro* and *in vivo* using the model host *Galleria mellonella*. Pilocarpine showed a direct effect in inhibiting *C. albicans* biofilm biomass and metabolic activity, and its administration to infected larvae increased larval survival. Because of the different behavior of pilocarpine compared to acetylcholine in the modulation of larva immune response, we concluded that the antifungal activity of pilocarpine might rely on muscarinic-like receptor activation on *C. albicans*, whereas the strong immunomodulatory effect of acetylcholine (but not of pilocarpine) might imply the engagement of nicotinic receptors. A similar approach, aimed at targeting both infection and inflammation, was used to investigate *A. fumigatus* persistence in CF patient lungs. Indeed, CF monocytes are characterized by altered intracellular lipid accumulation, that compromise pathogen clearance, and the infection resolution. We demonstrated that the treatment of patient monocytes with Myriocin, by inhibiting the synthesis of sphingolipids and hampering CF inflammation, ameliorate the *A. fumigatus* conidia internalization and clearance. On the host side, Myriocin

was able to reduce the over expression of genes encoding for pro-inflammatory cytokines and at the same time to increase the expression of gene encoding for pathogen recognizing receptors, crucial for its clearance.

Our results indicate that, despite we are still far from clinical practice, exploring alternative anti-biofilm strategies could pave the way to new target discovery and to integrated approaches able to promote the infection resolution.

TABLE OF CONTENTS

ABSTRACT	I
RIASSUNTO	II
TABLE OF CONTENTS	III
RESEARCH INTEGRITY	IV
LIST OF ABBREVIATIONS	V

1.INTRODUCTION

1.1 Clinical burden of fungal infections

1.1.1. *Candida* spp.

1.1.1.1. *Candida* virulence factors

1.1.1.2 Mucosal infections

1.1.1.3 Bloodstream infections

1.1.1.4 *Galleria mellonella*: an in vivo model of systemic infection

1.1.2. *Aspergillus* spp.

1.1.3. Antifungal resistance

1.2 Biofilm-related tolerance to antifungal and strategies to overcome it

1.2.1 *Candida albicans* biofilms

1.2.2 *Aspergillus fumigatus* biofilms

1.2.3 Biofilm-related antifungal tolerance

1.2.4 Alternative strategies for fungal infection management

1.3 The vicious cycle: infection-inflammation

1.3.1 *Candida albicans*: its role in Inflammation

1.3.2 *Aspergillus fumigatus*: its role in cystic Fibrosis

2.AIM

3 MATERIALS AND METHODS

3.1 Culture conditions and standardization

3.1.1 *Candida albicans*

3.1.2 *Aspergillus fumigatus*

3.2 Inhibitory effect of cranberry metabolites on *C. albicans* filamentation and biofilm-formation

3.2.1 Urinary fractions collection

3.2.2 Cranberry urinary metabolites

3.2.3 Biofilm formation and biomass quantification by Crystal Violet

3.2.4 Quantification of cell metabolic activity

3.2.5 CaCo-2 culture

3.2.6 Conditions and Cytotoxicity assay

3.2.7 Confocal laser scanning microscopy (CLSM)

3.2.8 Cell surface hydrophobicity assay

3.2.9 RNA extraction and real-time analysis for 5-(3',4'-dihydroxy phenyl)- γ -valerolactone on *Candida albicans* biofilm

3.3 Functionalized hydrogels as a strategy to prevent biofilm-related infection

3.3.1 Antimicrobial activity of hydrogels

3.4 Effect of inflammation on *Candida albicans* systemic *Galleria mellonella* pathogenicity assay

3.4.1 *Galleria mellonella* inoculation

3.4.2 Hemocytes

3.4.3 Histology

3.5 Effect of inflammation on *Aspergillus fumigatus* infection in cystic fibrosis patient

3.5.1 PBMC isolation and infection

3.5.2 Monocyte killing ability

3.5.3 RT-PCR

3.6 Statistical analysis

4. RESULTS

4.1 Strategies to counteract biofilm-related fungal Infections

4.1.1 Cranberry metabolites in urinary fractions activity against *Candida albicans* biofilm

4.1.2 Mass spectrometry (MS) analysis revealed that metabolites other than proanthocyanins are enriched in the most active urinary fractions

4.1.3 5-(3',4'-dihydroxy phenyl)- γ -valerolactone and 4-hydroxybenzoic acid are the most active metabolites in urinary fractions

4.1.4 5-(3',4'-dihydroxy phenyl)- γ -valerolactone and 4-hydroxybenzoic acid inhibitory activity does not involve changes in cell surface hydrophobicity

4.1.5 VAL and 4-HBA regulate the expression of *Candida albicans* genes involved in early phases of biofilm formation

4.1.6 Reducing *Candida albicans* surface attachment could be an effective strategy to prevent biofilm-formation and related infections

4.2 Strategies to counteract the vicious cycle of infection/-inflammation

4.2.1. Pilocarpine efficiently inhibits *Candida albicans* biofilm formation but fails to strongly modulate the host inflammatory response

4.2.2 Myriocin ameliorates the response to *A. fumigatus* infection in ex vivo CF monocytes

5. DISCUSSION

5.1 Cranberry metabolites and their effects on *Candida albicans* biofilm formation

5.2 Effect of Pilocarpine on *Candida albicans* virulence and host response

5.3 Myriocin modulate the response to inflammation and infection

7. CONCLUSIONS

8. REFERENCES

RESEARCH INTEGRITY DECLARATION

The research herein presented has been conducted in full compliance with the principles of Research Integrity of The European Code of Conduct for Research Integrity (ALLEA, Berlin, 2018), that are integrity and accuracy in conducting research and in recording the results. All the experiments were designed based on previous results obtained in the Laboratory of Medical and Clinical Microbiology under the supervision of Professor Elisa Borghi. All the methods applied were conform to research integrity criteria and were ethically sustainable. The published results are communicated in an open and responsible manner, according to the principle of dissemination of scientific knowledge.

LIST OF ABBREVIATION

ACE2P	Angiotensin converting enzyme
ACh	Acetylcholine
ALS3	Agglutinin-like protein 1
ASPF1	Allergene Aspergillus fumigatus 1
BCR1P	Biofilm and cell wall regulator 1
BMI	Body mass Index
BSI	Bloodstream infections
Caco-2	Colorectal adenocarcinoma cell line
CATB	Catalase B
CF	Cystic fibrosis
CFU	Colony-forming unit
CLSM	Confocal laser scanning microscopy
CSH	Cell surface hydrophobicity
CV	Crystal violet
CVC	Central venous catheters
DMEM	Dulbecco's Modified Eagle's Medium
DMSO	Dimethyl sulfoxide
DPPV	Dipeptidyl peptidase V
ECE1	Extent of cell elongation protein
ECM	Extracellular polymeric matrix
EDTA	Ethylenediaminetetraacetic Acid
EFG1P	Enhanced filamentous growth 1 protein
FBS	Fetal bovine serum

GAG	Galactosaminogalactan
GI	Gastrointestinal
4-HBA	4-hydroxybenzoic acid
HE	Hematoxylin and eosin
HG	Hydrogels
HWP1	Hyphal wall protein 1
HYR1	Hyphally regulated cell wall protein 1
ICU	Intensive care unit
IRIS	Immune reconstitution inflammatory syndrome
MACHRS	Muscarinic acetylcholine receptors
MEM	Minimum Essential Medium
MOI	Multiplicity of infection
MS	Mass spectrometry
MTT	Diphenyl tetrazolium bromide
NCAC	Non- <i>C. albicans Candida</i> species
PACs	Proanthocyanidins
PAMPs	Pathogen-associated molecular patterns
PAS	Periodic acid-Schiff
PBMCs	Peripheral blood mononuclear cells
PBS	Phosphate-buffered saline
PDA	Potato Dextrose Agar
PHCI	Pilocarpine hydrochloride
PRRs	Pattern recognition receptors
RPMI	Roswell Park Memorial Institute

RPMI	Roswell Park Memorial Institute Medium
SAB + CAF	Sabouraud dextrose agar supplemented with Chloramphenicol
SAP 4	Secreted Aspartyl Proteinase 4
SAP 6	Secreted Aspartyl Proteinase 6
SCP	Scopolamine
SPLs	Sphingolipids
TLRs	Toll-like receptors
TSA	Trypticase Soy Agar
TSB	Trypticase Soy Broth
UTIs	Urinary tract infections
VAL	5-(3',4'-dihydroxy phenyl)- γ -valerolactone
VVC	Vulvo vaginal candidiasis
XTT	2,3-bis(2-methoxy-4-nitro-5-sulfophenyl)-2H-tetrazolium-5-carboxanilide inner salt
YPD	Yeast extract peptone dextrose
ZAP1P	Zinc-responsive transcriptional regulator
A7NACHR	Alpha 7 nicotinic receptor

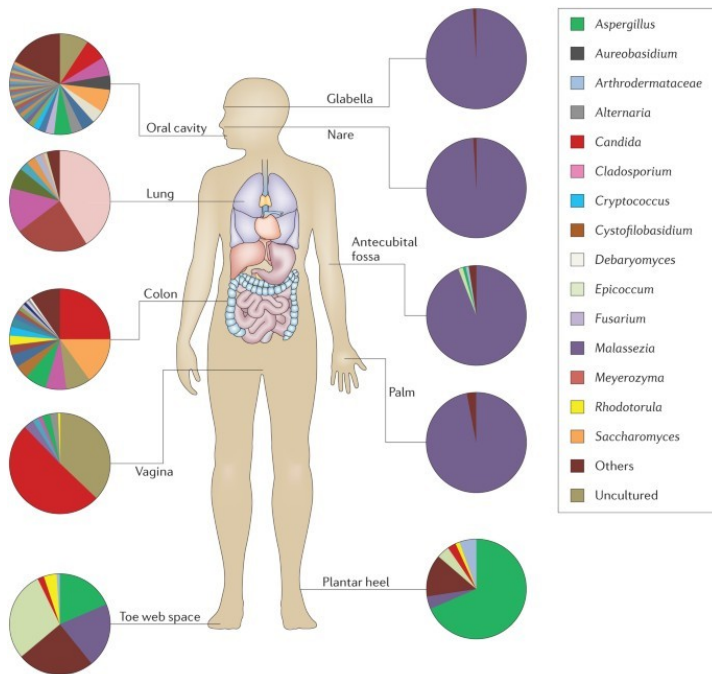
1.INTRODUCTION

1.1 Clinical burden of fungal infections

Fungi are opportunistic pathogens responsible for a variety of different diseases, ranging from mild superficial infections to life-threatening disseminated diseases. These latter represent a significant burden of infection within the hospital population. An estimated 1.5 to 2 million people/year die of a fungal infections, of which 30-40% for invasive candidiasis, 20–30% for disseminated cryptococcosis, and a similar percentage for invasive aspergillosis[1].

Candida, among yeast, and *Aspergillus* genus, among molds, are the most common etiological agents of human infection[1]. While *Candida* spp. are recognized as part of human microbiota (mycobiota, Figure 1) and colonize diverse niches such as skin, oropharynx, gastrointestinal and genitourinary tracts, *Aspergillus* spp. is a ubiquitous environmental fungus and has been less reported as true commensal[2]. Indeed, at least in the gastrointestinal tract, it can result from plant-derived food ingestion[3].

A. fumigatus and *C. albicans* are pathobionts as they can switch from a commensal state to pathogens, responsible for a variety of pathological processes (i.e. opportunistic infections). What mechanisms drive this switch is still not fully elucidated, but the host immune status and the local inflammation might exert a crucial role besides the microorganism virulence[4].



Nature Reviews | Immunology

Figure1. Human niches colonized by fungi. (From Underhill and Iliev, 2014)[5].

1.1.1. *Candida* spp.

Candida species normally colonize mucosal surfaces and the gastrointestinal tract in an asymptomatic manner, even if it can be responsible for of lethal infections. Clinical manifestations mediated by *Candida* spp. range from superficial to bloodstream infections, especially in individuals with known risk factors such as immune compromised patients or under corticosteroid or broad spectrum

antibiotic therapies[6]. In the last decades, fungi emerged as major causes of nosocomial infections, mainly affecting long-term hospitalized patients[7]. *Candida* spp. are considered relevant pathogens due to their versatility and their ability to adhere to different surfaces.

Candida genus is composed of a miscellaneous group of species. Among these, more than 17 are recognized to be etiological agents of human infections. *Candida albicans* is still the most reported species causing of invasive fungal infections[8] and represents a serious public health challenge with increasing medical and economic importance due to the high crude mortality rate.

Although *C. albicans* is the most widespread species, the incidence of infections due to *Candida glabrata* and other non-*C. albicans* species is increasing. In European countries, a surveillance study showed that 14% of the cases of candidemia are due to *C. glabrata* and *Candida parapsilosis*, 7% to *Candida tropicalis*, and 2% to *Candida krusei*[9].

Other species have been isolated in healthy subjects and patients. *Candida dubliniensis* is often co-isolated with other yeast species, especially *C. albicans*, with a high prevalence in the oral cavities of HIV-infected and AIDS patients[10]. *C. parapsilosis* complex has also emerged as a significant nosocomial pathogen, usually associated with invasive procedures or catheters and in neonatal intensive care units. This complex includes three species named *Candida parapsilosis sensu stricto*, *Candida orthopsilosis* and *Candida metapsilosis*[11].

The main source of infection is the endogenous route (Figure 1), i.e. when the commensal fungus exploiting host weakness behave as opportunistic pathogens. More rarely, exogenous transmission has also been reported, from contaminated medical devices or from healthcare staff[12].

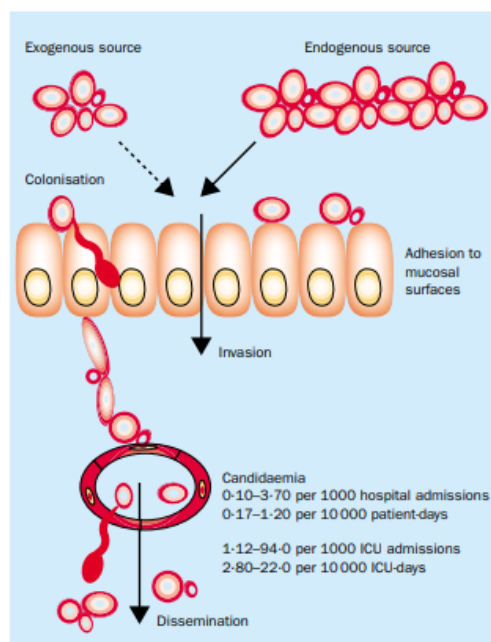


Figure2. Pathophysiology of invasive candidiasis from both exogenous and endogenous sources[6].

Despite candidiasis being the most common systemic infection by *Candida* spp., this yeast is well recognized etiological agent of

superficial and mucosal infections (involving the skin and mucosal surfaces) which have a greater incidence compared to the invasive infections and a strong impact on the quality of life of affected individuals (Figure 2).

1.1.1.1. Candida virulence factors

C. albicans is a pleomorphic fungus that can reversibly switch from unicellular yeast cells to either pseudohyphal or hyphal forms.

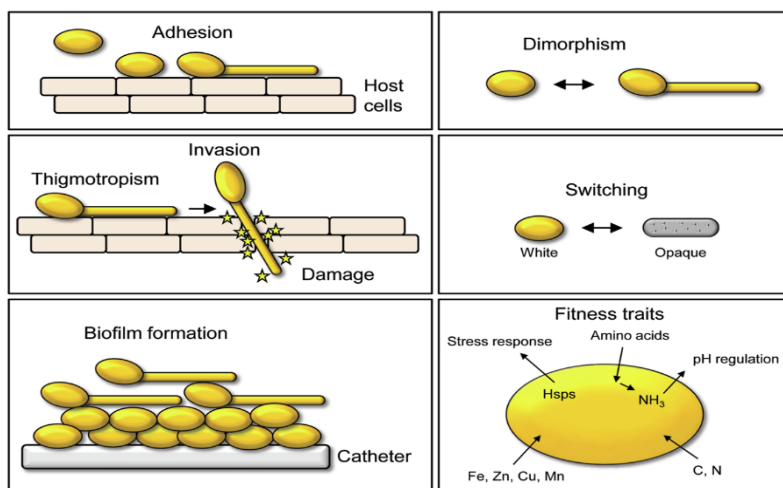


Figure3. *Candida albicans* virulence factors

The invasion should be facilitated by the transition between yeast cells, termed dimorphism, and filamentous growth in comparison to isotropic growth, the phenomenon of ‘phenotypic switching’ has been proposed to contribute to the plasticity of the organism[13]. The hyphal form is more invasive than the yeast, but the unicellular

form is primarily involved in dissemination[14]. Hypha formation is linked to the expression of a subset of genes encoding virulence factors, such as the hyphal wall protein *Hwp1*, the agglutinin-like sequence protein *Als3*, the hyphae-associated proteins *Ece1* and *Hyr1*, and the secreted aspartic proteases (*Sap4-Sap6*).

Adhesion and invasion are important determinant in invasive yeast infections. Indeed *C. albicans* presents a specialized set of proteins (adhesins) which mediate adherence to other fungi cells or other microorganisms, to abiotic surfaces and to host cells. *Hwp1* and *Als3* were also demonstrated to contribute to biofilm formation by acting as complementary adhesions[15]. *C. albicans* is a remarkable pathogen as it can utilize two mechanisms to invade into host cells: endocytosis and active penetration mediated by the hyphae.

Following adhesion to host cell surfaces and hyphal growth, filamentous *C. albicans* secretes hydrolases, which have been proposed to facilitate active penetration into host cells and to enhance the extracellular nutrient acquisition[16]. Another important virulence factor of *C. albicans* is its capacity to form biofilms on abiotic or biotic surfaces (see paragraph 1.2.1).

1.1.1.2 Mucosal infections

The most reported forms of mucosal infections are oral candidiasis and vulvovaginal candidiasis. Oral candidiasis is one of the most

common fungal infection affecting the oral mucosa. Other *Candida*-associated manifestations include denture stomatitis, angular cheilitis, and median rhomboid glossitis. Secondary oral candidiasis can also occur, which include chronic mucocutaneous candidiasis or chronic localized mucocutaneous candidiasis [17].

Oral candidiasis, which can involve both soft and hard tissues, can result in: i) an acute form of disease referred to as pseudomembranous candidiasis and estimated affecting ~5% of newborns and 10% of the elderly population, and ii) chronic candidiasis, referred to as oral leukoplakia, affecting mainly immunocompromised individuals[18]. The species *C. albicans* is the most reported etiological microorganism causing these lesions.

Vulvovaginal candidiasis (VVC) is another fungal mucosa infection and is the second most common cause of vaginitis after bacterial vaginosis. Transmission of this yeast from the vagina to the mouths of newborns during birth is a major portal of oral infections in newborns, leading to the development of thrush[19]. Furthermore, *Candida* inhabits the gastrointestinal (GI) tract, and the disruption of physiological barriers, such as gastric acidity and perturbations of the indigenous colon microbiota, facilitate *Candida* overgrowth. Within the GI tract, the most common site of infection is the esophagus. *Candida* may be associated with gastric ulcers as an opportunistic pathogen that delays ulcer healing and aggravates the disease[20].

1.1.1.3 Bloodstream infections

Bloodstream infections (BSI) caused by *Candida* species remain a frequent cause of morbidity and mortality, particularly in immunocompromised population. Overall, *Candida* species have been identified as the fourth most common organism responsible for all BSI, and are the third most common within the intensive care unit (ICU)[21]. Candidiasis is the mostly reported severe fungal infection in humans and its systemic involvement is associated with high mortality rates[21]. Around the turn of the millennium, it has been described as an emerging infection, particularly in the immunocompromised population, as a result of aggressive therapies (e.g. anticancer chemotherapy, long-term corticosteroids treatment or organ transplant) and immunosuppressive infections such as HIV.[22] Candidemia is often associated with the ability of *Candida* to adhere and form biofilms on medical devices, such as central venous catheters (CVC) and prosthesis.

Candida can invade through translocation or through anastomotic leakage and cause either localized, deep-seated infection (e.g., peritonitis), or candidemia. Once candidemia has developed, whether from a colonized intravascular catheter or by other means, the fungi may disseminate, leading to secondary, metastatic infections in the lung, liver, spleen, kidneys, bone, or eye. These deep-seated infections may remain localized or lead to further candidemia[23]. Although *C. albicans* has been reported as the most predominant species causing invasive fungal infections, a

significant increase in non-*C. albicans Candida* (NCAC) species such as *C. glabrata*, *C. parapsilosis*, or *Candida auris* in human candidiasis have been observed over the last decade [24].

Medical devices, including CVC, are the ideal surfaces for the colonization of *Candida* spp. and allowing for the development of mature biofilm communities whereby planktonic cells can detach cause acute candidemia and/or disseminated infection. A study investigating the pathogenicity reported a greater association of cells dispersed from biofilms with mortality rate than equivalent planktonic yeasts[25]. Infections associated with medical devices are essentially difficult to eradicate, with the only method of controlling such an infection being long-term use of antifungals and the removal of the implant. Although *C. glabrata*, *C. parapsilosis*, *C. dubliniensis*, *C. krusei* and *C. tropicalis* [26] are associated with biofilm formation and contribute to device-related bloodstream infections, *C. albicans* remains the dominant species responsible for human disease.

C. albicans is one of the most common fungi disease causing in humans and the most frequently isolated fungal pathogen in nosocomial urinary tract infections (UTIs) . Urological devices and procedures, diabetes and being female are the main factors linked to candiduria. Catheters, which are used in up to 20% of hospitalized subject, represent an adhesion substrate for microorganisms that can easily develop biofilm on plastic or silicone surfaces. The most important feature of microbial biofilms is their resistance to antimicrobial therapies, leading to recurrent or

persistent infections. *C. albicans* UTIs are increasingly common in hospital settings due to its high propensity to form biofilms on the mucosal surface and plastic surface of indwelling devices[27].

1.1.1.4 *Galleria mellonella*: an *in vivo* model of systemic infection

Although the mouse model is the most widely accepted experimental model to study candidiasis, immunological differences in the innate immune response between mouse and humans have been reported[28].

Taking into account the multifaceted interplay *Candida*-host, the use of a simple animal model can help providing elements to draw a coherent picture of the immunopathogenesis of systemic candidiasis.

The larvae of the greater wax moth, *Galleria mellonella* (Gmel), have emerged as an alternative model host for human pathogens including fungi[29]. This member of *Lepidoptera* is particularly useful to investigate fungal virulence, study immune defense responses and evaluate the efficacy of antimicrobial compounds. Indeed, the insect innate immune response shares high similarity with the mammalian immune system, starting from physical barriers (cuticle/skin, and midgut/intestinal microvilli) and two closely interconnected components, namely the cellular and humoral responses[30] (Figure 4).

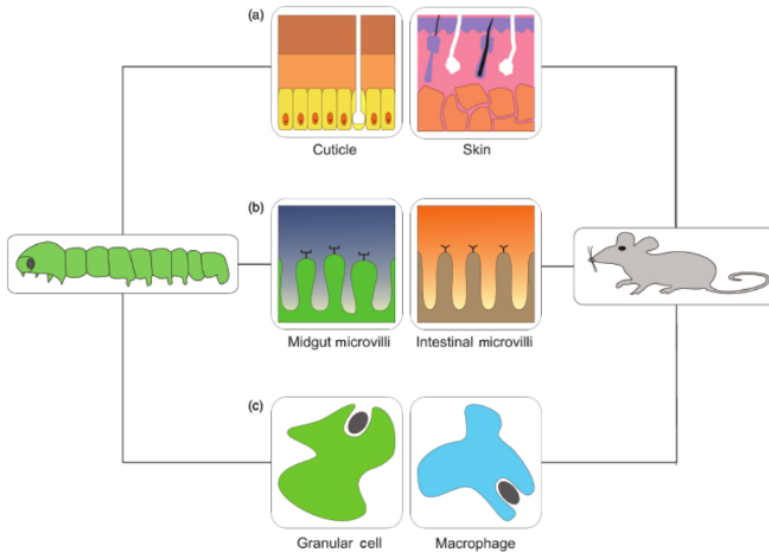


Figure 4. Correspondence between vertebrates and invertebrates response to microorganisms infection (a) at cuticle level, (b) at the intestinal level, and (c) at the cellular level[30].

Several types of hemocytes that mediate phagocytosis, nodulation, and encapsulation of the invading pathogen orchestrate the cellular immune response. Hemocytes are found circulating freely in the hemolymph or adhering to internal organs such as the fat body or the digestive tract of the insect.

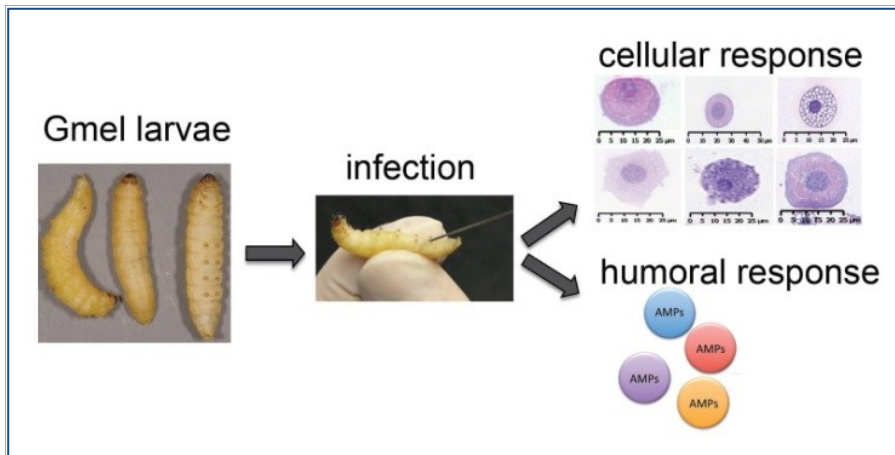


Figure5. The direct introduction of fungi into the body cavity of Gmel elicits multiple defense mechanisms. The easy inoculum delivery and handling of the insect Gmel make it a suitable model for the study of fungal pathogenesis. Larvae can be used in large numbers, resulting in an important reduction in time and costs for their maintenance.

Compared to other invertebrate hosts, for example *Caenorhabditis elegans* or *Drosophila melanogaster*, Gmel can survive at mammalian temperature (i.e. 37°C), allowing pathogens exploiting temperature-dependent virulence factors [31].

Moreover, the Gmel model will allow studying a high number of different clinical isolates that display clinical heterogeneity. This kind of study is extremely challenging in mammalian models due to the high number of animals required to reach a statistically significant results.

1.1.2. *Aspergillus* spp.

The genus *Aspergillus* encompasses a few hundred of ubiquitous and opportunistic mold species that can cause human diseases ranging from allergic responses to localized and systemic infections. *Aspergillus* species are filamentous fungi commonly found in soil, in decaying vegetation, and seeds, where they thrive as saprophytes[32]. The sensitivity to *Aspergillus* spp. is especially related to allergic diseases[33] and several species of *Aspergillus*, including *A. fumigatus*, *A. niger*, *A. flavus*, and *A. oryzae*, are the most common molds responsible for these forms.

Aspergillus fumigatus complex is the most common etiological agent isolated from human samples. Indeed, in comparison with conidia of most other molds, *Aspergillus fumigatus* conidia are more efficiently dispersed in the air. Even sparse air currents can disperse conidia due to their remarkable hydrophobicity. Due to the presence of melanin in their cell walls, these conidia are also protected from ultraviolet irradiation. Moreover, the presence of melanin in the conidial wall contributes to protection of *A. fumigatus* against host cell responses[34].

Aspergillus fumigatus can be isolated from a wide range of environmental conditions, and its thermotolerance facilitates the growth in several ecological niches, including mammalian respiratory tracts.

Similar to many other infectious diseases, the development of *Aspergillus* infection is dependent on the interactions between

the pathogen characteristics and the host status. To invade the tissues, *Aspergillus* spp. relies on a coordinated expression of a broad range of genes that are involved in conidial germination, cell wall assembly, nutrient acquisition, and resistance to adverse conditions such as oxidative stress.

The risk of developing fungal infections increase in ill patients with underlying debilitating diseases, such as cancer, or chronic lung diseases. *A. fumigatus* can cause a plethora of diseases, ranging from invasive pulmonary aspergillosis to allergic syndromes such as allergic rhinitis and asthma.

Moreover, recurrent antibacterial therapies can favor the insurgence of drug resistance and, by altering the commensal microbial community, can promote colonization by opportunistic pathogens. *Aspergillus fumigatus* is the most prevalent filamentous that affecting approximately 35% of CF patients, contributing to lung deterioration.

1.1.3. Antifungal resistance

Antifungal resistance is a complex and multifaceted process that can be inducible in response to a compound, or an irreversible genetic change resulting from prolonged exposure. Specifically, mechanisms mediating drug resistance encompass alterations of target molecules, active extrusion through efflux pumps, limited diffusion, tolerance, and cell density. Many fungi are intrinsically

resistant to certain antifungals. Whereas 20 years ago, azole-sensitive *C. albicans* were predominant as etiological agents, with NCAC rarely seen, after the broad use of systemic azole, this picture has changed. *C. glabrata* became particularly problematic: it is the second most-commonly isolated *Candida* species in the European Union (>10%) and United States (>20%) and it presents high rates of resistance to fluconazole and voriconazole, as well as (more recently) to echinocandins[35].

The emergence of azole resistance is a growing problem. Unlike bacteria, fungi are not known to transfer resistance genes between them, nor is patient-to-patient transmission common.

About 1.2 billion people worldwide are estimated to suffer from a fungal disease. Most are infections of the skin or mucosa, which respond readily to therapy, but a substantial minority is invasive or chronic and therefore difficult to diagnose and treat. An estimated 1.5 to 2 million people die of a fungal infection each year, surpassing those killed by either malaria or tuberculosis. Most of this mortality is caused by species belonging to four genera of fungi: *Aspergillus*, *Candida*, *Cryptococcus*, and *Pneumocystis*.

1.2 Biofilm-related tolerance to antifungal and strategies to overcome it

Biofilms are defined as communities of microorganisms attached to biotic or abiotic surfaces, surrounded by a self-produced

extracellular polymeric matrix (ECM)[36]. It has been confirmed that many fungal species can form biofilms and have a significant impact on the clinical outcome[37].

Biofilm is considered the most common form of growth for many microbial species and represents an important virulence factor since it implies a greater propensity to develop drug resistance or drug tolerance, and to evade the host immune response [38]. An intrinsic feature of biofilms is their tolerance to antimicrobial therapy, with higher drug concentrations required to kill the three-dimensional structure.

1.2.1 *Candida albicans* biofilms

C. albicans is the most studied *Candida* spp. because it is a highly adaptable pathogen with marked propensity to form biofilm on a variety of substrates[39].

C. albicans biofilm formation has been shown to proceed in three distinct developmental phases: early (0–11 h), intermediate (12–30 h), and mature (38–72 h) phase (Figure 4). The detailed structure of a mature *C. albicans* biofilm produced *in vitro* after 48 hours incubation has been shown to consist of a dense network of yeasts, hyphae, and pseudohyphae[40]. This mixture of yeasts, hyphae, and the matrix material is not seen when the organism is grown in liquid culture or onto agar surface, which suggests that the morphogenesis is triggered when the microorganism contacts a surface[41]. In addition, *in vivo* bacteria are often co-isolated with

Candida spp. in biofilms, indicating that extensive interspecies interactions probably occur.

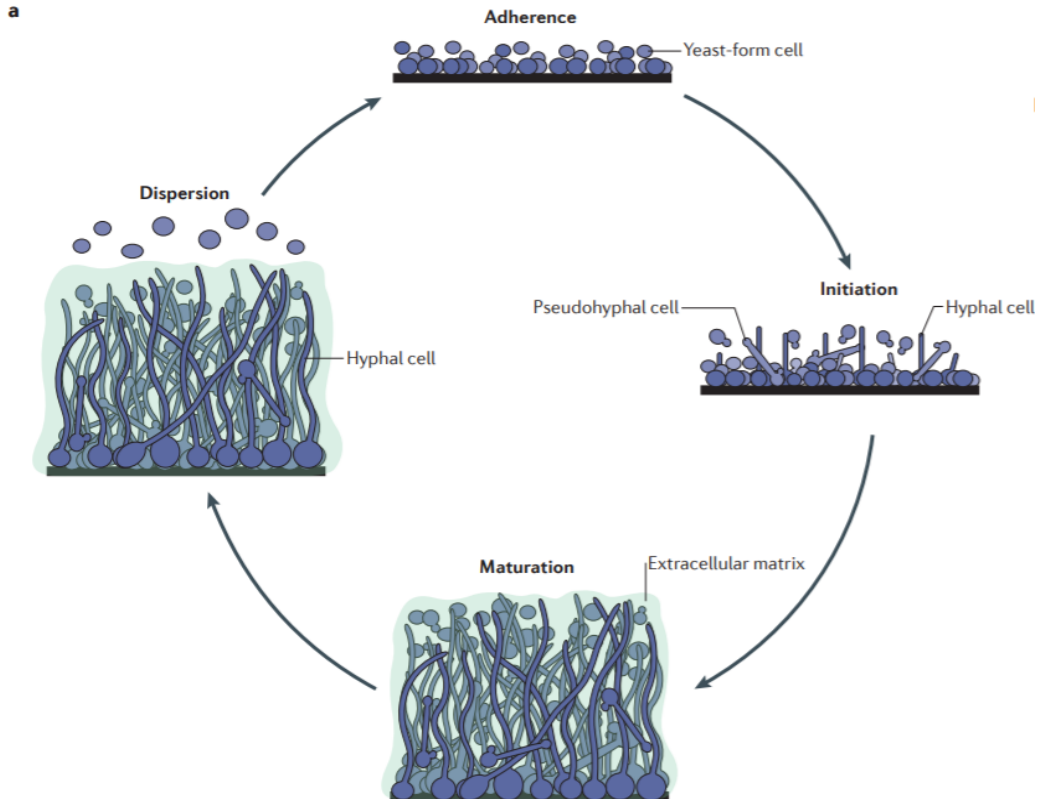


Figure 6. Stepwise biofilm formation (Nat Rev Microbiol 16, 19–31_2018) [42]

The initial attachment to the surface is controlled by several factors, including the flow of the surrounding medium (urine, blood, saliva, mucus), pH, temperature, osmolarity, other microorganisms, presence of antimicrobial substances, and host immune factors[39], [40].

These key factors include the presence of appropriate conditions such as substratum, adhesion, colonization, ECM production, biofilm maturation and dispersal[40].

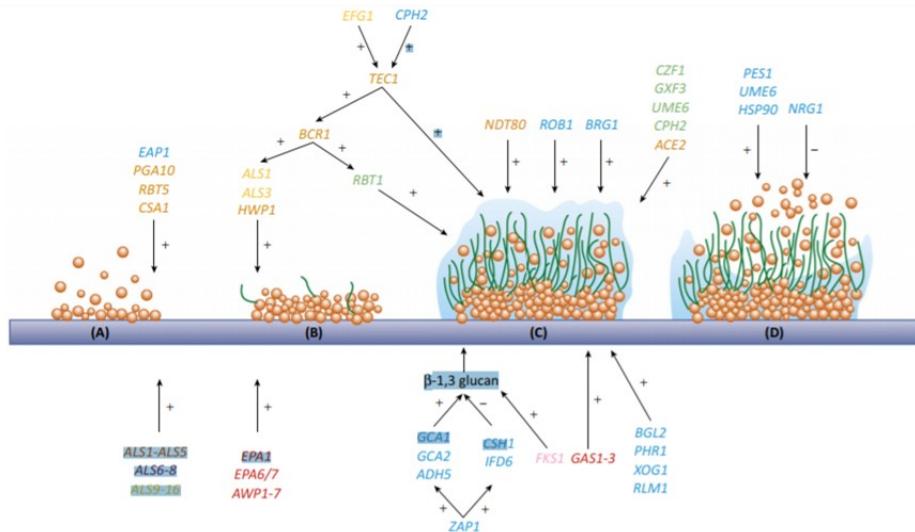


Figure 7. Genes involved in biofilm formation and development. (Adapted from Nobile, 2013)[42]

Simplistically, yeast cells attach to a surface via adhesins including, agglutinin like sequence protein Als3p and the cell wall protein Eap1p[43] . This leads to the formation of microcolonies and the morphology of yeast cells switches to hyphae by the regulator Efg1p to form a complex network of hyphal structures with budding yeast cells distributed throughout. Next, as the biofilm matures, a glucan rich extracellular matrix (ECM) provides a protective barrier from host defenses, antimicrobial agents, and environmental stresses. During the development of a mature biofilm, a hypoxic environment is created which induces the up-regulation of glycolytic

genes that control filamentation [44]. Finally, planktonic yeast cells are able to disperse from the mature biofilm and colonize a new surface to begin the development of a new biofilm even in other districts of the body[25].

Notably, yeast cells detaching from biofilms have been shown to be more cytotoxic than their planktonic counterparts and significantly increase mortality within a murine model of infection. These observations have been demonstrated clinically, where a significant association was observed between *C. albicans* biofilm formation and mortality rates in candidemia patients [25]

Several classes of genes govern *C. albicans* biofilm formation, encoding for adhesins, proteins required for filamentation, matrix proteins, and quorum-sensing molecules. The process of biofilm formation is complex, controlled by a variety of transcription factors including Bcr1p, Ace2p, Efg1p, and Zap1p, all of which are all involved in sophisticated molecular pathways[37], [45]. Their expression is finely regulated in a stepwise manner, and profound differences have been seen among different *Candida* isolates.

The importance of understanding this entire process of biofilm formation is essential to study possible alternative strategies to counteract biofilm-related infections.

1.2.2 *Aspergillus fumigatus* biofilms

Although *Candida* spp are great biofilm producers, other fungi can develop structures that confer resistance and ensure survival to the

pathogen. There are growing evidences of the capability of *A. fumigatus* to form biofilm with hyphae surrounded by an ECM[46]. This opportunistic pathogen can cause chronic pulmonary infections such as aspergilloma (localized), obstructive pulmonary disease, and allergic bronchopulmonary aspergillosis. In affected patients biofilms have been observed[47] [48]. On rare occasions, *A. fumigatus* biofilms are found on medical devices for healthcare[49]. The principal ECM components of *A. fumigatus* biofilms are galactomannan, α -1,3 glucan, proteins, polyols, and melanin. Immunostaining analysis of the *in vitro* secreted proteins in *A. fumigatus* ECM showed the presence of two major antigens, dipeptidyl peptidase V (DPPV) and catalase B (CatB), and the allergen, AspF1[50]. Also, several studies have demonstrated in the biofilm matrix the presence of an important virulence factor that permits the fungus to adhere to host cells and to elude the host innate immune system: galactosaminogalactan (GAG)[46][51][52]. The regulation of biofilm formation in *A. fumigatus* is relatively unknown, although probably involving a stepwise process similar to bacteria and yeasts[53].

1.2.3 Biofilm-related antifungal tolerance

Biofilms are universal, complex, interdependent communities of surface-associated microorganisms that can be composed of a

population that developed from a single species or multiple microbial species.

Some of the advantages of forming a biofilm include protection from the environment, nutrient availability, and metabolic cooperation. Biofilms are notoriously difficult to eliminate and are the source of many recalcitrant infections[54]. Microbial biofilms have two main consequences with profound clinical implications that are: i) the markedly enhanced resistance to antimicrobial agents, and ii) the highest protection from host defenses. Both features allow biofilm-associated infections being frequently refractory to conventional therapy.

Mechanisms mediating biofilm-related antifungal tolerance are still poorly understood. Factors considered to be responsible for the increased resistance to antibiotics in bacterial biofilms include restricted penetration of antimicrobials caused by the ECM production that protect biofilms and persister cells.

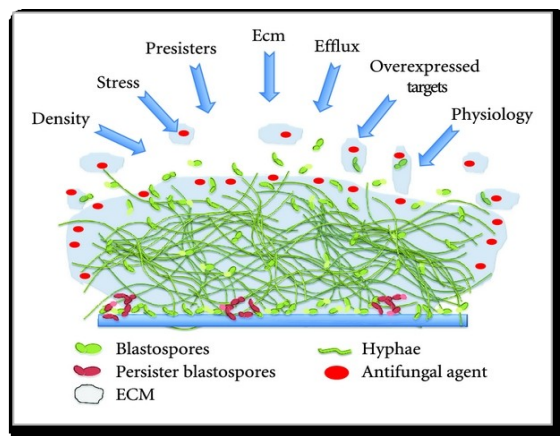


Figure 8. Biofilm-related antifungal strategies (*Adapted from Ramage, 2012*)[55]

Cell density is an important resistance factor within complex biofilm populations of yeasts and filamentous fungi, particularly towards azoles. It has been reported that both planktonic and mechanically dispersed biofilm cells exhibited azole sensitivity at low cell numbers. On contrary, an increase in cell density, as observed in biofilms, induces tolerance to antifungal agents[56].

Drug tolerance seems to be also associated, rather than the previously postulated slower growth rate, with an increase in metabolic activity of the developing biofilm, which suggests that drug resistance is a dynamic process, in parallel with biofilm maturation[40].

1.2.4 Alternative strategies for fungal infection management

Antifungal drug development is challenging because fungi are eukaryotes and many potential targets for therapy are also found in humans with substantial host toxicity risk. Current therapeutic choices for the treatment of invasive fungal infections are limited to three classes of drugs: azoles, echinocandins, and amphotericin B and its lipid formulations[57]. Therefore, the need for new antifungal agents is undeniable.

Most used antifungal agents are not completely efficient in eradicating the infection due to the resistance or tolerance development, often encompassing different antifungal classes. In fact, different compounds, such as fulvic acid and other natural

derivatives, have been investigated due to their antifungal activity to counteract fungal biofilm resistance[58].

Another approach under intensive study, is the use of antimicrobial peptides (AMP) as new antifungal candidates. AMPs are small soluble defense molecules, endogenously produced by virtually all organisms, displaying both anti-infective and immunomodulatory effects [59]. In humans, amongst the major AMPs produced, the cathelicidin LL-37 and defensins are suggested to have a good antifungal activity [60].

Two approaches are under investigation in our laboratories: natural products (i.e. cranberry) and sphingolipid metabolism inhibitors (i.e. Myriocin).

Vaccinium macrocarpon (Cranberry) is a rich source of polyphenols and it has been widely used for decades in the prevention of bacterial UTIs in the general population. Proanthocyanidins (PACs) are the main responsible for the inhibitory activity. PACs have been shown to possess beneficial properties fighting pathogenic infections including UTIs, dental caries, and stomach ulcers[61]. Nevertheless, there are controversial results on the PACs presence in human urine upon cranberry oral intake[62][63][64], [65]. The reason for such different results can rely on the use of different dosages as well as non-standardized cranberry products. Due to the common eukaryotic structure of fungi and humans, a limited number of antifungal drugs is tolerated by the host and available for therapeutic purposes, and new targets, as well as innovative

strategies to overcome primary and biofilm-related resistance, are needed.

Several sphingolipid metabolism inhibitors have been demonstrated to exert a broad-spectrum antifungal activity[66]. Sphingolipids (SPLs) are a class of molecules with structural and signaling activities conserved from fungi to humans, involved in infection-related mechanisms. Myriocin is a drug with a specific ability to inhibit *de novo* sphingolipid synthesis and its administration to human cells causes a re-arrangement of the endogenous pools of sphingolipids and an overall inhibition of proliferation without triggering cell death. Myriocin was used in research studies to inhibit highly proliferative cancerous cells with no sign of toxicity for normal cells[67]. In consideration of the opportunistic nature of fungal infection that takes advantage of the patient's pre-existing inflammatory conditions, and to the strict dependency of fungal survival on SPL synthesis, we aimed at investigating the Myriocin antifungal activity to counteract fungal infection.

1.3 The vicious cycle: infection-inflammation

The crude mortality rate of invasive candidiasis and aspergillosis has been estimated to be around 0.4 deaths per 100,000 people[68]. There are several risk factors thought to be responsible for the increased incidence of fungal infections. The primary causes are attributed to an ever-increasing population of

immunocompromised people. This population is not only composed of patients with primary or acquired immunodeficiencies but also conditions that are linked to intervention in medicine or surgery[11]. In fact, among the strongest risk factors for disseminated fungal infections are admitted to intensive care units, surgery and organ transplant, and use of broad-spectrum antibiotics, chemotherapy, and indwelling catheters[68]. Another apparent paradox is that, in addition to immunocompromised individuals, patients displaying hyperactivation of immune responses, such as those suffering from immune reconstitution inflammatory syndrome (IRIS), also display higher susceptibility to fungal infections[69]. The inflammatory milieu worsens the response to infection, which, in turn, perpetuates the inflammation. This situation triggers a vicious cycle between inflammation and infection that contribute to host diseases.

As a result of the long natural history of the co-evolution of fungi with their hosts, not only the human immune system has evolved mechanisms of recognition and control of fungi, but also fungi have evolved mechanisms of sensing and dealing with changes in the host environment[70]. To distinguish friends from foe, the immune system has evolved receptors that recognize molecules present on pathogenic microorganisms. These receptors, referred to as pattern recognition receptors (PRRs), function to promote the innate immune response, which is mainly described as a pro-inflammatory response. PRRs bind to conserved microbial structures called pathogen-associated molecular patterns (PAMPs). PRRs include

membranous Toll-like receptors (TLRs) and lectins, which confer additional extracellular surveillance mechanisms promoting phagocytosis and signaling[71]. TLR2, TLR4, and TLR9 are the main TLRs involved in sensing fungal components, such as zymosan, phosphor lipomannan, O-linked mannans, and fungal DNA. The role of TLRs is still unclear, although the contribution of individual TLRs varies depending on the fungal species and morphotypes, the route of infection and receptor cooperativity. Nevertheless, human studies have shown that a polymorphism in TLR4 is associated with increased susceptibility to pulmonary aspergillosis and bloodstream candidiasis[72].

An anti-inflammatory response during the initial interaction of yeasts with immune cells is necessary for the yeast to establish infection, showing that balancing the pro-/anti-inflammatory response is an important requisite for pathogenicity of infection mediated by fungi. However, the balance between resistance and tolerance to fungi may accommodate the host–fungus relationships, ranging from protection and immunopathology to fungal persistence and immunosuppression[72] (Figure 9).

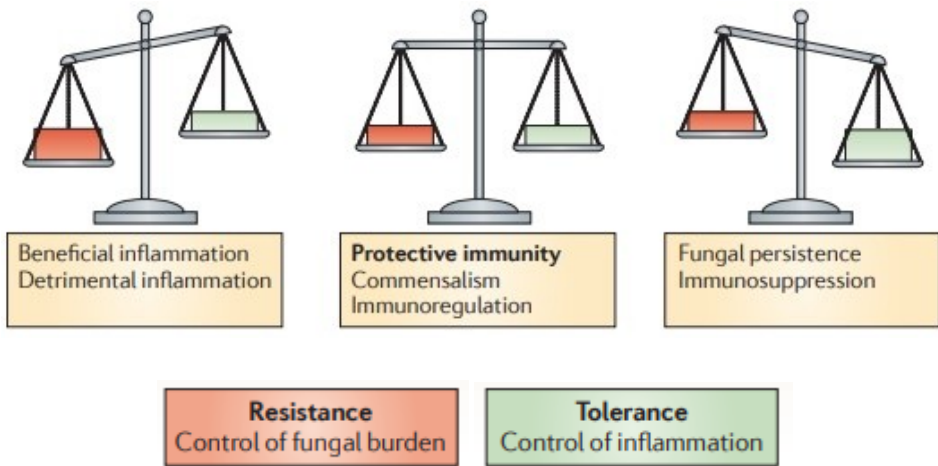


Figure 9. The balance between resistance and tolerance to fungi (Romani 2011)[72]

Excessive inflammation plays an important role in the pathogenesis of many infectious diseases and autoimmune conditions as well as in the development of malignancy. Targeting innate immune activation and signaling potentially holds great medical promise[73]

1.3.1 *Candida albicans*: its role in inflammation

The innate immune system plays a key role in protection against invasive *C. albicans* infections. Indeed, immunocompromised patients show increased susceptibility. Accumulating evidence suggests a complex interplay between the nervous and the immune

system in the regulation of immune responses, based on neurotransmitters, cytokines, and hormones. Acetylcholine (ACh), a classical neurotransmitter, is widely distributed in prokaryotic and eukaryotic cells, and almost every cell of a multicellular organism can synthesize and respond to ACh.

Recently, non-neuronally derived ACh has been demonstrated to play a role in regulating localized immune response, down-regulate potentially damaging chronic inflammatory responses, and promote favorable disease outcomes *in vivo* models of bacterial diseases[74].

This occurs via the cholinergic anti-inflammatory pathway which is mediated by the alpha 7 nicotinic receptor ($\alpha 7$ nAChR). Thanks to the wide distribution of cholinergic receptors, including a multitude of nicotinic and muscarinic receptors, ACh released by nerve terminals reaches discrete groups of cells in specific organs with minimum delay. Human immune cells, including neutrophils, possess the ability to respond to ACh because of the various repertoires of nAChRs and mAChRs, and the activation of specific receptors that can have different consequences for immune function[75].

The increase in our understanding of human cholinergic receptors and their roles in pathologies have led to the discovery of a plethora of small-molecule agonists and antagonists with therapeutic potential. Despite having been developed for the treatment of conditions whose pathology is defined by loss or gain of cholinergic function, cholinergic drugs have been utilized to evaluate the effects

of cholinergic receptors on non-neurological pathologies, including sepsis, for their therapeutic effects in inflammatory disease[76]. ACh is a neurotransmitter known to modulate pathogen-driven immune responses, downregulating potentially damaging chronic inflammation and promoting favorable outcome in bacterial sepsis[77]. Furthermore, human immune cells express both nicotinic and muscarinic acetylcholine receptors (nAChRs and mAChRs). These receptors have been demonstrated to modulate cellular immunity against pathogens via cholinergic-dependent mechanisms[78]. Evidence suggests that also bacteria and fungi are capable of synthesizing Ach, although very little is known about the cholinergic receptor repertoire of these microorganisms. Sequencing of the *C. albicans* genome has suggested that this organism possesses putative cholinergic receptor genes[79]. ACh modulates the pathogenicity of *C. albicans* by inhibiting morphogenesis, biofilm formation, and the expression of virulence factors. Besides, ACh promotes an effective cellular immune response to fungal infection, facilitating rapid clearance from infected tissues and affording protection from chronic-inflammation-induced damage of vital tissues[80]. The research of similar compounds paves the way to new therapeutic strategies.

1.3.2 *Aspergillus fumigatus*: its role in cystic fibrosis

Lung disease and recurrent lung infections are undoubtedly the major cause of morbidity and mortality in Cystic Fibrosis (CF) patients. The achieved increase in the life expectancy of CF patients goes in parallel with new challenges in their clinical management, such as fungal infection therapies[81]. *Aspergillus fumigatus* is the most frequently cultured fungal pathogen from the sputum of CF patients, with a reported prevalence ranging from 10–57%[82].

Several studies have indicated that, in healthy individuals, the innate defenses are primarily responsible for the elimination of inhaled conidia from the lungs, due to beating cilia and the presence of mucus and macrophages of the innate immune system that rapidly eliminates conidia via non-inflammatory mechanisms[83]. Failure to remove conidia, as in CF patients, results in rapid fungal germination that reveals pro-inflammatory substrates such as inner cell wall-derived beta-glucans that bind to fungal pattern-recognition receptors and elicit the innate immune response. The pathogenic significance of fungal colonization is still a matter of debate, although recent studies suggested that persistently colonized patients have a higher rate of pulmonary exacerbations requiring hospital admission[84]. On the other hand, the chronic inflammatory state of the CF lung mucosa is often

responsible for the shift from microbial colonization to infection, perpetuating the vicious cycle of infection-inflammation[85].

Targeting simultaneously infection and inflammation has been suggested as a useful antifungal strategy. Moreover, in previous studies conducted in our laboratories, we demonstrated a direct antifungal activity of Myriocin on *A. fumigatus* biofilm, suggesting that inhibition of sphingolipid metabolism could represent a new target to overcome biofilm-related fungal infections[86].

2.AIM

Biofilm formation represents a key factor in fungal survival in harsh environments as well as a virulence trait in human fungal infections, with important clinical consequences. Alternative or complementary approaches to conventional antifungal therapy or to prevent biofilm-related disease are thus desirable.

The aim of my Ph.D. project was to investigate the mechanisms promoting biofilm development and assess new strategies to prevent or eradicate biofilm-related infections. Since fungal pathogenesis can be related to either pathogen characteristics or host immune response to infection, the research has been carried out considering both aspects.

Based on the reported efficacy of cranberry in preventing and/or inhibiting *Escherichia coli* UTIs, we studied whether cranberry or its metabolites might exert an anti-biofilm effect on *C. albicans* biofilm formation. Moreover, we assessed the antimicrobial activity of hydrogels, newly synthesized biocompatible material meant for assembly medical devices reducing the risk of biofilm formation.

Since altered host immune status and inflammatory milieu can worsen the outcome of the infection, we also explored some strategies aimed at targeting both fungal biofilms and host inflammatory status: cholinergic agonists in systemic candidiasis, and Myriocin, a sphingolipid synthesis inhibitor, in *A. fumigatus* infection in CF patients.

3.MATERIALS and METHODS

3.1 Culture conditions and standardization

3.1.1 *Candida albicans*

The reference strain *C. albicans* SC5314, a strong biofilm producer, has been used as a control strain in all the experiments. Clinical *C. albicans* isolates, used to validate the obtained results, were chosen among strains collected during a previous study [87]. In particular, 10 selected isolates were chosen because isolated from the genitourinary tract (8 from vaginal swabs and 2 from urine).

C. albicans strains were stored at -80°C in yeast extract peptone dextrose (YPD) broth supplemented with glycerol (30% w/v), in cryovials.

YPD medium was prepared by diluting 1% w/v yeast extract, 2% w/v peptone, 2% w/v dextrose in distilled water, and sterilized by autoclave at 120°C for 30 minutes.

Before experiments, yeast strains were thawed in 3 ml of YPD broth and incubated overnight at 30°C under an orbital shaker. Cells were collected by centrifugation at 1500g for 10 minutes at 4°C, washed with 10 mL of cold phosphate-buffered saline (PBS), and resuspended in 3 mL of PBS. The washing steps were repeated two times to completely remove the media. After the last centrifugation, cells were resuspended in 2 ml of PBS and counted by hemocytometer (Neubauer counting chamber). Finally, the suspension was standardized to the desired final concentration by

further diluting in PBS. The final concentration was also checked by plating the final suspension onto Sabouraud dextrose agar supplemented with Chloramphenicol (SAB+CAF) and incubating for 24 h for colony forming unit (CFU) count.

3.1.2 *Aspergillus fumigatus*

The reference strain *A. fumigatus* Af293 (ATCC MYA-4609, CBS 101355) was used in the study. Frozen conidia were stored in glycerol stocks at -80°C. Prior to experiments, conidia were streaked out directly on fresh Potato Dextrose Agar (PDA) slants and incubated at 30° C, until sporulation. After 72–96 h conidia were harvested in PBS supplemented with Tween-20 (0.01% w/V), centrifuged at 1500g for 5 minutes, and washed three times with PBS, until final suspension in 1.5 ml of PBS. Conidia suspension was counted by hemocytometer as above described and the final concentration checked by (CFU) count.

3.2 Inhibitory effect of cranberry metabolites on *C. albicans* filamentation and biofilm-formation

3.2.1 Urinary fractions collection

Urine fractions to be tested were obtained by a randomized, double-blind, 2-arm study with a design. The enrolled cohort consisted of a

total of 13 volunteers (age, mean \pm SD: 25 \pm 4, and BMI, mean \pm SD: 20.6 \pm 2.0 kg m⁻²) recruited from students and staff of the University of Milan.

Inclusion criteria were: women, 18–40 years of age, normal weight for height (BMI 18–25 kg m⁻²), non-smokers, no history of diabetes, renal, hepatic, or gastrointestinal diseases.

Exclusion criteria were: allergy and/or aversion to cranberry or derived products, consumption of any dietary supplement, drug or medication for at least one month before the start of the study. A list of foods to be avoided has been provided to the volunteers (fruits and vegetables rich in polyphenols for such as red/purple fruits/vegetables, chocolate, and some beverages such as coffee, tea, wine, and fruit juice). All participants signed an informed consent form. The study was according to the ethical standards established in the 2013 Declaration of Helsinki and approved by the Ethics Committee of the University of Milan (December 18, 2018, ref. 57/18) and was registered at www.isrctn.org as ISRCTN32556347.

Participants took 2 capsules of Anthocran® /day for 7-days. Urine samples were collected before starting the supplementation (day 1, time 0) and at the following time-points: 1,2, 4, 6, 10, 12, 24 h, after the last dosage (day 7).

Three volunteers consumed two placebo capsules (same shape, size, color, flavor, and excipients of the products tested). Collected urine samples were freeze-dried and stored at 4 °C until use.

The urinary fractions were kept freeze-dried at 4°C until the test. Before experiments, the samples were rehydrated in 2 ml of warm RPMI-1640 and used within 2 days.

3.2.2 Cranberry urinary metabolites

The characterization of metabolites in urine was carried out by Prof. Aldini's group. Both targeted and untargeted analyses based on high-resolution mass spectrometry (MS) were used for the identification. Based on the results obtained, the following compounds were purchased from Merck KGaA, Darmstadt, Germany: 2-hydroxybenzoic acid, 4-hydroxybenzoic acid (4-HBA), 2,3-dihydroxybenzoic acid, 2,5-dihydroxybenzoic acid, and 3-(4-hydroxyphenyl)-propionic acid. Protocatechuic acid, kaempferol, quercetin, syringe were purchased from Extrasynthese (Genay Cedex, France). A 10 µM concentration was used in the initial phase for all the compounds, whereas, after MS quantitative analyses, each compound concentration was adjusted according to the amount recovered in the most active urine fractions. Due to the lack of commercial availability of valerolactone standards, the 5-(3',4'-dihydroxy phenyl)-γ-valerolactone (VAL) was synthesized in Fumagalli's laboratories. For 4-HBA and VAL, various concentrations were assessed. All the compounds were dissolved in 100% methanol filtered in a 0.22 µm filter (Merk Millipore) and diluted to the final concentration in the desired medium.

3.2.3 Biofilm formation and biomass quantification by Crystal Violet

For evaluating and quantifying biofilm biomass, the well-established Crystal violet (CV) assay was employed.

C. albicans inocula were standardized, as specified in the section culture conditions, to 10^6 yeast cells/mL in Roswell Park Memorial Institute (RPMI)-1640 medium supplemented with 2% glucose and buffered with 0.165 M MOPS [3-(N-morpholino) propane sulfonic acid]. At first, 200 μ L of inoculum was seeded in each well of polystyrene 96-well plate and incubated at 37°C for 1 hour to promote adhesion. To evaluate the inhibitory effect of various cranberry metabolites, as well as of urinary fractions, the compound was added in this initial phase by plating 100 μ L of 2×10^6 yeast cells/mL and 100 μ L of with 0,1 mg/ml Anthocran®, 30 μ M and 245 μ M of 5-(3',4'-dihydroxy phenyl)- γ -valerolactone (VAL) or 3,5 μ M 4-HBA.

Non-adherent cells were then removed, and wells were washed with warm RPMI-1640; eventually, the medium was replaced, and the plate further incubated at 37°C for 24 h.

At the end of incubation, wells were washed two times with warm PBS to remove non-adherent cells and the medium. Biofilms were fixed with 100% methanol for 15 minutes and then stained by CV staining (0.1% w/v in distilled water) for 5 minutes. The excess of staining was removed by washing with distilled water and let dry for 5 minutes. Eventually, CV was dissolved in 33% acetic acid for 10 minutes before absorbance reading at 540 nm using an EnSight

Microplate Reader (PerkinElmer). Three independent experiments were carried out with five technical replicates for each condition. The reference strain *C. albicans* SC5314 was used as control. Negative controls containing no biofilms were used for background correction.

3.2.4 Quantification of cell metabolic activity

The formazan salt-based XTT (2,3-bis(2-methoxy-4-nitro-5-sulfophenyl)-2H-tetrazolium-5-carboxanilide inner salt) reduction assay is a semi-quantitative measure of cell viability.

For this assay, *C. albicans* biofilms (treated or untreated) were allowed forming as above described.

After 24h-incubation, at 37°C, the culture medium was removed from each well of a 96-well plate, and biofilms were carefully washed three times with 200µl of warm PBS to avoid mechanical biofilm detachment. Meanwhile, a solution of 0.5mg/ml XTT and 10 mM of menadione (AppliChem) was prepared and 100µl were added to each well. The plate was incubated at 37°C, in the dark, for 2 hours. Metabolically active cells reduce the XTT formazan (yellow color) and the dye formed directly correlates to the number of viable cells in the culture. The absorbance of colorimetric changes was read by EnSight Microplate Reader at 450nm with a reference scanning of 620nm[88].

Three independent experiments were carried out with three replicates for each condition. Negative controls containing no biofilms were used for background correction.

3.2.5 CaCo-2 culture

Colorectal adenocarcinoma cell line, Caco-2 (ATCC® HTB-37™), was cultured in Dulbecco's Modified Eagle's Medium (DMEM) supplemented with 10% fetal bovine serum (FBS) (Gibco®), 2 mM L-glutamine (Gibco®) and 1 mM sodium pyruvate (Gibco®) and incubated at 37°C and 5% CO₂ atmosphere. The cells were detached from the culture flasks with trypsin-EDTA solution (Lonza Bioscience) for 5 minutes when reaching 70-80% confluence. The cell viability was performed by Trypan blue 0.4% (Sigma-Aldrich) exclusion assay.

3.2.6 Conditions and Cytotoxicity assay

The cytotoxicity of VAL and 4-HBA was assessed by 3-(4,5-dimethylthiazol-2-yl)-2,5-diphenyl tetrazolium bromide (MTT) assay[89]. The compounds' stock solutions were prepared in dimethyl sulfoxide (DMSO) as a vehicle and the dilutions were prepared in complete medium and filtered. After dilution, the final concentration of DMSO was 0.1% and the concentrations of the compounds tested were 245, 100, 30, 10 µM for VAL and 36, 18, 3.5, 1 µM for 4-HBA. In addition, the untreated (control) and vehicle

(DMSO 0.1%) samples were prepared. Briefly, 1×10^4 Caco-2 cells/well were seeded in a 96-well plate in the complete medium as previously described and incubated for 24 h. Then, the cells were incubated with the treatments for 24 h. The MTT solution (0.5 mg/mL) was added into each well for 3-4 h at 37°C. Formazan crystal was solubilized with 100 μ L/well of lysis buffer (8 mM HCl + 0.5% NP-40 in DMSO) and the absorbance was measured at 575 nm by a microplate reader (Power Wave HT, Biotek, Bad Friedrichshall, Germany). The fraction of cell viability was calculated as follows: *Cell viability (%) = (absorbance sample/absorbance control) \times 100*. Three independent experiments were performed with four technical replicates for each condition.

3.2.7 Confocal laser scanning microscopy (CLSM)

To investigate the morphological and structural changes induced by *Vaccinium macrocarpon* (Cranberry) and its metabolites both on filamentation and biofilm architecture, *C. albicans* reference strain SC5314 was allowed forming biofilm for 24h in presence or not of treatments and then biofilm was visualized by confocal laser scanning microscopy (CLSM). Untreated and treated (exposure to 30 μ M or 245 μ M of VAL and 0.1 mg/ml of Anthocran®) biofilms were studied. To allow direct visualization under CLSM, biofilms were grown on tissue culture coverslips (Starstedt) in a 24-well plate, fixed with methanol 100%, and stained by 0,05% calcofluor white (Sigma-Aldrich). Biofilms thickness was measured by CLSM Z-

stacking. The samples were stored in the dark until observation by CLSM (inverted Nikon A1R with SIM-Super Resolution, 115 nm X, Y; 270 nm Z). The excitation line 300nm and the emission filters 440nm were used for Calcofluor white and images were acquired with the program NIS Viewer (Nikon).

3.2.8 Cell surface hydrophobicity assay

To determine the effect of cranberry metabolites on *C. albicans* cell surface hydrophobicity (CSH), the ability of cells to adhere to a hydrocarbon source (Octane, Sigma) was measured.

Cells of *C. albicans* SC5314 were grown overnight in YPD with 0,1 mg/ml Anthocran®, 30µM and 245µM of 5-(3',4'-dihydroxy phenyl)-γ-valerolactone (VAL) or 3,5 µM 4-HBA under orbital shaking at 30°C. Cell suspensions were then diluted in PBS to an OD600 of 1 and 1.2mL of the fungal suspensions were transferred to a glass tube with the addition of 300µl of octane. The samples were then mixed by vortex for 2 min and phases (aqueous and hydrophobic) were allowed separating for 10 minutes at 30°C. The aqueous phase was harvested and its optical density was measured spectrophotometrically. The hydrophobicity index was calculated as follows: %CSH= $[(A-B)/A] \times 100$ (A= absorbance of fungal suspension; B= absorbance of aqueous phase). Data from three independent experiments were collected. Negative controls grown in medium alone were used for background correction.

3.2.9 RNA extraction and real-time analysis for 5-(3',4'-dihydroxy phenyl)- γ -valerolactone on *Candida albicans* biofilm

The expression of genes encoding for proteins involved in filamentation and biofilm formation was evaluated by quantitative Real-Time PCR (qPCR). Total RNA was isolated from *C. albicans* SC5314 culture at two different time points: 4 h for early biofilm and 24 h for mature biofilm.

C. albicans RNA was extracted with TRI-reagent (Sigma-Aldrich) from cells culture, treated/untreated with 30 μ M and 245 μ M VAL or 3,5 μ M 4-HBA or Anthocran® (0.1 mg/mL).

A standardized inoculum of 1×10^6 was seeded, in a T25 flask containing 5mL of RPMI-1640 medium, supplemented or not with the above-mentioned compounds. After 4 hours or 24 hours of incubation, cells were harvested directly by scraping in TRI-reagent, keeping flasks on ice to preserve the RNA fraction, and the collected samples were stored at -80°C. For RNA extraction, samples were thawed and 200mg of glass beads (106 μ m, Sigma-Aldrich) were added to each tube and vortexed at maximum speed in a Tissue lyser for 3 minutes, and then kept in ice to avoid the heating. This step was repeated 3 times. Beads were removed by centrifugation and 200 μ l of acid phenol were added to allow the complete fungal cell wall rupture. The aqueous phase was obtained by adding 200 μ l chloroform to each sample. After adding 500 μ l isopropanol and mixing by vortex, samples were centrifuged to

obtain the RNA pellets which were washed with ethanol 95% and, finally, dissolved in 30µl DNase-RNase free water. Total RNA was quantified by NanoDrop (Implen).

Complementary DNA was synthesized from a total amount of 1000 ng of purified RNA by the Applied Biosystems™ High-Capacity cDNA Reverse Transcription Kit (Life Technologies Italia) according to the manufacturer's instructions, with a final volume of 20 µL made up using RNase free water.

The thermal cycler (Applied Biosystems) was set up with cycle conditions of 5 min at 25°C, 60 min at 42°C, 5 min at 70°C and a final hold stage at 4°C. cDNA was then stored at -20°C until used in subsequent q-PCR.

The real-time reaction was prepared using the primers listed in table 1. 50 ng of cDNA was used in the reaction and each sample was run in triplicate. The reaction mix was prepared using TB Green Premix Ex Taq /ROX qPCR Master Mix (Takara Bio Europe) and conducted in a Step One Plus Real-Time PCR System thermocycler. The thermal profile cycle consisted of a holding stage of 20 sec at 95°C followed by 40 cycles of 3 s at 95°C and 30 s at 60°C. A melt curve was also carried out after the end of the PCR thermal profile to confirm that only one product had been amplified. Relative expression levels were calculated using the $\Delta\Delta C_t$ method and all samples were normalized to the expression of the housekeeping gene and the control condition whose values were normalized to 1. Three independent experiments were carried out.

Table 1. List of primers used in qRT-PCR for VAL and 4-HBA on *C. albicans* biofilm markers

Target	Primer forward	Primer reverse
HWP1	TGCTATCGCTTATTACATGTTATC	GAGCTTCTTCTGTTTCACCTTGAC
ALS3	CAACTTGGGTATTGAAACAAAAAC A	AGAAACAGAAACCCAAGAACAACC T
IMH3	TATTCATATGGCATTATTGGGTGGT A	AACCATTTCTGCTTGTTCTTCAGA

3.3 Functionalized hydrogels as a strategy to prevent biofilm-related infection

3.3.1 Antimicrobial activity of hydrogels

Hydrogel synthesis was performed at the Department of Chemistry, Materials and Chemical Engineering, Milan, Italy as reported in Mauri et al. 2019 [90]. Hydrogels antibacterial activity was assessed by an *in vitro* test against *Staphylococcus aureus* ATCC 6538 and *C. albicans* SC5314, two common etiological agents of hospital-acquired infections related to biofilm formation.

Before testing, hydrogels were placed in a 24-well-plate and sterilized under UV light for 30 min for each side. Microbial strains were thawed from glycerol stock at $-80\text{ }^{\circ}\text{C}$ by seeding them on fresh Trypticase Soy Agar (TSA, for *S. aureus*) or Sabouraud

Dextrose agar (SAB, for *C. albicans*) and incubated for 24 h at 37°C.

A single colony was picked and suspended in phosphate buffer saline (PBS) to obtain a 0.5 McFarland inoculum corresponding to about 10^8 CFU/mL for *S. aureus* and 10^6 CFU/mL for *C. albicans*. Serial dilutions were performed in Trypticase Soy Broth (TSB, for *S. aureus*) or RPMI-1640 medium (for *C. albicans*) until the desired concentration, which was assessed to be 10^4 and 10^5 CFU/mL, respectively. Two ml of the suspension were added drop-by-drop to hydrogels, allowing gradual absorption. As positive growth controls, *S. aureus* ATCC 6538 and *C. albicans* SC5314 were cultured without hydrogels or with non-functionalized samples. After 24 h incubation at 37°C, both supernatant and hydrogels were collected in 50 ml tubes containing 18 ml of PBS and mixed by vortex to disperse microbial cells for CFU count. Plates were incubated at 37°C and colonies were counted after 24 h of growth.

3.4 Effect of inflammation on *Candida albicans* systemic *Galleria mellonella* pathogenicity assay

3.4.1 *Galleria mellonella* inoculation

The host model *Galleria mellonella* (Gmel) was used to study *C. albicans* pathogenicity and the effect of the administration of ACh and pilocarpine (Pilo), dissolved in DMSO in modulating the

invertebrate immune response and, in turn, the outcome of the infection.

G. mellonella larvae were purchased from Allevamento Cira, Como, Italy. At arrival, larvae were kept in the dark at 18°C in wood shavings and used within 7 days of shipment. Before experiments, 16 last-instar larvae, with a bodyweight comprise between 250mg and 300 mg, were selected for each experimental condition. Two further groups were included: un-injected larvae (for batch control) and PBS- injected larvae (to monitor the trauma related to injection). Larvae were inoculated, using a Hamilton syringe with a 26-gauge needle, into the hemocoel through the hindmost left proleg with a standardized inoculum of *C. albicans* 5×10^5 cells/larva, in the presence and absence of ACh (50 µg/ larva) or Pilo (25 µg/ larva). Inoculated larvae were placed into sterile Petri dishes (90 mm diameter) with filter paper at the bottom and incubated at 37°C. The number of dead larvae was scored daily for 9 days. A larva was considered dead when it displayed no movement in response to gentle touch. Three independent experiments were carried out.

3.4.2 Hemocytes

To study the effect of ACh and Pilo administration on the insect immune response, hemolymph of three *G. mellonella* larvae/group were collected to study hemocytes composition. Two approaches were used: an *ex-vivo* stimulation of insect hemocytes and an *in vivo* study, by extracting hemocyte after *C. albicans* infection. For

the first part, five larvae were stunned in ice, and hemolymph was harvested into ice-cold Grace's medium (Sigma-Aldrich, Italy) by lateral bleeding corresponding to the last right proleg. Hemocytes were counted and plated onto coverslips in a 24-well plate. The plate was incubated for 2 h to allow hemocytes to adhere prior to stimulation with *C. albicans* SC5314 (10^2 yeast cells/well) for 24 h, in the presence and absence of treatments. At 24h, hemocytes were fixed in 4% paraformaldehyde and stained with hematoxylin and eosin. Hemocytes incubated in media alone was used as a control.

For the *in vivo* experiments, larvae were inoculated as described for the killing assay. After 24h treatment, hemocytes were isolated from larvae as described above pooling three animals for the condition. Hemocytes were plated onto coverslips in a 24-well plate, and the coverslips were centrifuged for 3 min at 300 g at room temperature and fixed in 4% paraformaldehyde and stained with hematoxylin and eosin (HE). In both *ex-vivo* and *in vivo* experiments, hemocyte, subtype differentiation, and nodule formation were assessed in comparison to hemocytes incubated in media only (*in vitro*) or hemocytes from sham-inoculated larvae (*in vivo*) Characterization and quantification were achieved with the help of Dr. Monica Falleni, experienced pathology at our Department.

3.4.3 Histology

After hemolymph extraction, the same larvae were processed for histology, as previously described[91]. Briefly, the larvae were inoculated with buffered formalin and sectioned through transverse cutting. Tissue sections were embedded in paraffin and stained with HE or periodic acid-Schiff stain (PAS). Image acquisition was performed by the NanoZoomer-XR C12000 series (Hamamatsu Photonics). To investigate *C. albicans* filamentation and the effect on cellular immunity *in vivo*, two-time points were chosen, 24 and 48 h. Data were confirmed in three independent experiments.

3.5 Effect of inflammation on *Aspergillus fumigatus* infection in cystic fibrosis patient

3.5.3 PBMC Isolation and Infection

CF patient monocytes were infected *ex-vivo* to study the inflammatory response. We collected 43 blood samples from CF patients referred to the Ancona Cystic Fibrosis Centre. 22 out of 43 subjects were homozygotes for the F508 del mutation of the CFTR gene and 21 heterozygotes with one F508 del allele (United Hospital Le Torrette, Ancona, Italy, CE Regionale Marche -CERM-, protocol number 2016 0606OR).

Peripheral blood mononuclear cells (PBMCs) were freshly isolated in the Ancona Cystic Fibrosis Centre using Leucosep protocol according to the manufacturer's instructions, and stored at -80°C. Frozen PBMCs were shipped to our laboratory in dry-ice and immediately put at -80°C at their arrival.

To avoid the influence of anti-CD14-coated microbeads selection on cytokine production, we isolated monocytes by plastic adherence[92].

Before experiments, thawed PBMCs were counted by hemocytometer using trypan blue to detect non-viable cells. About 1×10^6 cells per well were seeded into 6-well plate (Corning Inc. Costar, New York, NY, USA) containing 2 mL RPMI-1640 medium supplemented with 10% FBS and 1% penicillin/streptomycin. Plate was finally incubated in a 5% CO₂ incubator at 37°C for 2 hours. Free-floating cells were then removed by washing and the adhering fraction enriched in monocytes was used for *A. fumigatus* infection.

3.5.4 Monocyte killing ability

To assess monocyte killing ability, cells were pre-treated with 50µM Myriocin or medium for 1 h at 37°C and then infected with *A. fumigatus* conidia at a multiplicity of infection (MOI) of 1:1. Myriocin powder (Sigma Aldrich, Milan, Italy) was weighted and dissolved in DMSO by warming up at 37°C and the solution was filtered and stored at -80°C until used. One hour after infection, cells were washed twice with warm medium to remove non-internalized

conidia, and incubated for a further 4 h to allow conidia killing. Cells were then harvested, counted, and lysed by osmotic shock induced by adding distilled water, to recover live internalized conidia. Cellular lysis was confirmed by microscopy. Supernatants were mixed by vortex, serially diluted in PBS, and plated onto Sabouraud Dextrose Agar (SAB). Plates were incubated at 37°C, and CFU were counted after 48 and 72 h of growth.

3.5.5 RT-PCR

RNA was isolated from cell cultures as *in vitro* model of CF. IB3-1 cells, an adeno-associated virus-transformed human bronchial epithelial cell line derived from a CF patient (DF508/W1282X) provided by LGC Promochem (US), were used. This cell line was growth in LHC-8 medium supplemented with 10% FBS and 1% penicillin/streptomycin at 37°C and 5% CO₂.

Human lung bronchial epithelial cells 16HBE14o-, originally developed by Dieter C. Gruenert, were provided by Luis J. Galletta (Telethon Institute of Genetics and Medicine TIGEM, Napoli), and used as a control cell line. Cells (1×10^6 cells) were cultured overnight at 37°C and 5% CO₂, in 100 mm Petri dishes containing 5 ml of Minimum Essential Medium (MEM) Earle's salt, supplemented with 10% FBS and 1% penicillin/streptomycin.

After 24 hours of incubation, cells were pre-treated with 50 mM Myriocin for 1 h and then stimulated with *A. fumigatus* conidia with a MOI of 1:100 for 1 h. Cells were washed three times in PBS to

eliminate non internalized conidia and incubated for further 3 h with 5 mL medium supplemented or not with 50 mM Myriocin. Cells were collected at this time point, or after 12 h, for the RNA extraction. Adherent cells were harvested with lysis buffer of SV Total RNA Isolation Kit (Promega) and the extraction was performed as the manufacturer's instructions. RNA was quantified and quality assessed using a NanoDrop spectrophotometer (Implen).

A total amount of 1000 ng of purified RNA was used to synthesized complementary DNA by the Applied Biosystems™ High-Capacity cDNA Reverse Transcription Kit (Life Technologies Italia) according to the manufacturer's instructions, with a final volume of 20 µL made up using RNase free water.

The thermal cycler (Applied Biosystems) was set up with cycle conditions of 5 min at 25°C, 60 min at 42°C, 5 min at 70°C and a final hold stage at 4°C. cDNA was then stored at -20°C until used in subsequent q-PCR.

The Real-time PCR was performed using TB Green Premix Ex Taq /ROX qPCR Master Mix (Takara Bio Europe), for target genes listed in Table 2.

Table 2. List of primers used in qRT-PCR for gene expression in CF cell lines.

Target	Primer forward	Primer reverse
<i>IL-1β</i>	TGCTATCGCTTATTACATGTTATC	GAGCTTCTTCTGTTTCACCTTGAC
<i>IL-8</i>	CAACTTGGGTATTGAAACAAAAAC A	AGAAACAGAAACCCAAGAACAACC T
<i>NOD2</i>	TATTCATATGGCATTATTGGGTGGT A	AACCATTTCTGCTTGTTCTTCAGA
<i>TLR2</i>	CTGCAAGCTGCGGAAGATAAT	AGGACTTTATCGCAGCTCTCAGA
<i>TLR7</i>	TTTACCTGGATGGAAACCAGCTA	TCAAGGCTGAGAAGCTGTAAGCTA

The thermal profile cycle set up in a Step One Plus Real-Time PCR System thermocycler, consisted of a holding stage of 20 sec at 95°C followed by 40 cycles of 3 s at 95°C and 30 s at 60°C. A melt curve was also carried out after the end of the PCR thermal profile to confirm that only one product had been amplified.

Relative mRNA expression of target genes was normalized to the endogenous *GAPDH* gene, whose values were normalized to 1 and calculated by the comparative $\Delta\Delta CT$ method. Three independent experiments were carried out.

3.6 Statistical analysis

All the experiments were carried out at least three times, with at least three replicates for each condition. Student's t-test and one-way ANOVA analyses of variance were used to compare two or multiple groups, respectively. Mann-Whitney was used for non-parametric tests. For *in vivo* experiments, *G. mellonella* Kaplan Meier survival curves were analyzed using Log-rank Mantel-Cox test. Statistical significance was achieved if $p < 0.05$. Graph production, data distribution and statistical analysis were performed using GraphPad Prism (version 7; La Jolla, CA, USA, www.graphpad.com).

4. RESULTS

4.1 Strategies to counteract biofilm-related fungal infections

4.1.1 Cranberry metabolites in urinary fractions activity against *Candida albicans* biofilm

Ten healthy volunteers were asked to take Anthocran®, a concentrated extract of cranberry, once a day for one week. The ability of Anthocran® urinary metabolites to reduce *C. albicans* adhesion and biofilm formation was measured using urine fractions collected at different time points (pre-administration, 1h, 2h, 4h, 6h, 10h, 12h, and 24h).

First, metabolite activity was tested against the reference strain *C. albicans* SC5314, a high biofilm producer, by means of CV assay. In particular, two urinary fractions efficiently inhibited biofilm production and biomass formation ($p < 0.001$), 1h and 12 h, whereas all others, including the urine collected before cranberry intake, were ineffective (Figure 10).

Anthocran® itself, solubilized in DMSO at 0.1 mg/mL, dramatically impacted on *C. albicans* SC5314 biofilm-forming ability ($p < 0.0001$).

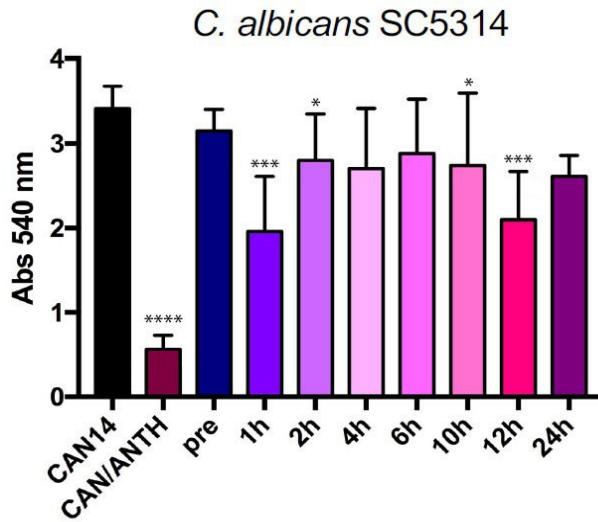


Figure 10- Activity of Anthocran® (CRAN, 0.1 mg/mL)(CAN/ANTH), urine before Anthocran® intake (pre) and urinary fractions on the reference strain *C. albicans* SC5314 (CAN14). Crystal violet assay was used to evaluate biofilm biomass reduction. Significant differences are indicated by * $p < 0.05$, *** $p < 0.001$, **** $p < 0.0001$, Mann-Whitney test.

To confirm this observation, clinical isolates from genitourinary infections were selected from a collection of strains isolated during a national survey on yeast infections[87]. Ten strains were chosen for this purpose (Table 3). Because of the highly strain-dependent variability in biofilm-forming ability, strains were firstly assessed for their propensity to form biofilm on 96-well polystyrene plates. Five strains resulted good biofilm producers (+++), and five low/medium (+/-; ++) producers.

Table 3- Clinical isolates used in the study and biofilm-forming ability

ID strain	Species	Source	Biofilm production
g11	<i>Candida albicans</i>	Vaginal swab	++
g23	<i>Candida albicans</i>	Vaginal swab	+++
g29	<i>Candida albicans</i>	Vaginal swab	+++
g35	<i>Candida albicans</i>	Vaginal swab	++
g44	<i>Candida albicans</i>	Vaginal swab	++
g49	<i>Candida albicans</i>	Vaginal swab	+/-
g67	<i>Candida albicans</i>	Vaginal swab	++
g69	<i>Candida albicans</i>	Vaginal swab	+++
g14	<i>Candida albicans</i>	UTI*	+++
g53	<i>Candida albicans</i>	UTI*	+++

*Urinary tract infection

Clinical strains were then tested in the presence of urinary fractions (1:2 diluted in RPMI) as previously done for the reference strain SC5314. Despite strain-dependent variability, 12 h fraction (and to a lesser extent 1h fraction) was confirmed to efficiently reduce adhesion and biofilm formation, more efficiently compared to other fractions (Figure 11).

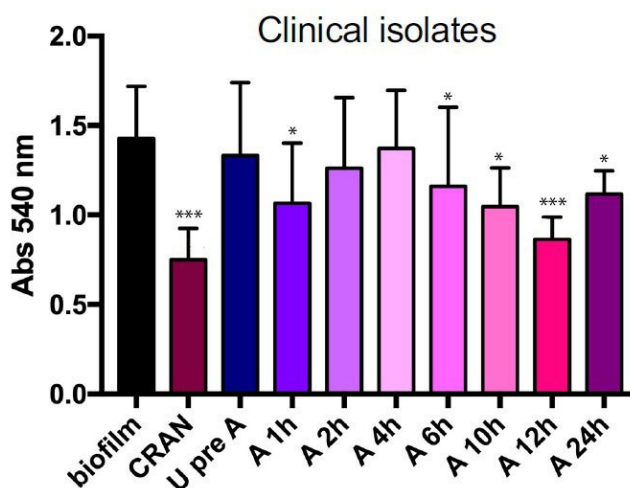


Figure 11– Activity of Anthocran® (CRAN, 0.1 mg/mL), untreated reference strain SC5314 (biofilm), urine before Anthocran® intake (U pre A), and urinary fractions against ten *C. albicans* clinical isolates from genitourinary infections. Crystal violet assay was used to evaluate biofilm biomass reduction. Significant differences are indicated by * $p < 0.05$, *** $p < 0.001$, Mann-Whitney test.

4.1.2 Mass spectrometry (MS) analysis revealed that metabolites other than proanthocyanins are enriched in the most active urinary fractions

In collaboration with Prof. Giancarlo Aldini and Dr. Giovanna Baron (Department of Pharmaceutical Sciences, Università Degli Studi di Milano), a combined targeted and untargeted MS approach was applied to identify the most concentrated metabolites in various urinary fractions. Particular attention was used for those metabolites picking in the most active ones. The combined strategy allowed

identifying 35 analytes including Cranberry components, known metabolites, and metabolites hitherto unreported in the literature. Each compound identified with the targeted and untargeted approach was extracted and normalized to that of the internal standard to obtain semiquantitative ratios of the compounds present in each urine fraction. A selection was made (Table 4) by choosing those metabolites which were present at their maximum relative concentration in the two most active urine fractions (1 h and 12 h after the last capsule intake).

Table 4 Urinary fraction at 1h and 12h resulted in the most active *in vitro*. The most abundant cranberry metabolites in these fractions are listed in the table.

NAME	TMAX	IDENTIFICATION APPROACH
Protocatechuic acid	1 h	Targeted
kaempferol	1/12 h	Targeted
Quercetin	12 h	Targeted
Syringetin	1/12 h	Targeted
Quercetin 3-O-rhamnoside	1 h	Targeted
2-hydroxybenzoic acid	1 h	Targeted
4-hydroxybenzoic acid	1 h	Targeted
2,3-dihydroxybenzoic acid	1 h	Targeted
2,5-dihydroxybenzoic acid	1 h	Targeted
3-(4-hydroxyphenyl)-propionic acid	1 h	Targeted
5-(3'-4'-dihydroxyphenyl)-gamma-valerolactone	1/12 h	Untargeted
5-(4'-hydroxyphenyl)- gamma-valerolactone-3'-O-sulphate	1 h	Untargeted
5-(3'-hydroxyphenyl)- gamma-valerolactone-4'-O-sulphate	1 h	Untargeted

First, we tested the most represented urinary metabolites obtained by MS targeted analysis (Figure 12). 4-HBA was the most active compound in inhibiting *C.albicans* SC5314 adhesion and biofilm formation ($p < 0.001$). Moreover, compared to 3-(4-hydroxyphenyl)-

propionic acid (HPPA) its inhibitory action was more pronounced and more reliable within different experiments.

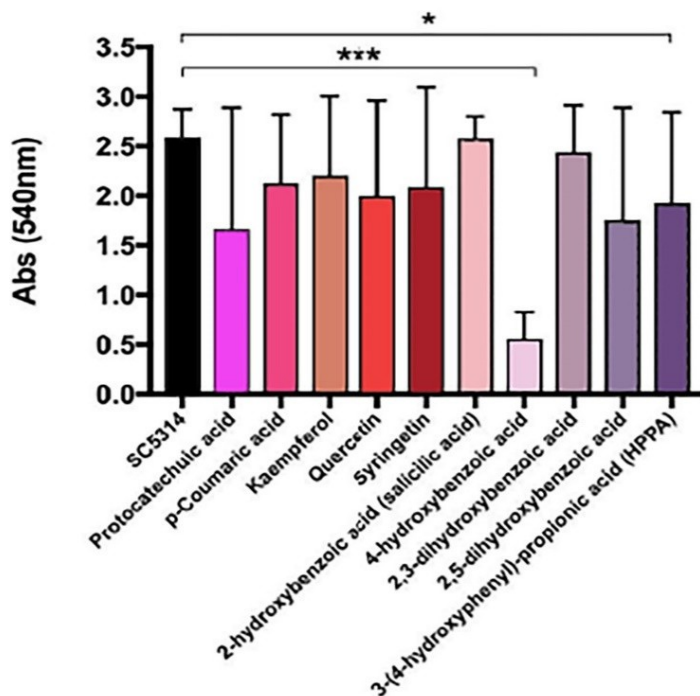


Figure 12- Activity of metabolites identified by targeted MS analysis on *C. albicans* SC5314. Crystal violet assay was used to evaluate biofilm biomass reduction. Significant differences are indicated by * $p < 0.05$, *** $p < 0.001$, Mann-Whitney test.

The untargeted analysis revealed the presence, in the two most active urinary fractions, of 5-(3',4'-dihydroxy phenyl)- γ -valerolactone. This metabolite reached its maximum concentration at 12h. Because of its commercial unavailability, to further study the 5-(3',4'-dihydroxy phenyl)- γ -valerolactone activity against *C.*

albicans, this metabolite was synthesized by Prof. Laura Fumagalli ((Department of Pharmaceutical Sciences, Università Degli Studi di Milano)[93].

4.1.3 5-(3',4'-dihydroxy phenyl)- γ -valerolactone and 4-hydroxybenzoic acid are the most active metabolites in urinary fractions

We focused the second part of this study on the two most abundant compounds identified by MS in the most active urinary fractions: 5-(3',4'-dihydroxy phenyl)- γ -valerolactone and 4-hydroxybenzoic acid. To assess whether the inhibitory effect against *Candida* was strain-independent and dose-dependent, we tested selected concentrations, starting from the concentration detected in urine fractions and descaling, of both metabolites on polystyrene 96-well plates by CV assay.

4-HBA significantly inhibited biofilm formation only at concentrations equal (3.5 μ M) or above the value found in urinary fraction (Figure 13, Panel A). VAL activity was more pronounced and a dose-dependent response, starting from 30 μ M concentration, was observed (Figure 13, Panel B).

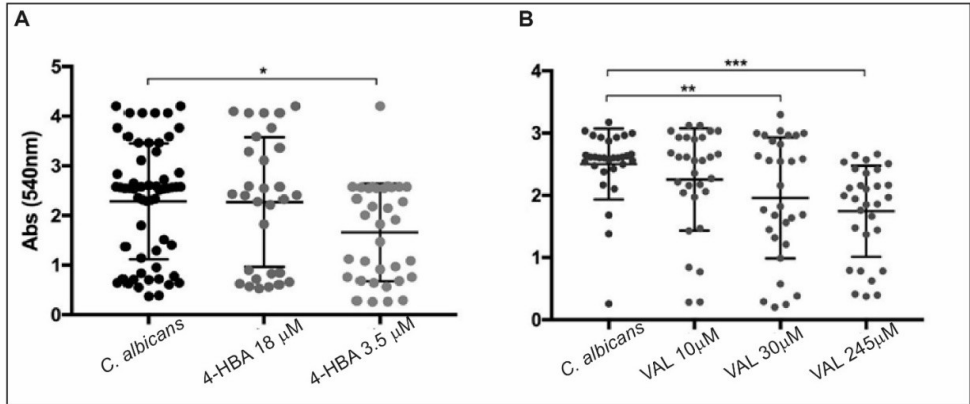


Figure 13. Inhibition of *C. albicans* clinical isolates biofilm-formation in the presence of a different concentration of 4-HBA (panel A) and VAL (panel B). The results are shown as scatter plot, when horizontal bars indicate. Significant differences are indicated by * $p < 0.05$, ** $p < 0.01$, *** $p < 0.001$, Mann-Whitney test.

To get insights into biofilm modification by VAL and 4-HBA, in terms of cell morphology, biofilm architecture, and thickness, we performed confocal microscopy of biofilms grown on plastic coverslips (Figure 14). Both Val and 4-HBA reduced biofilm thickness.

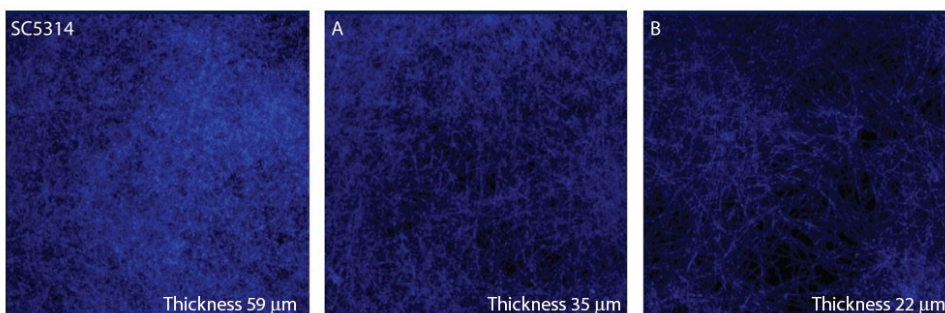


Figure 14- Visualization of *C. albicans* SC5314 biofilms in the presence of 4-HBA (3.5 μ M, panel A) and VAL (245 μ M, panel B), compared to control. Thickness was measured by z-scanning using the instrument software.

Despite the concentrations tested were close to those identified in urine, we assessed *in vitro* whether VAL and 4-HBA can have toxic effects on intestinal cells. We thus performed a cytotoxicity test using Caco-2 cells. We tested four different concentrations of each compound and none of them resulted in a decrease of cell viability (Figure 15).

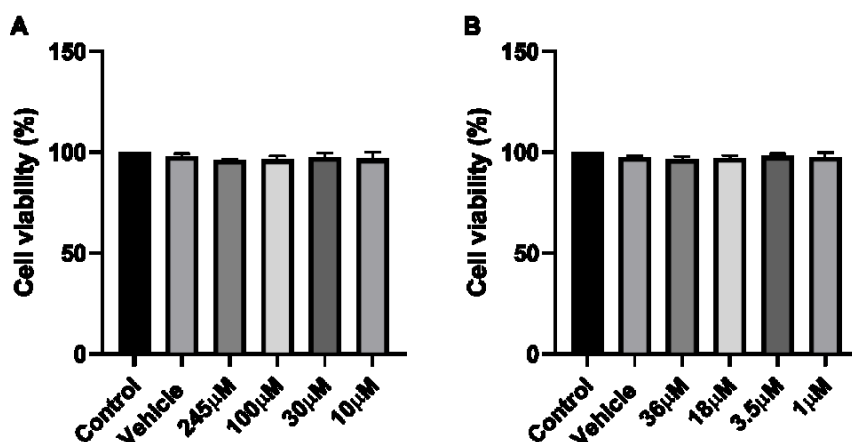


Figure 15. Caco-2 cell viability. (A) VAL and (B) 4-HBA cytotoxicity assay. Data represent the mean \pm SD of three different experiments performed in quadruplicates, compared by one-way ANOVA. Control: untreated cells; Vehicle: DMSO 0.1%.

4.1.4 5-(3',4'-dihydroxy phenyl)- γ -valerolactone and 4-hydroxybenzoic acid inhibitory activity does not involve changes in cell surface hydrophobicity

Together with adhesion ability, cell surface hydrophobicity (CSH) is another characteristic usually related to biofilm formation. Indeed, the same strain (i.e. *C. albicans* SC5314) cultured in the planktonic form or the sessile form (biofilm) showed a dramatic increase in CSH (35% vs 99%). To understand whether VAL and/or 4-HBA could exert their inhibitory activity by reducing the CSH, we measured the parameter in *C. albicans* SC5314 upon induction of biofilm formation in the presence of two concentrations of VAL and 4-HBA. Figure 15 shows that both compounds did not significantly alter the yeast surface hydrophobicity. On contrary, the treatment with whole cranberry extract (0.1 mg/mL) reduced biofilm hydrophobicity ($p=0.0042$).

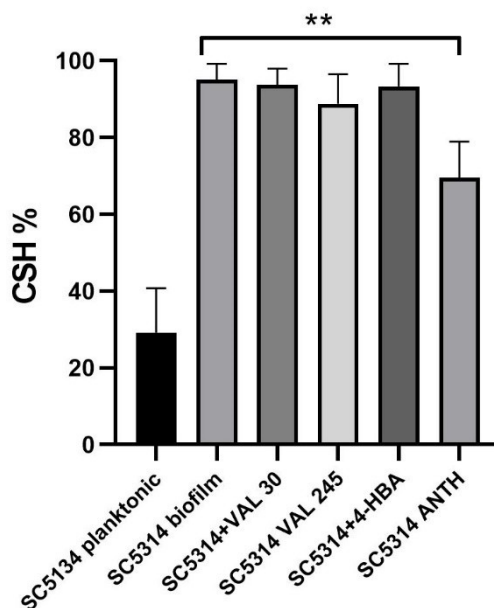


Figure 16. Cell surface hydrophobicity (CSH) is not altered by 4-HBA (3.5 μ M) and VAL alone, whereas Anthocran® 0.1 mg/ml significantly affects the yeast surface hydrophobicity. Data represented the mean \pm SD of three independent experiments. Data set were compared by one-way ANOVA, ** p <0.01.

4.1.5 VAL and 4-HBA regulate the expression of *Candida albicans* genes involved in early phases of biofilm formation

To get insight into other mechanisms possible involved in the observed inhibitory effects by VAL and 4-HBA, we evaluated the

expression of genes encoding for proteins involved in the initial phases of *C.albicans* biofilm formation. We evaluated the expression of *HWP1* and *ALS3* genes, both involved in adhesion mechanisms, and the first one also in yeast filamentation. As shown in figure 17, 4h after biofilm induction both genes are downregulated in yeast cells treated with VAL and with 4-HBA (also by cranberry itself), compared to controls. This activity was not confirmed at 24h, in line with the precocity of the mechanism. In fact, our results show that both treatments inhibit primary phases of biofilm formation.

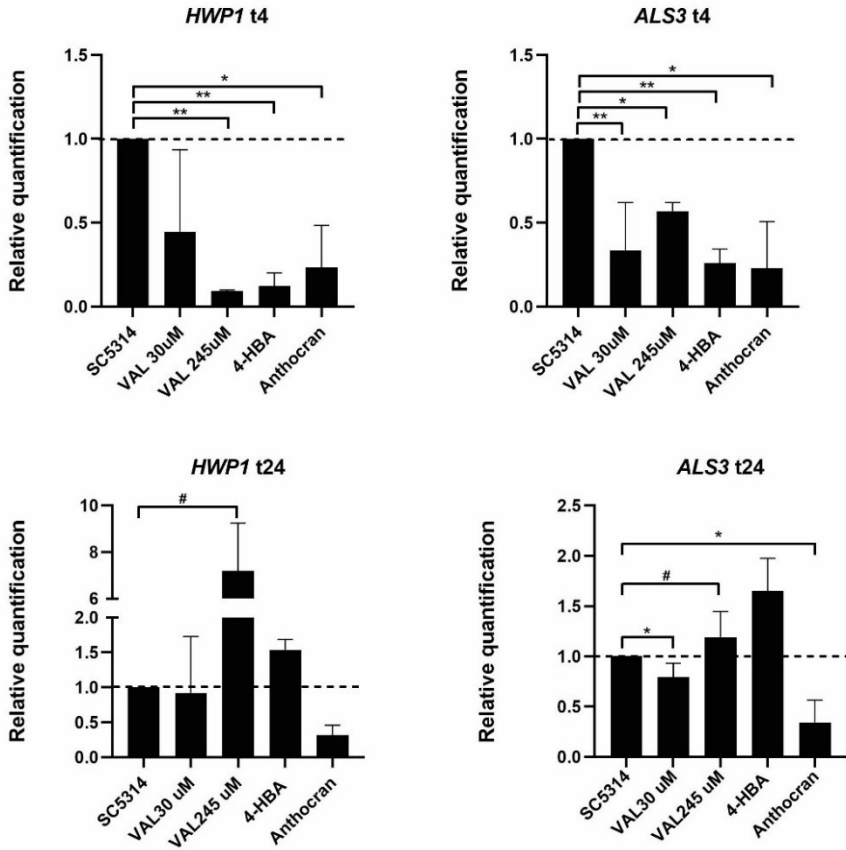


Figure 17. *C. albicans* gene expression modulation by cranberry metabolites. *C. albicans* were induced to form biofilm in the presence/absence of two concentrations of VAL (30µM and 245µM) and of 4-HBA (3.5µM). At 4h, both *HWP1* and *ALS3* genes were significantly downregulated by either VAL or 4-HBA (* $p < 0.05$; ** $p < 0.01$). At 24h, the modulatory effect was lost and, especially with VAL 245µM a paradoxical effect, i.e. upregulation, was seen (# $p < 0.05$). Data represent the mean \pm SD of three different experiments performed in triplicates.

4.1.6 Reducing *C. albicans* surface attachment could be an effective strategy to prevent biofilm-formation and related infections

In the last years, researchers have strongly focused their studies on the development of antibacterial and antimicrobial materials. The design of polymeric systems able to inhibit bacterial growth and biofilm formation has become pivotal not only in biological fields, hospitals, and healthcare environments but also in some industrial applications.

Scientific literature suggests that advanced antibacterial materials[90], and among them hydrogels, are extensively studied as a promising tool to reduce microorganism adhesion and replication on indwelling medical devices, thus preventing biofilm-related infections.

In collaboration with the Chemistry laboratory of the Politecnico di Milano (Professors Mauri and Rossi), we assessed the inhibitory activity of functionalized hydrogels (chem-HG) against *C. albicans*. For comparative purposes, the activity against *S. aureus* was also tested. Hydrogels were loaded with two molecules: i) SF, sodium salt or ii) RhB a neutral molecule at pH = 7.4 and slightly positive at acidic pH[90].

The *in vitro* assay revealed a strong efficacy of chem-HG in microbial growth inhibition.

Indeed, after 24 h incubation (Figure 18), we observed an almost complete inhibition of *S. aureus* growth (> 99% reduction in CFUs

count, $p=0.0159$) and a significant reduction (about 30%, $p=0.015$) for *C. albicans*, compared with controls (growth on non-functionalized hydrogel).

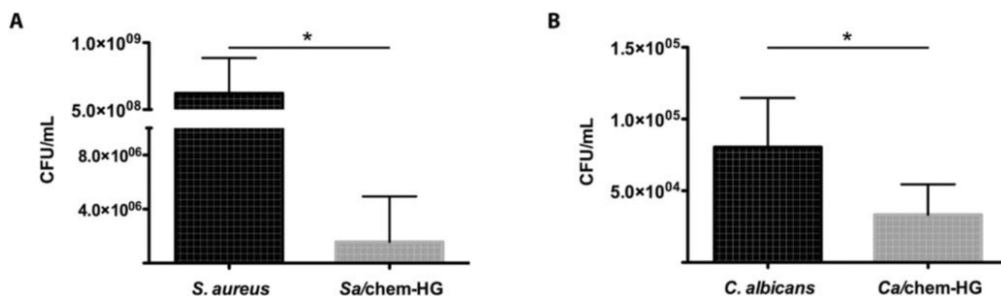


Figure 18. Microbial inhibitory activity of chem-HG hydrogels. Colony-forming units (CFU) count of (A) *S. aureus* and (B) *C. albicans*, after 24 h incubation in appropriated media. Black bars represent growth controls (with non-functionalized hydrogel); grey bars show microorganisms grew in the presence of chem-HG hydrogel. Values represent the mean of two independent experiments for each strain. Pairwise lines denote statistical significance; $*p<0.05$.

4.2 Strategies to counteract the vicious cycle of infection/-inflammation

4.2.1. Pilocarpine efficiently inhibits *Candida albicans* biofilm formation but fails to strongly modulate the host inflammatory response

Based on previous results of our laboratory that demonstrated that acetylcholine inhibits *C. albicans* biofilm development and pathogenicity, we attempted to better delineate the role of cholinergic receptors in candidemia (Figure 19).

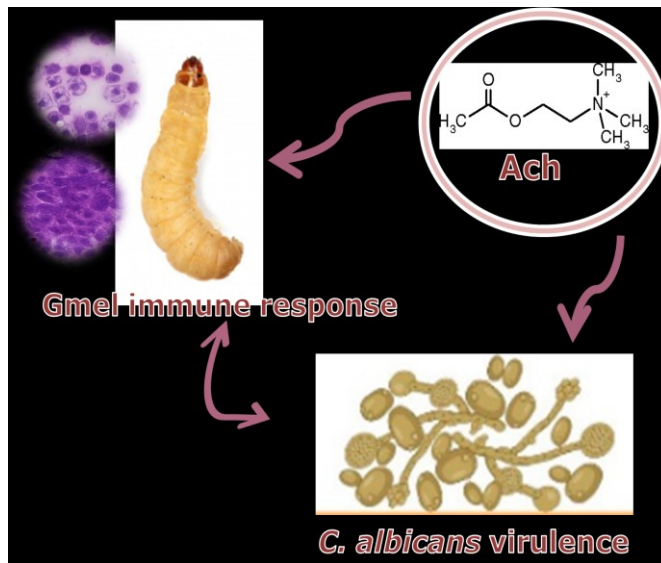


Figure 19. Dual role for acetylcholine in *C. albicans* pathogenesis: inhibition of *C. albicans* virulence factors and regulation host cellular immune responses to allow the rapid clearance of *C. albicans* infection[80].

To this end, the effects of a non-specific nicotinic receptor agonist, SIB1508Y maleate (SIBm), and a nonspecific muscarinic receptor agonist, pilocarpine hydrochloride (PHCl), were investigated for

determining which subtype of cholinergic receptors could be engaged in *C. albicans*.

Comparing the effect on *C. albicans* biomass formation (Figure 20, panel A and B), was clear that SIBm did not affect biofilm formation, while in PHCl there was a dose-dependent activation and a statistically significant decrease in biomass in the highest concentrations ($p < 0.001$). The metabolic activity was also evaluated (Figure 20, panels C and D), showing no effect for SIBm. However, a significant reduction in *C. albicans* metabolic activity compared to the control was observed when treated with PHCl concentrations ranging between 3.125 and 50 mM (all p values < 0.01).

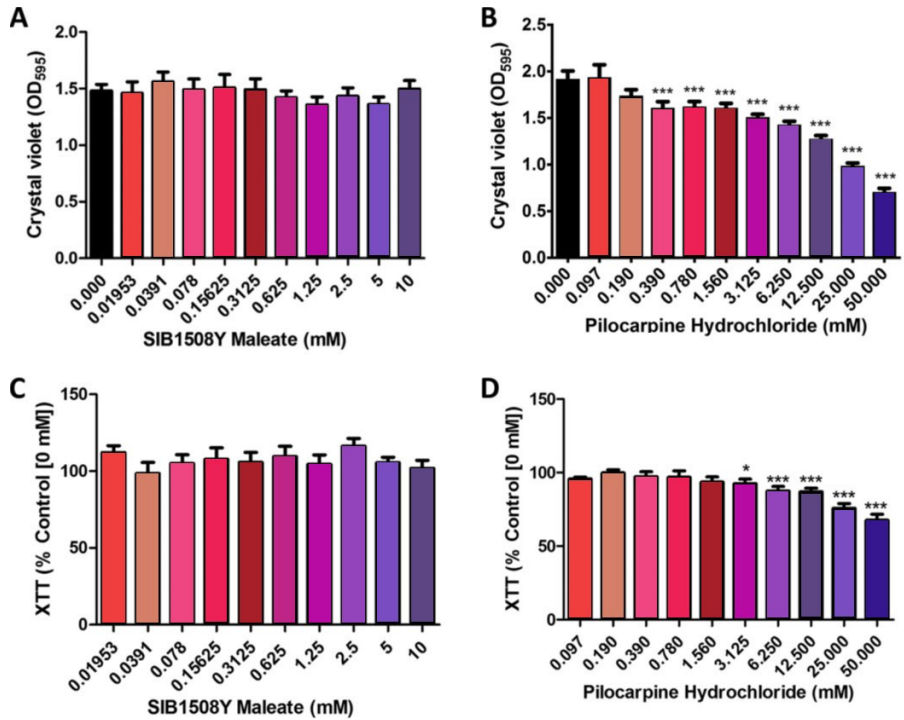


Figure 20. The broad muscarinic receptor pilocarpine inhibits both *C. albicans* biofilm formation and metabolic activity *in vitro*. Biofilm biomass was quantified using the crystal violet assay at 24h post *C. albicans* biofilm induction in the presence of SIB 15008Y (0 to 10 mM) (panel A) and PHCl (0 to 50 mM) (panel B). (Panels C and D) Biofilm metabolic activity was assessed using the XTT assay at the same conditions described. Bars represent the mean values (\pm SD) of three independent experiments. (* $p < 0.05$; *** $p < 0.001$). Crystal violet and XTT data were found to be abnormally distributed; therefore, all concentrations were compared to the control using a Kruskal-Wallis nonparametric test with a Dunns post-test.

To corroborate the data obtained with PHCl, we performed the same experiment by adding different concentrations of the nonspecific muscarinic receptor antagonist scopolamine (SCP). The

simultaneous administration of an agonist and an antagonist totally revokes the inhibitory effect. Indeed, SCP inhibits the reduction in biofilm formation induced by PHCl in a dose-dependent manner, revealing no significant differences in biofilm biomass in the presence of 25 mM PHCl compared to the control (Figure 21, panel A). Additionally, all concentrations of SCP abolished any PHCl induced reductions in metabolic activity (Figure 21, panel B).

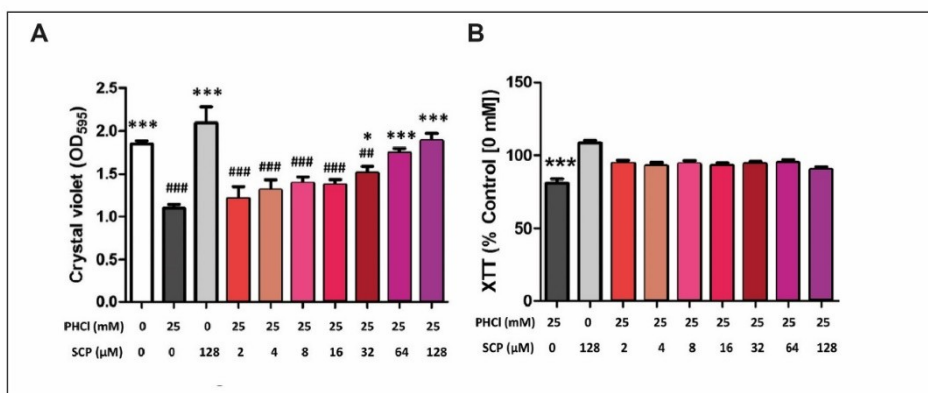


Figure 21. Pilocarpine hydrochloride activates a specific muscarinic-like receptor resulting in biofilm inhibition. (A) Biofilm biomass assessed with CV assay after 25 mM PHCl treatment and different concentrations of the nonspecific muscarinic receptor antagonist scopolamine (SCP). The bars represent the mean values (\pm SD) from triplicate wells of three independent experiments. #, significantly different from cells cultured in the absence of any compound; *, significantly different from cells cultured in PHCl alone; * or # $p < 0.05$; *** or ###, $p < 0.001$. (B) Biofilm metabolic activity assessed with XTT assay with the same conditions. The bars represent the mean values (\pm SD) from triplicate wells of three independent experiments. (***) $p < 0.001$.

The formation of biofilm *in vivo*, has been demonstrated to worsen *Candida* infection in the *Gmel* candidemia model[94]. We thus evaluated the effect of PHCl administration on *Gmel* larva survival during *C. albicans* systemic infection (Figure 22, panel A). PHCl protects *Gmel* larvae from mortality induced by *C. albicans* infection in a dose-dependent manner compared to larvae inoculated with *C. albicans* alone (PHCl 10.5mM, $p<0.001$; PHCl 6.25 mM, $p<0.05$, respectively). Moreover, we determined the possible toxic effects of PHCl alone (10.5 mM) and found no adverse effects on the survival of the larvae (Figure 22, panel A).

As performed for *in vitro* experiments, the addition of SCP was used to confirm the specificity of PHCl activity. When SCP was added to PHCl-treated larvae, the mortality rate was comparable to untreated *C. albicans*-infected larvae, suggesting that SCP inhibited the PHCl-induced protection. The possible toxic effects of SCP (6.25 mM) was also assessed, revealing no adverse effects per se on larva survival.

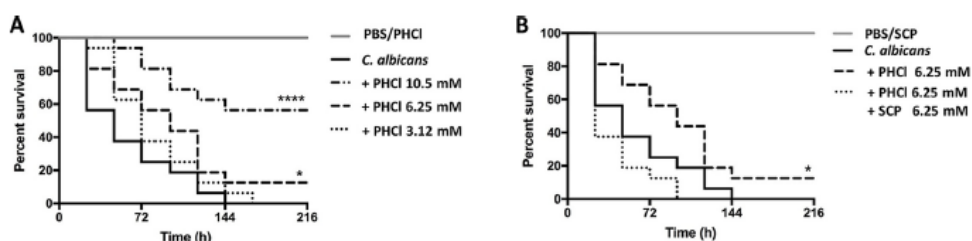


Figure 22. Pilocarpine hydrochloride effect on the outcome of systemic infection *in vivo* using *G. mellonella* infection model. (A) A

Kaplan-Meier plot indicate the effects of PHCI on the survival of *C. albicans*-infected larvae. **** $p < 0.0001$; * $p < 0.05$, in comparison to larvae inoculated with *C. albicans* alone. (B) To verify receptor specificity, infected larvae were also treated with PHCI and SCP in combination. * $p < 0.05$. The simultaneous treatment of PHCI and SCP had no effect on larva survival.

To get insight into the pathophysiology of *C. albicans* SC5314 systemic infection, we performed histological analyses of Gmel infected larvae, treated or not with PHCI (\pm SCP). PBS-, PHCI- or SCP-injected larvae were included as a control.

Both drugs, at 24 and 48 h post-inoculation alone, induced the formation of small hemocyte aggregates, adjacent to the gut and the tracheal system, crucial tissues for larva survival. Moreover, hemocytes were also visualized close to the fat body (Figure. 23, panels A and D). 24 hours post-inoculation, PHCI-injected larvae showed a cellular response characterized by small dispersed melanized nodules and an increase in circulating hemocytes (Figure 23, panel B). SCP failed to induce melanization.

In larvae inoculated with *C. albicans* alone, the hemocyte response was characterized by melanized nodules close to the fat body (Figure 23, panel C). By contrary, the cellular response in larvae inoculated with *C. albicans* and treated with PHCI was characterized by the presence of very small aggregates of hemocytes with melanin deposition surrounding yeast cells, uniformly distributed in the hemolymph (Figure 23, panel D). In contrast, larvae inoculated with *C. albicans* and treated with PHCI

and SCP showed the presence of medium-sized nodules with scanty melanization and poor hemocyte recruitment into the invaded tissues (Figure 23, panel E). Thus, SCP administration to larvae inoculated with *C. albicans* and treated with PHCI abrogates PHCI effect and larval tissue appeared very similar to larvae infected only with *C. albicans* (Figure 23, panel C).

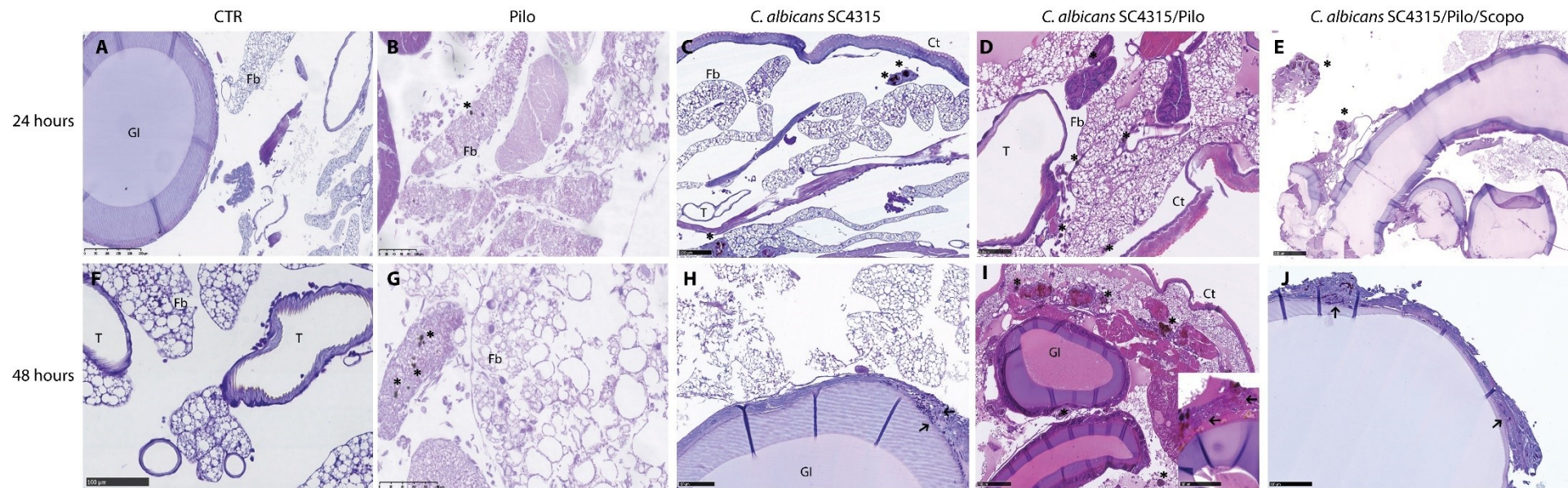


Figure 23. Histological analysis of injected and un-injected larvae at 24 and 48 h inoculation stained with haematoxylin and eosin (HE). (A, and F) control larvae and (panels B and G) larvae inoculated with PHCI alone. (C and H) larvae infected with *C. albicans* SC5314. (D and I) larvae infected and treated with PHCI. (E and J) larvae infected in the co-presence of PHCI and SCP.

Asterisks indicate melanized nodules, while arrows highlight *C. albicans* cells and hyphae. Fb, fat body; Ct, cuticle; GI, gastrointestinal tract; T, trachea; Nd, nodule.

At 48 hours, larvae infected with *C. albicans* alone revealed an increase of hemocytes in the subcuticular, intestinal, and tracheal areas with large nodules and diffuse melanization. The fat body appeared strongly damaged. Hyphal invasion of the intestinal walls (Figure 23, panel H) was clearly visible. In contrast, larvae infected with *C. albicans* plus PHCl showed a decreased inflammation and a less aggressive fungal infiltration, with small melanized nodules distributed in subcuticular areas. *C. albicans* filamentous forms were not recorded (Figure 23, panel I).

As observed at 24 h, the simultaneous treatment with PHCl and SCP in *C. albicans*-infected larvae resulted in hyphal invasion of the intestinal walls (Figure 23, panel J), with a histological aspect comparable to larvae infected with *C. albicans* without treatment (Figure 23, panel I).

Because of the strong effect of acetylcholine in inducing the activation of different hemocyte subtypes, we evaluated PHCl behavior and compare it with ACh (Figure 24).

We studied Gmel hemocytes infection both *ex vivo*, by isolating hemocytes from healthy larvae, and *in vivo*, by isolating hemocytes from infected larvae. For each condition, the *in vivo* and the *in vitro* observations overlapped.

Extracted hemocytes were cultured and treated and/or infected with *C. albicans in vitro* (Figure 24, panel A). At 24 h, *C. albicans*-infected hemocytes showed an increase in plasmatocytes, granulocytes, and spherulocytes. The infection promoted the cell aggregation into nodules and melanin deposition (Figure 24, panel A-ii).

ACh alone induced an increase in cellularity, mainly plasmatocytes, granulocytes and spherulocytes, and cell aggregation was evidenced by multidimensional nodule formation (Figure 24, panel A-iii). PHCl alone induced nodules of smaller dimension (Figure 24, panel A-iv), and spherulocytes were poorly present.

C. albicans-infected ACh-treated group was characterized by a strong induction of aggregation and multidimensional nodule formation with low deposition of melanin (Figure 24, panel A-v). *C. albicans*-infected Pilo-treated group showed massive aggregation and strong melanization (Figure 24, panel A-vi).

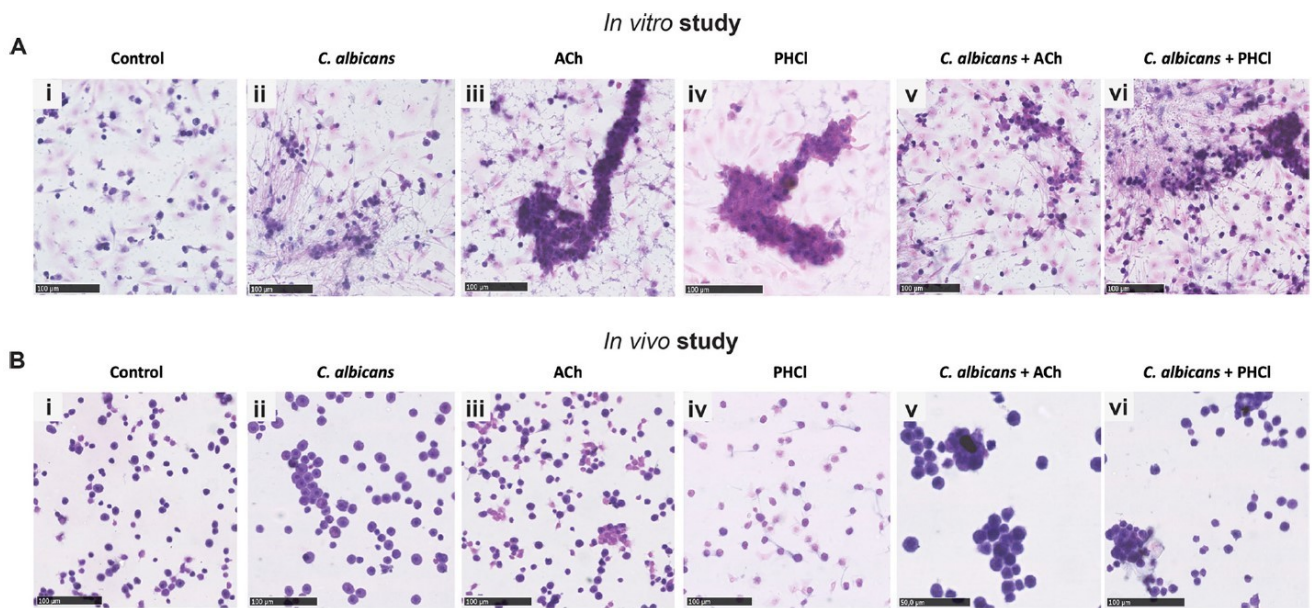


Figure 24. Effects of PHCl and ACh on hemocyte responses to *C. albicans* infection *in vitro* (panel A) and *in vivo* (panel B) using hematoxylin and eosin (HE) staining.

Panel A- (i) hemocytes isolated from control larvae; (ii) hemocytes infected with *C. albicans* (ii); hemocytes stimulated with ACh (iii) or PHCl (iv) alone; (v) hemocytes infected and treated with ACh; (vi) hemocytes infected and treated with Pilo.

Panel B- hemocytes were collected from larvae inoculated with PBS (i) or with *C. albicans* (ii), ACh (iii), PHCl (iv); *C. albicans* + ACh; *C. albicans* + Pilo.

Because the high impact of fat body in hemocyte production and orchestration, we performed the same experiment by infecting and treating living larvae and by extracting hemocytes subsequently (Figure 24, panel B).

Overall cellularity was slightly reduced *in vivo* compared to *in vitro* experiments due to tissue sequestration of hemocytes.

Hemocytes isolated from larvae inoculated with ACh or PHCl alone and with *C. albicans* plus PHCl (Figure 24, panel B-iii, B-iv, and B-vi, respectively) showed similar cellularity and hemocytes subtypes exposed compared to the same condition *in vitro*.

Nevertheless, hemocytes isolated from larvae infected with *C. albicans* plus ACh (Figure 24, panel B-v) showed more melanization compared to hemocytes cultured *in vitro* and infected with *C. albicans* alone (Figure 24, panel A-v).

4.2.2 Myriocin ameliorates the response to *A. fumigatus* infection in ex vivo CF monocytes

Myriocin is another compound with suggested activity on both inflammation and fungal infections[86], [95].

To evaluate the possible direct effects of Myriocin in promoting fungal clearance in CF patients, we isolated monocytes from CF patients. Monocytes were selected by adherence from PBMCs of CF patients with both homozygous and heterozygous $\Delta F508$ *CFTR* mutation. Two experimental conditions/patients (three replicates for each group) were set up. Once stabilized in culture, monocytes were pre-treated or not with Myriocin, and in both conditions, *A. fumigatus* conidia were added.

CFU count, performed upon incubation to allow conidia internalization and killing, revealed that Myriocin treatment significantly increases *A. fumigatus* conidia killing by patient monocytes (Figure 25).

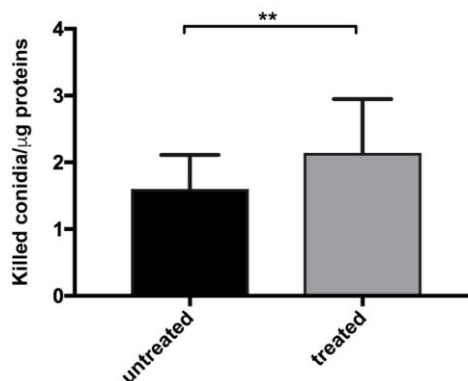


Figure 25. Monocyte killing ability improved by Myriocin treatment. The patient's monocytes were pre-treated with 50 μ M Myr or medium alone for 1 hour at 37°C and then infected with *A. fumigatus* conidia (MOI 1:1). Non-internalized conidia were removed by washing and the cells incubated for further 4h before proceeding with the lysis. Data were obtained by CFU count performed upon incubation.

To determine whether the observed effects of Myriocin could depend on the activation/repression of regulatory pathways involved in infection and inflammation, we evaluated by qRT-PCR the effect of drug administration on gene expression. We studied genes involved in the pathogen recognition, i.e. gene encoding for the pattern recognition

receptors *NOD2*, *TLR2*, and *TLR7*, and in the altered inflammatory process, i.e. genes encoding for interleukin-1 β and interleukin-8.

Myriocin treatment was efficient in downregulating both *IL-1 β* and *IL-8* (Figure 26) gene expression following *A. fumigatus* stimulus. At the same time, the expression of the studied PRRs, crucial in activating a microbicidal and pro-inflammatory response, was up-regulated (Figure 26). Basal expression of the selected genes was also assessed in the absence of *A. fumigatus* conidia to verify whether Myriocin could restore the inflammatory milieu, interrupting the vicious cycle that promotes *A. fumigatus* colonization in CF patient lungs.

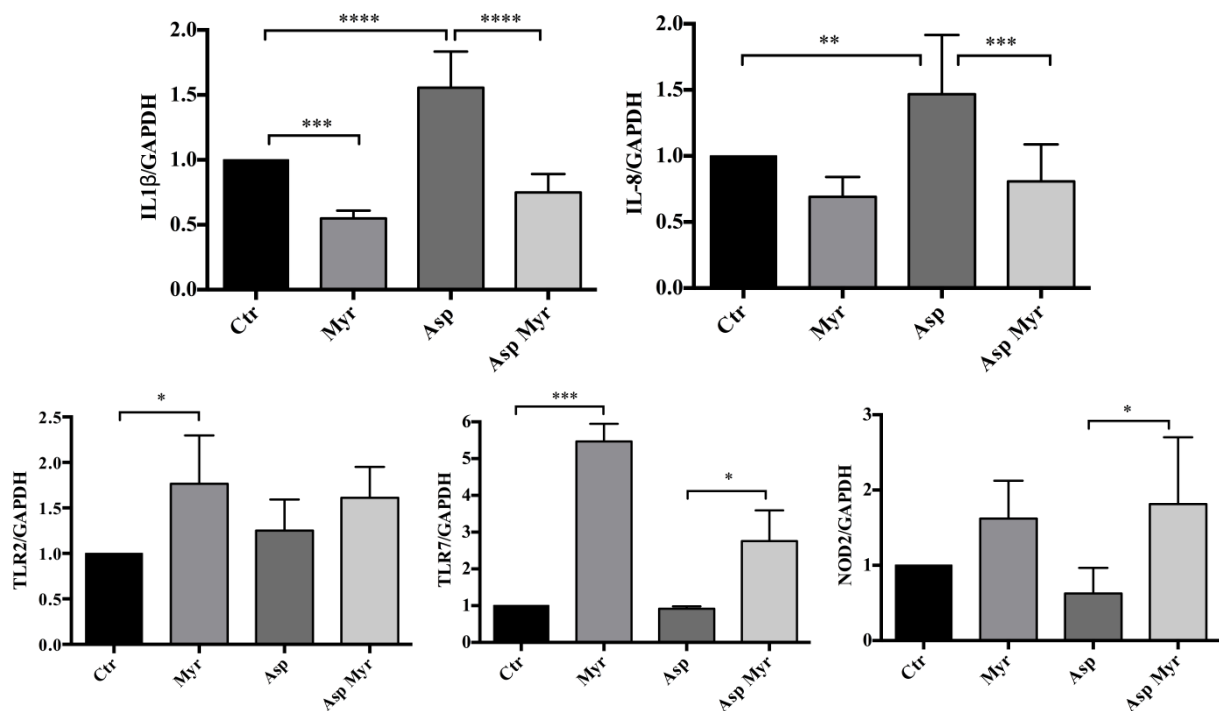


Figure 26. Gene expression of specific markers for inflammation and response to infection. Pro-inflammatory cytokine genes *IL-1 β* and *IL-8*; pathogen recognition receptors (PRRs): *NOD2*, *TLR2*, and *TLR7*; by qRT-PCR in Myr treated (Myr and Asp Myr) and untreated (Ctr and Asp) and *A. fumigatus*-infected (Asp and Asp Myr) and uninfected CF cells (Ctr and Myr) (12 h after infection). GAPDH was used as a housekeeping gene. Data, derived for triplicate samples, are expressed as mean \pm SE (* $p < 0.05$; ** $p < 0.01$; *** $p < 0.001$).

5. DISCUSSION

5.1 Cranberry metabolites and their effects on *Candida albicans* biofilm formation

The results reported in the present study stem out from a multidisciplinary collaboration with the Department of Pharmaceutical Sciences and are based on the identification of several cranberry metabolites present in human urine upon oral cranberry intake.

The antiadhesive properties of cranberry extract have long been reported[63], [96]–[99] mainly concerning *Escherichia coli*, which represents the main uropathogenic agent responsible for about 80% of UTIs.

The activity of cranberry products is principally attributed to proanthocyanidins (PACs), but we did not recover in urinary fractions any (A-type and B-type). Our data are in line with other reports that failed to identify this class of polyphenols, in particular procyanidin A2, in human urine[62], [64], [65], [100], but in contrast with few studies demonstrating that low concentration of PACs are detectable in urine[101], [102]. Controversial results might rely on the very low bioavailability of PACs. Moreover, the gut human microbiota can catabolize PACs into phenolic compounds: catechin and epicatechin, also valerolactones from procyanidin B2; and phenylacetic and phenyl propionic acids from procyanidins A2[103] [104].

In our study, we assessed the activity of cranberry, both crude extract and its urinary metabolites upon oral intake, in reducing *C. albicans* adhesion and biofilm formation on polystyrene. Indeed, *Candida* spp. are responsible for a high percentage of catheter related UTIs within the nosocomial setting that can eventually lead to bloodstream invasion if not efficiently treated[105]. *Candida* spp. and in particular *C. albicans* are prone to develop biofilms on indwelling devices[106] that can serve as entry route to trigger an infectious process. Amongst genitourinary infections, *Candida* is a common etiological[19] agent also of vulvovaginitis, affecting a high percentage of women in reproductive age. Vulvovaginal candidiasis often develops in a recurrent form of disease that dramatically impacts patient quality of life[19].

Candida recalcitrant infection are often sustained by strains able to switch from a yeast form to a filamented morphology, which helps the fungus in adhesion and immune evasion, and biofilm producers[15].

Because of the high impact of these virulence factors in the pathophysiology and in the outcome of the infection, a therapeutic approach addressing adhesion, filamentation and biofilm formation is strongly desirable.

Cranberry extract has been reported to inhibit *in vitro* *Candida* growth (REF), thus we reasoned whether urinary derived metabolites could retain the observed inhibitory effects. Starting from the most active urinary fractions in inhibiting *Candida*, i.e., 1 hour and 12 hours following the last capsule ingestion, we investigated if increased metabolites in these fractions could *per se* be responsible for the anti-biofilm effects.

Amongst several identified metabolites, two resulted in the most promising in *C. albicans* virulence modulation: 5-(3',4' -dihydroxy phenyl)-gamma-valerolactone and 4-hydroxybenzoic acid. Valerolactone derivatives have been already reported by authors investigating urinary cranberry metabolites[103], [107], however, probably due to the highly concentrated amount of crude extract in the Anthocran® formulation, the urinary fractions at 1 hour and 12 hours were particularly enriched in valerolactones.

A recent study demonstrated that valerolactones and their conjugates can counteract *E. coli*[107] adhesion, confirming that the inhibitory activity is not only due to whole PACs but also to the derived metabolites.

5-(3',4' -dihydroxy phenyl)-gamma-valerolactone, at the concentration found in urine fractions, was efficient in reducing *C. albicans* biofilm biomass and thickness, probably affecting the stability of the whole biofilm structure.

Many natural compounds[108] have been investigated for their anti-*Candida* effects, but for several of them the *in vitro* determined minimal inhibitory concentration (MIC) is beyond reasonable values and thus probably ineffective *in vivo*. Zida and coworkers[108] suggested that only compounds with MIC values below 1 mg/mL are considered noteworthy of further analysis.

Notably, both the VAL and 4-HBA concentrations tested in our study are below the suggested cut-off MIC value, as the higher dose assessed was 245 μ M (0.05 mg/mL) and 3.5 μ M (0.0005 mg/mL), respectively.

Another issue concerning natural compounds is that the exact mechanism of action is often unknown. To get some insights on the possible mechanism, we evaluated two important features in biofilm formation: modifications of *Candida* cell wall, i.e. cell surface hydrophobicity, and the expression of genes directly involved in biofilm-formation.

We first investigated the possible modulation by the studied compounds of *C. albicans* cell surface hydrophobicity; Anthocran® but not VAL and 4-HBA alone was able to significantly reduce the CSH. The highest dose of VAL, 245 μ M, only partially modified the hydrophobic

nature of *C. albicans* SC5314 cell wall. CSH value has been suggested as a possible marker for a strain propensity to form biofilm[109], as mediate non-specific interactions with the substrate for cell attachment.

To this end, i.e. surface attachment, a plethora of genes, including *BCR1*, *ALS1*, *ALS3*, *ECE1*, and *HWP1*, have been shown to be required for the initial phase of biofilm formation[110]. We focused, in our preliminary screening, on *ALS3* and *HWP1*, two genes encoding for Glycosyl Phosphatidyl Inositol (GPI)-anchored proteins, interacting with each other and promoting the adhesion to abiotic and biotic (host cells) surface[111].

At 4h post-biofilm-induction in the presence of cranberry metabolites, we observed a significant modulation of *HWP1* and *ALS3* genes by both VAL and 4-HBA. Despite filamentation is not necessary for biofilm formation, as shown for other *Candida* species whose biofilm lacks the presence of pseudohyphae and/or hyphae, *C. albicans* filamented forms stabilize the three-dimensional structure of the biofilm.

The inhibitory activity on *ALS3* and *HWP1* not only was not confirmed at 24h but we observed an up-regulation in their expression by VAL 245 μ M and 4-HBA. This observation suggests an overproduction of the two proteins, especially the hyphal protein to support the growth of hyphae and attachment. On the other hand, we did not investigate the kinetics of the two compounds, and their repeated administration to mature biofilms might restore the inhibitory effects.

5.2 Effect of Pilocarpine on *C. albicans* virulence and host response

Previous results demonstrated the ACh effects in inhibiting *C. albicans* biofilm formation, both *in vitro* and *in vivo*, assuming the putative presence of the cholinergic receptor in *C. albicans*[80][58]. Because both nicotinic and muscarinic receptors can be activated by ACh, a deeper understanding of the fungal target could provide new hints for anti-biofilm compounds. In this study, we investigated the direct effect of SIB1508Y maleate (SIB), a general nicotinic agonist, and of pilocarpine (PHCI), a nonspecific muscarinic agonist, on *C. albicans* adhesion and filamentation. PHCI, but not SIB, was able to reproduce ACh anti-biofilm effects, suggesting the presence of a muscarinic-like receptor in *Candida*. To verify the hypothesis, we tested *in vitro* and *in vivo* PHCI in combination with a general muscarinic receptor antagonist, scopolamine. The simultaneous administration of a muscarinic agonist and antagonist abrogated the previously observed inhibition of biofilm

biomass and metabolic activity. These results confirmed the presence of an uncharacterized cholinergic receptor involved in the filamentation of *C. albicans* that shows a similar phenotype to the human muscarinic receptor.

ACh is not suitable in the medical field, PHCI instead is used clinically in the treatment of xerostomia and glaucoma[112], [113]. Pharmacological studies indicate that PHCI has a predominance for M₁ and M₃ muscarinic receptors in mammals[75]. M₁ and M₃ are coupled with the G_q protein and promote the mobilization of intracellular calcium via phospholipase C signaling pathway[114].

Calcium homeostasis is crucial in all eukaryotic organisms and fungi regulates many virulence traits. In *C. albicans*, the Calcium Cell Survival Complex (CSS), encompassing calcium ions, calmodulin, and calcineurin proteins, is involved in hypha formation and maintenance and in invasive growth[115].

We speculate that *C. albicans* possesses a muscarinic-like receptor that can modulate its virulence. Additional research is required to confirm this hypothesis, but if a fungal-specific subunit exists, it can represent a desirable target for antifungal drug development.

C. albicans-triggered diseases constitute an interesting example of an altered balance between pathogen tolerance and immune system response[72].

Normally, the host immune response eliminates the fungus limiting collateral damage of tissues and rapidly restore the homeostatic environment. The invasive infection mediated by *C. albicans*, trigger a strong inflammatory response that can damage infected tissues and organs[116]. The biofilm lifestyle is an active part of *C. albicans* pathogenicity, as demonstrated by a previous study on *Galleria mellonella* experimental model, and promote more rapid larval death *in vivo* leads to larvae death[94]. In a previous study, we demonstrate that acetylcholine, besides inhibiting *Candida* biofilm formation and filamentation, promotes a rapid clearance of *C. albicans*, and protect the larvae against inflammation-induced tissue injury[80].

The data herein presented shows that, although similarities between ACh and PHCI action against *C. albicans*, the two compounds differ in the ability of hemocyte response modulation.

G. mellonella possesses six immune cell types that differentiate from prohemocytes: granulocytes, plasmatocytes, oenocytes, spherulocytes, prohemocytes, and adipohemocytes[117]. Granulocytes are the first-line response to pathogen invasion and share similar characteristics to human neutrophils[118]. Granulocyte recruitment is

strongly activated in the presence of ACh, *in vivo*, but not of PHCl. Moreover, PHCl was found to promote less nodulation and encapsulation *in vivo* than ACh.

We speculate that PHCl does not induce strong hemocyte recruitment and nodulation because the immune modulation observed with ACh relies mainly on nicotinic rather than muscarinic receptors.

5.3 Myriocin modulate the response to inflammation and infection

It has been demonstrated that the ability of immune cells in CF patients is altered by the mutated *CFTR* gene and results in a reduced clearance of pathogens, contributing to patient susceptibility to opportunistic infection[119], [120]. The local and systemic inflammatory status characterizing this disease also contributes to the reduced microorganism clearance.

Altered lipid metabolism is a common feature of chronic inflammatory diseases and it has been observed in CF patients, possibly contributing to the CF pathophysiology. The specific sphingolipid *de novo* synthesis inhibitor Myriocin reduces lipid accumulation in CF cells[120], resulting in a decrease in pro-inflammatory cytokine release.

Moreover, fungi and mammals share the very first enzyme involved in sphingolipid synthesis – the palmitoyl serin transferase- and previous studies demonstrated that sphingolipid inhibitors exert direct antifungal activity[66].

We investigated whether Myriocin administration could enhance, by reducing inflammation and simultaneously inhibiting the fungal growth, the CF defective killing ability in CF patient monocytes. Indeed, monocytes play a key role in fungi eradication and CF susceptibility to *A. fumigatus* colonization or recurrent infections[121].

CF monocytes infected with *A. fumigatus* and treated with Myriocin displayed a significant increase of conidia killing. This observation is of relevance because, in the lungs, the most affected organs in CF patients, macrophage dysfunction is associated with elevated production of proinflammatory cytokines, reduced bacteria clearance, and altered tissue repair capability[122].

To have a more complete picture of the effects of Myriocin modulatory action, we studied the expression of pro-inflammatory cytokines in CF bronchial epithelial cell lines. Indeed, CF lung environment shows a typical proinflammatory phenotype, with high levels of IL-8, IL-6, and IL-1 β and low levels of IL-10[123].

Our data suggest a significant shaping by Myriocin treatment of genes mediating the inflammation, as both *IL-8* and *IL-1 β* gene expression was downregulated either in basal condition or after *A. fumigatus* conidia stimulus.

The innate immune response is crucial in hampering fungal infection[85]. In the lungs as in other tissues, the innate response is primarily mediated via Toll-like receptor (TLR) signaling. Altogether, pattern recognition receptors (PRRs), involved in pathogens-recognizing mechanisms are known to be downregulated in CF[121], [124]. We thus investigated whether Myriocin treatment could balance this altered PRR expression. As expected, possibly by ameliorating the cell homeostasis, Myriocin increases *NOD2*, *TLR2*, and *TLR7* expressions. It is reported that *Candida* spp. stimulate cytokine production downstream of various PRR, including TLRs, and nucleotide oligomerization domain (NOD)-like receptors[125].

Our data indicate that acting on lipid accumulation could be a successful therapeutic approach to restore an adequate response to infection in CF patients or in diseases characterized by local and systemic chronic inflammation.

7. CONCLUSIONS

Biofilm formation has received much attention in the last decades, as it has become clear that all types of microorganisms, including fungi, can virtually form biofilms, and that this may be the preferred mode of microbial existence in nature. In human medicine, microbial biofilms are implicated in more than 80% of chronic inflammatory and infectious diseases, particularly in people with indwelling medical devices made of polymeric material (intravascular and bladder catheters, artificial heart valves, bone, and joint prosthesis).

The treatment of biofilm-related infections poses a significant clinical challenge. The biofilm matrix itself and the microenvironment characteristic of these microbial communities seem to interfere with the antimicrobial response and virulence traits, promoting drug tolerance and pathogen persistence.

In spite of the wide significance of fungal biofilms and relative drug resistance, individuating new strategies is necessary.

In our study, we assessed various strategies to counteract biofilm-related infections, targeting both pathogens and host immune response. Indeed, in fungal infections, the host pro-inflammatory milieu and the altered immune response could participate in determining the infection outcome.

Among preventive approaches for targeting the very early phases of biofilm formation (attachment to surfaces), the study of cranberry metabolites for genitourinary *Candida* infections appears to offer new perspectives for drug development. Indeed, VAL and 4-HBA resulted effective in inhibiting *Candida* adhesion and biofilm biomass production. Further researches investigating the mechanism of action and the possible inducible tolerance in *Candida* spp. (including NCAC) will provide a comprehensive picture on the possible use of VAL and 4-HBA for treating fungal infections.

Moreover, because biofilm infections are often related to the wide use of indwelling medical devices, we explored the use of materials with inhibitory activities against microbial growth. Hydrogel made up of a novel matrix showed an excellent ability to counteract *C. albicans* biofilm formation *in vitro*. Further investigation is required to better delineate the possible applications for these materials, especially in terms of functionalization by embedding in hydrogels antifungal compounds.

We also explored the possibility of addressing simultaneously fungal virulence factors and host immune response, as the strategy to overcome fungal persistence and clear the infection.

We investigated, stemming out from data demonstrating the dual anti-inflammatory and anti-biofilm effect of acetylcholine on systemic candidiasis, the effects of pilocarpine on both *Candida* biofilm-formation and the modulation of host immune response. Indeed, pilocarpine, contrary to acetylcholine, has already several clinical uses and it could represent a good candidate as a repurposing drug. Although pilocarpine showed a good anti-biofilm effect, overlapping acetylcholine one, its immune-modulatory effect was less remarkable. Notably, acetylcholine activates both muscarinic and nicotinic receptors, whereas pilocarpine is a muscarinic agonist engaging preferentially receptors. We thus speculate that the anti-inflammatory activity of ACh could rely on nicotinic receptors instead of muscarinic ones. Alpha7 nicotinic receptors are widely distributed in human cells, including circulating immune cells and such receptors are believed to play a role in regulating immune progenitor cell differentiation and maturation. On the other hand, muscarinic receptors, particularly M₁ and M₃ regulate intracellular calcium homeostasis, known to be crucial for a variety of fungal processes, including yeast-to-hypha transition. Further research using specific cholinergic receptor agonists and antagonists is required for better elucidating the role of cholinergic receptors in *Candida* pathogenesis.

CF is a genetic disease characterized by both chronic inflammation and recurrent microbial infections that exacerbate both the inflammation and patient wellbeing. In this context, we explored the dual activity of Myriocin, a sphingolipid synthesis inhibitor that targets a common enzyme in the mammal and fungal sphingolipid pathway.

We demonstrated that treating patient monocytes with Myriocin prior to *A.fumigatus* infection, ameliorates the pathogen clearance and the expression in genes encoding for pathogen recognizing receptors. Moreover, Myriocin was able to reduce the basal inflammatory milieu by downregulating the expression of genes encoding for pro-inflammatory cytokines.

As observed for acetylcholine and pilocarpine, Myriocin can directly inhibit fungal growth and could represent a drug candidate for alternative approaches to fungal infections.

In light with the importance of targeting both infection and inflammation during fungal diseases, potentiating the antimicrobial peptide-related response could offer a further strategy to improve antifungal treatment.

In conclusion, although the unmet need for biofilm-targeting therapeutic strategies is far from clinical practice, results from the present thesis showed that tackling different aspects of biofilm production using different fungal species and modeling systems will indicate avenues for drugs/therapeutic approaches development.

References

- [1] S. Campoy and J. L. Adrio, "Antifungals," *Biochem. Pharmacol.*, vol. 133, pp. 86–96, 2017, doi: 10.1016/j.bcp.2016.11.019.
- [2] D. J. Baumgardner, "Oral Fungal Microbiota: To Thrush and Beyond," *J. Patient-Centered Res. Rev.*, vol. 6, no. 4, pp. 252–261, 2019, doi: 10.17294/2330-0698.1705.
- [3] H. E. Hallen-Adams and M. J. Suhr, "Fungi in the healthy human gastrointestinal tract," *Virulence*, vol. 8, no. 3, pp. 352–358, 2017, doi: 10.1080/21505594.2016.1247140.
- [4] Y. and T. H. Belkaid, "Role of the Microbiota in Immunity and inflammation Yasmine," *Cell*, vol. 157, no. 1, pp. 121–141, 2015, doi: 10.1016/j.cell.2014.03.011.Role.
- [5] D. M. Underhill and I. D. Iliev, "The mycobiota: Interactions between commensal fungi and the host immune system," *Nature Reviews Immunology*, vol. 14, no. 6. Nature Publishing Group, pp. 405–416, May 23, 2014, doi: 10.1038/nri3684.
- [6] P. Eggimann, J. Garbino, D. Pittet, and P. Didier Pittet, "For personal use. Only reproduce with permission from The Lancet. Epidemiology of Candida species infections in critically ill non-immunosuppressed patients," 2003. doi: 10.1016/S1473-3099(03)00801-6.
- [7] P. G. Vidigal and T. I. E. Svidzinski, "Yeasts in the urinary and respiratory tracts: Is it a fungal infection or not?," *J. Bras. Patol. e Med. Lab.*, vol. 45, no. 1, pp. 55–64, 2009, doi: 10.1590/s1676-24442009000100009.
- [8] D. L. Horn *et al.*, "Epidemiology and outcomes of candidemia in 2019 patients: Data from the prospective antifungal therapy alliance registry," *Clin. Infect. Dis.*, vol. 48, no. 12, pp. 1695–1703, Jun. 2009, doi: 10.1086/599039.
- [9] A. M. Tortorano, C. Kibbler, J. Peman, H. Bernhardt, L. Klingspor, and R. Grillot, "Candidaemia in Europe: epidemiology and resistance," *International Journal of Antimicrobial Agents*, vol. 27, no. 5. Int J Antimicrob Agents, pp. 359–366, May 2006, doi: 10.1016/j.ijantimicag.2006.01.002.
- [10] M. A. Nunn, S. M. Schäfer, M. A. Petrou, and J. R. M. Brown, "Environmental source of *Candida dubliniensis*," *Emerg. Infect. Dis.*, vol. 13, no. 5, pp. 747–750, 2007, doi: 10.3201/eid1305.061179.
- [11] E. Cantón *et al.*, "Prospective multicenter study of the epidemiology, molecular identification, and antifungal susceptibility of *Candida parapsilosis*, *Candida orthopsilosis*, and *Candida metapsilosis* isolated from patients with candidemia," *Antimicrob. Agents Chemother.*, vol. 55, no. 12, pp. 5590–5596, Dec. 2011, doi: 10.1128/AAC.00466-11.
- [12] J. C. O. Sardi, L. Scorzoni, T. Bernardi, A. M. Fusco-Almeida, and M. J. S. Mendes Giannini, "Candida species: Current epidemiology, pathogenicity, biofilm formation, natural antifungal products and new therapeutic options," *Journal of Medical Microbiology*, vol. 62, no. PART1. Microbiology Society, pp. 10–24, Jan. 01, 2013, doi: 10.1099/jmm.0.045054-0.

- [13] R. A. Calderone and W. A. Fonzi, "Virulence factors of *Candida albicans*," *Trends in Microbiology*, vol. 9, no. 7. Trends Microbiol, pp. 327–335, Jul. 01, 2001, doi: 10.1016/S0966-842X(01)02094-7.
- [14] S. P. Saville, A. L. Lazzell, C. Monteagudo, and J. L. Lopez-Ribot, "Engineered control of cell morphology in vivo reveals distinct roles for yeast and filamentous forms of *Candida albicans* during infection," *Eukaryot. Cell*, vol. 2, no. 5, pp. 1053–1060, 2003, doi: 10.1128/EC.2.5.1053-1060.2003.
- [15] F. L. Mayer, D. Wilson, and B. Hube, "Candida albicans pathogenicity mechanisms," *Virulence*, vol. 4, no. 2. Taylor and Francis Inc., pp. 119–128, Feb. 15, 2013, doi: 10.4161/viru.22913.
- [16] J. R. Naglik, S. J. Challacombe, and B. Hube, "Candida albicans Secreted Aspartyl Proteinases in Virulence and Pathogenesis," *Microbiol. Mol. Biol. Rev.*, vol. 67, no. 3, pp. 400–428, Sep. 2003, doi: 10.1128/mubr.67.3.400-428.2003.
- [17] Arya N. R; Naureen B. Rafiq., "Candidiasis," in *Stat pearls*, Springer Berlin Heidelberg, 2020, pp. 1261–1267.
- [18] L. P. Samaranayake, W. Keung Leung, and L. Jin, "Oral mucosal fungal infections," *Periodontol. 2000*, vol. 49, no. 1, pp. 39–59, Feb. 2009, doi: 10.1111/j.1600-0757.2008.00291.x.
- [19] F. Vicariotto, M. Del Piano, L. Mogna, and G. Mogna, "Effectiveness of the association of 2 probiotic strains formulated in a slow release vaginal product, in women affected by vulvovaginal candidiasis: A pilot study," *J. Clin. Gastroenterol.*, vol. 46, no. SUPPL. 1, Oct. 2012, doi: 10.1097/MCG.0b013e3182684d71.
- [20] M. Zwolinska-Wcislo *et al.*, "Effect of *Candida* colonization on human ulcerative colitis and the healing of inflammatory changes of the colon in the experimental model of Colitis ulcerosa," *J. Physiol. Pharmacol.*, vol. 60, no. 1, pp. 107–118, 2009.
- [21] G. Morace and E. Borghi, "Fungal infections in ICU patients: Epidemiology and the role of diagnostics," *Minerva Anesthesiol.*, vol. 76, no. 11, pp. 950–956, 2010.
- [22] M. C. Arendrup, "Candida and Candidaemia: Susceptibility and Epidemiology," *Dan. Med. J.*, vol. 60, no. 11, pp. 1–32, 2013.
- [23] B. J. Kullberg and M. C. Arendrup, "Invasive candidiasis," *N. Engl. J. Med.*, vol. 373, no. 15, pp. 1445–1456, 2015, doi: 10.1056/NEJMra1315399.
- [24] A. Cortegiani, G. Misseri, T. Fasciana, A. Giammanco, A. Giarratano, and A. Chowdhary, "Epidemiology, clinical characteristics, resistance, and treatment of infections by *Candida auris*," *J. Intensive Care*, vol. 6, no. 1, pp. 1–13, 2018, doi: 10.1186/s40560-018-0342-4.
- [25] P. Uppuluri *et al.*, "Dispersion as an important step in the *Candida albicans* biofilm developmental cycle," *PLoS Pathog.*, vol. 6, no. 3, pp. 1–13, 2010, doi: 10.1371/journal.ppat.1000828.
- [26] M. Tumbarello *et al.*, "Biofilm production by *Candida* species and inadequate antifungal therapy as predictors of mortality for patients with candidemia," *J. Clin. Microbiol.*, vol. 45, no. 6, pp. 1843–1850, 2007, doi: 10.1128/JCM.00131-07.

- [27] J. M. Achkar and B. C. Fries, "Candida infections of the genitourinary tract," *Clin. Microbiol. Rev.*, vol. 23, no. 2, pp. 253–273, 2010, doi: 10.1128/CMR.00076-09.
- [28] D. Ermert, M. J. Niemiec, M. Röhm, A. Glenthøj, N. Borregaard, and C. F. Urban, "Candida albicans escapes from mouse neutrophils," *J. Leukoc. Biol.*, vol. 94, no. 2, pp. 223–236, Aug. 2013, doi: 10.1189/jlb.0213063.
- [29] M. Moreno-García, R. Condé, R. Bello-Bedoy, and H. Lanz-Mendoza, "The damage threshold hypothesis and the immune strategies of insects," *Infection, Genetics and Evolution*, vol. 24. *Infect Genet Evol*, pp. 25–33, Jun. 2014, doi: 10.1016/j.meegid.2014.02.010.
- [30] L. R. Scully and M. J. Bidochka, "Developing insect models for the study of current and emerging human pathogens," *FEMS Microbiology Letters*, vol. 263, no. 1. *FEMS Microbiol Lett*, pp. 1–9, Oct. 2006, doi: 10.1111/j.1574-6968.2006.00388.x.
- [31] C. J. Y. Tsai, J. M. S. Loh, and T. Proft, "Galleria mellonella infection models for the study of bacterial diseases and for antimicrobial drug testing," *Virulence*, vol. 7, no. 3, pp. 214–229, 2016, doi: 10.1080/21505594.2015.1135289.
- [32] "The current role of Aspergillus and Penicillium in human and animal health - PubMed." <https://pubmed.ncbi.nlm.nih.gov/7722784/> (accessed Oct. 07, 2020).
- [33] "WHO/IUIS Allergen Nomenclature Home Page." <http://www.allergen.org/> (accessed Oct. 07, 2020).
- [34] K. J. Kwon-Chung and J. A. Sugui, "Aspergillus fumigatus-What Makes the Species a Ubiquitous Human Fungal Pathogen?," *PLoS Pathog.*, vol. 9, no. 12, pp. 1–4, 2013, doi: 10.1371/journal.ppat.1003743.
- [35] M. Slavin *et al.*, "Invasive infections due to filamentous fungi other than Aspergillus: Epidemiology and determinants of mortality," *Clin. Microbiol. Infect.*, vol. 21, no. 5, pp. 490.e1-490.e10, 2015, doi: 10.1016/j.cmi.2014.12.021.
- [36] G. Ramage, E. Mowat, B. Jones, C. Williams, and J. Lopez-Ribot, "Our Current Understanding of Fungal Biofilms Fungal biofilms Gordon Ramage et al.," *Critical Reviews in Microbiology*, vol. 35, no. 4. *Crit Rev Microbiol*, pp. 340–355, Nov. 2009, doi: 10.3109/10408410903241436.
- [37] S. Fanning and A. P. Mitchell, "Fungal biofilms.," *PLoS Pathog.*, vol. 8, no. 4, pp. 1–4, 2012, doi: 10.1371/journal.ppat.1002585.
- [38] J. W. Costerton *et al.*, "Bacterial biofilms in nature and disease.," *Annual review of microbiology*, vol. 41. *Annu Rev Microbiol*, pp. 435–464, 1987, doi: 10.1146/annurev.mi.41.100187.002251.
- [39] G. Ramage, J. P. Martínez, and J. L. López-Ribot, "Candida biofilms on implanted biomaterials: A clinically significant problem," *FEMS Yeast Res.*, vol. 6, no. 7, pp. 979–986, 2006, doi: 10.1111/j.1567-1364.2006.00117.x.
- [40] J. Chandra, D. M. Kuhn, P. K. Mukherjee, L. L. Hoyer, and M. A. Ghannoum, "Biofilm Formation by the Fungal Pathogen," *Society*, vol. 183, no. 18, pp. 5385–5394, 2001, doi: 10.1128/JB.183.18.5385.
- [41] F. L. Mayer, D. Wilson, and B. Hube, "Candida albicans pathogenicity mechanisms,"

Virulence, vol. 4, no. 2, pp. 119–128, 2013, doi: 10.4161/viru.22913.

- [42] M. B. Lohse, M. Gulati, A. D. Johnson, and C. J. Nobile, “Development and regulation of single- and multi-species *Candida albicans* biofilms,” *Nature Reviews Microbiology*, vol. 16, no. 1. Nature Publishing Group, pp. 19–31, Oct. 03, 2018, doi: 10.1038/nrmicro.2017.107.
- [43] X. Zhao *et al.*, “*Candida albicans* Als3p is required for wild-type biofilm formation on silicone elastomer surfaces,” *Microbiology*, vol. 152, no. 8, pp. 2287–2299, Aug. 2006, doi: 10.1099/mic.0.28959-0.
- [44] J. Bonhomme, M. Chauvel, S. Goyard, P. Roux, T. Rossignol, and C. D’Enfert, “Contribution of the glycolytic flux and hypoxia adaptation to efficient biofilm formation by *Candida albicans*,” *Mol. Microbiol.*, vol. 80, no. 4, pp. 995–1013, 2011, doi: 10.1111/j.1365-2958.2011.07626.x.
- [45] Y. Li *et al.*, “Teasaponin suppresses *Candida albicans* filamentation by reducing the level of intracellular cAMP,” *Ann. Transl. Med.*, vol. 8, no. 5, pp. 175–175, 2020, doi: 10.21037/atm.2020.01.124.
- [46] A. Beauvais, T. Fontaine, V. Aimanianda, and J. P. Latgé, “*Aspergillus* cell wall and biofilm,” *Mycopathologia*, vol. 178, no. 5–6, pp. 371–377, 2014, doi: 10.1007/s11046-014-9766-0.
- [47] P. R. Taylor, S. M. Leal, Y. Sun, and E. Pearlman, “*Aspergillus* and *Fusarium* Corneal Infections Are Regulated by Th17 Cells and IL-17–Producing Neutrophils,” *J. Immunol.*, vol. 192, no. 7, pp. 3319–3327, Apr. 2014, doi: 10.4049/jimmunol.1302235.
- [48] Y. Xu *et al.*, “Characterization of the biosynthetic genes for 10,11- dehydrocurvularin, a heat shock response-modulating anticancer fungal polyketide from *Aspergillus terreus*,” *Appl. Environ. Microbiol.*, vol. 79, no. 6, pp. 2038–2047, Mar. 2013, doi: 10.1128/AEM.03334-12.
- [49] N. Robbins *et al.*, “Hsp90 governs dispersion and drug resistance of fungal biofilms,” *PLoS Pathog.*, vol. 7, no. 9, 2011, doi: 10.1371/journal.ppat.1002257.
- [50] R. Rajendran *et al.*, “Biofilm formation is a risk factor for mortality in patients with *Candida albicans* bloodstream infection-Scotland, 2012-2013,” *Clin. Microbiol. Infect.*, vol. 22, no. 1, pp. 87–93, Jan. 2016, doi: 10.1016/j.cmi.2015.09.018.
- [51] P. Robinet *et al.*, “A Polysaccharide Virulence Factor of a Human Fungal Pathogen Induces Neutrophil Apoptosis via NK Cells,” *J. Immunol.*, vol. 192, no. 11, pp. 5332–5342, Jun. 2014, doi: 10.4049/jimmunol.1303180.
- [52] “Gravelat *et al.*, 2013; Gresnigt *et al.*, 2014; Robinet *et al.*, 2014 - Cerca con Google.”
<https://www.google.com/search?q=Gravelat+et+al.%2C+2013%3B+Gresnigt+et+al.%2C+2014%3B+Robinet+et+al.%2C+2014&oq=Gravelat+et+al.%2C+2013%3B+Gresnigt+et+al.%2C+2014%3B+Robinet+et+al.%2C+2014&aqs=chrome..69i57.721j0j4&sourceid=chrome&ie=UTF-8> (accessed Oct. 03, 2020).
- [53] A. O. Manfiolli *et al.*, “Mitogen activated protein kinases (MAPK) and protein phosphatases are involved in *Aspergillus fumigatus* adhesion and biofilm formation,”

Cell Surf., vol. 1, no. March, pp. 43–56, 2018, doi: 10.1016/j.tcs.2018.03.002.

- [54] M. A. Jabra-Rizk, W. A. Falkler, and T. F. Meiller, “Fungal Biofilms and Drug Resistance,” *Emerg. Infect. Dis.*, vol. 10, no. 1, pp. 14–19, 2004, doi: 10.3201/eid1001.030119.
- [55] G. Ramage, R. Rajendran, L. Sherry, and C. Williams, “Fungal biofilm resistance,” *International Journal of Microbiology*, vol. 2012. *Int J Microbiol*, 2012, doi: 10.1155/2012/528521.
- [56] G. Ramage, R. Rajendran, L. Sherry, and C. Williams, “Fungal biofilm resistance,” *Int. J. Microbiol.*, vol. 2012, 2012, doi: 10.1155/2012/528521.
- [57] D. W. Denning and M. J. Bromley, “How to bolster the antifungal pipeline,” *Science (80-.)*, vol. 347, no. 6229, pp. 1414–1416, 2015, doi: 10.1126/science.aaa6097.
- [58] E. Borghi *et al.*, “New strategic insights into managing fungal biofilms,” *Front. Microbiol.*, vol. 6, no. OCT, p. 1077, Oct. 2015, doi: 10.3389/fmicb.2015.01077.
- [59] C. D. Fjell, J. A. Hiss, R. E. W. Hancock, and G. Schneider, “Designing antimicrobial peptides: Form follows function,” *Nature Reviews Drug Discovery*, vol. 11, no. 1. Nature Publishing Group, pp. 37–51, Dec. 16, 2012, doi: 10.1038/nrd3591.
- [60] M. Swidergall and J. F. Ernst, “Interplay between *Candida albicans* and the Antimicrobial Peptide Armory,” 2014, doi: 10.1128/EC.00093-14.
- [61] M. Heinonen, “Antioxidant activity and antimicrobial effect of berry phenolics - A Finnish perspective,” *Molecular Nutrition and Food Research*, vol. 51, no. 6. *Mol Nutr Food Res*, pp. 684–691, Jun. 2007, doi: 10.1002/mnfr.200700006.
- [62] R. P. Feliciano *et al.*, “Identification and quantification of novel cranberry-derived plasma and urinary (poly)phenols,” *Arch. Biochem. Biophys.*, vol. 599, pp. 31–41, Jun. 2016, doi: 10.1016/j.abb.2016.01.014.
- [63] G. Peron *et al.*, “The antiadhesive activity of cranberry phytocomplex studied by metabolomics: Intestinal PAC-A metabolites but not intact PAC-A are identified as markers in active urines against uropathogenic *Escherichia coli*,” *Fitoterapia*, vol. 122, pp. 67–75, Oct. 2017, doi: 10.1016/j.fitote.2017.08.014.
- [64] I. Iswaldi *et al.*, “Identification of polyphenols and their metabolites in human urine after cranberry-syrup consumption,” *Food Chem. Toxicol.*, vol. 55, pp. 484–492, May 2013, doi: 10.1016/j.fct.2013.01.039.
- [65] K. Valentová *et al.*, “Biosafety, antioxidant status, and metabolites in urine after consumption of dried cranberry juice in healthy women: A pilot double-blind placebo-controlled trial,” *J. Agric. Food Chem.*, vol. 55, no. 8, pp. 3217–3224, Apr. 2007, doi: 10.1021/jf0636014.
- [66] A. H. Groll, A. J. De Lucca, and T. J. Walsh, “Emerging targets for the development of novel antifungal therapeutics,” *Trends in Microbiology*, vol. 6, no. 3. *Trends Microbiol*, pp. 117–124, Mar. 01, 1998, doi: 10.1016/S0966-842X(97)01206-7.
- [67] Y. S. Lee *et al.*, “Myriocin, a serine palmitoyltransferase inhibitor, suppresses tumor growth in a murine melanoma model by inhibiting de novo sphingolipid synthesis,” *Cancer Biol. Ther.*, vol. 13, no. 2, pp. 92–100, Jan. 2012, doi:

10.4161/cbt.13.2.18870.

- [68] M. A. Pfaller and D. J. Diekema, "Epidemiology of invasive candidiasis: A persistent public health problem," *Clinical Microbiology Reviews*, vol. 20, no. 1. American Society for Microbiology (ASM), pp. 133–163, Jan. 2007, doi: 10.1128/CMR.00029-06.
- [69] L. Romani *et al.*, "Defective tryptophan catabolism underlies inflammation in mouse chronic granulomatous disease," *Nature*, vol. 451, no. 7175, pp. 211–216, Jan. 2008, Accessed: Oct. 03, 2020. [Online]. Available: <https://go.gale.com/ps/i.do?p=HRCA&sw=w&issn=00280836&v=2.1&it=r&id=GALE%7CA193476618&sid=googleScholar&linkaccess=fulltext>.
- [70] A. Casadevall, F. C. Fang, and L. Pirofski, "Microbial Virulence as an Emergent Property: Consequences and Opportunities," *PLoS Pathog.*, vol. 7, no. 7, p. e1002136, Jul. 2011, doi: 10.1371/journal.ppat.1002136.
- [71] P. R. Taylor, L. Martinez-Pomares, M. Stacey, H. H. Lin, G. D. Brown, and S. Gordon, "Macrophage receptors and immune recognition," *Annu. Rev. Immunol.*, vol. 23, pp. 901–944, 2005, doi: 10.1146/annurev.immunol.23.021704.115816.
- [72] L. Romani, "Immunity to fungal infections," *Nat. Rev. Immunol.*, vol. 11, no. 4, pp. 275–288, 2011, doi: 10.1038/nri2939.
- [73] N. T. H. Mai *et al.*, "Dexamethasone in Vietnamese Adolescents and Adults with Bacterial Meningitis," *N. Engl. J. Med.*, vol. 357, no. 24, pp. 2431–2440, Dec. 2007, doi: 10.1056/NEJMoa070852.
- [74] X. Su, M. A. Matthay, and A. B. Malik, "Requisite Role of the Cholinergic $\alpha 7$ Nicotinic Acetylcholine Receptor Pathway in Suppressing Gram-Negative Sepsis-Induced Acute Lung Inflammatory Injury," *J. Immunol.*, vol. 184, no. 1, pp. 401–410, Jan. 2010, doi: 10.4049/jimmunol.0901808.
- [75] K. Kawashima, T. Fujii, Y. Moriwaki, H. Misawa, and K. Horiguchi, "Non-neuronal cholinergic system in regulation of immune function with a focus on $\alpha 7$ nAChRs," *Int. Immunopharmacol.*, vol. 29, no. 1, pp. 127–134, Feb. 2015, doi: 10.1016/j.intimp.2015.04.015.
- [76] C. Nile *et al.*, "Repurposing pilocarpine hydrochloride for treatment of *Candida albicans* infections," *mSphere*, vol. 4, no. 1, 2019, doi: 10.1128/mSphere.00689-18.
- [77] M. Rosas-Ballina and K. J. Tracey, "Cholinergic control of inflammation," doi: 10.1111/j.1365-2796.2009.02098.x.
- [78] S. Neumann *et al.*, "The non-neuronal cholinergic system in peripheral blood cells: Effects of nicotinic and muscarinic receptor antagonists on phagocytosis, respiratory burst and migration," *Life Sci.*, vol. 80, no. 24–25, pp. 2361–2364, May 2007, doi: 10.1016/j.lfs.2007.01.010.
- [79] "CGD Paper." <http://www.candidagenome.org/cgi-bin/reference/reference.pl?pubmed=22064862> (accessed Oct. 03, 2020).
- [80] R. Rajendran *et al.*, "Acetylcholine protects against *Candida albicans* infection by inhibiting biofilm formation and promoting hemocyte function in a *Galleria mellonella*

- infection model,” *Eukaryot. Cell*, vol. 14, no. 8, pp. 834–844, 2015, doi: 10.1128/EC.00067-15.
- [81] S. H. Chotirmall and N. G. McElvaney, “Fungi in the cystic fibrosis lung: Bystanders or pathogens?,” *International Journal of Biochemistry and Cell Biology*, vol. 52. Elsevier Ltd, pp. 161–173, 2014, doi: 10.1016/j.biocel.2014.03.001.
- [82] B. Briard, C. Heddergott, and J. P. Latgé, “Volatile compounds emitted by pseudomonas aeruginosa stimulate growth of the fungal pathogen aspergillus fumigatus,” *MBio*, vol. 7, no. 2, Mar. 2016, doi: 10.1128/mBio.00219-16.
- [83] C. R. Bonnett, E. J. Cornish, A. G. Harmsen, and J. B. Burritt, “Early neutrophil recruitment and aggregation in the murine lung inhibit germination of *Aspergillus fumigatus* conidia,” *Infect. Immun.*, vol. 74, no. 12, pp. 6528–6539, Dec. 2006, doi: 10.1128/IAI.00909-06.
- [84] A. C. Tang, S. E. Turvey, M. P. Alves, N. Regamey, B. Tümmler, and D. Hartl, “Current concepts: Host-pathogen interactions in cystic fibrosis airways disease,” *European Respiratory Review*, vol. 23, no. 133. European Respiratory Society, pp. 320–332, 2014, doi: 10.1183/09059180.00006113.
- [85] A. M. Cantin, D. Hartl, M. W. Konstan, and J. F. Chmiel, “Inflammation in cystic fibrosis lung disease: Pathogenesis and therapy,” *Journal of Cystic Fibrosis*, vol. 14, no. 4. Elsevier, pp. 419–430, Jul. 01, 2015, doi: 10.1016/j.jcf.2015.03.003.
- [86] F. Perdoni *et al.*, “Antifungal activity of Myriocin on clinically relevant *Aspergillus fumigatus* strains producing biofilm,” *BMC Microbiol.*, vol. 15, no. 1, pp. 1–8, 2015, doi: 10.1186/s12866-015-0588-0.
- [87] G. Morace and L. Polonelli, “Voriconazole activity against clinical yeast isolates: A multicentre Italian study,” *Int. J. Antimicrob. Agents*, vol. 26, no. 3, pp. 247–253, 2005, doi: 10.1016/j.ijantimicag.2005.06.005.
- [88] A. Summers, “Susceptibility Testing,” *Genet. Test. Care, Consent. Liabil.*, vol. 3, no. 9, pp. 268–291, 2006, doi: 10.1002/0471748897.ch11.
- [89] J. A. Plumb, “Cell sensitivity assays: the MTT assay.,” *Methods Mol. Med.*, vol. 88, pp. 165–169, 2004, doi: 10.1007/978-1-61779-080-5_20.
- [90] E. Mauri *et al.*, “Design of polymer-based antimicrobial hydrogels through physico-chemical transition,” *Mater. Sci. Eng. C*, vol. 103, 2019, doi: 10.1016/j.msec.2019.109791.
- [91] F. Perdoni *et al.*, “A histological procedure to study fungal infection in the wax moth *Galleria mellonella*,” *Eur. J. Histochem.*, vol. 58, no. 3, pp. 258–262, 2014, doi: 10.4081/ejh.2014.2428.
- [92] E. Elkord, P. E. Williams, H. Kynaston, and A. W. Rowbottom, “Human monocyte isolation methods influence cytokine production from in vitro generated dendritic cells,” *Immunology*, vol. 114, no. 2, pp. 204–212, 2005, doi: 10.1111/j.1365-2567.2004.02076.x.
- [93] G. Baron *et al.*, “Profiling *Vaccinium macrocarpon* components and metabolites in human urine and the urine ex-vivo effect on *Candida albicans* adhesion and biofilm-

formation,” *Biochem. Pharmacol.*, vol. 173, 2020, doi: 10.1016/j.bcp.2019.113726.

- [94] D. Cirasola, R. Sciota, L. Vizzini, V. Ricucci, G. Morace, and E. Borghi, “Experimental biofilm-related *Candida* infections,” *Future Microbiol.*, vol. 8, no. 6, pp. 799–805, Jun. 2013, doi: 10.2217/fmb.13.36.
- [95] A. Caretti *et al.*, “Inhibition of ceramide de novo synthesis by myriocin produces the double effect of reducing pathological inflammation and exerting antifungal activity against *A. fumigatus* airways infection,” *Biochim. Biophys. Acta - Gen. Subj.*, vol. 1860, no. 6, pp. 1089–1097, 2016, doi: 10.1016/j.bbagen.2016.02.014.
- [96] G. Ermel, S. Georgeault, C. Inisan, and M. Besnard, “Inhibition of adhesion of uropathogenic *Escherichia coli* bacteria to uroepithelial cells by extracts from cranberry,” *J. Med. Food*, vol. 15, no. 2, pp. 126–134, Feb. 2012, doi: 10.1089/jmf.2010.0312.
- [97] J. P. Lavigne, G. Bourg, C. Combescure, H. Botto, and A. Sotto, “In-vitro and in-vivo evidence of dose-dependent decrease of uropathogenic *Escherichia coli* virulence after consumption of commercial *Vaccinium macrocarpon* (cranberry) capsules,” *Clin. Microbiol. Infect.*, vol. 14, no. 4, pp. 350–355, 2008, doi: 10.1111/j.1469-0691.2007.01917.x.
- [98] K. Gupta, M. Y. Chou, A. Howell, C. Wobbe, R. Grady, and A. E. Stapleton, “Cranberry Products Inhibit Adherence of P-Fimbriated *Escherichia coli* to Primary Cultured Bladder and Vaginal Epithelial Cells,” *J. Urol.*, vol. 177, no. 6, pp. 2357–2360, Jun. 2007, doi: 10.1016/j.juro.2007.01.114.
- [99] A. Turner, S. N. Chen, M. K. Joike, S. L. Pendland, G. F. Pauli, and N. R. Farnsworth, “Inhibition of uropathogenic *Escherichia coli* by cranberry juice: A new antiadherence assay,” *J. Agric. Food Chem.*, vol. 53, no. 23, pp. 8940–8947, Nov. 2005, doi: 10.1021/jf052035u.
- [100] R. P. Feliciano, E. Mecha, M. R. Bronze, and A. Rodriguez-Mateos, “Development and validation of a high-throughput micro solid-phase extraction method coupled with ultra-high-performance liquid chromatography-quadrupole time-of-flight mass spectrometry for rapid identification and quantification of phenolic metabolites in human plasma and urine,” *J. Chromatogr. A*, vol. 1464, pp. 21–31, Sep. 2016, doi: 10.1016/j.chroma.2016.08.027.
- [101] D. L. McKay, C. Y. O. Chen, C. A. Zampariello, and J. B. Blumberg, “Flavonoids and phenolic acids from cranberry juice are bioavailable and bioactive in healthy older adults,” *Food Chem.*, vol. 168, pp. 233–240, Feb. 2015, doi: 10.1016/j.foodchem.2014.07.062.
- [102] J. M. Walsh *et al.*, “Liquid chromatography with tandem mass spectrometry quantification of urinary proanthocyanin A2 dimer and its potential use as a biomarker of cranberry intake,” *J. Sep. Sci.*, vol. 39, no. 2, pp. 342–349, Jan. 2016, doi: 10.1002/jssc.201500922.
- [103] K. Ou, P. Sarnoski, K. R. Schneider, K. Song, C. Khoo, and L. Gu, “Microbial catabolism of procyanidins by human gut microbiota,” *Mol. Nutr. Food Res.*, vol. 58, no. 11, pp. 2196–2205, Nov. 2014, doi: 10.1002/mnfr.201400243.
- [104] M. Monagas *et al.*, “Insights into the metabolism and microbial biotransformation of

dietary flavan-3-ols and the bioactivity of their metabolites,” *Food and Function*, vol. 1, no. 3. Food Funct, pp. 233–253, Dec. 2010, doi: 10.1039/c0fo00132e.

- [105] A. I. H. Phua, K. Y. Hon, A. Holt, M. O’Callaghan, and S. Bihari, “Candida catheter-related bloodstream infection in patients on home parenteral nutrition - Rates, risk factors, outcomes, and management,” *Clinical Nutrition ESPEN*, vol. 31. Elsevier Ltd, pp. 1–9, Jun. 01, 2019, doi: 10.1016/j.clnesp.2019.03.007.
- [106] C. Tsui, E. F. Kong, and M. A. Jabra-Rizk, “Pathogenesis of *Candida albicans* biofilm,” *Pathogens and disease*, vol. 74, no. 4. Pathog Dis, p. ftw018, Jun. 01, 2016, doi: 10.1093/femspd/ftw018.
- [107] P. Mena *et al.*, “5-(3’,4’-Dihydroxyphenyl)- γ -valerolactone and its sulphate conjugates, representative circulating metabolites of flavan-3-ols, exhibit anti-adhesive activity against uropathogenic *Escherichia coli* in bladder epithelial cells,” *J. Funct. Foods*, vol. 29, pp. 275–280, Feb. 2017, doi: 10.1016/j.jff.2016.12.035.
- [108] A. Zida, S. Bamba, A. Yacouba, R. Ouedraogo-Traore, and R. T. Guiguemdé, “Substances naturelles actives sur *Candida albicans*, sources de nouveaux médicaments antifongiques : revue de la littérature,” *Journal de Mycologie Médicale*, vol. 27, no. 1. Elsevier Masson SAS, pp. 1–19, Mar. 01, 2017, doi: 10.1016/j.mycmed.2016.10.002.
- [109] E. Borghi *et al.*, “Cell surface hydrophobicity: A predictor of biofilm production in *Candida* isolates?,” *Journal of Medical Microbiology*, vol. 60, no. 5. Microbiology Society, pp. 689–690, May 01, 2011, doi: 10.1099/jmm.0.026898-0.
- [110] C. J. Nobile *et al.*, “Complementary Adhesin Function in *C. albicans* Biofilm Formation,” *Curr. Biol.*, vol. 18, no. 14, pp. 1017–1024, Jul. 2008, doi: 10.1016/j.cub.2008.06.034.
- [111] C. J. Nobile, J. E. Nett, D. R. Andes, and A. P. Mitchell, “Function of *Candida albicans* adhesin hwp1 in biofilm formation,” *Eukaryot. Cell*, vol. 5, no. 10, pp. 1604–1610, Oct. 2006, doi: 10.1128/EC.00194-06.
- [112] C. Ciurtin, A. Ostas, V. M. Cojocar, S. B. Walsh, and D. A. Isenberg, “Advances in the treatment of ocular dryness associated with Sjögren’s syndrome,” *Semin. Arthritis Rheum.*, vol. 45, no. 3, pp. 321–327, Dec. 2015, doi: 10.1016/j.semarthrit.2015.06.007.
- [113] J. Burr, A. Azuara-Blanco, A. Avenell, and A. Tuulonen, “Medical versus surgical interventions for open angle glaucoma,” *Cochrane Database Syst. Rev.*, no. 9, Sep. 2012, doi: 10.1002/14651858.cd004399.pub3.
- [114] C. Xue, Y. P. Hsueh, and J. Heitman, “Magnificent seven: Roles of G protein-coupled receptors in extracellular sensing in fungi,” *FEMS Microbiology Reviews*, vol. 32, no. 6. FEMS Microbiol Rev, pp. 1010–1032, Nov. 2008, doi: 10.1111/j.1574-6976.2008.00131.x.
- [115] Y. Li, L. Sun, C. Lu, Y. Gong, M. Li, and S. Sun, “Promising antifungal targets against *Candida albicans* based on ion homeostasis,” *Frontiers in Cellular and Infection Microbiology*, vol. 8, no. SEP. Frontiers Media S.A., p. 286, Sep. 04, 2018, doi: 10.3389/fcimb.2018.00286.

- [116] M. S. Lionakis, "New insights into innate immune control of systemic candidiasis," *Medical Mycology*, vol. 52, no. 6. Oxford University Press, pp. 555–564, 2014, doi: 10.1093/mmy/myu029.
- [117] K. Kavanagh and E. P. Reeves, "Exploiting the potential of insects for in vivo pathogenicity testing of microbial pathogens," *FEMS Microbiology Reviews*, vol. 28, no. 1. Elsevier, pp. 101–112, 2004, doi: 10.1016/j.femsre.2003.09.002.
- [118] N. Browne, M. Heelan, and K. Kavanagh, "An analysis of the structural and functional similarities of insect hemocytes and mammalian phagocytes," *Virulence*, vol. 4, no. 7. Taylor and Francis Inc., pp. 597–603, 2013, doi: 10.4161/viru.25906.
- [119] V. Teichgräber *et al.*, "Ceramide accumulation mediates inflammation, cell death and infection susceptibility in cystic fibrosis," *Nat. Med.*, vol. 14, no. 4, pp. 382–391, Apr. 2008, doi: 10.1038/nm1748.
- [120] A. Mingione *et al.*, "Inhibition of Sphingolipid Synthesis as a Phenotype-Modifying Therapy in Cystic Fibrosis," *Cell. Physiol. Biochem.*, vol. 54, no. 1, pp. 110–125, Jan. 2019, doi: 10.33594/000000208.
- [121] S. Zhang, C. L. Shrestha, and B. T. Kopp, "Cystic fibrosis transmembrane conductance regulator (CFTR) modulators have differential effects on cystic fibrosis macrophage function," *Sci. Rep.*, vol. 8, no. 1, Dec. 2018, doi: 10.1038/s41598-018-35151-7.
- [122] E. M. Bruscia and T. L. Bonfield, "Cystic Fibrosis Lung Immunity: The Role of the Macrophage," *Journal of Innate Immunity*, vol. 8, no. 6. S. Karger AG, pp. 550–563, Nov. 01, 2016, doi: 10.1159/000446825.
- [123] T. L. Bonfield *et al.*, "Inflammatory cytokines in cystic fibrosis lungs," *Am. J. Respir. Crit. Care Med.*, vol. 152, no. 6 I, pp. 2111–2118, 1995, doi: 10.1164/ajrccm.152.6.8520783.
- [124] S. Chillappagari *et al.*, "Impaired TLR4 and HIF expression in cystic fibrosis bronchial epithelial cells downregulates hemeoxygenase-1 and alters iron homeostasis in vitro," *Am. J. Physiol. - Lung Cell. Mol. Physiol.*, vol. 307, no. 10, pp. L791–L799, Nov. 2014, doi: 10.1152/ajplung.00167.2014.
- [125] E. C. Patin *et al.*, "IL-27 Induced by Select *Candida* spp. via TLR7/NOD2 Signaling and IFN- β Production Inhibits Fungal Clearance," *J. Immunol.*, vol. 197, no. 1, pp. 208–221, Jul. 2016, doi: 10.4049/jimmunol.1501204.

ACKNOWLEDGMENTS

Throughout the writing of this dissertation I have received a great support.

I would first like to thank my supervisor, Professor Elisa Borghi, whose expertise was fundamental in formulating the research proposal and outcome. Her feedback helped me to give always the best of myself. She provided me with the tools that I needed to choose the right direction and successfully complete my dissertation.

I would also like to thank the reviewers Prof. Di Bonaventura, Prof. Tavanti, Prof. Blasi and Prof. Bujdàková, to kindly revise my dissertation work with thoughtful suggestions.

I would like to acknowledge the laboratories with whom I collaborated during my PhD. All of them enriched my skills both personally and professionally.

I also want to thank my colleague Giulia Bassanini for the memorable time we spent working together, and Professor Giulia Morace for her valuable guidance throughout my studies.

Finally, I could not have completed this dissertation without the support of my parents, my brother, my sister and my dear Luca, to be always there for me.



ELSEVIER

Contents lists available at ScienceDirect

Biochemical Pharmacology

journal homepage: www.elsevier.com/locate/biochempharm

Profiling *Vaccinium macrocarpon* components and metabolites in human urine and the urine *ex-vivo* effect on *Candida albicans* adhesion and biofilm-formation

Giovanna Baron^a, Alessandra Altomare^a, Luca Regazzoni^a, Laura Fumagalli^a, Angelica Artasensi^a, Elisa Borghi^b, Emerenziana Ottaviano^b, Cristian Del Bo^c, Patrizia Riso^c, Pietro Allegrini^d, Giovanna Petrangolini^d, Paolo Morazzoni^d, Antonella Riva^d, Lolita Arnoldi^d, Marina Carini^a, Giancarlo Aldini^{a,*}

^a Department of Pharmaceutical Sciences, Università degli Studi di Milano, Via Luigi Mangiagalli 25, 20133 Milan, Italy

^b Department of Health Sciences, Università degli Studi di Milano, Via Di Rudini 8, 20142 Milan, Italy

^c Department of Food, Environmental and Nutritional Sciences, Università degli Studi di Milano, Via Luigi Mangiagalli 25, 20133 Milan, Italy

^d Indena S.p.A, Viale Ortles 12, 20139 Milan, Italy

ARTICLE INFO

Keywords:

Mass spectrometry
Cranberry
Vaccinium macrocarpon
Candida albicans
Urine metabolites
UTIs

ABSTRACT

The aim of this work was to profile, by using an HPLC-MS/MS method, cranberry compounds and metabolites found in human urine after ingestion of a highly standardized cranberry extract (Anthocran®). Two different strategies were adopted for the data analysis: a targeted and an untargeted approach. These strategies allowed the identification of 42 analytes including cranberry components, known metabolites and metabolites hitherto unreported in the literature, including six valerolactones/valeric acid derivatives whose presence in urine after cranberry consumption has never been described before. Absolute concentrations of 26 over 42 metabolites were obtained by using pure available standards. Urine collected at different time points after the last dosage of Anthocran® were tested on the reference strain *C. albicans* SC5314, a biofilm-forming strain. Fractions collected after 12 h were found to significantly reduce the adhesion and biofilm formation compared to the control ($p < 0.05$). A similar effect was then obtained by using Anthocran™ Phytosome™, the lecithin formulation containing 1/3 of standardized cranberry extract and formulated to enhance the absorption of the cranberry components. The urinary profile of cranberry components and metabolites in the urine fractions collected at 1 h, 6 h and 12 h after the last capsule intake were then reproduced by using the pure standards at the concentration ranges found in the urine fraction, and tested on *C. albicans*. Only the mixture mimicking the urinary fraction collected at 12 h and containing as main components, quercetin and 5-(3',4'-dihydroxyphenyl)- γ -valerolactone was found effective thus confirming the *ex-vivo* results.

1. Introduction

Candida albicans is one of the most common fungi causing disease in humans and the most frequently isolated fungal pathogen in nosocomial urinary tract infections (UTIs) [1,2]. Urological devices, urological procedures, diabetes and being female are the main factors linked to candiduria [3]. Catheters, which are used in up to 20% of hospitalized subjects [4], represent an adhesion substrate for microorganisms that can easily develop biofilm on plastic or silicone surfaces. The most important feature of microbial biofilms is their tolerance to

antimicrobial therapies [5], leading to recurrent or persistent infections. Therefore, alternative approaches to conventional antifungal therapy are desirable and among these the search of botanical products provides opportunities for new therapeutic approaches.

Cranberry (*Vaccinium macrocarpon*) is a rich source of polyphenols, which possess beneficial properties towards pathogenic infections including urinary tract infections (UTIs), dental caries and stomach ulcers [6]. Moreover, berry phenolics showed antioxidant, anti-inflammatory and anticancer properties [7,8]. A synergy of all the phytochemicals could explain the great health benefits of cranberry reported *in vitro*

Abbreviations: UTIs, urinary tract infections; PACs, proanthocyanidins; CFM-ID, competitive fragmentation modeling for metabolite identification

* Corresponding author.

E-mail address: giancarlo.aldini@unimi.it (G. Aldini).

<https://doi.org/10.1016/j.bcp.2019.113726>

Received 30 September 2019; Accepted 18 November 2019

Available online 26 November 2019

0006-2952/ © 2019 The Authors. Published by Elsevier Inc. This is an open access article under the CC BY license

(<http://creativecommons.org/licenses/by/4.0/>).

studies [9–11]. Despite all these potential applications, thus far prevention of UTIs remains the main application for cranberry based products [12]. The major constituents of cranberry are flavonols, anthocyanins, proanthocyanidins (PACs), flavan-3-ols and phenolic acids and derivatives [13]. Several *in vitro* studies have supported the hypothesis that the antiadhesive properties of cranberry are due to PACs, and in particular to the A-type [14]. However, controversial results regarding their presence in human urine are reported: many *in vivo* studies have demonstrated that they are not detected after cranberry intake [15–19], but two works have shown their presence in urine at a very low concentration [20,21]. The use of different dosages and non-standardized cranberry products could explain these controversial results. The purpose of the present work is to profile the components and metabolites in human urine after ingestion of a highly standardized cranberry extract (Anthocran®, Indena S.p.A.) which has been found effective in human studies [22–24]. Furthermore, the evaluation of the activity of urinary fractions on *C. albicans* adhesion collected at different times following cranberry intake was performed. The quantitative analysis of the metabolites identified in each urine fraction combined with the urine activity on *C. albicans* adhesion has permitted the identification of an array of compounds responsible for inhibiting fungal adherence. Finally, the *ex-vivo* activity of Anthocran™ Phytosome™, lecithin formulation of the standardized cranberry extract was tested in order to evaluate whether the lipid matrix can improve the bioavailability and bioactivity of the extract.

2. Materials and methods

2.1. Reagents

Formic acid, ethyl gallate, protocatechuic acid, p-coumaric acid, gallic acid, sinapinic acid, 2-hydroxybenzoic acid, 3-hydroxybenzoic acid, 4-hydroxybenzoic acid, 2,3-dihydroxybenzoic acid, 2,5-dihydroxybenzoic acid, 2,4-dihydroxybenzoic acid, 3-(4-hydroxyphenyl)-propionic acid, 3,4-dihydroxyphenylacetic acid, hippuric acid, 3,4-dihydroxyhydrocinnamic acid, 2-hydroxyhippuric acid, quinic acid, 2-methylhippuric acid, YPD medium, Roswell Park Memorial Institute 1640 medium (RPMI), phosphate buffered saline (PBS), crystal violet, methanol and LC-MS grade solvents were purchased from Merck KGaA, Darmstadt, Germany. Kaempferol, quercetin, syringetin, quercetin-3-O-rhamnoside, quercetin-3-O-galactoside were from Extrasynthese (Genay Cedex, France). Quercetin-3-O-arabinofuranoside, 3-hydroxyhippuric acid and 4-hydroxyhippuric acid were from Carbosynth (Compton Berkshire, UK). LC-grade H₂O (18 MΩ cm) was prepared with a Milli-Q H₂O purification system (Millipore, Bedford, MA, USA). SPE Hypersep C18 column (100 mg/mL) were from Thermo Scientific (Milan, Italy). Standardized cranberry extract (*V. macrocarpon*) and the capsules containing 36 mg PACs/capsule (Anthocran®), 12 mg PACs/capsule Anthocran™ Phytosome™ and placebo capsule were supplied by Indena S.p.A (Milan, Italy).

2.2. Synthesis of 5-(3',4'-dihydroxyphenyl)-γ-valerolactone (I)

¹H NMR spectra were recorded operating at 300 MHz while ¹³C NMR at 75.43 MHz. Chemical shifts are reported in ppm relative to residual solvent (CHCl₃ or DMSO) as internal standard. Signal multiplicity is designed according to the following abbreviations: s = singlet, d = doublet, dd = doublet of doublets, t = triplet, m = multiplet, br s = broad singlet, br t = broad triplet. Purifications were performed by flash chromatography using silica gel (particle size 40–63 μm, Merck) on Isolera™ (Biotage, Uppsala, Sweden) apparatus.

Palladium on carbon, 3,4-bis(benzyloxy)benzaldehyde, 2(5H)-furanone, *tert*-butyldimethylsilyl trifluoromethanesulfonate (TBDMSOTf), 1,8-Diazabicyclo[5.4.0]undec-7-ene (DBU), sodium bisulfite, 37% HCl, cyclohexane, ethyl acetate, tetrahydrofuran, ethanol and methanol were purchased from Merck KGaA, Darmstadt, Germany.

Compound I was afforded (Fig. 1) by Mukaiyama aldol addition

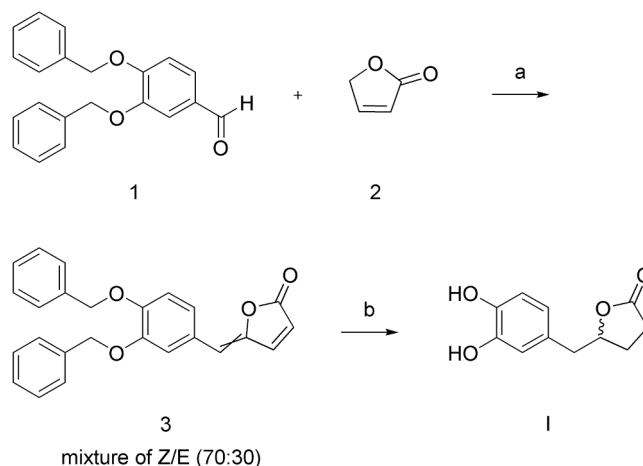


Fig. 1. Synthesis of compound I – a) DBU, TBDMSOTf, THF dry, –10 °C; b) H₂, Pd/C, CH₃OH, RT.

between 3,4-bis(benzyloxy)benzaldehyde (1) and 2(5H)-furanone (2) in presence of *tert*-butyldimethylsilyl trifluoromethanesulfonate and DBU. 5-(3',4'-bis(benzyloxy)benzylidene)furan-2(5H)-one (3) was obtained as a mixture of Z/E isomers (70:30). Reduction of 3 by H₂ Pd/C provided the final compound 5-(3',4'-dihydroxyphenyl)-γ-valerolactone (I) as racemic mixture.

5-(3',4'-Bis(benzyloxy)benzylidene)furan-2(5H)-one (3). Under nitrogen atmosphere, DBU (0.28 mL, 1.88 mmol) was added dropwise to a solution of 2 (158 mg, 1.88 mmol) in dry THF (16 mL). The mixture was stirred for 30 min at room temperature. After cooled down to –10 °C *tert*-butyldimethylsilyl trifluoromethanesulfonate (0.48 mL, 2.07 mmol) and 1 (600 mg, 1.88 mmol) were added dropwise and the mixture was stirred 1 h at –10 °C, then DBU (0.56 mL, 3.76 mmol) was added dropwise. The reaction mixture was stirred overnight at room temperature, then solvent was removed under vacuum. Ethyl acetate (20 mL), EtOH (5 mL) and saturated solution of sodium bisulfite (5 mL) were added to the crude residue and stirred overnight at 40 °C. The phases were separated and the organic layer was diluted with ethyl acetate (15 mL), treated with 2.9 N HCl (3 × 20 mL), washed with brine (20 mL), dried and concentrated to afford a sticky black oil. The crude product was purified on silica gel (75:25 cyclohexane/ethyl acetate) to afford the title compound as an orange/brown oil (137 mg, 0.36 mmol, 19% yield).

¹H NMR (300 MHz, CDCl₃) Z isomer: δ = 7.53 (d, *J* = 7.0 Hz, 4H), 7.49–7.24 (m, 9H), 6.92 (d, *J* = 8.4 Hz, 1H), 6.15 (d, *J* = 5.3 Hz, 1H), 5.91 (s, 1H), 5.22 (s, 2H), 5.20 (s, 2H).

¹H NMR (300 MHz, CDCl₃) E isomer: δ = 7.53 (d, *J* = 7.0 Hz, 4H), 7.49–7.24 (m, 9H), 6.92 (d, *J* = 8.4 Hz, 1H), 6.21 (d, *J* = 5.3 Hz, 1H), 5.91 (s, 1H), 5.18 (s, 2H), 5.14 (s, 2H).

5-(3',4'-dihydroxyphenyl)-γ-valerolactone (I). 3 (275 mg, 0.72 mmol) was dissolved in CH₃OH (16.50 mL), and 3% Pd/C (40 mg) was added. The reaction mixture was stirred overnight under hydrogen atmosphere at room temperature, then the catalyst was removed by filtration. The filtrate was concentrated in vacuo to afford the desired product as an orange oil (125 mg, 0.60 mmol, 83% yield).

¹H NMR (300 MHz, CD₃OD) δ = 6.71–6.67 (m, 2H), 6.56 (dd, *J* = 7.9, 2.2 Hz, 1H), 4.77–4.66 (m, 1H), 2.87 (dd, *J* = 14.1, 6.1 Hz, 1H), 2.78 (dd, *J* = 14.0, 6.1 Hz, 1H), 2.52–2.41 (m, 1H), 2.35 (dd, *J* = 9.4, 4.7 Hz, 1H), 2.29–2.17 (m, 1H), 2.03–1.88 (m, 1H).

¹³C NMR (75 MHz, CD₃OD) δ = 173.17, 144.88, 143.80, 127.60, 120.45, 116.20, 114.90, 81.86, 40.03, 28.14, 26.44.

2.3. Subject selection

A total of thirteen volunteers (mean age 25 ± 4 years and BMI 20.6 ± 2.0 kg m⁻²) were recruited from students and staff of the

University of Milan according to the following inclusion criteria: women, 18–40 years of age, normal weight for height ($18\text{--}25\text{ kg m}^{-2}$), non-smokers, no history of cardiovascular, diabetes, hepatic, renal, or gastrointestinal diseases. Subjects with allergy and/or aversion to cranberry and/or cranberry products were excluded. Other exclusion criteria were as follow: consumption of any dietary supplement, drug or medication for at least one month before the beginning of the study. The study was performed in accordance with the ethical standards established in the 2013 Declaration of Helsinki and approved by the Ethics Committee of the University of Milan (December 18, 2018, ref. 57/18). The study was registered at www.isrctn.org as ISRCTN32556347. All participants signed an informed consent form.

2.4. Study design on healthy volunteers

Subjects were instructed to limit the consumption of polyphenols at least 72 h before experimentation and during the trial. A list of foods to be avoided has been provided to the volunteers. The list included: fruits and vegetables rich in polyphenols (e.g. berries, red/purple fruits/vegetables), chocolate and some beverages such as coffee, tea, wine and fruit juice. The study consisted of a randomized, double blind, 2-arm repeated measure cross-over design. One group of subjects consumed 2 capsules of Anthocran® per day, while the other group 2 the capsules of Anthocran™ Phytosome™ per day. The experiment was 7-day long. Urine samples were collected before starting supplementation (day 1, time 0) and after the last dosage (day 7) at the following time-points: 1, 2, 4, 6, 10, 12, 24 h. After one week of wash-out the groups inverted the treatment. Each subject received a box containing the number of capsules to consume during the experiment. Capsules were provided in a blind condition. Subjects were instructed to swallow two capsules per day, the first one in the morning before breakfast and the second one before dinner with a glass of water. Three volunteers consumed two placebo capsules with the same shape, size, colour, flavour and excipients of the products tested. Urine samples were collected at the same time-points as previously reported and used as control to verify the influence of diet and circadian rhythm on *C. albicans* activity. Ethyl gallate 10 μM was added as internal standard in the sample used for the MS analysis and all the samples were stored at $-80\text{ }^\circ\text{C}$ until analysis.

2.5. Sample preparation

An aliquot (1 mL) of each of the 10 subjects' urine was centrifuged at $10000 \times g$ for 5 min and the supernatant was extracted on the SPE column, working at 1 mL/min. Salts were removed with water and then all the compounds retained were eluted with 1 mL 100% acetonitrile. The fractions collected were dried under vacuum and then solubilized in 100 μL $\text{H}_2\text{O}-\text{CH}_3\text{OH}-\text{HCOOH}$ (90:10:0.1, v/v). For the quantitative analysis, the stock solutions of the standards were prepared in methanol and then diluted in a pool of the pre-treatment urine samples to obtain the final concentrations for each calibration curve. The samples were then added with ethyl gallate 10 μM as internal standard and processed as described.

2.6. Chromatographic conditions

Cranberry components and urine metabolite separation was performed on a reversed-phase Agilent Zorbax SB-C18 column ($150 \times 2.1\text{ mm}$, i.d. $3.5\text{ }\mu\text{m}$, CPS analitica, Milan, Italy), protected by an Agilent Zorbax guard column, kept at $40\text{ }^\circ\text{C}$, by an UltiMate 3000 system (Dionex) equipped with an autosampler kept at $4\text{ }^\circ\text{C}$ working at a constant flow rate (200 $\mu\text{L}/\text{min}$). Each sample (10 μL) was injected into the column and both cranberry components and urine metabolites were eluted with an 80 min multistep gradient of phase A $\text{H}_2\text{O}-\text{HCOOH}$ (100:0.1, v/v) and phase B $\text{CH}_3\text{CN}-\text{HCOOH}$ (100:0.1, v/v): 0–45 min, from 10% B to 20% B; 45–65 min, from 20% B to 60% B; 65–66 min, from 60% B to 90% B; 66–70 min, isocratic of 90% B; 70–71 min, from

90% B to 10% B, and then 71–80 min of isocratic 10% B.

2.7. Polyphenol class identification by HPLC-UV analysis

The identification of polyphenol classes was carried out by HPLC-UV analysis on a HPLC Surveyor LC system (Thermo Fisher Scientific, Milan, Italy) equipped with a quaternary pump, UV-VIS detector (PDA) and an autosampler. The scan range was set from 200 nm to 600 nm. A solution of 4 mg/mL of cranberry extract in $\text{H}_2\text{O}/\text{CH}_3\text{OH}/\text{HCOOH}$ (90/10/0.1% v/v) was used for the analysis.

2.8. Cranberry component profiling and urine metabolite characterization by high resolution mass spectrometry

Each sample (10 μL) was injected into the RP column as previously described: the cranberry extract was analyzed at a concentration of 4 mg/mL in $\text{H}_2\text{O}-\text{CH}_3\text{OH}-\text{HCOOH}$ (90:10:0.1, v/v), while the urine samples were analyzed after the treatment described in section 2.3. The analyses were performed on a LTQ-Orbitrap XL mass spectrometer using an ESI source. Mass spectra were acquired in positive and in negative ion modes. A list of 20 background ions was adopted as lock mass values for real time mass calibration [25]. The source parameters used for the positive mode are: spray voltage 4 kV, capillary temperature $300\text{ }^\circ\text{C}$, capillary voltage 30 V, tube lens offset 90 V; for the negative ion mode: spray voltage 4 kV, capillary temperature $300\text{ }^\circ\text{C}$, capillary voltage -23 V , tube lens offset -140 V . The instrument was set up to work in a data-dependent scan mode to acquire both full MS and MS/MS spectra. Full MS spectra were acquired in profile mode by the FT analyzer in a scan range of m/z 100–1200, using AGC scan target 5×10^5 and resolution 30,000 FWHM at m/z 400. Tandem mass spectra were acquired by the linear ion trap (LTQ) which was set up to fragment the 3 most intense ions exceeding 1×10^4 counts. Mass acquisition settings were: centroid mode, AGC scan target 5×10^4 , precursor ion isolation width of m/z 3, and collision energy (CID) of 35 eV. Dynamic exclusion was enabled to reduce redundant spectra acquisition: 2 repeat counts, 20 sec repeat duration, 30 sec of exclusion duration. Moreover, only singly and unassigned charged ions were fragmented. Instrument control and spectra analysis were provided by the software Xcalibur 2.0.7 and Chromeleon Xpress 6.80.

2.9. Targeted and untargeted analyses of cranberry components and metabolites in human urine

An in-house database was created for the targeted analysis by adding all the characterized cranberry extract components as well as known cranberry metabolites identified in other studies and cranberry components deriving from other cranberry sources even if not present in the extract under investigation. The identification was carried out on the QualBrowser tool of Xcalibur 2.0.7 by using the accurate mass and the isotopic and fragmentation patterns.

The untargeted analysis consisted of searching for all the ions present in the urine samples collected after the cranberry consumption that were not present or present at intensity relative to noise ($< 5 \times 10^2$ counts) in the pre-treatment sample. Spectra analyses were carried out on the QualBrowser tool of Xcalibur 2.0.7 by screening the full MS spectra acquired in negative ion mode in mass ranges of m/z 5 with 10 min as acquisition time for each sample. Each ion detected with these filters was exported with the relative MS/MS spectrum, if present. Identification was performed by following two different approaches based on the accurate mass and isotopic and fragmentation patterns. The first approach consists of giving the precursor ion and the MS/MS spectrum list as inputs in the Compound Identification tool of CFM-ID [26], using as mass tolerance error 10 ppm for the precursor ion and 0.3 Da for the fragments. CFM-ID performs a search for candidates in available databases (HMDB and KEGG) based on the accurate mass, then generating *in-silico* MS/MS spectra of all the candidates and then

comparing the experimental data with those obtained *in-silico*. The top candidates were ranked (Jaccard Score) according to how closely they matched and returned to a list. The second approach was initially focused on the calculation of the elemental composition performed on the Elemental Composition page of Xcalibur 2.0.7 by using the following parameters: mass tolerance 10 ppm, charge -1 , C, H, O, N, P, S as elements in use. The top 5 formulae were searched in available databases such as PubChem, METLIN, MassBank and in the literature in order to obtain a list of candidates. Following this, the Peak Assignment tool of CFM-ID was used to predict the MS/MS spectra of the putative identified compounds and to compare the *in-silico* spectra obtained with the experimental spectra.

2.10. Quantitative analysis

The calibration curves for each available metabolite were built by plotting the peak area ratios of metabolite/ethyl gallate versus the nominal concentrations of the metabolite by weighted (1/x²) least-squares linear regression. Table 1 shows all the obtained linear curves and the relative limit of quantification (LOQ). All the samples and calibration solutions were analyzed in triplicates. The areas under the curve of the extracted ion chromatogram of each identified metabolite was integrated by using the Genesis peak algorithm of the Qual Browser tool of Xcalibur 2.0.7.

2.11. *Candida albicans* biofilm formation assay

The biofilm-forming ability of *C. albicans* under various conditions (i.e. medium supplementation with cranberry extract or urine fractions) was evaluated on polystyrene 96-well plates using the reference strain *C. albicans* SC5314 [27]. Prior to experiments, *C. albicans* was grown overnight in yeast extract, peptone, dextrose (1% w/v yeast extract, 2% w/v peptone, 2% w/v dextrose) broth (YPD) at 30 °C in an orbital shaker. Cells were then harvested and washed with cold phosphate-buffered saline (PBS) and counted by hemocytometer. A standard inoculum of 5×10^5 yeast cells/mL was prepared in Roswell Park Memorial Institute 1640 medium (RPMI) and incubated in presence and absence of urine fractions as well as in the presence of Anthocran™

Table 1

Calibration curve parameters for the available metabolites.

Metabolite	[M – H] ⁻	Slope	Intercept	R ²	Limit of Quantification (µM)
Protocatechuic acid	153.0189	0.1529	-0.04789	0.991	0.25
p-Coumaric acid	163.0408	0.2786	-0.03032	0.995	0.01
Gallic acid	169.0146	0.0253	-0.00585	0.991	1
Sinapinic acid	223.0608	0.0452	-0.00523	0.990	0.005
Kaempferol	285.0407	1.0160	0.07999	0.991	0.001
Quercetin	301.0353	1.1520	-0.05015	0.999	0.005
Syringetin	345.0618	0.6626	0.00924	0.981	0.005
Quercetin-3-O-arabinofuranoside	433.0731	0.7625	-0.01439	0.997	0.0025
Quercetin-3-O-rhamnoside	447.0920	0.9010	-0.02547	0.997	0.001
Quercetin-3-O-galactoside	463.0884	0.5151	-0.02053	0.996	0.0025
2-hydroxybenzoic acid	137.0243	1.1470	-0.13480	0.998	0.25
3-hydroxybenzoic acid	137.0231	0.1113	-0.01402	0.996	0.05
4-hydroxybenzoic acid	137.0232	0.1204	-0.04054	0.999	1
2,3-dihydroxybenzoic acid	153.0201	1.2380	-1.89800	0.984	1.5
2,5-dihydroxybenzoic acid	153.0194	0.2438	0.67780	0.998	5
2,4-dihydroxybenzoic acid	153.0175	0.3176	-0.33540	0.989	1.5
3-(4-hydroxyphenyl)-propionic acid	165.0561	0.0048	0.00106	0.999	0.25
3,4-dihydroxyphenylacetic acid	167.0349	0.0228	0.05486	0.981	1.5
Hippuric acid	178.0509	0.3032	120.80000	0.993	1
3,4-dihydroxyhydrocinnamic acid	181.0506	0.2474	0.37710	0.997	0.25
p-Hydroxyhippuric acid	194.0450	0.2756	10.42000	0.995	1
m-Hydroxyhippuric acid	194.0446	0.3605	-2.94400	0.991	1
o-Hydroxyhippuric acid	194.0461	0.6801	-4.23000	0.996	1
2-methylhippuric acid	192.0670	0.7954	3.60500	0.999	1
Quinic acid	191.0554	0.01012	0.0097	0.999	0.05
5-(3',4'-dihydroxyphenyl)-γ-valerolactone	207.0666	0.2411	-0.47450	0.999	0.1

0.1 mg/mL. 100 µL/well of the inoculum was firstly incubated at 37 °C for 1 h to promote adhesion. Non-adherent cells were removed and wells washed with PBS; medium was replaced and the plate further incubated for 24 h. Biofilm-forming ability was quantified by crystal violet (CV) staining for total biomass measurement [28]. Two independent experiments were carried out with six replicates for each condition. The statistical analysis was performed by GraphPad Prism 6.02 for Windows, GraphPad Software, La Jolla California USA, (www.graphpad.com) using the one-way ANOVA with Dunnett's multiple comparisons test.

3. Results and discussion

3.1. Compliance

Volunteers confirmed the consumption of the capsules and the compliance was also verified by counting the capsules in the returned boxes. All the participants had 100% compliance and declared no adverse effects following the intervention.

3.2. Characterization of Anthocran® components

Polyphenol classes of the cranberry extract were characterized by HPLC-UV analysis at typical wavelength: 310–320 nm for phenolic acids, 350–370 nm for flavonols, 520 nm for anthocyanins, 278 nm for benzoic acids, flavanols and PACs. The identification of each compound in the extract was then obtained on the basis of the accurate mass and of the isotopic and the fragmentation patterns, by acquiring the mass spectra in positive and in negative ion mode. All identified compounds are reported in Table 2, Tables 3 and 4.

3.3. Targeted analysis of human urine after cranberry extract intake

The targeted analysis consisted of searching in the urine samples for the compounds listed in an in-house database (total number of compounds = 138), which comprises the cranberry extract components characterized as reported in section 3.2 and cranberry compounds and metabolites as reported elsewhere [15–21,29,30]. Identification was

Table 2
Anthocyanins composition in Anthocran®.

Name	RT (min)	[M] ⁺	Fragments
Anthocyanins			
Cyanidin	19	287.0556	259 + 255 + 251 + 245 + 242 + 125
Peonidin	24	301.0712	268 + 258 + 230 + 177 + 151
Cyanidin-3-O-arabinoside	6.2	419.0978	287
Peonidin-3-O-arabinoside	10	433.1135	301
Cyanidin-3-O-galactoside	4.2	449.1084	287
Cyanidin-3-O-glucoside	4.6	449.1084	287
Petunidin-3-O-arabinoside	5	449.1084	317
Peonidin-3-O-galactoside	7.3	463.1240	301
Peonidin 3-O-glucoside	7.6	463.1240	301
Malvidin-3-O-galactoside	8	493.1346	331
Malvidin-3-O-glucoside	8.4	493.1346	331

Table 3
Phenolic acids in Anthocran®.

Name	RT (min)	[M - H] ⁻	Fragments
Phenolic acids			
Benzoic acid	8.3	121.0290	77
Protocatechuic acid	4	153.0188	109
<i>p</i> -Coumaric acid	13.6	163.0395	119
Gallic acid	2.5	169.0137	125
Caffeic acid	7.9	179.0344	135
Ferulic acid	4.9	193.0501	149 + 134
Sinapinic acid	6.2	223.0607	179 + 164 + 149 + 135
Caffeoyl glucose	5	341.0873	179 + 135
Chlorogenic acid	6	353.0873	191 + 179 + 161

performed by considering the following parameters: accurate mass, isotopic pattern, MS/MS fragments and the retention time. In more details for each of the compound listed in the database, the SIC was reconstituted setting as filter ion the *m/z* calculated for the target compound; when a peak with the same RT of the targeted compound was found, the *m/z* of the parent ion, the isotopic pattern and MS/MS data were retrieved and compared with that of the standard. For some cranberry components (gallic acid, kaempferol, quercetin, syringetin, quercetin-3-O-arabinofuranoside, quercetin 3-O-rhamnoside and quercetin-3-O-galactoside) the intensity of the parent compound was not intense enough to perform CID experiments and their identity was confirmed by comparing the RT and isotopic pattern with those of genuine standards.

Tables 5 and 6 report the compounds and metabolites identified by using such an approach and setting the ion source in negative ion mode. Specifically, the identification of metabolites reported in Table 5 was confirmed by pure standards, while metabolites listed in Table 6 were putatively identified on the base of the accurate mass, isotopic pattern and, when present, fragmentation pattern. Analyses were also carried out in positive ion mode but no additional components were detected, nor were anthocyanins, which are characterized by an high response in such a polarity mode. The lack of detection of anthocyanins can be explained by considering their biotransformation mediated by the colonic microflora into small phenolic compounds, such as protocatechuic acid, phloroglucinaldehyde, ferulic acid, syringic acid, gallic acid, caffeic acid and vanillic acid [31–33], some of which were detected in the urine.

Some flavonols were found as well as some of their glycosylated forms such as kaempferol, quercetin and traces of its glycosides (quercetin-3-O-arabinofuranoside, quercetin-3-O-rhamnoside and quercetin-3-O-galactoside), syringetin and traces of isorhamnetin-3-O-arabinopyranoside. The low abundance of the glycosylated forms can be explained by considering the enzymatic hydrolysis into the corresponding aglycones mediated by cellular and bacterial β -glucosidases and occurring in the intestine [34]. The aglycones can be transformed by microbiota in the intestinal tract into phenolic acids by C-ring

cleavage and/or can undergo phase-II metabolism (i.e. glucuronidation) or methylation [35]. Metabolic studies performed on quercetin (the most representative flavonol) and related glycoside in the intestine showed that the main metabolites are represented by hydroxyphenylacetic acid catabolites [36,37]. In fact, 3,4-dihydroxyphenylacetic acid was found in urine as possible metabolite of flavonols deriving from intestinal microbiota metabolism.

Proanthocyanidins present in the extract (procyanidins A-type and B-type) were not detected in urine in the present study. Results from previous studies on this class of polyphenols are quite controversial, in particular concerning procyanidin A2, to which several studies attributed the activity of cranberry products in UTI prevention. In most cases [15–19], as in the present study, PACs were not detected in human urine while two works reported PACs in human urine: one work was performed on men and postmenopausal women of 50–70 years who took a single dose of 237 mL of cranberry juice (PACs content in the juice was not reported) [20]; in the second study, performed by the same research group, five young women (20–30 years) consumed 237 mL/day of cranberry juice (140 mg of PACs) according to a weekly schedule for 7 weeks [21]. The results that they obtained showed very low levels of PAC-A2 quantified in human urine ($C_{MAX} = 24$ ng/mg creatinine) and they concluded that PAC-A2 cannot be used as biomarker of cranberry intake since there was no correlation with the amount of juice consumed. Taking into consideration all these results, it is commonly accepted that PACs have a very low bioavailability, which decreases as the degree of their polymerization increases [38]. Moreover, it is reported that human microbiota degrades PACs in the colon into phenolic compounds: phenylacetic acids and phenylpropionic acids as metabolites of procyanidins A2, B2, catechin and epicatechin; for procyanidin B2, catechin and epicatechin, valerolactones and valeric acids derivatives have also been reported [39,40]. Although in the present paper the valerolactones origin has not been investigated, we can suggest they come from a microbiota-based transformation of cranberry catechin/epicatechin/PACs. This assumption is supported by independent researchers showing the catechin/epicatechin/PACs biotransformation to valerolactones is driven by gut microbiota. In particular, a metabolome study based on [2-¹⁴C] (–)-epicatechin in humans showed valerolactones as epicatechin metabolites [41]. Moreover, the bacteria *Eggerthella lenta* and *Flavonifractor plautii* were identified as responsible for catechin/epicatechin degradation to valerolactone derivatives by M. Kutschera et al. [42]. Li et al. described phenyl-valerolactones as the main tea catechin metabolites produced by gut microorganisms and detected in human urine and blood [43]. A gamma valerolactone was identified by Appeldoorn M.M. et al. as a main metabolite of procyanidin dimer metabolized by human microbiota [44]. Valerolactones were also detected in human urine by Ottaviani et al. after the consumption of flavanols and PACs [45].

In the present study, the following metabolites deriving from phenylpropionic acids [46] were detected: 3,4-dihydroxyphenylacetic acid, 3-(4-hydroxyphenyl)-propionic acid, dihydroxybenzoic acids,

Table 4
Flavanols, Flavonols and PACs in Anthocran®.

Name	RT (min)	[M + H] ⁺	Fragments	[M - H] ⁻	Fragments
Flavanols, Flavonols, PACs					
Coumarin	14	147.0446	119 + 91	145.0289	-
Scopoletin	17.8	193.0501	165 + 152 + 133 + 119 + 105	191.0344	-
Kaempferol	55	287.0556	259 + 251 + 241 + 231 + 213 + 165 + 153 + 137 + 121	285.0399	-
Epicatechin	5.7	291.0869	169 + 165 + 151 + 147 + 139 + 123	289.0712	245 + 205 + 179 + 161 + 151 + 137 + 125 + 109
Catechin	9	291.0869	169 + 165 + 151 + 147 + 139 + 123	289.0712	245 + 205 + 179 + 161 + 151 + 137 + 125 + 109
Quercetin	48.5	303.0505	257 + 247 + 229 + 165 + 153 + 149 + 137 + 121	301.0348	273 + 257 + 229 + 179 + 151 + 121 + 107
Epigallocatechin	4.4	307.0818	-	305.0661	261 + 221 + 219 + 179 + 137 + 125
Gallocatechin	3.1	307.0818	-	305.0661	261 + 221 + 219 + 179 + 137 + 125
Isorhamnetin	55.8	317.0661	299 + 285 + 281 + 274 + 257 + 165 + 153 + 139	315.0505	287 + 271 + 259 + 243 + 203 + 163 + 151
Myricetin	32	319.0454	290 + 273 + 255 + 245 + 165 + 153 + 137	317.0298	255 + 227 + 193 + 179 + 151 + 137 + 107
3-O-methylmyricetin	50	333.0610	301 + 287 + 277 + 273 + 245 + 193 + 165 + 153 + 139	331.0454	287 + 271 + 263 + 179 + 151
Syringetin	55.8	347.0767	315 + 291 + 287 + 269 + 181 + 165 + 153 + 139	345.0610	315
Quercetin-3-O-arabinofuranoside	25.2	435.0927	303	433.0771	301
Quercetin-3-O-arabinopyranoside	28.4	435.0927	303	433.0771	301
Quercetin-3-O-xylopyranoside	26.6	435.0927	303	433.0771	301
Catechin-3-O-gallate	16.6	443.0978	291 + 273 + 151 + 139	441.0822	315 + 297 + 289 + 161 + 153
Epicatechin-3-O-gallate	20	443.0978	291 + 273 + 151 + 139	441.0822	330 + 305 + 289 + 161 + 139
Kaempferol-7-O-glucoside	27.2	449.1084	287	447.0927	284
Isorhamnetin-3-O-arabinofuranoside	37	449.1084	317	447.0927	314
Isorhamnetin-3-O-xylopyranoside	38.5	449.1084	317	447.0927	314
Isorhamnetin-3-O-arabinopyranoside	41	449.1084	317	447.0927	314
Quercetin-3-O-rhamnoside	30.5	449.1084	303	447.0928	301
Myricetin-3-O-arabinofuranoside	16.6	451.0877	319	449.0720	317
Myricetin-3-O-arabinopyranoside	19.6	451.0877	319	449.0720	317
Myricetin-3-O-xylopyranoside	19	451.0877	319	449.0720	317
Quercetin-3-O-glucoside	22.4	465.1033	303	463.0877	301
Quercetin-3-O-galactoside	21.5	465.1033	303	463.0877	301
Isorhamnetin-3-O-glucopyranoside	34.5	479.1189	317	477.1033	315
Isorhamnetin-3-O-glucoturanoside	32.8	479.1189	317	477.1033	315
Isorhamnetin-3-O-galactoside	31.1	479.1189	317	477.1033	315
Syringetin-3-O-arabinofuranoside	38.8	479.1189	347	477.1033	345
Syringetin-3-O-xylopyranoside	39.8	479.1189	347	477.1033	345
Syringetin-3-O-arabinopyranoside	43.5	479.1189	347	477.1033	345
Myricetin-3-O-glucoside	15.1	481.0982	319	479.0826	317
Myricetin-3-O-galactoside	14.5	481.0982	319	479.0826	317
Syringetin-3-O-rhamnoside	43.8	493.1346	347	491.1189	-
Proanthocyanidin A-type dimer	17/23	577.1346	437 + 425 + 397 + 287	575.1189	425 + 289 + 287
Proanthocyanidin B-type dimer	22.6	579.1502	453 + 439 + 427 + 409 + 301 + 291	577.1346	425 + 407 + 289
Proanthocyanidin A-type trimer	16/25/27.3	865.1980	713 + 577 + 425 + 287	863.1823	575 + 423 + 289
Proanthocyanidin B-type trimer	11.5/14.3/24	867.2136	579 + 427 + 409 + 291	865.1979	577 + 425 + 407 + 287

Table 5
Cranberry components and metabolites identified using the targeted analysis.

Metabolite identification	RT (min)	Calculated [M – H] [–]	Observed [M – H] [–]	MS/MS fragments	Delta ppm
Protocatechuic acid	4.1	153.0188	153.0189	109	–0.588
<i>p</i> -Coumaric acid	14.1	163.0395	163.0408	119	–8.035
Gallic acid	2.5	169.0137	169.0146	–	–5.325
Sinapinic acid	19.4	223.0607	223.0608	179 + 164 + 149	–0.717
Kaempferol	55	285.0399	285.0407	–	–2.877
Quercetin	48.9	301.0348	301.0353	–	–1.395
Syringetin	55.8	345.0610	345.0618	–	–2.289
Quercetin-3-O-arabinofuranoside	28.5	433.0771	433.0731	–	9.306
Quercetin 3-O-rhamnoside	30.6	447.0928	447.0920	–	1.789
Quercetin-3-O-galactoside	21.6	463.0877	463.0884	–	–1.684
2-hydroxybenzoic acid	24.2	137.0239	137.0243	93	–3.065
3-hydroxybenzoic acid	8.9	137.0239	137.0231	–	5.984
4-hydroxybenzoic acid	6.6	137.0239	137.0232	93	4.671
2,3-dihydroxybenzoic acid	9.1	153.0187	153.0201	109	–8.561
2,5-dihydroxybenzoic acid	6.8	153.0187	153.0194	109	–3.856
2,4-dihydroxybenzoic acid	8.6	153.0187	153.0175	109	8.169
3-(4-hydroxyphenyl)-propionic acid	12.1	165.0552	165.0561	–	–5.816
3,4-dihydroxyphenylacetic acid	4.5	167.0344	167.0349	–	–2.574
Hippuric acid	8.2	178.0504	178.0509	134	–2.640
3,4-dihydroxyhydrocinnamic acid	7.1	181.0499	181.0506	137 + 121	–3.811
<i>p</i> -Hydroxyhippuric acid	3.6	194.0456	194.0450	150 + 100 + 93	3.401
<i>m</i> -Hydroxyhippuric acid	4.5	194.0456	194.0446	150 + 100 + 93	5.256
<i>o</i> -Hydroxyhippuric acid (salicyluric acid)	14.1	194.0456	194.0461	150 + 100 + 93	–2.628
5-(3',4'-dihydroxyphenyl)- γ -valerolactone	12	207.0657	207.0659	163 + 122 + 109	–0.821

Table 6
Metabolites putatively identified using the targeted analysis.

Metabolite putative identification	RT (min)	Calculated [M – H] [–]	Observed [M – H] [–]	MS/MS fragments	Delta ppm
Isorhamnetin-3-O-arabinopyranoside	41	447.0927	447.0954	–	–5.882
4-methylcatechol-O-sulphate	9.7	203.0014	203.0021	123	–3.300
Pyrogallol-O-2-sulphate	3.9	204.9807	204.9814	125	–3.269
Vanillic acid-4-O-sulphate	4.2	246.9912	246.9918	167	–2.105
5-(3',4'-dihydroxyphenyl)- γ -valerolactone-4'-O-sulphate	9.5	287.0225	287.0236	207	–3.658
Dihydroxyhydrocinnamic acid-3-O-glucuronide	9.5	357.0821	357.0827	181 + 137	–1.484

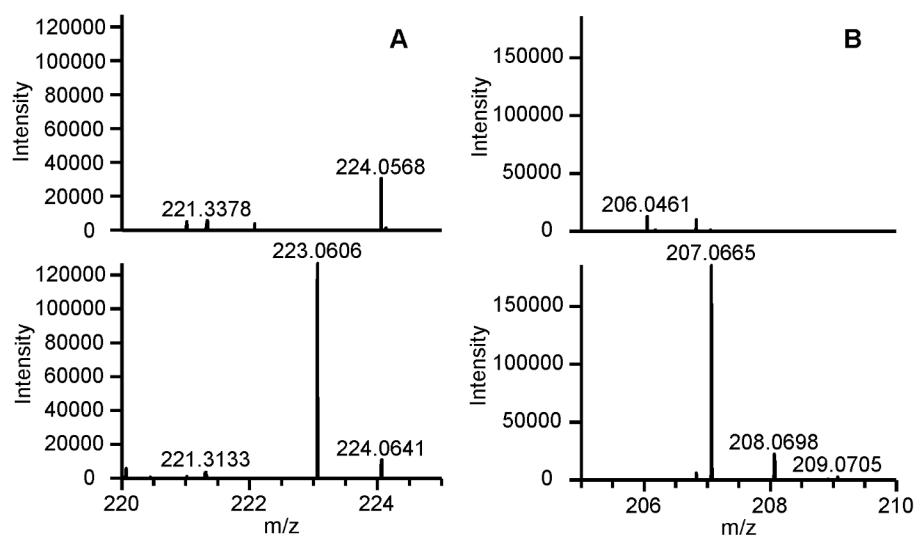


Fig. 2. Searching ions in untargeted analysis – Examples of ions not present in urine before cranberry intake (upper panels), but present in urine samples after the treatment (lower panels): ions at m/z 223.0606 and m/z 207.0665 are present only after the treatment and identified as sinapinic acid (A) and as 5-(3',4'-dihydroxyphenyl)- γ -valerolactone (B), respectively.

hydroxybenzoic acid and hydroxyhippuric acids, which presence can be related to PACs metabolism.

Phenolic acids represent the main class of identified polyphenols: protocatechuic acid, *p*-coumaric acid, gallic acid and sinapinic acid were found to be already present in the extract, but they can also derive from the metabolism of other polyphenols as mentioned above; 3,4-dihydroxyhydrocinnamic acid, dihydroxyhydrocinnamic acid-3-O-

glucuronide and 3-(4-hydroxyphenyl)-propionic acid can derive from the metabolism of PACs, chlorogenic acid or anthocyanins [17,39,46], while hydroxybenzoic acid, dihydroxybenzoic acids, hippuric acid and hydroxyhippuric acids can derive from the metabolism of all the other flavonoid components [46]. Catechol and pyrogallol derivatives, such as 4-methylcatechol-O-sulphate and pyrogallol-O-2-sulphate that we identified, can be generated from phenolic acids or anthocyanins [46].

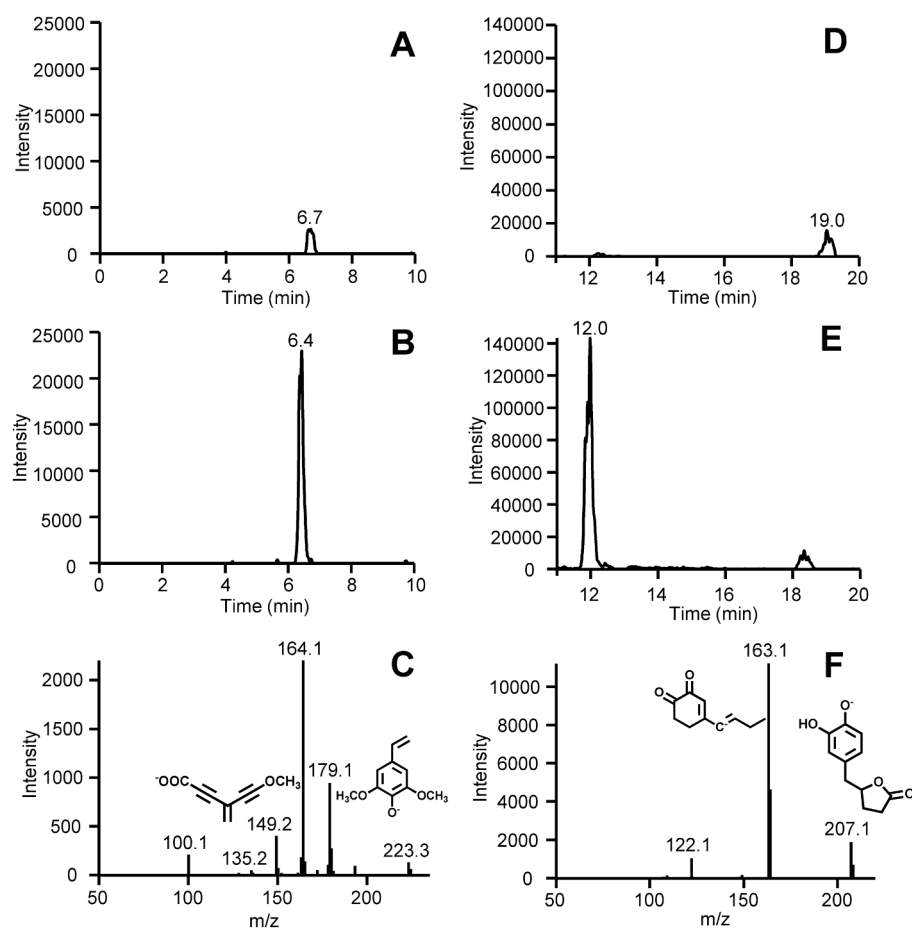


Fig. 3. Compounds identification in untargeted analysis – Single ion chromatograms relative to sinapinic acid and 5'-(3',4'-hydroxyphenyl)- γ -valerolactone (D) in urine sample before cranberry intake (panels A and D, respectively) and after 10 h and 12 h from cranberry intake (panels B and E, respectively). Peaks with the same RT of genuine standards are only detected after cranberry intake. Final confirmation of identities was achieved by tandem MS analyses. MS/MS spectra of sinapinic acid (C) and 5'-(3',4'-hydroxyphenyl)- γ -valerolactone (F) with the predicted structure for each fragment assigned by the Compound Identification tool of CFM-ID.

Table 7

Metabolites identified using the untargeted analysis. *identity confirmed by pure standard.

Metabolite putative identification	RT (min)	Calculated [M - H] ⁻	Observed [M - H] ⁻	MS/MS fragments	Delta ppm	Database
3,4-dihydroxyhydrocinnamic acid*	7.1	181.0499	181.0506	137 + 121	-3.811	HMDB
Quinic acid*	1.72	191.0556	191.0554	173 + 129	1.047	HMDB
2-methylhippuric acid*	11.1	192.0661	192.0670	74	-4.894	HMDB
<i>p</i> -Hydroxyhippuric acid*	3.6	194.0456	194.0450	150 + 100 + 93	3.401	HMDB
<i>m</i> -Hydroxyhippuric acid*	4.5	194.0456	194.0446	150 + 100 + 93	5.256	HMDB
<i>o</i> -Hydroxyhippuric acid (salicylic acid)*	14.1	194.0456	194.0461	150 + 100 + 93	-2.628	HMDB
Sinapinic acid*	19.4	223.0607	223.0608	179 + 164 + 149	-0.717	HMDB
5-(3',4'-dihydroxyphenyl)- γ -valerolactone*	12	207.0657	207.0659	163 + 122 + 109	-0.821	HMDB
5-(3',4'-dihydroxyphenyl)- γ -valerolactone-3'-O-sulphate	9.5	287.0225	287.0236	207	-3.658	HMDB
5-(3',4'-dihydroxyphenyl)- γ -valerolactone-4'-O-sulphate	10.2	287.0225	287.0233	207	-2.474	HMDB
5-(3',4',5'-trihydroxyphenyl)- γ -valerolactone-3'-O-sulphate	6.6	303.0175	303.0167	223	2.442	HMDB
4-Hydroxy-5-(dihydroxyphenyl)-valeric acid-O-sulphate	6.4	305.0331	305.0341	225	-3.213	HMDB
Dihydroxyhydrocinnamic acid-3-O-glucuronide	9.5	357.0821	357.0826	181 + 137	-1.484	HMDB
Salicylic acid glucuronide	9.2	370.0774	370.0783	194 + 150	-2.513	PubChem
3-O-Methylcatechin-sulphate	12.3	383.0437	383.0442	303 + 285 + 259 + 244 + 217 + 137	-1.279	PubChem
5-(3',4'-dihydroxyphenyl)- γ -valerolactone-3'-O-glucuronide	8.1	383.0978	383.0981	207	-0.783	HMDB
5-(3',4'-dihydroxyphenyl)- γ -valerolactone-4'-O-glucuronide	9.4	383.0978	383.0982	207	-1.044	HMDB
Sinapinic acid glucuronide	6.8	399.0928	399.0931	223	-0.877	HMDB
5-(3',4'-dihydroxyphenyl)- γ -valerolactone sulphoglucuronide	4.6	463.0546	463.0548	383/287/207	-0.302	[47]

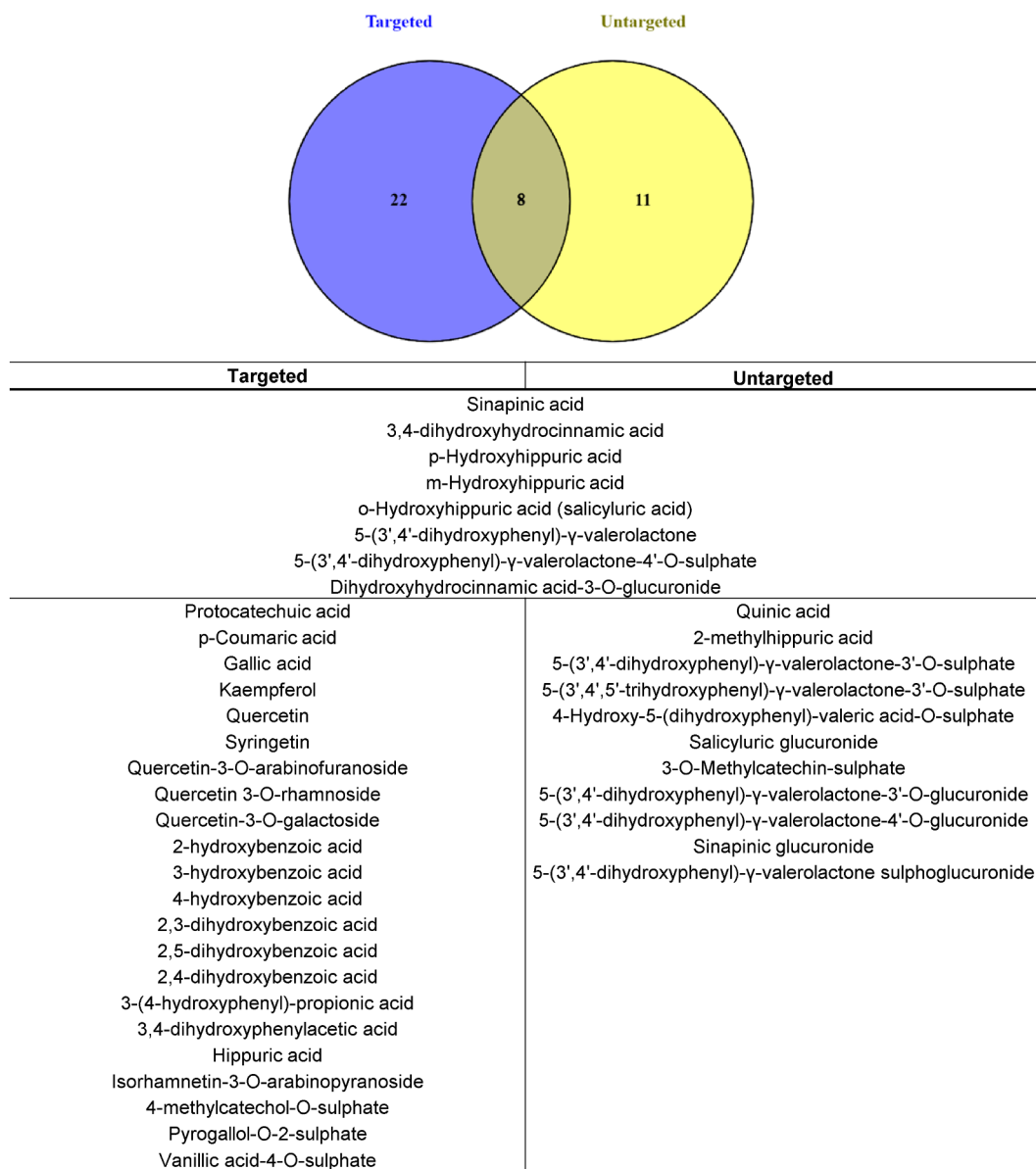


Fig. 4. Targeted and untargeted identifications – Venn diagram reporting all of the 42 compounds identified with the targeted (blue circle) and untargeted (yellow circle) analyses.

3.4. Untargeted analysis of human urine after cranberry extract intake

As described in the method session, the untargeted approach consists of searching for all the ions present in the urine samples collected after cranberry consumption that were not present or present at intensity relative to noise less than 5×10^2 counts in the pre-treatment sample. The analysis was performed using the negative ion mode because all the compounds identified using the targeted analysis were mainly detected in this polarity mode. The unidentified compounds, or those recognized as coming from the human basal metabolism (e.g. amino acids), were not included on the list. The search of ions was performed by screening the full MS spectra acquired in negative ion mode using a mass ranges of m/z 5 and with 10 min as acquisition time for each sample. As an example, Fig. 2A reports the MS spectra resulting by setting a MS range between m/z 220 and 225 and considering a time window between 0 and 10 min and relative to urine collected before (upper panel) and after 10 h (lower panel) the cranberry intake; Fig. 2B reports the MS spectra resulting by setting a MS range between m/z 205 and 210 and considering a time window between 10 and 20 min and

relative to urine collected before (upper panel) and after 12 h (lower panel) the cranberry intake. The ions at m/z 223.0606 and m/z 207.0665 are well evident only in the urine samples collected after the cranberry administration but not before. Identification of the unknown compounds was carried out by setting the precursor ion and the MS/MS fragment ions as inputs in the Compound Identification tool of CFM-ID. Fig. 3C and Fig. 3F reports the experimental MS/MS spectra used as input for the Compound Identification tool of CFM-ID which gave sinapinic acid and 5'-(3',4'-dihydroxyphenyl)-γ-valerolactone as best matched results. Final attribution was obtained by comparing RT, MS isotopic pattern and MS/MS fragmentation with those of pure standards (when commercially available). Fig. 3 shows the SIC chromatograms of sinapinic acid (Fig. 3B) and 5'-(3',4'-dihydroxyphenyl)-γ-valerolactone (Fig. 3E) in the urine fraction in which they reached their maximum concentration (10 h for sinapinic acid and 12 h for 5'-(3',4'-dihydroxyphenyl)-γ-valerolactone), while in the control sample (Figs. 3A and 3D, respectively) they were not present.

Several metabolites were identified in the untargeted analysis as reported in Table 7. Some of them had already been identified using the

Table 8
Results of known studies on metabolite characterization after cranberry products intake. The comparison regards: cranberry treatment, PACs content in the cranberry product used, the time of the treatment, the number of cranberry metabolites identified, the eventual presence of PACs and the number of known PACs metabolites including phenolic acid and valerolactone derivatives. NA: not available.

	Present study	Valentova et al. [15]	McKay et al. [20]	Walsh et al. [21]	Iswaldi et al. [16]	Feliciano et al. [17,18]	Peron et al. [19]
Cranberry Treatment	2 capsules/day standardized cranberry extract	1200 mg/day of dried cranberry juice	237 mL cranberry juice cocktail	237 mL/day cranberry juice cocktail	0.6 mL/kg of cranberry syrup	450 mL of a single-strength cranberry juice beverage	360 mg of cranberry extract
PACs content	36 mg/capsule	14.4 mg	NA	140 mg	0.71% (w/v)	710 mg	42.6% w/w of PAC-A/ 14.6% w/w of PAC-B
Treatment time	7 days	8 weeks	Single dose (24 h)	7 weeks	Single dose (24 h)	Single dose (24 h)	Single dose (24 h)
Number of metabolites	42	NA	26	19	32	67	14
PACs presence	no	no	yes	yes	no	no	no
N PACs metabolites (N valerolactones)	15 (8)	NA	8 (0)	7 (0)	3 (0)	17 (1)	12 (6)

targeted analysis, such as 3,4-dihydroxyhydrocinnamic acid, dihydroxyhydrocinnamic acid-3-O-glucuronide, sinapinic acid, the three hydroxyhippuric acid isomers, 5-(3',4'-dihydroxyphenyl)- γ -valerolactone and 5-(3',4'-dihydroxyphenyl)- γ -valerolactone-4'-O-sulphate. Fig. 4 shows an overview of all the 42 compounds which have been identified in the present study with the targeted (blue circle) and untargeted (yellow circle) analyses.

Besides quinic acid, which can derive from chlorogenic acid, and 2-methylhippuric acid, a methyl derivative of hippuric acid, different valerolactones and one valeric acid derivative were identified and listed in Table 7. Among these metabolites, 5-(3'-hydroxyphenyl)- γ -valerolactone-4'-O-sulphate had been identified in previous studies [17,18]. Also 5-(3',4'-dihydroxyphenyl)- γ -valerolactone has already been reported as cranberry metabolite [19]. None of the other valerolactones here described had previously been identified in urine after cranberry intake, although they are known as PACs metabolites [39,47].

Table 8 summarizes the overall cranberry components and metabolites, including PACs and their metabolites, so far identified in human studies, in comparison with those reported in the present study. Information on the treatment (dose and PACs content of the given cranberry) are also summarized. As already discussed above, PACs were detected only in two studies [20,21] and in one of these [20] the amount of PACs in the cranberry juice was not reported. In these two studies, phenolic acids were reported as PACs metabolites and no valerolactone derivatives were detected as in the study performed by Valentova et al. [15]. Feliciano et al. [17,18] identified several PAC metabolites by using standards, and among these only one valerolactone derivative was identified, while Peron et al. [19] reported a lower amount of metabolites but a higher number of valerolactone/valeric acid derivatives, one of which was also detected in this study. Hence, the untargeted approach here reported has permitted the identification of six valerolactones/valeric acid whose presence in urine after cranberry consumption has never been described before.

3.5. Ex-vivo inhibition of *Candida albicans* biofilm-formation by urine fractions

Anthocran® (0.1 mg/mL), urine collected before administration of Anthocran®, Anthocran™ Phytosome™ or placebo and urine fractions collected after 1 h, 2 h, 4 h, 6 h, 10 h, 12 h and 24 h of each treatment were tested to investigate their potential ability to reduce *C. albicans* adhesion and biofilm formation on polystyrene 96-well plates. Anthocran® 0.1 mg/mL was able to strongly reduce the adhesion and biofilm formation ($p < 0.0001$) of the biofilm-producing strain SC5314 (data not shown). Results expressed as mean \pm SD of urine fractions are reported in Fig. 5. Urine samples before (U-Pre) each treatment were inactive, while among the seven fractions tested those collected after 12 h the Anthocran® consumption (Fig. 5A) as well as Anthocran™ Phytosome™ (Fig. 5B) were shown to significantly inhibit the adhesion compared with the control ($p < 0.05$ and $p < 0.01$, respectively for Anthocran® and Anthocran™ Phytosome™). Urine fractions after placebo intake showed no activity at all, meaning that diet and the circadian rhythm does not influence activity. It should be noted that the effect of Anthocran™ Phytosome™ at 12 hr superimposes that of Anthocran®, despite the dose of Anthocran® per capsule being 1/3 in the phytosomal preparation (12 mg PACs/capsule Anthocran™ Phytosome™ vs 36 mg PACs/capsule Anthocran®). Phytosomes are lecithin formulations demonstrated to enhance botanical ingredients oral bioavailability both at preclinical and clinical levels [48–51]. The similar ability to reduce *C. albicans* adhesion and biofilm despite the reduced cranberry extract dose can be consequently explained by considering an increased absorption of active principles allowed by the Phytosome technology. This figure can positively contribute to a more rational and convenient modulation of clinical dosage and posology.

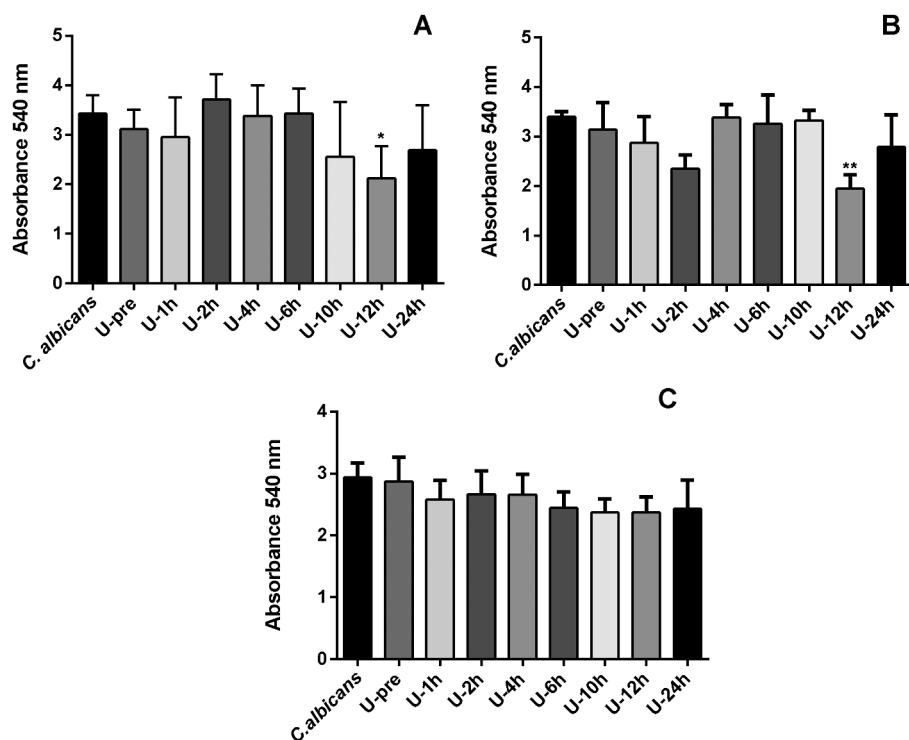


Fig. 5. Inhibition of *Candida albicans* biofilm formation – Biofilm biomass was assessed using the crystal violet assay after *C. albicans* SC5314 strain was cultured for 24 h in RPMI 1640 with/without treatments. A) Activity of urine before Anthocran® intake (U-Pre) and urinary fractions after treatment (U-1 h – U-24 h). Biomass of untreated *C. albicans* biofilm was used as control (*C. albicans*). B) Activity of urine fractions (U-1 h – U-24 h) after oral intake of Anthocran™ Phytosome™ and of urine before Anthocran™ Phytosome™ intake (U-Pre). Untreated *C. albicans* biofilm (*C. albicans*) was used as control. C) Activity of urine fractions (U-1 h – U-24 h) after oral intake of placebo (U-1 h – U-24 h). Control as described for B). Values represent the mean of three independent experiments, and of at least three sample replicates. Significant differences are indicated by *p < 0.05, **p < 0.01, ANOVA test.

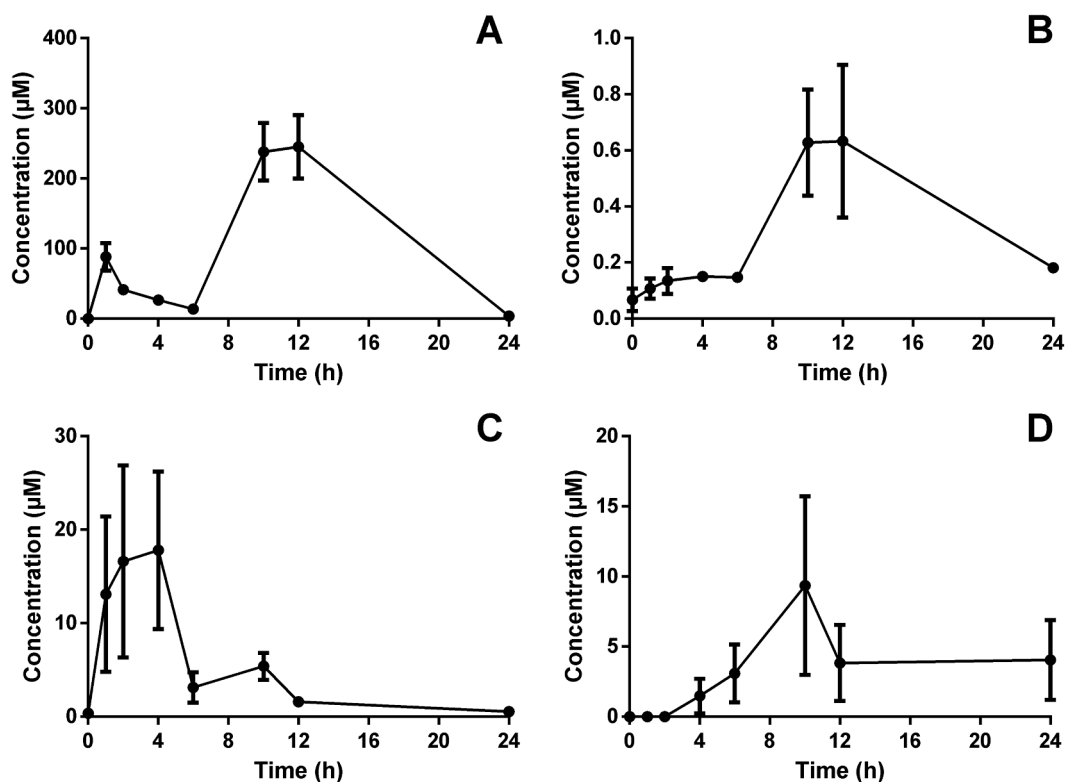


Fig. 6. Urinary profile of some metabolites – Excretion profiles of 5-(3',4'-dihydroxyphenyl)-γ-valerolactone (A), quercetin (B), p-coumaric acid (C) and 3,4-dihydroxyphenylacetic acid (D).

3.6. Metabolite concentration in urine samples

In order to identify the cranberry components/metabolites characteristic of the bioactive fractions and hence most likely responsible for the ability to reduce *C. albicans* adhesion and biofilm formation, the concentration of the available metabolites for each urinary fraction was

obtained through the quantitative analysis explained in the method section. Concentrations of the urinary components are reported as µM in order to allow the reassemble of the mixtures by using pure compounds and confirm their activities (see below). As examples, Fig. 6 shows two compounds which reached their maximum abundance in the active fraction and two compounds that reached this value in other

Table 9
Cranberry components and metabolites mean (± SD) concentration (µM) in urine fractions. N.D.: not detected.

Name	Pre-treatment	1 h	2 h	4 h	6 h	10 h	12 h	24 h
Protocatechuic acid	1.20 ± 1.00	7.24 ± 3.31	4.97 ± 1.52	10.81 ± 4.45	2.12 ± 1.33	3.78 ± 1.47	2.03 ± 0.82	2.51 ± 0.94
p-Coumaric acid	0.39 ± 0.24	13.11 ± 8.30	16.63 ± 10.27	17.81 ± 8.43	3.13 ± 1.62	5.40 ± 1.43	1.60 ± 0.31	0.55 ± 0.28
Gallic acid	< LOQ	2.28 ± 1.34	< LOQ	1.45 ± 1.06	< LOQ	3.02 ± 1.56	2.18 ± 0.91	1.22 ± 0.53
Sinapinic acid	0.29 ± 0.19	47.02 ± 46.73	25.36 ± 24.52	68.25 ± 67.50	118.75 ± 117.77	255.90 ± 247.79	84.29 ± 80.26	111.53 ± 109.32
Kaempferol	N.D.	0.083 ± 0.033	0.04 ± 0.03	N.D.	N.D.	0.02 ± 0.01	0.04 ± 0.03	N.D.
Quercetin	< LOQ	0.108 ± 0.036	0.14 ± 0.04	0.15 ± 0.01	0.15 ± 0.01	0.63 ± 0.19	0.63 ± 0.27	0.18 ± 0.01
Syringetin	N.D.	0.15 ± 0.14	0.02 ± 0.02	N.D.	N.D.	0.15 ± 0.14	0.03 ± 0.02	N.D.
Quercetin-3-O-arabinofuranoside	N.D.	0.01 ± 0.01	0.03 ± 0.01	0.01 ± 0.01	0.01 ± 0.01	0.02 ± 0.01	0.03 ± 0.01	N.D.
Quercetin 3-O-rhamnoside	N.D.	0.04 ± 0.02	0.03 ± 0.01	0.02 ± 0.01	N.D.	N.D.	N.D.	N.D.
Quercetin-3-O-galactoside	N.D.	N.D.	0.02 ± 0.12	0.08 ± 0.06	N.D.	N.D.	N.D.	N.D.
2-hydroxybenzoic acid	< LOQ	0.26 ± 0.11	< LOQ	< LOQ	< LOQ	0.85 ± 0.44	0.01 ± 0.01	N.D.
3-hydroxybenzoic acid	N.D.	N.D.	N.D.	1.19 ± 1.07	1.31 ± 1.15	N.D.	0.36 ± 0.15	0.38 ± 0.18
4-hydroxybenzoic acid	4.58 ± 2.73	23.84 ± 14.69	18.10 ± 9.90	13.91 ± 8.35	2.51 ± 1.44	7.74 ± 4.65	3.71 ± 2.07	4.29 ± 3.75
2,3-dihydroxybenzoic acid	< LOQ	2.44 ± 0.53	2.20 ± 1.16	2.50 ± 0.80	1.62 ± 0.69	2.99 ± 1.23	1.62 ± 0.64	< LOQ
2,5-dihydroxybenzoic acid	< LOQ	10.48 ± 4.20	< LOQ	< LOQ	< LOQ	14.56 ± 5.40	5.07 ± 1.37	6.04 ± 2.03
2,4-dihydroxybenzoic acid	< LOQ	1.51 ± 1.18	3.58 ± 2.40	4.61 ± 3.44	< LOQ	3.40 ± 3.04	1.55 ± 1.22	2.88 ± 2.57
3-(4-hydroxyphenyl)-propionic acid	0.58 ± 0.55	25.79 ± 19.77	4.22 ± 2.85	20.23 ± 7.92	17.74 ± 16.76	4.10 ± 1.91	1.18 ± 0.64	N.D.
3,4-dihydroxyphenylacetic acid	N.D.	N.D.	N.D.	1.49 ± 1.24	3.10 ± 2.06	9.36 ± 6.36	3.85 ± 2.70	4.06 ± 2.85
Hippuric acid	666.15 ± 29.07	230.12 ± 19.82	557.72 ± 26.45	409.82 ± 17.03	656.46 ± 24.06	531.84 ± 68.23	192.91 ± 31.13	648.52 ± 27.88
3,4-dihydroxyhydrocinnamic acid	0.45 ± 0.40	4.39 ± 4.03	2.99 ± 2.69	3.24 ± 2.43	2.50 ± 2.45	7.15 ± 4.89	4.46 ± 2.05	5.08 ± 2.12
p-Hydroxyhippuric acid	47.16 ± 12.68	1.48 ± 0.49	14.14 ± 3.15	30.64 ± 4.53	59.89 ± 14.55	9.04 ± 4.13	< LOQ	46.19 ± 4.34
m-Hydroxyhippuric acid	24.80 ± 13.21	21.91 ± 3.37	37.88 ± 12.61	25.57 ± 8.15	43.60 ± 10.17	32.36 ± 3.54	29.03 ± 13.24	24.89 ± 3.74
o-Hydroxyhippuric acid	36.65 ± 8.21	10.84 ± 1.14	8.44 ± 3.31	7.86 ± 2.68	17.99 ± 3.42	19.79 ± 1.20	13.32 ± 2.78	27.48 ± 3.30
2-methylhippuric acid	N.D.	2.070 ± 1.11	4.85 ± 0.97	< LOQ	N.D.	N.D.	N.D.	N.D.
Quinic acid	5.49 ± 3.80	12.71 ± 8.02	6.42 ± 4.38	10.15 ± 8.29	9.23 ± 2.26	17.36 ± 9.82	14.74 ± 7.32	8.50 ± 4.92
5-(3',4'-dihydroxyphenyl)-γ-valerolactone	N.D.	88.34 ± 61.63	41.51 ± 15.10	26.40 ± 14.03	13.83 ± 11.89	238.22 ± 129.46	245.24 ± 143.59	3.83 ± 2.08

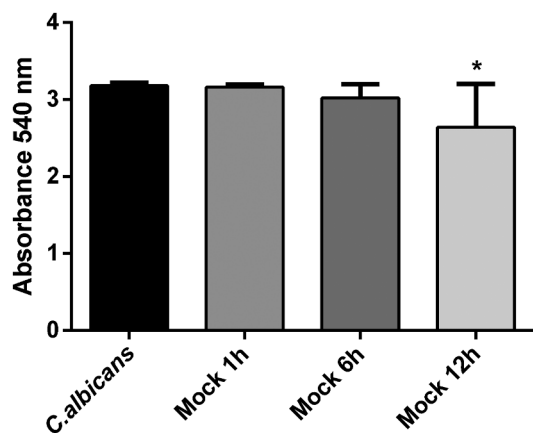


Fig. 7. Inhibition of *Candida albicans* biofilm formation by mock mixtures – The activity of the mixtures, prepared using available standards in RPMI medium, representing the inactive fractions (1 h and 6 h) and the active fraction (12 h, * $p < 0.05$) is reported.

urine fractions: Fig. 6A and B are relative to 5-(3',4'-dihydroxyphenyl)- γ -valerolactone and quercetin, respectively, whose T_{MAX} was 12 h; Fig. 6C is relative to *p*-coumaric acid, with a T_{MAX} reached after 4 h; Fig. 6D shows the excretion profile of 3,4-dihydroxyphenylacetic acid ($T_{MAX} = 10$ h). Table 9 shows the mean cranberry metabolite concentrations (μ M) in the control and in the urine fractions after cranberry intake.

The mixture of the active urine fractions (12 h) and of two inactive fractions (1 h and 6 h) were then reassembled by using available standards dissolved in RPMI and tested on *C. albicans*. The 12 h mixture was found to significantly reduce adhesion while the other two mixtures were inactive, thus confirming the results of the ex-vivo urine samples (Fig. 7). It is important to underline that the 12 h reconstituted mixture only contained one of the 8 valerolactone derivatives identified (namely, 5-(3',4'-dihydroxyphenyl)- γ -valerolactone) due to the lack of commercial availability of valerolactone standards (their synthesis is on-going in our laboratories). Hence if the bioactivity is related to this class of compounds, as expected, a greater activity could be obtained by integrating the reconstituted mixture with the other seven valerolactones.

The antiadhesive properties of cranberry, both *in vitro* and *in vivo*, have long been reported [52–55] mainly with regard to *E. coli*, which is the principal uropathogen that causes UTIs. An *in vitro* study showed that cranberry PACs prevent *C. albicans* biofilm formation in artificial urine [56]. In the present work, we demonstrate for the first time that cranberry extract as well as some urine fractions, collected after one week of cranberry administration, reduce both *C. albicans* adhesion and biofilm biomass. Since 12 h urine fractions were the most active, we focused our attention on the components that reached their highest concentration at this time point. The components found to have the highest concentration in this urine fraction are quercetin and 5-(3',4'-dihydroxyphenyl)- γ -valerolactone. A recent *in vitro* study [57] demonstrates that valerolactone derivatives display anti-adhesive activity against *E. coli*, confirming that the *in vivo* activity is due to PACs metabolites rather than intact PACs. Moreover, quercetin was reported to have *in vitro* anti-adhesive properties on *E. coli* [58]. However, the activity could derive not only by a single component but from a synergy of all the metabolites present in that mixture, thus explaining the possible activity of cranberry as a phytocomplex. In fact, many components present in the mixture showed an activity against biofilm formation or anti-adhesive properties against *E. coli*, like protocatechuic acid, 3,4-dihydroxyphenylacetic acid and 2-hydroxybenzoic acid [59–61].

In conclusion, the HR-MS method developed allowed the identification of several cranberry components and metabolites in human urine after a highly standardized cranberry extract consumption which has

been found to be effective in human studies. PACs were not detected as reported by previous studies, but several metabolites deriving from their catabolism presumably operated by the gut microflora and hereto not found *in vivo* were identified. The crude extract and the urine fraction collected at 12 h after cranberry intake were found to be active against *C. albicans* adhesion *ex-vivo*. The known metabolite of PACs, 5-(3',4'-dihydroxyphenyl)- γ -valerolactone was identified as the most abundant metabolite (245 μ M) in the bioactive urine fraction. To our knowledge, this is the first work which demonstrates an *ex-vivo* inhibition of *C. albicans* adhesion by human urine after cranberry intake. As a future perspective, as soon as all the identified compounds peaking at 12 h will be available (the synthesis of valerolactones derivatives is on-going) their activity against *C. albicans* will be evaluated, with a particular interest focused on valerolactone derivatives which represent the most abundant metabolites in urine after cranberry intake. Furthermore, in order to understand whether a synergistic action is involved, compounds will be tested in pure form or in mixture.

A further interesting result of our study derives from the use of the lecithin formulation of the cranberry extract which has shown to markedly increase oral bioavailability and organ target accessibility of cranberry active principles. A clinical study in catheterized subjects is on-going to confirm the effectiveness of Anthocran™ Phytosome™.

Author contributions

GB and GA were the principal responsible for the experimental part and for writing the manuscript. PA, GP, PM AR, MC, GB and GA conceived and designed the study. LF and A. Artasensi contributed to the synthesis of valerolactone derivative. EB and EO contributed to the microbiological studies. CDB and PR contributed to the design of the human volunteers study. GB, AA, LC, LA performed the analyses. All the authors assisted with the manuscript preparation.

Acknowledgments

We are grateful to Gerard Davy for his assistance in revising the English style of the paper.

Conflict of interest and sponsorship

None of the academic researcher listed as co-Authors served as consultant for Indena or received any personal compensation. The research was partially supported by a research contract signed in 2015 between UNIMI and Indena (GA as PI) entitled “Development of liquid chromatography methods coupled with mass spectrometry to assess the bioavailability of standardised extracts of vaccinium macrocarpon and vaccinium myrtillus”. AR, PA, GP, PM are employees of Indena SpA.

References

- [1] J.M. Achkar, B.C. Fries, *Candida* infections of the genitourinary tract, *Clin. Microbiol. Rev.* 23 (2) (2010) 253–273.
- [2] C.J. Nobile, A.D. Johnson, *Candida albicans* Biofilms and Human Disease, *Annu. Rev. Microbiol.* 69 (2015) 71–92.
- [3] C.A. Kauffman, Diagnosis and management of fungal urinary tract infection, *Infect. Dis. Clin. North Am.* 28 (1) (2014) 61–74.
- [4] S. Saint, J. Wiese, J.K. Amory, M.L. Bernstein, U.D. Patel, J.K. Zemencuk, S.J. Bernstein, B.A. Lipsky, T.P. Hofer, Are physicians aware of which of their patients have indwelling urinary catheters? *Am. J. Med.* 109 (6) (2000) 476–480.
- [5] S. Tobudic, C. Kratzer, A. Lassnigg, E. Prestler, Antifungal susceptibility of *Candida albicans* in biofilms, *Mycoses* 55 (3) (2012) 199–204.
- [6] M. Heinonen, Antioxidant activity and antimicrobial effect of berry phenolics—a Finnish perspective, *Mol. Nutr. Food Res.* 51 (6) (2007) 684–691.
- [7] S.H. Nile, S.W. Park, Edible berries: bioactive components and their effect on human health, *Nutrition* 30 (2) (2014) 134–144.
- [8] S. Skrovankova, D. Sumczynski, J. Mlcek, T. Jurikova, J. Sochor, Bioactive compounds and antioxidant activity in different types of berries, *Int. J. Mol. Sci.* 16 (10) (2015) 24673–24706.
- [9] C. Bodet, F. Chandad, D. Grenier, Cranberry components inhibit interleukin-6, interleukin-8, and prostaglandin E production by lipopolysaccharide-activated

- gingival fibroblasts, *Eur. J. Oral Sci.* 115 (1) (2007) 64–70.
- [10] N.P. Seeram, L.S. Adams, M.L. Hardy, D. Heber, Total cranberry extract versus its phytochemical constituents: antiproliferative and synergistic effects against human tumor cell lines, *J. Agric. Food Chem.* 52 (9) (2004) 2512–2517.
- [11] X. Yan, B.T. Murphy, G.B. Hammond, J.A. Vinson, C.C. Neto, Antioxidant activities and antitumor screening of extracts from cranberry fruit (*Vaccinium macrocarpon*), *J. Agric. Food Chem.* 50 (21) (2002) 5844–5849.
- [12] I. Vasileiou, A. Katsargyris, S. Theocharis, C. Giaginis, Current clinical status on the preventive effects of cranberry consumption against urinary tract infections, *Nutr. Res.* 33 (8) (2013) 595–607.
- [13] E. Pappas, K.M. Schaich, Phytochemicals of cranberries and cranberry products: characterization, potential health effects, and processing stability, *Crit. Rev. Food Sci. Nutr.* 49 (9) (2009) 741–781.
- [14] A.B. Howell, J.D. Reed, C.G. Krueger, R. Winterbottom, D.G. Cunningham, M. Leahy, A-type cranberry proanthocyanidins and uropathogenic bacterial anti-adhesion activity, *Phytochemistry* 66 (18) (2005) 2281–2291.
- [15] K. Valentova, D. Stejskal, P. Bednar, J. Vostalova, C. Cihalik, R. Vecerova, D. Koukalova, M. Kolar, R. Reichenbach, L. Sknouril, J. Ulrichova, V. Simanek, Biosafety, antioxidant status, and metabolites in urine after consumption of dried cranberry juice in healthy women: a pilot double-blind placebo-controlled trial, *J. Agric. Food Chem.* 55 (8) (2007) 3217–3224.
- [16] I. Iswaldi, D. Arráez-Román, A.M. Gómez-Caravaca, M.E.M. Contreras, J. Uberos, A. Segura-Carretero, A. Fernández-Gutiérrez, Identification of polyphenols and their metabolites in human urine after cranberry-syrup consumption, *Food Chem. Toxicol.* 55 (2013) 484–492.
- [17] R.P. Feliciano, A. Boeres, L. Massaccesi, G. Ista, M.R. Ventura, C. Nunes Dos Santos, C. Heiss, A. Rodriguez-Mateos, Identification and quantification of novel cranberry-derived plasma and urinary (poly)phenols, *Arch. Biochem. Biophys.* 599 (2016) 31–41.
- [18] R.P. Feliciano, E. Mecha, M.R. Bronze, A. Rodriguez-Mateos, Development and validation of a high-throughput micro solid-phase extraction method coupled with ultra-high-performance liquid chromatography-quadrupole time-of-flight mass spectrometry for rapid identification and quantification of phenolic metabolites in human plasma and urine, *J. Chromatogr. A* 1464 (2016) 21–31.
- [19] G. Peron, S. Sut, A. Pellizzaro, P. Brun, D. Voinovich, I. Castagliuolo, S. Dall'Acqua, The antiadhesive activity of cranberry phytocomplex studied by metabolomics: intestinal PAC-A metabolites but not intact PAC-A are identified as markers in active urines against uropathogenic *Escherichia coli*, *Fitoterapia* 122 (2017) 67–75.
- [20] D.L. McKay, C.Y. Chen, C.A. Zampariello, J.B. Blumberg, Flavonoids and phenolic acids from cranberry juice are bioavailable and bioactive in healthy older adults, *Food Chem.* 168 (2015) 233–240.
- [21] J.M. Walsh, X. Ren, C. Zampariello, D.A. Polasky, D.L. McKay, J.B. Blumberg, C.Y. Chen, Liquid chromatography with tandem mass spectrometry quantification of urinary proanthocyanin A2 dimer and its potential use as a biomarker of cranberry intake, *J. Sep. Sci.* 39 (2) (2016) 342–349.
- [22] A. Ledda, A. Bottari, R. Luzzi, G. Belcaro, S. Hu, M. Dugall, M. Hosoi, E. Ippolito, M. Corsi, G. Gizzi, P. Morazzoni, A. Riva, L. Giacomelli, S. Togni, Cranberry supplementation in the prevention of non-severe lower urinary tract infections: a pilot study, *Eur. Rev. Med. Pharmacol. Sci.* 19 (1) (2015) 77–80.
- [23] A. Ledda, G. Belcaro, M. Dugall, B. Feragalli, A. Riva, S. Togni, L. Giacomelli, Supplementation with high titer cranberry extract (Anthocran®) for the prevention of recurrent urinary tract infections in elderly men suffering from moderate prostatic hyperplasia: a pilot study, *Eur. Rev. Med. Pharmacol. Sci.* 20 (24) (2016) 5205–5209.
- [24] A. Ledda, G. Belcaro, M. Dugall, A. Riva, S. Togni, R. Eggenhoffner, L. Giacomelli, Highly standardized cranberry extract supplementation (Anthocran®) as prophylaxis in young healthy subjects with recurrent urinary tract infections, *Eur. Rev. Med. Pharmacol. Sci.* 21 (2) (2017) 389–393.
- [25] B.O. Keller, J. Sui, A.B. Young, R.M. Whittall, Interferences and contaminants encountered in modern mass spectrometry, *Anal. Chim. Acta* 627 (1) (2008) 71–81.
- [26] F. Allen, A. Pon, M. Wilson, R. Greiner, D. Wishart, CFM-ID: a web server for annotation, spectrum prediction and metabolite identification from tandem mass spectra, *Nucl. Acids Res.* 42 (Web Server issue) (2014) W94–W99.
- [27] D. Cirasola, R. Sciota, L. Vizzini, V. Ricucci, G. Morace, E. Borghi, Experimental biofilm-related *Candida* infections, *Future Microbiol.* 8 (6) (2013) 799–805.
- [28] C.G. Pierce, P. Uppuluri, A.R. Tristan, F.L. Wormley, E. Mowat, G. Ramage, J.L. Lopez-Ribot, A simple and reproducible 96-well plate-based method for the formation of fungal biofilms and its application to antifungal susceptibility testing, *Nat. Protoc.* 3 (9) (2008) 1494–1500.
- [29] R. Ohnishi, H. Ito, N. Kasajima, M. Kaneda, R. Kariyama, H. Kumon, T. Hatano, T. Yoshida, Urinary excretion of anthocyanins in humans after cranberry juice ingestion, *Biosci. Biotechnol. Biochem.* 70 (7) (2006) 1681–1687.
- [30] R. Rajbhandari, N. Peng, R. Moore, A. Arabshahi, J.M. Wyss, S. Barnes, J.K. Prasain, Determination of cranberry phenolic metabolites in rats by liquid chromatography-tandem mass spectrometry, *J. Agric. Food Chem.* 59 (12) (2011) 6682–6688.
- [31] R.M. de Ferrars, C. Czank, Q. Zhang, N.P. Botting, P.A. Kroon, A. Cassidy, C.D. Kay, The pharmacokinetics of anthocyanins and their metabolites in humans, *Br. J. Pharmacol.* 171 (13) (2014) 3268–3282.
- [32] S.C. Forester, A.L. Waterhouse, Identification of Cabernet Sauvignon anthocyanin gut microflora metabolites, *J. Agric. Food Chem.* 56 (19) (2008) 9299–9304.
- [33] A. Rodriguez-Mateos, D. Vauzour, C.G. Krueger, D. Shanmuganayagam, J. Reed, L. Calani, P. Mena, D. Del Rio, A. Crozier, Bioavailability, bioactivity and impact on health of dietary flavonoids and related compounds: an update, *Arch. Toxicol.* 88 (10) (2014) 1803–1853.
- [34] A. Scalbert, G. Williamson, Dietary intake and bioavailability of polyphenols, *J. Nutr.* 130 (8S Suppl) (2000) 2073S–2085S.
- [35] K. Kawabata, R. Mukai, A. Ishisaka, Quercetin and related polyphenols: new insights and implications for their bioactivity and bioavailability, *Food Funct.* 6 (5) (2015) 1399–1417.
- [36] I.B. Jaganath, W. Mullen, C.A. Edwards, A. Crozier, The relative contribution of the small and large intestine to the absorption and metabolism of rutin in man, *Free Radic Res* 40 (10) (2006) 1035–1046.
- [37] H. Schneider, A. Schwiertz, M.D. Collins, M. Blaut, Anaerobic transformation of quercetin-3-glucoside by bacteria from the human intestinal tract, *Arch. Microbiol.* 171 (2) (1999) 81–91.
- [38] R.P. Feliciano, C.G. Krueger, J.D. Reed, Methods to determine effects of cranberry proanthocyanidins on extraintestinal infections: Relevance for urinary tract health, *Mol. Nutr. Food Res.* 59 (7) (2015) 1292–1306.
- [39] M. Monagas, M. Urpi-Sarda, F. Sánchez-Patán, R. Llorach, I. Garrido, C. Gómez-Cordovés, C. Andres-Lacueva, B. Bartolomé, Insights into the metabolism and microbial biotransformation of dietary flavan-3-ols and the bioactivity of their metabolites, *Food Funct.* 1 (3) (2010) 233–253.
- [40] K. Ou, P. Sarnoski, K.R. Schneider, K. Song, C. Khoo, L. Gu, Microbial catabolism of procyanidins by human gut microbiota, *Mol. Nutr. Food Res.* 58 (11) (2014) 2196–2205.
- [41] J.I. Ottaviani, G. Borges, T.Y. Momma, J.P. Spencer, C.L. Keen, A. Crozier, H. Schroeter, The metabolome of [2-(14C)](-)-epicatechin in humans: implications for the assessment of efficacy, safety, and mechanisms of action of polyphenolic bioactives, *Sci. Rep.* 6 (2016) 29034.
- [42] M. Kutschera, W. Engst, M. Blaut, A. Braune, Isolation of catechin-converting human intestinal bacteria, *J. Appl. Microbiol.* 111 (1) (2011) 165–175.
- [43] C. Li, M.J. Lee, S. Sheng, X. Meng, S. Prabhu, B. Winnik, B. Huang, J.Y. Chung, S. Yan, C.T. Ho, C.S. Yang, Structural identification of two metabolites of catechins and their kinetics in human urine and blood after tea ingestion, *Chem. Res. Toxicol.* 13 (3) (2000) 177–184.
- [44] M.M. Appeldoorn, J.P. Vincken, A.M. Aura, P.C. Hollman, H. Gruppen, Procyanidin dimers are metabolized by human microbiota with 2-(3,4-dihydroxyphenyl)acetic acid and 5-(3,4-dihydroxyphenyl)-gamma-valerolactone as the major metabolites, *J. Agric. Food Chem.* 57 (3) (2009) 1084–1092.
- [45] J.I. Ottaviani, C. Kwik-Urbe, C.L. Keen, H. Schroeter, Intake of dietary procyanidins does not contribute to the pool of circulating flavanols in humans, *Am. J. Clin. Nutr.* 95 (4) (2012) 851–858.
- [46] D. Del Rio, A. Rodriguez-Mateos, J.P. Spencer, M. Tognolini, G. Borges, A. Crozier, Dietary (poly)phenolics in human health: structures, bioavailability, and evidence of protective effects against chronic diseases, *Antioxid. Redox Signal.* 18 (14) (2013) 1818–1892.
- [47] R. Llorach, I. Garrido, M. Monagas, M. Urpi-Sarda, S. Tulipani, B. Bartolomé, C. Andres-Lacueva, Metabolomics study of human urinary metabolome modifications after intake of almond (*Prunus dulcis* (Mill.) D.A. Webb) skin polyphenols, *J. Proteome Res.* 9 (11) (2010) 5859–5867.
- [48] J. Hüsch, J. Bohnet, G. Fricker, C. Skarke, C. Artaria, G. Appendino, M. Schubert-Zsilavecz, M. Abdel-Tawab, Enhanced absorption of boswellic acids by a lecithin delivery form (Phytosome®) of Boswellia extract, *Fitoterapia* 84 (2013) 89–98.
- [49] A. Babazadeh, M. Zeinali, H. Hamishehkar, Nano-phytosome: a developing platform for herbal anti-cancer agents in cancer therapy, *Curr. Drug Targets* 19 (2) (2018) 170–180.
- [50] A. Riva, M. Ronchi, G. Petrangolini, S. Bosisio, P. Allegrini, Improved Oral Absorption of Quercetin from Quercetin Phytosome®, a New Delivery System Based on Food Grade Lecithin, *Eur. J. Drug Metab. Pharmacokinet.* 44 (2) (2019) 169–177.
- [51] G.S. Ravi, R.N. Charyulu, A. Dubey, P. Prabhu, S. Hebbar, A.C. Mathias, Nano-lipid Complex of Rutin: Development, Characterisation and In Vivo Investigation of Hepatoprotective, Antioxidant Activity and Bioavailability Study in Rats, *AAPS PharmSciTech* 19 (8) (2018) 3631–3649.
- [52] G. Ermel, S. Georgeault, C. Inisan, M. Besnard, Inhibition of adhesion of uropathogenic *Escherichia coli* bacteria to uroepithelial cells by extracts from cranberry, *J. Med. Food* 15 (2) (2012) 126–134.
- [53] J.P. Lavigne, G. Bourg, C. Combesure, H. Botto, A. Sotto, In-vitro and in-vivo evidence of dose-dependent decrease of uropathogenic *Escherichia coli* virulence after consumption of commercial *Vaccinium macrocarpon* (cranberry) capsules, *Clin. Microbiol. Infect.* 14 (4) (2008) 350–355.
- [54] K. Gupta, M.Y. Chou, A. Howell, C. Wobbe, R. Grady, A.E. Stapleton, Cranberry products inhibit adherence of p-fimbriated *Escherichia coli* to primary cultured bladder and vaginal epithelial cells, *J. Urol.* 177 (6) (2007) 2357–2360.
- [55] A. Turner, S.N. Chen, M.K. Joike, S.L. Pendland, G.F. Pauli, N.R. Farnsworth, Inhibition of uropathogenic *Escherichia coli* by cranberry juice: a new anti-adherence assay, *J. Agric. Food Chem.* 53 (23) (2005) 8940–8947.
- [56] M.L. Porter, C.G. Krueger, D.A. Wiebe, D.G. Cunningham, J.D. Reed, Cranberry proanthocyanidins associate with low-density lipoprotein and inhibit in vitro Cu²⁺-induced oxidation, *J. Sci. Food Agric.* 81 (2001) 1306–1313.
- [57] P. Mena, D. Gonzalez de Llano, N. Brindani, A. Esteban-Fernandez, C. Curti, M.V. Moreno-Arribas, D. Del Rio, 5-(3',4'-Dihydroxyphenyl)-γ-valerolactone and its sulphate conjugates, representative circulating metabolites of flavan-3-ols, exhibit anti-adhesive activity against uropathogenic *Escherichia coli* in bladder epithelial cells, *J. Funct. Food* 29 (2017) 275–280.
- [58] C. Rodríguez-Pérez, R. Quirantes-Piné, J. Uberos, C. Jiménez-Sánchez, A. Peña, A. Segura-Carretero, Antibacterial activity of isolated phenolic compounds from cranberry (*Vaccinium macrocarpon*) against *Escherichia coli*, *Food Funct.* 7 (3) (2016) 1564–1573.
- [59] A.T. Bernal-Mercado, F.J. Vazquez-Armenta, M.R. Tapia-Rodriguez, M.A. Islas-Osuna, V. Mata-Haro, G.A. Gonzalez-Aguilar, A.A. Lopez-Zavala, J.F. Ayala-Zavala, Comparison of single and combined use of catechin, protocathechuic, and vanillic

- acids as antioxidant and antibacterial agents against uropathogenic, *Molecules* 23 (11) (2018).
- [60] D.G. de Llano, A. Esteban-Fernández, F. Sánchez-Patán, P.J. Martínlvarez, M.V. Moreno-Arribas, B. Bartolomé, Anti-adhesive activity of cranberry phenolic compounds and their microbial-derived metabolites against uropathogenic *Escherichia coli* in bladder epithelial cell cultures, *Int. J. Mol. Sci.* 16 (6) (2015) 12119–12130.
- [61] C. Cattò, G. Grazioso, S. Dell'Orto, A. Gelain, S. Villa, V. Marzano, A. Vitali, F. Villa, F. Cappitelli, F. Forlani, The response of *Escherichia coli* biofilm to salicylic acid, *Biofouling* 33 (3) (2017) 235–251.



Design of polymer-based antimicrobial hydrogels through physico-chemical transition

Emanuele Mauri^{a,1}, Davide Naso^a, Arianna Rossetti^a, Elisa Borghi^b, Emerenziana Ottaviano^b, Gianmarco Griffini^a, Maurizio Masi^a, Alessandro Sacchetti^{a,*}, Filippo Rossi^{a,*}

^a Department of Chemistry, Materials and Chemical Engineering "Giulio Natta", Politecnico di Milano, piazza Leonardo da Vinci 32, 20133 Milan, Italy

^b Department of Health Sciences, Università degli Studi di Milano, via Di Rudinì 8, 20142 Milan, Italy

ARTICLE INFO

Keywords:

Antimicrobial
Drug delivery
Hydrogels
Polymer
Rheology

ABSTRACT

The antimicrobial activity represents a cornerstone in the development of biomaterials: it is a leading request in many areas, including biology, medicine, environment and industry. Over the years, different polymeric scaffolds are proposed as solutions, based on the encapsulation of metal ions/particles, antibacterial agents or antibiotics. However, the compliance with the biocompatibility criteria and the concentration of the active principles to avoid under- and over-dosing are being debated. In this work, we propose the synthesis of a versatile hydrogel using branched polyacrylic acid (carbomer 974P) and aliphatic polyetherdiamine (elastamine®) through physico-chemical transition, able to show its ability to counteract the bacterial growth and infections thanks to the polymers used, that are not subjected to further chemical modifications. In particular, the antimicrobial activity is clearly demonstrated against *Staphylococcus aureus* and *Candida albicans*, two well-known opportunistic pathogens. Moreover, we discuss the hydrogel use as drug carrier to design a unique device able to combine the antibacterial/antimicrobial properties to the controlled drug delivery, as a promising tool for a wide range of biomedical applications.

1. Introduction

In the last years researchers have strongly focused their efforts in the development of antibacterial and antimicrobial materials. Although the study of antimicrobial field dates back about one hundred years, the design of polymeric systems able to exhibit efficient inhibition of bacterial infections is a discussed and thriving technology, that has become pivotal not only in biological fields, hospital and healthcare environments, but also in laboratory, marine and some industrial applications [1–4]. The direct use of antibiotic agents could be the approach to counteract many infections, but the main constraints are related to the potential environmental toxicity, the bacterial resistance, the short-term antimicrobial activity and the proteolytic instability and degradation [5,6]. In addition, conventional antibiotics show problems about the solubility and overdose concentration range [7–9]. Therefore, the design of a biocompatible and efficient therapeutic delivery system, which can satisfy both the cytotoxicity issues and the antimicrobial criteria, is in high demand. Moreover, in biomedical applications, the loading of drugs or other active molecules over this kind of substrate represents a challenge to maximize the performance of the therapeutic

cargo without inflammations and secondary side-effects during the medical treatment [6,10,11]. Scientific literature suggests different advanced antibacterial materials combining metal ions, natural compounds and modified polymers [12–14]. Among them, hydrogels are extensively studied as an alternative and promising tool due to their key properties. Defined as three-dimensional (3D) scaffolds composed by the chemical or physical entanglement of natural and/or synthetic polymer chains, hydrogels appear as suitable materials counteracting the microbial effects thanks to their biostability, biocompatibility and biomimetic physico-chemical properties, including swelling behavior [15,16]. Different strategies have emerged to develop hydrogels for antimicrobial applications: through the adsorption of antimicrobial agents [17,18], the encapsulation of metal particles or polycationic groups [19–22], the material modification with covalent linkers to graft antibacterial peptides or synthetic compounds [23–25].

The use of metal nanoparticles, involving silver, gold, copper, zinc oxide, has to overcome two main constraints: the first one related to a high spatial dispersion to avoid the agglomeration within the gel scaffold, the second one about the compatibility and satisfying combination of an inorganic component with an organic environment [12,26].

* Corresponding authors.

E-mail addresses: alessandro.sacchetti@polimi.it (A. Sacchetti), filippo.rossi@polimi.it (F. Rossi).

¹ Present address: Department of Engineering, Università Campus Bio-Medico di Roma, via Alvaro del Portillo 21, 00128 Rome, Italy.

Alternatively the chemical modification of antimicrobial agents through covalent bonds, exploiting the peptides amino and carboxyl terminal groups [27,28], offers many advantages to achieve long-term antimicrobial activity, but with a special attention towards their structural integrity [29,30]. All these considerations could be skipped through the proposal of a hydrogel able to show antimicrobial features thanks to the starting polymers used in the sol/gel synthesis, without any further additions of antibacterial peptides, antibiotics or metal derivatives. In this work, we propose the synthesis of antimicrobial hydrogels via physico-chemical transition using two polymers: branched polyacrylic acid (carbomer 974P) and aliphatic polyetherdiamine (elastamine®). The simple synthesis approach and the lack of compliance problems related to the biocompatibility and antimicrobial molecule dosage dependency in the final applications qualify this hydrogel able to conquer the vast issue of the traditional therapies and its promising application also in industrial fields. Finally, we have tested this hydrogel as a controlled drug delivery system. In the first case-study, we have considered the release kinetics of two drug-mimetics: fluorescein sodium salt (SF) and rhodamine B (RhB) (commonly used as mimetic drugs [31]), entrapped by steric hindrance within the network meshes. In the second case-study, we have investigated the effect of a cleavable linker between the mimetic drug and the polymeric network using polyethylene glycol (PEG) modified ester to graft RhB: the cleavability of the ester linker allows a more prolonged and sustained drug release over time. These results show the promising use of the synthesized hydrogels not only in the antimicrobial field, but also as a therapeutic tool for the delivery and controlled release of active agents in biomedical applications, providing a potential solution to the design of a tool able to combine antibacterial/antimicrobial and therapeutic care.

2. Materials and methods

2.1. Materials

Hydrogel synthesis was performed using: carbomer 974P (MW \cong 1 MDa, Fagron, The Netherlands) and elastamine® RE-2000 amine (MW = 2 kDa, Huntsman Corporation, Italy) as polyetherdiamine. Polyethylene glycol (MW = 8 kDa) and all other chemicals involved in this work were purchased from Merck (Merck KGaA, Darmstadt, Germany). The materials were used as received, without further purification. Solvents were of analytical laboratory grade. Synthesized products containing fluorescein sodium salt or rhodamine B were stored at 4 °C in dark, until their use.

2.2. Synthesis of physical hydrogels

The first step of the hydrogel design concerns the synthesis of the physical polymeric network. Carbomer 974P (140 mg, 1.94 mmol of COOH) and elastamine (1200 mg, 1.2 mmol of NH₂) were independently dissolved in distilled water (respectively, 1.5 mL for carbomer and 8.5 mL for the polyetherdiamine). The resulting solutions were separately loaded into two syringes and the latter connected through a syringe mixing tube. Then, the polymeric solutions were mixed together for 2 min to obtain a homogeneous system. The physical mixture, representing the physical gel system, was placed in steel cylinders (0.4 mL each and with the cylinder diameter of 1.1 cm) and frozen at -20 °C. Lastly, the molds were taken off and the final physical hydrogel configuration was obtained coming back to room temperature (r.t.). Referring to their nature, these hydrogels will be referred as phys-HG.

2.3. Synthesis of chemical hydrogels via physico-chemical transition

Physical hydrogels were freeze-dried and then subjected to microwave irradiation (500 W) for 25 min to induce the direct amidation of carbomer carboxyl groups with elastamine terminal -NH₂, that gave

rise to the formation of covalent linkers in the 3D hydrogel network. In this way, the microwave-assisted reaction allowed the transition from physical to chemical polymeric matrix. The resulting physico-chemical hydrogels (hereafter labeled chem-HG) were cooled down to r.t. and then stored at 4 °C.

2.4. Characterization techniques

2.4.1. FT-IR analysis

FT-IR spectra were recorded using a Thermo Nexus 6700 spectrometer coupled to a Thermo Nicolet Continuum microscope equipped with a 15 × Refflachromat Cassegrain objective, at room temperature in air in the 4000–500 cm⁻¹ wavenumber range with 64 accumulated scans and at a resolution of 4 cm⁻¹, using the KBr pellet technique for all samples.

2.4.2. Rheology

Hydrogels rheological properties were evaluated using a Rheometrics DSR200 rheometer with a 25 mm plate-cone configuration at 30 °C. Dynamic stress sweep (DSS) tests were performed in the range 5–300 Pa, at 1 Hz. The oscillatory responses (*G'*, elastic modulus and *G''*, loss/viscous modulus) were determined at low values of strain over the frequency range 0.1–100 Hz. The pseudoplastic behavior was also investigated. The behaviors of shear stress and viscosity as a function of shear rate were examined and the linearity of the viscoelastic properties was verified.

2.4.3. Swelling behavior

Physico-chemical hydrogel swelling was studied in distilled water, buffer phosphate saline (PBS) solution, at pH = 10 and at pH = 3. The first two conditions resemble a physiologic-like environment with a focal point related to the potential influence of salts in the responsive swelling behavior; the basic and acid environment mimic the conditions of inflammatory disorders. After the microwave-assisted synthesis, the hydrogel samples were weighed (*W_d*) and poured into an excess of the corresponding neutral, alkaline or acid aqueous solution to achieve the complete swelling at 37 °C under a 5% CO₂ atmosphere. Gravimetric measures were recorded to estimate the swelling kinetics: the samples were removed from the aqueous solution at fixed time points (range 1 h–300 h) and the surfaces were wiped with moistened filter paper in order to remove the excess solution, then they were weighed (*W_t*). The swelling ratio (*Q_m*) was calculated according to the following equation:

$$Q_m = \frac{W_t - W_d}{W_d} \cdot 100 \quad (1)$$

W_t represents the weight of the wet hydrogel as a function of time, and *W_d* is the weight of the dry sample.

2.4.4. Scanning electron microscope (SEM) analysis

Environmental SEM analysis was performed on gold sputtered samples at 10 kV with Evo 50 EP Instrumentation (Zeiss, Jena, Germany). To preserve the morphology of the physico-chemical hydrogel under complete swelling, freeze-drying (for 24 h) was applied to remove all the liquid phase by sublimation. Due to the low operating values of temperature and pressure, the polymer chains were expected to retain the same conformation they had in wet conditions. Evaluations of the superficial and internal morphology of the investigated chem-HG samples (triplicate) were carried out.

2.4.5. UV/vis spectroscopy

The drug release studies were conducted through the evaluation of SF and RhB absorbance. It was measured by Tecan® Microplate Reader with UV/vis spectroscopy applying the Lambert–Beer method.

2.5. Antimicrobial analysis

Hydrogels were placed in a 24-well-plate and sterilized under UV light for 30 min. The reference strain *Staphylococcus aureus* ATCC 6538 and *Candida albicans* SC5314 were used for *in vitro* assays. Before each test, microbial strains were thaw from glycerol stock stored at -80°C by seeding them on fresh Trypticase soy agar (TSA, for *S. aureus*) or Saboraud Dextrose agar (SAB, for *C. albicans*) and culturing them for 24 h at 37°C . A single colony was harvested in phosphate buffer saline (PBS) to obtain a 0.5 McFarland suspension (corresponding to about 10^8 CFU/mL for *S. aureus* and 10^6 CFU/mL for *C. albicans*). Serial dilutions were then performed in Trypticase soy broth (TSB, for *S. aureus*) or RPMI 1640 medium (for *C. albicans*) until the desired concentration (10^4 – 10^5 CFU/mL, respectively). Two ml of the suspension were added drop-by-drop to hydrogels, allowing gradual absorption. Positive growth controls, consisting of *S. aureus* ATCC 6538 and *C. albicans* SC5314 cultured without hydrogels, were run in parallel. After 24 h incubation at 37°C , both supernatant and hydrogels were collected in 50-mL tubes containing 18 mL of PBS and vigorously mixed to harvest microbial cells for CFU counting. Plates were incubated at 37°C and colonies were counted after 24 h of growth.

2.6. Drug loading within hydrogels

The drug mimetic loading was performed by adding SF or RhB in the phys-HG synthesis step. SF is a sodium salt like several drugs already listed and in water it is dissociated into fluorescein anion and sodium cation [32], whereas RhB is a neutral molecule at $\text{pH} = 7.4$ and slightly positive at acidic pH [33,34]. In details, regarding SF studies, the traceable molecule (10 mg) was dissolved into the elastamine solution (1.5 mL) to obtain a SF concentration of 6.67 mg/mL; consequently, the resulting mixture was mixed with carbomer solution (8.5 mL) using the syringe mixing tube technique. Then, the gelling system was poured into steel cylinders (0.4 mL), frozen and lyophilized as discussed in the previous sections, and finally treated with microwave irradiation to obtain the final chem-HG containing SF. The final concentration of the drug mimetic was recorded 1 mg/mL. The same approach was developed to synthesize hydrogels encapsulating RhB: in this case, the RhB concentration in elastamine solution was 1 mg/mL due to the water solubility constraints [35–37], and the final concentration in the chem-HG was calculated equal to 0.15 mg/mL.

2.7. Synthesis of hydrogels with drug modified ester

The study of the antimicrobial hydrogels as tunable drug delivery systems characterized by a cleavable RhB linkage was planned using a chemoselective functionalized PEG with ester bond grafting RhB, synthesized in our previous work [38]. Following a procedure similar to the one discussed in the SF and RhB loading by steric hindrance, PEG modified ester-RhB (32 mg) and elastamine (960 mg) were dissolved in distilled water (1.2 mL) and then mixed with the carbomer aqueous solution (112 mg in 6.8 mL of distilled water) using the two syringes and the mixing connection-tube.

Then, the resulting homogeneous mixture was partitioned in 0.4 mL in each steel cylinder, freeze-dried and subjected to the electromagnetic stimulation by microwave (25 min) to give rise to the final amide-based hydrogel scaffold. These hydrogels are named chem-HG-ester-RhB, with regard to the presence of the cleavable linker between the mimetic drug and the polymeric network.

2.8. In vitro drug release

Chem-HG entrapping SF and RhB and chem-HG-ester-RhB were individually submerged in 2 mL of water-based solution (physiologic pH) and stored at 37°C , under a 5% CO_2 atmosphere. At defined time points, for each sample, a volume of 100 μL was collected and poured

into a 96-wells plate; each withdrawal was made in triplicate, removing overall 300 μL . The aliquots were used in UV/vis measurements and they were substituted in the release media with 300 μL of distilled water in order to keep the volume invariable and preserve the diffusion regime. The SF and RhB released amounts were respectively measured via spectrophotometer at $\lambda = 485$ nm and $\lambda = 570$ nm and quantified referring to the standard calibration curve of the two drug mimetics. The percentage of the released molecule was defined as the ratio of the released absolute amount in the aqueous media to the sum of the total amounts of the released and unreleased SF or RhB. Three samples per type were used in this experimental procedure and the results were averaged.

2.9. Statistical analysis

The experimental data related to swelling behavior and drug release were analyzed using Analysis of Variance (ANOVA). Statistical significance was set to p value < 0.05 . The results are presented as mean value \pm standard deviation.

3. Results and discussion

3.1. The role of the physico-chemical transition

The proposed hydrogel synthesis protocol takes advantages of the chemical structure of the raw polymeric materials to define the optimal configuration of a 3D stable and biocompatible scaffold. The intermediate physical hydrogel represents a key point for the adequate spatial orientation, mobility and distribution of the polyacrylic acid and elastamine chains. In addition, it provides the condition to form stable covalent cross-linking in solid phase, without the use of any solvent. Carbomer is a branched polyacrylic acid characterized by side-chain carboxyl groups that cause the formation of a gel-like solution, according to the increased viscosity, when the polymer is dissolved in water. The resulting high viscous consistency is correlated to the carbomer ability to absorb and retain water; the polymer chains are involved in the interactions with the water self-ionization that provides hydroxide and hydronium ions: $-\text{COOH}$ are deprotonated and the formation of carboxylate anions occurs. Carbomer also shows anti-inflammatory properties and high biocompatibility in therapeutic application and tissue engineering [15,39,40]. Used elastamine is a water soluble polyetherdiamine formed by propylene oxide and ethylene oxide, with terminal-chain primary amine groups; it is able to increase the hydrophilicity and the flexibility of the final material. In water, elastamine can be protonated, resulting in $-\text{NH}_3^+$ terminal groups. When the polymer aqueous solutions are mixed with each other, the presence of anions and cations promotes ionic interactions, with a further viscosity increase and the formation of a physical gel system. The electrostatic bonds are the cause of the 3D carbomer-elastamine entanglement but, due to their nature, they can be easily disrupted when the hydrogel is submerged in water or PBS solution, because the added ions interfere with the physical gel cross-linking and the structure simply dissolves.

For these reasons, the freeze-drying approach allows preserving the hydrogel structure and the subsequent microwave irradiation ensures the formation of covalent bonds, only exploiting the carboxyl and amine moiety, that represent strong interconnections of the polymeric meshes. The transition from physical to chemical regime occurs in solid-state without the introduction of any solvent, polymer chain functionalization or specific/critical experimental conditions and is the keystone for the design of biocompatible antimicrobial scaffolds without introducing tailored antibacterial molecules (the use of which would require additional synthesis steps, cost or care). A schematic representation of the discussed strategy and the putative structures of the physical and chemical (with amidic bonds) hydrogels are illustrated in Fig. 1.

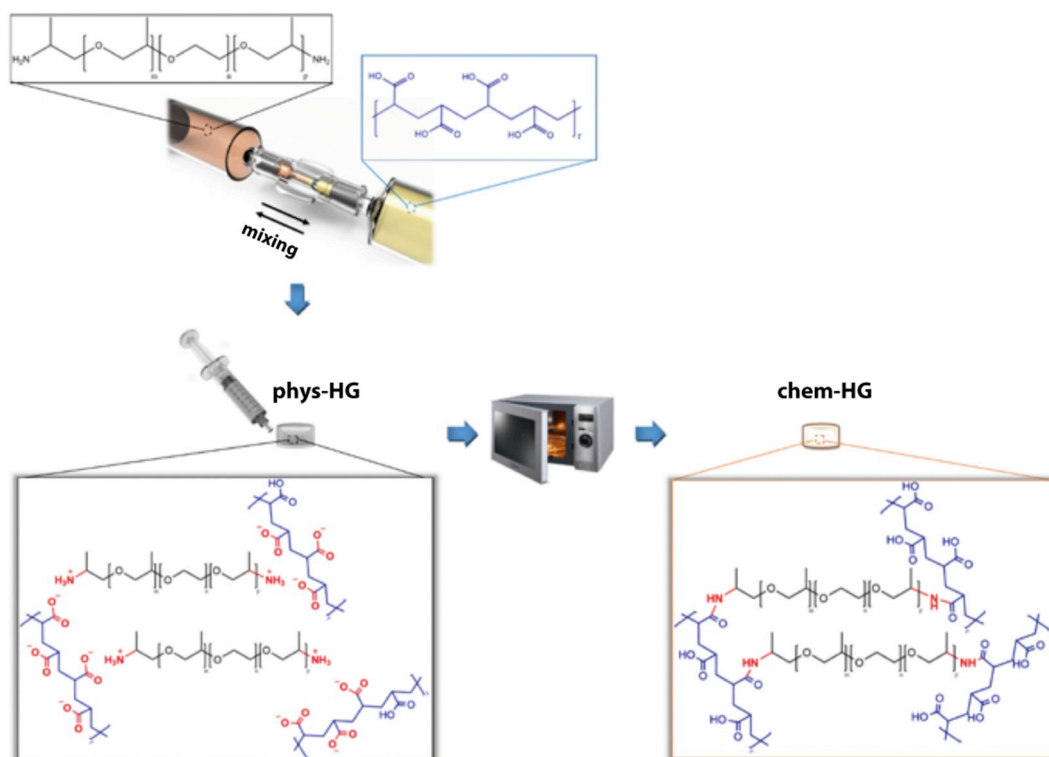


Fig. 1. Scheme of hydrogel synthesis exploiting the physico-chemical transition. In red are highlighted the electrostatic interactions between the ionic groups of carbomer and elastamine to give rise to phys-HG and the amidic bonds to form the crosslinked scaffold of chem-HG. (For interpretation of the references to color in this figure legend, the reader is referred to the web version of this article.)

The use of polyetherdiamines is detected in biomedical applications due to its *in vitro* and *in vivo* biocompatibility. For example, Javan and coworkers [41] introduced a jeffamine chemical functionalization in hyaluronic acid-based hydrogels to formulate a prolonged and sustained drug release and reduce the number of hydrogel injections: *in vivo* studies showed the efficiency of this material thanks to the improved biocompatibility and no signal of cell viability reduction. Similar biocompatibility aims were achieved in other works: the jeffamine was used as monomer to preserve some physico-mechanical properties, blood compatibility and cargo release [42–45], as copolymer with acrylamides derivatives to design 3D scaffolds able to modulate the lower critical solution temperature (LCST) and internalize cells [46] or as cross-linker to satisfy the no-cytotoxicity criteria [47]. However, the evaluation of the polymer antimicrobial features and the design of a 3D scaffold able to preserve them is not widely investigated.

3.2. Material characterization

Amidic bonds are demonstrative of the intermolecular association between carbomer and elastamine chains and the formation of a chemical network. Especially in the amidation reactions, the use of microwave irradiation is defined as a comfortable technique compared to the common way of synthesis [48,49]. The main benefits of microwave-assisted polymer synthesis are the reduced reaction time, the absence of organic solvents, the limitation of side reactions and the removal of unreacted species. In this work, the direct irradiation of polyacrylic acid and amine groups was efficient enough to obtain the desired product in a high yield after a short reaction time. The chemical characterization of the hydrogel was performed through FT-IR analysis. Moreover, the FT-IR spectroscopy could also provide information about the amide formation, noting the evolution of the corresponding absorption band. In this way, it was possible to draw the conversion-time chart at different time points.

Fig. 2 shows the FT-IR spectra of phys-HG (A) and chem-HG at fixed

time points ($B = 5$ min, $C = 15$ min, $D = 25$ min). In all spectra the polymers characteristic bands are detectable: with regards to carbomer, the wavenumbers range $3650\text{--}3300\text{ cm}^{-1}$ shows the stretching vibration of --OH residual groups, at 2950 cm^{-1} the C--H chain stretching is recorded, whereas the C=O stretching band is detectable around 1655 cm^{-1} . The --CH_2 narrow peak is visible at $1435\text{--}1300\text{ cm}^{-1}$ and the signal at 1256 cm^{-1} is associated to the C--O vibrations [50,51]. The elastamine polyether backbone (C--O--C) is well visible around 1100 cm^{-1} (symmetric and asymmetric stretching [52]) and the C--H stretch is around 2870 cm^{-1} , whereas the amine end groups are recognizable as weak signal at 3225 cm^{-1} . The other signals in the wavenumber range $1500\text{--}500\text{ cm}^{-1}$ are generally related to combination of vibrations, bending, scissoring and deformation of --CH_2 and --CH_3 moieties [53].

The amide bond (*) is clearly detectable at 1713 cm^{-1} : in particular, chem-HG FT-IR spectra show the signal increase at different time points, confirming the reaction between carboxyl and amine groups. According to this trend, amide formation could be evaluated over time as percentage of covalent bond within the hydrogel scaffold [54]. The appearance of the peak at 1713 cm^{-1} , which does not exist in the samples before microwave irradiation, was used to evaluate the conversion. The peak at 1100 cm^{-1} was chosen as an internal standard because representative of an invariant and well-defined group (elastamine polyether chains) and all spectra were signal-normalized to this reference. Absorbances were correlated to the IR peak intensity and the conversion of the reactive groups to amide was determined by the Lambert–Beer law [55,56] from the normalized changes of absorbance at 1713 cm^{-1} (A_{am}) scaled to the elastamine area at 1100 cm^{-1} (A_{ref}), as reported in Eq. (2) (Supporting Information):

$$\alpha_{\%} = \frac{A_{\text{am}}}{A_{\text{ref}}} \cdot 100 \quad (2)$$

where with $\alpha_{\%}$ the amount of formed bond was indicated. It was experimentally evaluated that not all the elastamine was involved in the

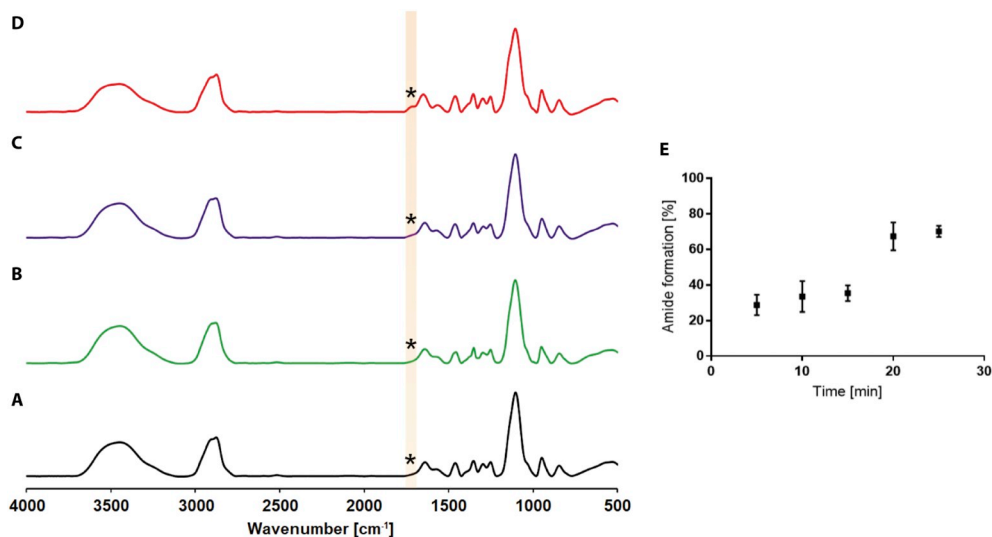


Fig. 2. FT-IR spectra of hydrogel during the microwave-assisted physico-chemical transition, at different time points: phys-HG (A), 5 min of microwave irradiation (B), 15 min of microwave irradiation (C) and 25 min of microwave irradiation (D) corresponding to final chem-HG; (E) plot of amide bond formation over time.

reaction, but only the 72.5% (Supporting Information): as a consequence, the obtained amide bond percentage was calculated and reported in the plot according to this consideration. The performed investigation showed that our hydrogels were characterized by covalent bonds, but the presence of residual elastamine amine groups (that is the limiting reagent) indicated continuing electrostatic interactions between $-\text{COOH}$ and $-\text{NH}_2$. For this reason, we classified the final network as physico-chemical hydrogel and we previously discussed the physical to chemical transition step. The amide formation trend (Fig. 2, pointed out in yellow) highlights a progressive microwave-assisted reaction, with a slow increase in the range 5–20 min (from 28% to 35.5%) and the achievement of the final polymer interconnections at 25 min (72.5%).

This behavior could be explained considering the hydrogel structure and the microwave mean free path: at first, the reaction occurred at the phys-HG surface, then the irradiation was able to achieve the functional groups inside the meshes and gave rise to covalent linkages in the inner core. In addition, the samples were subjected to the electromagnetic stimulation for further periods of time but, as showed, already at 30 min the reaction did not move forward (71.2%), indicating the achievement of an amide formation plateau; with longer times, the hydrogel underwent thermos-oxidative degradation and collapsed.

3.3. Hydrogel physical properties

Rheological studies were carried out to characterize the elastic/viscous hydrogel behavior. In particular, a comparison between the rheology of phys-HG and chem-HG was conducted in order to investigate the potential effect of the microwave irradiation and the physico-chemical transition in the network. The obtained data are showed in Fig. 3.

The storage modulus G' was found to be approximately one order of magnitude higher than the corresponding loss modulus G'' both in phys-HG and in chem-HG samples, with a frequency-dependent behavior at low frequencies: physical gels were characterized by $G' = 1490$ Pa and $G'' = 372$ Pa at 10 rad/s and by $G' = 780$ Pa and $G'' = 145$ Pa at 0.1 rad/s, whereas the amide-based samples recorded a variation of G' from 5160 Pa to 4380 Pa and G'' from 545 Pa to 680 Pa, in the same frequency sweep. The marked phys-HG storage modulus trend is detectable in colloidal gels and it is indicative of the physical nature and interconnections [57,58]; instead, G' in chem-HG exhibits frequency dependence only at low frequency values, below 0.5 rad/s, which may be indicative of a reduction of the physical macromolecular interchain

interactions and of the viscoelastic response of the system, matching the typical characteristic signature of a solid-like gel. The different order of magnitude observed for G' and G'' is also indicative of an elastic rather than viscous material. Moreover, the corresponding G' and G'' values in chem-HG are higher than in phys-HG, pointing out the elastic property and the improved stiffness due to the amide cross-linking. Through DSS test, the crossover strain can be evaluated as the value at which the contribution of the material damping $\tan(\delta)$ is predominant with respect to G' . At low values of strain, the G' trends of phys-HG (Fig. 3B) and chem-HG (Fig. 3C) indicate a network of packed polymeric chains and the correlation with $\tan(\delta)$ confirmed for both hydrogels liquid-like behaviors rather than a solid-like nature. Moreover, the intersection of G' and G'' occurs at lower values in chem-HG than in phys-HG (at shear stress $\tau = 131$ Pa and $\tau = 345$ Pa) indicating more stiffness in the chemical network according to the presence of both amide and electrostatic cross-linking that probably create preferential break-lines compared to the physical gel under the same strain [59]. One hydrogel distinctive feature is the ability to retain high amount of water.

The hydrogel swelling occurs due to the polymer chain stretching during the exposure to aqueous solvents, counterbalanced by an elastic force acting in the opposite direction generated by increasing the elongation of the system. Chem-HG swelling behavior was investigated in distilled water and in PBS solution and the results are reported in Fig. 4A.

The same study was not feasible for phys-HG because in aqueous environment the physical bonds between carboxyl and amine groups became weaker due to the auto-dissociation of water or the addition of salts (PBS) that interfered and dissolved the gel in < 30 min (data not shown). The experimental results suggest that chem-HG exhibited fast swelling kinetics and their swelling equilibrium was reached within 4 h. Moreover different swelling ratios were recorded in water (about 900%) and in PBS solution (375%).

The changed behavior in PBS could be considered related to the increased ionic strength and so ionic interactions between the salts and the polymeric chains: PBS dissociation is able to generate interactions with the oxygen and carboxyl moieties creating physical bindings that move closer the polymeric chains and result in a mesh reduction. This effect was not observed in samples immersed in distilled water: the amount of entrapped water was higher and limited only by the chains elongation and the cross-linking points. In summary, in both cases hydrogel swelling behavior was expressed, preserving the peculiar feature of the polymeric network and the presence of saline solution could affect the behavior due to the physico-chemical nature of the

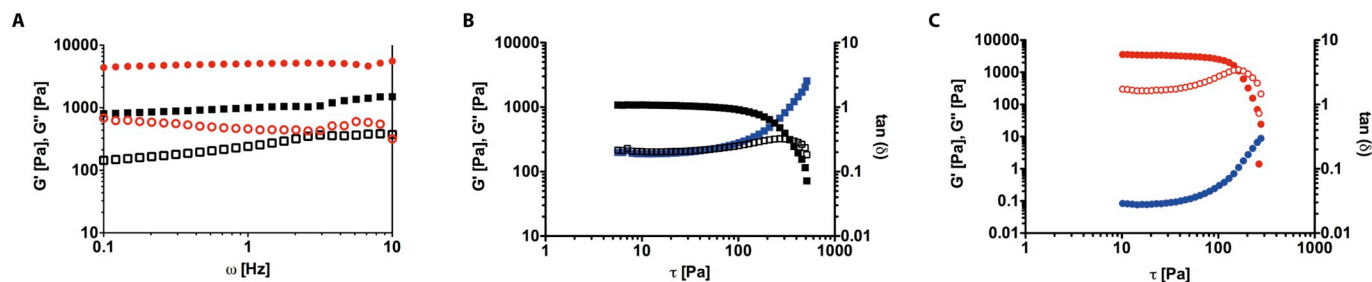


Fig. 3. Rheological behavior of phys-HG (G' ■ black, G'' □ black, $\tan(\delta)$ ■ blue) and chem-HG (G' ● red, G'' ○ red, $\tan(\delta)$ ● blue) samples. (A) G' and G'' trends in frequency range 0.1–10 Hz; (B) crossover point in phys-HG; (C) crossover point in chem-HG. (For interpretation of the references to color in this figure legend, the reader is referred to the web version of this article.)

system. Considering the potential application in conditions dissimilar from the neutral ones, the swelling studies were also performed in acid and alkaline environments; pH = 3 is representative of gastric conditions, whereas alkaline pH is indicative of pancreatic environment and fluid (pH = 8.8) [60,61]. Moreover, the study of hydrogels in low and high pH represents an approach to produce materials potentially useful for chronic wounds [62,63], for the re-alkalization of carbonated materials [64], for antitumoral administrations or to counteract undesired pH changes [60]. In this work, the swelling evaluation was conducted at pH 3 and 10 (Supporting Information) and compared the hydrogels state once they reached the equilibrium to the physiologic pH 7.4. Fig. 4B illustrates the hydrogel swelling after 48 h: at acid pH the recorded value was 445%, whereas in alkaline system was around 600%. Both conditions exhibited lower swelling than in samples treated with distilled water and this could be explained considering the ions at stake. The polyacrylic acid pK_a is reported to be 4.7 [65]. When the pH was less than pK_a of PAA, the H^+ ionic strength was high and able to suppress the ionization of the carboxylic acid groups; as result, carbomer neutral chains were rather flexible due to their compact conformation [66].

The principal acid pH effect is related to the formation of hydrogen bindings (van der Waals forces) in the elastamine polyethoxylate moiety that reduces the mean free space among the elastamine and carbomer chains; as a result, a reduction of hydrogel meshes occurs and the swelling appeared reduced than in water. At pH = 10, the same effect of net mesh sizes constraint is due to the Na^+ (alkaline conditions are performed using NaOH 1 M) interactions with carbomer carboxylate ions. In all experimental procedures, hydrogel scaffolds were able to preserve their structural integrity over the investigated time. The morphology of the chem-HG was also investigated through SEM analysis, as reported in Fig. 5.

The results revealed that dried samples possess a highly entangled structure, with small and big pores in the diameter range 70–270 μm , that seem to define a sponge-like state. In addition, most of the pores

are interconnected. This demonstrates their microscopic porous structure with a complex 3D construction.

3.4. Antimicrobial results

For this study, we used *S. aureus* and *C. albicans* as representative of biofilm-producing organisms and opportunistic pathogens. Both microorganisms were grown adsorbed on hydrogels. The *in vitro* assay revealed the chem-HG to be the most effective in microbial inhibition. Indeed, after 24 h incubation (Fig. 6), we observed a dramatic inhibition of *S. aureus* growth (> 99% reduction in CFUs count, $p = 0.0159$) and a significant reduction (about 30%, $p = 0.015$) for *C. albicans*, compared with controls (growth in absence of hydrogels).

3.5. Drug release

Once demonstrated the antimicrobial property of the synthesized hydrogels, their application as drug carriers was studied. The aim is the approval of the fundamental controlled drug delivery principles and offering the potential combination of therapeutic curative and sterile effects in only one scaffold.

The developed method is based on the evaluation of mimetic drugs release considering the steric hindrance or using a cleavable ester linker that temporarily graft the molecule to the hydrogel. Release studies were performed at 37 °C, at physiologic pH that mimic the classic *in vitro* and *in vivo* environment. As previously assessed, SF was chosen to represent the behavior of drugs in salt form, able to dissociate in anions and cations in aqueous system, like corticosteroids and anti-inflammatory drugs [31,67], whereas RhB resembles the characteristics of carbonyl-based drugs as those involved in the treatment of cancer or spinal cord injury [15,68,69].

3.5.1. Release by steric hindrance

SF and RhB were loaded within the hydrogels during the physical

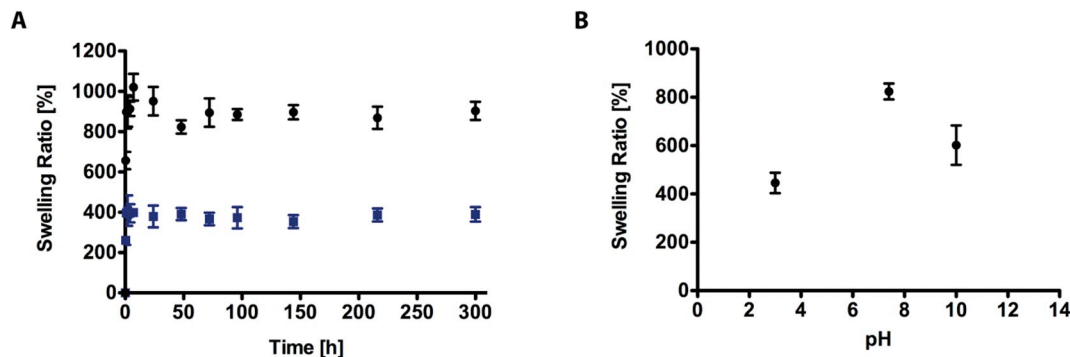


Fig. 4. (A) Swelling behavior of hydrogels in distilled water (●, black) and in PBS solution (■, blue). (B) Swelling trend of hydrogels at different pH values: 3 (acid), 7.4 (physiologic) and 10 (alkaline). The swelling data are recorded to 48 h. (For interpretation of the references to color in this figure legend, the reader is referred to the web version of this article.)

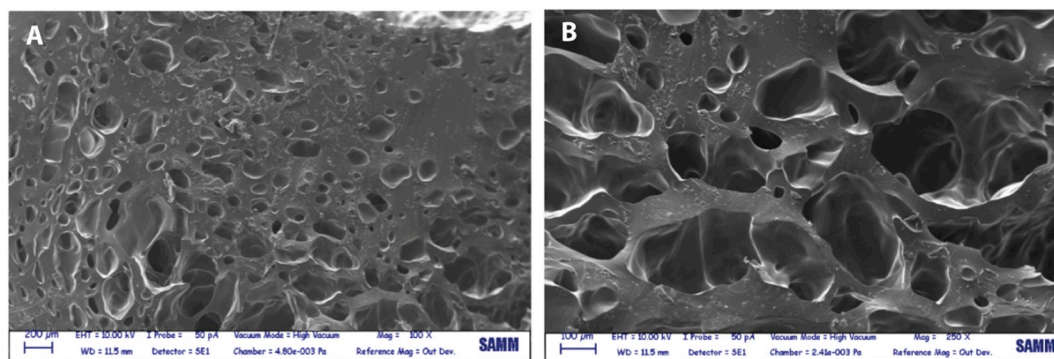


Fig. 5. SEM images of chem-HG hydrogels after freeze-drying at amplification 100 \times (A) and 250 \times (B).

formation of the 3D network. The different drug concentrations are evaluated according to the general concentration range proposed in hydrogels field and the solubility limit in water. However, the percentage drug release depends on drug concentration gradient generating the diffusion flow and it was normalized respect to the mass loaded (percentage), so that the kinetics became concentration independent [70]. The percentage of SF and RhB released was defined as the ratio between the released amount in the aqueous media and the total amount entrapped by steric hindrance within the hydrogel. Fig. 7 shows the SF and RhB release profiles at pH values 7.4 (A, D), 3 (B, E) and 10 (C, F).

Considering the neutral release environment, SF release is faster than RhB in the first hours (after 48 h, the percentage of released SF is 80%, whereas for RhB 60%) and similar amounts of released drug are recorded only after 250 h. The different trends are related to the electrostatic and ionic interactions with the polymer chains: the presence of fluorescein anions causes repulsion with the dominant carboxylate moieties and the mimetic drug comes out from the meshes more quickly than RhB, which is neutral.

These repulsive effects overlap the attractive interaction between residual amine groups and the fluorescein anion. SF indeed is present in salt form at basic pH and its solubility is higher respect to acid and neutral pH. Salt form of SF resembles the behavior of many drugs saled in salt form like ibuprofene and ketoprofene. On the other hand, the RhB delivery rate is minimally influenced by the scaffold. In both cases, the hydrogels are able to sustain drug release, without introducing any polymeric modification. The influence of the system in delivering SF or RhB can be evaluated plotting release percentage against time square root, as showed in Fig. 7D. A linear plot is indicative of Fickian diffusion and the y-axis intercept value is indicative of the burst release. The condition of ideal controlled release system is characterized by linear trend during time and its y-axis intercept equal to zero [31,71]. Both RhB and SF release highlight linear trends in the first 8 h, approaching then plateau trends. The SF burst release value is higher (40%) than

RhB (19%) according to the SF ionic interactions with the polymeric scaffold that facilitates the quick release of small hydrophilic molecules in the aqueous medium; on the other hand, the ability to control the drug release is slightly improved in the RhB case due to the absence anion-cation interactions. The drug releases in acid and basic conditions are characterized by different trends, compared to pH 7.4. In particular, at pH 3 RhB release profile is faster and it is almost completed after 72 h, while the escaped SF is 33% at the same time point suggesting a prolonged release over a longer period of time. In this condition, the high concentration of H⁺ in the release medium counteracts the negative charge of carboxyl groups reducing the repulsion against fluorescein anions and promoting the attractive effect related to the elastamine protonation: as result, the SF release is delayed. The same electrostatic re-organization occurs in sample containing RhB, but the mimetic drug is characterized by a slightly positive charge at pH 3 and the repulsion with the polymeric scaffold encourages a modest enlargement of the meshes and a quick release of drug molecules. In alkaline aqueous medium, the release profiles are reversed: SF comes out faster than RhB, due to the high repulsion between the drug anions and the carboxylate groups.

As discussed in the evaluation of hydrogel swelling behavior, the presence of COO⁻ allows the elongation of the polymeric chains increasing the free spaces in the scaffold and the improved release of the loaded drug. This also explains the increased amount of released RhB compared to the corresponding study at pH 7.4, considering that RhB is neutral at basic pH and no ionic interactions arise. The linear plots at pH 3 and 10 show that the Fickian diffusion regime is well visible in the first 8 h, then the drugs release reaches a plateau. In particular, at pH 3, the SF burst release contribution is extremely small (1%) suggesting the ability of the synthesized gels to control the release of salt form-drugs in acid conditions. This effect is less visible in the RhB samples, where the burst release value is about 20%. In alkaline environment these release behaviors are reversed: RhB presents 15% of burst release (comparable to the neutral release environment), whereas SF about 36%. The RhB

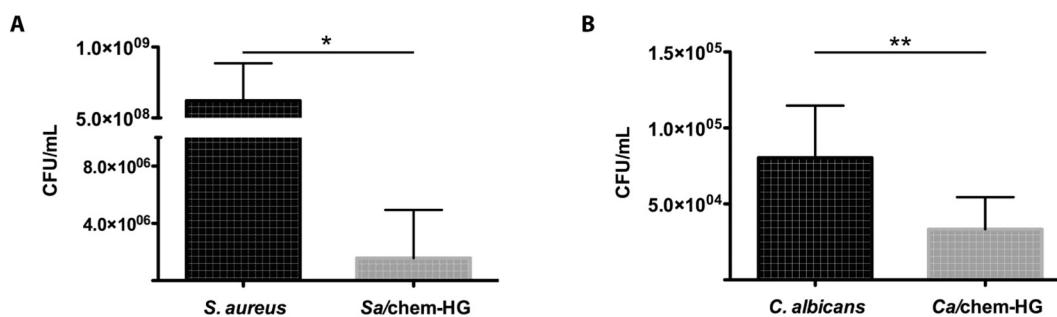


Fig. 6. Microbial growth-inhibition activity of chem-HG hydrogel. Colony-forming units of (A) *S. aureus*; or (B) *C. albicans*, after 24 h incubation in either TSB or RPMI media, respectively. Black bars represent growth controls (without hydrogel); grey bars show microorganisms grew in the presence of chem-HG hydrogel. Values represent the mean of two independent experiments for each strain. Pairwise lines denote statistical significance; * $p < 0.05$; ** $p < 0.01$.

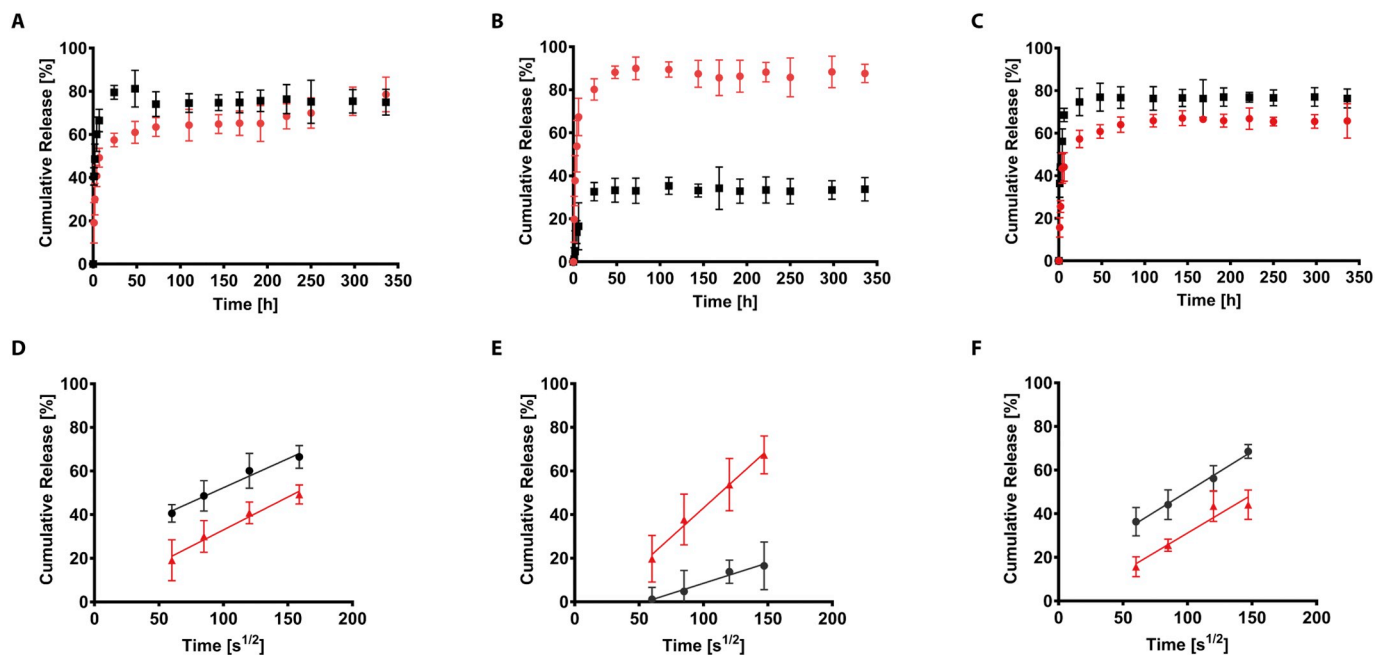


Fig. 7. *In vitro* release profile of RhB (•, red) and SF (•, black) delivered from hydrogels at pH 7.4 (A), pH 3 (B) and pH 10 (C). The slope of the rhodamine and sodium fluorescein release from the hydrogel scaffold is plotted against the square root time at pH 7.4 (D), pH 3 (E) and pH 10 (F): it is representative of the Fickian diffusion coefficient of the drug in the gel system ($p < 0.0001$ between all the groups). The diffusion-controlled release is affected by the pH value and the nature of the mimetic drug. The values are calculated as a percentage with respect to the total mass loaded (mean value \pm standard deviation is plotted). (For interpretation of the references to color in this figure legend, the reader is referred to the web version of this article.)

non-ionic nature allows a drug release not affected by the chemical behaviors of the carbomer and elastamine, which otherwise tune the SF escape from the network meshes.

3.5.2. Release by ester hydrolysis

These hydrogels were also tested as tunable drug delivery systems through the introduction of PEG carrying RhB through ester bond. The choice of a modified polymer instead of the direct chemical modification of the polymeric network is related to the intention to preserve the elastamine component, avoiding any reaction that could affect its properties. PEG reacted with carbomer carboxyl groups to bind to the scaffold in a stable manner [38] (IR, Supporting information) and the ester-RhB cleavability was investigated. The evaluations were performed, also in this case, at acid, neutral and alkaline pH. Fig. 8 shows the amount of released RhB over time: at pH 7.4, only 30% of entrapped mimetic drug was escaped after 250 h, indicating that the release kinetic is prolonged and dependent on the ester hydrolysis, which delay the release associated to this strategy.

The same trend is observed in the RhB release at pH 10, whereas in acid medium, there is a slight increase in the released amount due to the ester acid hydrolysis.

The linear trends plotting release percentage against $s^{1/2}$ are indicative of increased performances in terms of pure diffusive mass transport and of burst release contribution that results to be very small. In particular, it is recognizable a double diffusion regime with different slopes. The transition of the two regimes depends on the allocation of ester-RhB bond: when it is near the hydrogel/medium interface it can be more easily hydrolyzed (regime *i*) than the linker present in the inner core (regime *ii*). The obtained results make possible to state that the proposed hydrogels can be used as drug carriers also introducing cleavable linkers designing a system characterized by a delayed drug release with consequent higher performance with respect to hydrogels where drugs are only physically entrapped.

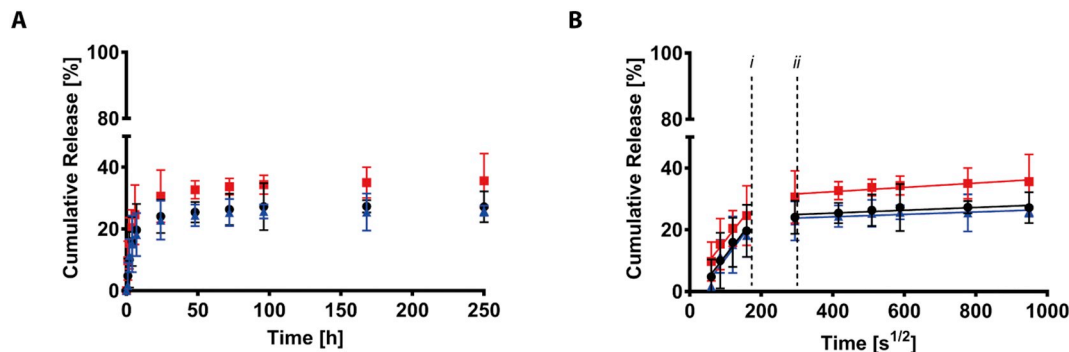


Fig. 8. A: *In vitro* release profile of RhB linked to the hydrogels scaffold through ester bond, at pH 7.4 (●, black), pH 3 (■, red) and pH 10 (▲, blue). B: Evaluation of RhB cumulative release percentage against $s^{1/2}$ at the different pH: the linear trends are representative of the Fickian diffusion regime of the drug from the hydrogel ($p < 0.0001$ between all the groups), according to the ester cleavability. The values are calculated as a percentage with respect to the total mass loaded (mean value \pm standard deviation is plotted). (For interpretation of the references to color in this figure legend, the reader is referred to the web version of this article.)

4. Conclusions

This work proposes the design of innovative hydrogel systems using a simple synthesis approach based on a physical-chemical transition that exploits the physico-chemical interactions among carbomer and elastamine, preserving their peculiar properties. The main advantage is related to the non-use of inorganic particles, antibacterial agents or antibiotics to perform a suitable antimicrobial effect, overcoming all questionable aspects related to the cytotoxicity or the concentration of the active molecules to avoid side-effects: here, the antimicrobial activity is due to the polymeric components. Moreover, the hydrogels are able to preserve their structure in environments at different pH and could be used as controlled drug delivery systems. In particular, thanks to the nature and the polymeric chains spatial organization, it is possible to prepare drug carriers with drug loading and release *via* steric hindrance or polymer functionalization, offering a wide range of release kinetics, that can be chosen according to the needs of the final therapeutic application. The opportunity to synthesize a system able to perform the double effect of antimicrobial and drug delivery is a pivotal challenge to reduce the number of administrations, injections or dosing in biomedical fields, and these scaffolds appear as a promising tool. Finally, the antimicrobial property could be useful in other fields, such as for environmental and industrial applications, and this shows the potential of this material.

Acknowledgements

We would like to acknowledge the financial support from Regione Lombardia and European Community FESR program, project POR FESR 2014-2020 FOODTECH ID20337.

Appendix A. Supplementary data

Supplementary data to this article can be found online at <https://doi.org/10.1016/j.msec.2019.109791>.

References

- [1] K.E. Boehle, J. Gilliland, C.R. Wheelton, A. Holder, J.A. Adkins, B.J. Geiss, et al., Utilizing paper-based devices for antimicrobial-resistant bacteria detection, *Angew Chem Int Edit* 56 (2017) 6886–6890.
- [2] B. Nabil, E. Ahmida, C. Christine, V. Julien, A. Abdelkrim, Polyfunctional cotton fabrics with catalytic activity and antibacterial capacity, *Chem. Eng. J.* 351 (2018) 328–339.
- [3] F.J. Rodriguez, A. Torres, A. Penalzo, H. Sepulveda, M.J. Galotto, A. Guarda, et al., Development of an antimicrobial material based on a nanocomposite cellulose acetate film for active food packaging, *Food Addit Contam A* 31 (2014) 342–353.
- [4] C.M. Gonzalez-Henriquez, M.A. Sarabia-Vallejos, J. Rodriguez-Hernandez, Advances in the fabrication of antimicrobial hydrogels for biomedical applications, *Materials* 10 (2017).
- [5] W.W. Gao, Y.J. Chen, Y. Zhang, Q.Z. Zhang, L.F. Zhang, Nanoparticle-based local antimicrobial drug delivery, *Adv Drug Deliver Rev* 127 (2018) 46–57.
- [6] J. Hoque, B. Bhattacharjee, R.G. Prakash, K. Paramanandham, J. Haldar, Dual function injectable hydrogel for controlled release of antibiotic and local antibacterial therapy, *Biomacromolecules* 19 (2018) 267–278.
- [7] M.H. Xiong, Y. Bao, X.Z. Yang, Y.H. Zhu, J. Wang, Delivery of antibiotics with polymeric particles, *Adv Drug Deliver Rev* 78 (2014) 63–76.
- [8] F.S. Taccone, O. Bond, F.Z. Cavicchi, M. Hites, Individualized antibiotic strategies, *Curr Opin Anesthesiol* 29 (2016) 166–171.
- [9] T.W. Felton, W.W. Hope, J.A. Roberts, How severe is antibiotic pharmacokinetic variability in critically ill patients and what can be done about it? *Diagn Microb Infect Dis* 79 (2014) 441–447.
- [10] S. Sattari, A.D. Tehrani, M. Adeli, pH-responsive hybrid hydrogels as antibacterial and drug delivery systems, *Polymers-Basel* 10 (2018).
- [11] W.G. Xu, S.J. Dong, Y.P. Han, S.Q. Li, Y. Liu, Hydrogels as antibacterial biomaterials, *Curr Pharm Design* 24 (2018) 843–854.
- [12] S.Q. Li, S.J. Dong, W.G. Xu, S.C. Tu, L.S. Yan, C.W. Zhao, et al., Antibacterial hydrogels, *Adv Sci* 5 (2018).
- [13] A.O. Adebisi, B.R. Conway, Modification of drug delivery to improve antibiotic targeting to the stomach, *Ther. Deliv.* 6 (2015) 741–762.
- [14] Q.F. Wang, H.J. Yu, L. Zhong, J.Q. Liu, J.Q. Sun, J.C. Shen, Incorporation of silver ions into ultrathin titanium phosphate films: in situ reduction to prepare silver nanoparticles and their antibacterial activity, *Chem. Mater.* 18 (2006) 1988–1994.
- [15] G. Perale, F. Rossi, M. Santoro, M. Peviani, S. Papa, D. Llupi, et al., Multiple drug delivery hydrogel system for spinal cord injury repair strategies, *J. Control. Release* 159 (2012) 271–280.
- [16] N. Annabi, A. Tamayol, J.A. Uquillas, M. Akbari, L.E. Bertassoni, C. Cha, et al., 25th anniversary article: rational design and applications of hydrogels in regenerative medicine, *Adv. Mater.* 26 (2014) 85–124.
- [17] R.R. Choudhury, J.M. Gohil, S. Mohanty, S.K. Nayak, Antifouling, fouling release and antimicrobial materials for surface modification of reverse osmosis and nano-filtration membranes, *J. Mater. Chem. A* 6 (2018) 313–333.
- [18] P.M. Nguyen, N.S. Zacharia, E. Verploegen, P.T. Hammond, Extended release antibacterial layer-by-layer films incorporating linear-dendritic block copolymer micelles, *Chem. Mater.* 19 (2007) 5524–5530.
- [19] A.S. Veiga, J.P. Schneider, Antimicrobial hydrogels for the treatment of infection, *Biopolymers* 100 (2013) 637–644.
- [20] D. Sun, M.B. Shahzad, M. Li, G. Wang, D. Xu, Antimicrobial materials with medical applications, *Mater. Technol.* 30 (2015) (B90-B5).
- [21] X. Yi, J.P. He, X.L. Wang, Y. Zhang, G.X. Tan, Z.N. Zhou, et al., Tunable mechanical, antibacterial, and cytocompatible hydrogels based on a functionalized dual network of metal coordination bonds and covalent crosslinking, *ACS Appl Mater Inter* 10 (2018) 6190–6198.
- [22] H. Tang, A. Lu, L. Li, W.J. Zhou, Z.X. Xie, L.N. Zhang, Highly antibacterial materials constructed from silver molybdate nanoparticles immobilized in chitin matrix, *Chem. Eng. J.* 234 (2013) 124–131.
- [23] I. Irwansyah, Y.Q. Li, W.X. Shi, D.P. Qi, W.R. Leow, M.B.Y. Tang, et al., Gram-positive antimicrobial activity of amino acid-based hydrogels, *Adv. Mater.* 27 (2015) 648–654.
- [24] A.L. Lakes, R. Peyyala, J.L. Ebersole, D.A. Puleo, J.Z. Hilt, T.D. Dziubla, Synthesis and characterization of an antibacterial hydrogel containing covalently bound vancomycin, *Biomacromolecules* 15 (2014) 3009–3018.
- [25] Y. Lee, K.H. Choi, K.M. Park, J.M. Lee, B.J. Park, K.D. Park, In situ forming and H₂O₂-releasing hydrogels for treatment of drug-resistant bacterial infections, *ACS Appl Mater Inter* 9 (2017) 16891–16900.
- [26] D. Chudobova, S. Dostalova, B. Ruttkay-Nedecky, R. Guran, M.A.M. Rodrigo, K. Tmejova, et al., The effect of metal ions on *Staphylococcus aureus* revealed by biochemical and mass spectrometric analyses, *Microbiol. Res.* 170 (2015) 147–156.
- [27] Y.M. Wan, L.B. Liu, S.S. Yuan, J. Sun, Z.B. Li, pH-responsive peptide supramolecular hydrogels with antibacterial activity, *Langmuir* 33 (2017) 3234–3240.
- [28] I. Caron, F. Rossi, S. Papa, R. Aloe, M. Sculco, E. Mauri, et al., A new three dimensional biomimetic hydrogel to deliver factors secreted by human mesenchymal stem cells in spinal cord injury, *Biomaterials* 75 (2016) 135–147.
- [29] M. Barbosa, M. Martins, P. Gomes, Grafting techniques towards production of peptide-tethered hydrogels, a novel class of materials with biomedical interest, *Gels* 1 (2015) 194.
- [30] J. Sestak, M. Mullins, L. Northrup, S. Thati, M.L. Forrest, T.J. Siahaan, et al., Single-step grafting of aminoxy-peptides to hyaluronan: a simple approach to multifunctional therapeutics for experimental autoimmune encephalomyelitis, *J. Control. Release* 168 (2013) 334–340.
- [31] E. Mauri, G.M.F. Chincarini, R. Rigamonti, L. Magagnin, A. Sacchetti, F. Rossi, Modulation of electrostatic interactions to improve controlled drug delivery from nanogels, *Mat Sci Eng C-Mater* 72 (2017) 308–315.
- [32] T. Casalini, M. Salvalaglio, G. Perale, M. Masi, C. Cavallotti, Diffusion and aggregation of sodium fluorescein in aqueous solutions, *J. Phys. Chem. B* 115 (2011) 12896–12904.
- [33] H. Sun, J. Chen, X. Han, H.L. Liu, Multi-responsive hydrogels with UCST- and LCST-induced shrinking and controlled release behaviors of rhodamine B, *Mat Sci Eng C-Mater* 82 (2018) 284–290.
- [34] B.S. Kim, Y.C. Shin, pH-sensitive swelling and release behaviors of anionic hydrogels for intelligent drug delivery system, *J. Appl. Polym. Sci.* 105 (2007) 3656–3661.
- [35] R.W. Ramette, E.B. Sandell, Rhodamine B Equilibria, *J. Am. Chem. Soc.* 78 (1956) 4872–4878.
- [36] R.Y. Zhang, M. Hummelgard, G. Lv, H. Olin, Real time monitoring of the drug release of rhodamine B on graphene oxide, *Carbon* 49 (2011) 1126–1132.
- [37] M. Obata, M. Morita, K. Nakase, K. Mitsuo, K. Asai, S. Hirohara, et al., Synthesis and photophysical properties of rhodamine B dye-bearing poly(isobutyl methacrylate-co-2,2,2-trifluoroethyl methacrylate) as a temperature-sensing polymer film, *J Polym Sci Pol Chem* 45 (2007) 2876–2885.
- [38] E. Mauri, F. Rossi, A. Sacchetti, Tunable drug delivery using chemoselective functionalization of hydrogels, *Mat Sci Eng C-Mater* 61 (2016) 851–857.
- [39] N.A. Peppas, J.B. Thomas, J. McGinty, Molecular aspects of mucoadhesive carrier development for drug delivery and improved absorption, *J Biomat Sci-Polym E* 20 (2009) 1–20.
- [40] Y. Zheng, W.Q. Ouyang, Y.P. Wei, S.F. Syed, C.S. Hao, B.Z. Wang, et al., Effects of Carbopol (R) 934 proportion on nanoemulsion gel for topical and transdermal drug delivery: a skin permeation study, *Int. J. Nanomedicine* 11 (2016) 5971–5987.
- [41] N.B. Javan, H. Montazeri, L.R. Shirmard, N.J. Omid, G.R. Barbari, M. Amini, et al., Preparation, characterization and in vivo evaluation of a combination delivery system based on hyaluronic acid/jeffamine hydrogel loaded with PHBV/PLGA blend nanoparticles for prolonged delivery of Teriparatide, *Eur. J. Pharm. Sci.* 101 (2017) 167–181.
- [42] T.Y. Lo, Y.J. Wang, D.M. Liu, W.T. Whang, Surface characteristics and bio-functionality of a novel high-performance, hydrophilic Jeffamine-added fluoro-containing polyimide for biomedical applications, *J. Polym. Res.* 22 (2015).
- [43] A.S. Erturk, M.U. Gurbuz, M. Tulu, New-generation Jeffamine (R) D230 core amine, TRIS and carboxyl-terminated PAMAM dendrimers: synthesis, characterization and the solubility application for a model NSAID drug Ibuprofen, *Marmara Pharm J* 21 (2017) 385–399.

- [44] K. Ozturk, A.S. Erturk, C. Sansozen, M. Tulu, S. Calis, Cytotoxicity and in vitro characterization studies of synthesized Jeffamine-cored PAMAM dendrimers, *J. Microencapsul.* 31 (2014) 127–136.
- [45] A. Zeynep, A. Fahri, S. Mehmet, K.S. Naci, Evaluation of Jeffamine®-cored PAMAM dendrimers as an efficient in vitro gene delivery system, *J. Biomed. Mater. Res. A* 100A (2012) 2623–2628.
- [46] J.M. Heffernan, J.B. McNamara, S. Borwege, B.L. Vernon, N. Sanai, S. Mehta, et al., PNIPAAm-co-Jeffamine (R) (PNJ) scaffolds as in vitro models for niche enrichment of glioblastoma stem-like cells, *Biomaterials* 143 (2017) 149–158.
- [47] A. Erdem, F.A. Ngwabebhoh, U. Yildiz, Fabrication and characterization of soft macroporous Jeffamine cryogels as potential materials for tissue applications, *RSC Adv.* 6 (2016) 111872–111881.
- [48] O. Kretschmann, S. Schmitz, H. Ritter, Microwave-assisted synthesis of associative hydrogels, *Macromol Rapid Comm* 28 (2007) 1265–1269.
- [49] M. Iannelli, H. Ritter, Microwave-assisted direct synthesis and polymerization of chiral acrylamide, *Macromol. Chem. Phys.* 206 (2005) 349–353.
- [50] J. Dong, Y. Ozaki, K. Nakashima, Infrared, Raman, and near-infrared spectroscopic evidence for the coexistence of various hydrogen-bond forms in poly(acrylic acid), *Macromolecules* 30 (1997) 1111–1117.
- [51] M. Todica, R. Stefan, C.V. Pop, L. Olar, IR and Raman investigation of some poly(acrylic) acid gels in aqueous and neutralized state, *Acta Phys. Pol. A* 128 (2015) 128–135.
- [52] A. Sanchez-Ferrer, D. Rogez, P. Martinoty, Synthesis and characterization of new polyurea elastomers by sol/gel chemistry, *Macromol. Chem. Phys.* 211 (2010) 1712–1721.
- [53] V.D. Bermudez, L.D. Carlos, L. Alcacer, Sol-gel derived urea cross-linked organically modified silicates. 1. Room temperature mid-infrared spectra, *Chem. Mater.* 11 (1999) 569–580.
- [54] X. Ramis, J.M. Salla, C. Mas, A. Mantecon, A. Serra, Kinetic study by FTIR, TMA, and DSC of the curing of a mixture of DGEBA resin and gamma-butyrolactone catalyzed by ytterbium triflate, *J. Appl. Polym. Sci.* 92 (2004) 381–393.
- [55] C. Mas, X. Ramis, J.M. Salla, A. Mantecón, A. Serra, Copolymerization of diglycidyl ether of bisphenol A with γ -butyrolactone catalyzed by ytterbium triflate: shrinkage during curing, *J. Polym. Sci. A Polym. Chem.* 41 (2003) 2794–2808.
- [56] J.M. Parnis, K.B. Oldham, Beyond the Beer–Lambert law: the dependence of absorbance on time in photochemistry, *J. Photochem. Photobiol. A Chem.* 267 (2013) 6–10.
- [57] M. Wang, H.H. Winter, G.K. Auernhammer, Time and frequency dependent rheology of reactive silica gels, *J. Colloid Interf Sci* 413 (2014) 159–166.
- [58] C.Q. Yan, D.J. Pochan, Rheological properties of peptide-based hydrogels for biomedical and other applications, *Chem. Soc. Rev.* 39 (2010) 3528–3540.
- [59] V.V. Erramreddy, S. Tu, S. Ghosh, Rheological reversibility and long-term stability of repulsive and attractive nanoemulsion gels, *RSC Adv.* 7 (2017) 47818–47832.
- [60] G.K. Schwalfenberg, The alkaline diet: is there evidence that an alkaline pH diet benefits health? *J. Environ. Public Health* 2012 (2012) 727630.
- [61] L.R.N. Angeloco, G.C.A. de Souza, E.A. Romao, P.G. Chiarello, Alkaline diet and metabolic acidosis: practical approaches to the nutritional management of chronic kidney disease, *J. Renal Nutr* 28 (2018) 215–220.
- [62] J. Koehler, L. Verheyen, S. Hedtrich, F.P. Brandl, A.M. Goepferich, Alkaline poly(ethylene glycol)-based hydrogels for a potential use as bioactive wound dressings, *J. Biomed. Mater. Res. A* 105 (2017) 3360–3368.
- [63] C.C. Deng, W.L.A. Brooks, K.A. Abboud, B.S. Sumerlin, Boronic acid-based hydrogels undergo self-healing at neutral and acidic pH, *ACS Macro Lett.* 4 (2015) 220–224.
- [64] A. Jung, O. Weichold, Preparation and characterisation of highly alkaline hydrogels for the re-alkalisation of carbonated cementitious materials, *Soft Matter* 14 (2018) 8105–8111.
- [65] N.A. Peppas, S.L. Wright, Drug diffusion and binding in ionizable interpenetrating networks from poly(vinyl alcohol) and poly(acrylic acid), *Eur. J. Pharm. Biopharm.* 46 (1998) 15–29.
- [66] N. Sheikh, L. Jalili, F. Anvari, A study on the swelling behavior of poly(acrylic acid) hydrogels obtained by electron beam crosslinking, *Radiat. Phys. Chem.* 79 (2010) 735–739.
- [67] H.S. Jamwal, G.S. Chauhan, Designing silica-based hybrid polymers and their application in the loading and release of fluorescein as a model drug and diagnostic agent, *Adv. Polym. Technol.* 37 (2018) 411–418.
- [68] Y.T. Kim, J.M. Caldwell, R.V. Bellamkonda, Nanoparticle-mediated local delivery of methylprednisolone after spinal cord injury, *Biomaterials* 30 (2009) 2582–2590.
- [69] J.L. Arias, F. Linares-Molinero, V. Gallardo, A.V. Delgado, Study of carbonyl iron/poly(butylcyanoacrylate) (core/shell) particles as anticancer drug delivery systems - loading and release properties, *Eur. J. Pharm. Sci.* 33 (2008) 252–261.
- [70] Y. Fu, W.J. Kao, Drug release kinetics and transport mechanisms of non-degradable and degradable polymeric delivery systems, *Expert Opin Drug Del* 7 (2010) 429–444.
- [71] K. Vulic, M.S. Shoichet, Tunable growth factor delivery from injectable hydrogels for tissue engineering, *J. Am. Chem. Soc.* 134 (2012) 882–885.



Repurposing Pilocarpine Hydrochloride for Treatment of *Candida albicans* Infections

Christopher Nile,^a Monica Falleni,^b Daniela Cirasola,^c Abeer Alghamdi,^a Oliver F. Anderson,^a Christopher Delaney,^a Gordon Ramage,^a Emerenziana Ottaviano,^c Delfina Tosi,^b Gaetano Bulfamante,^b Giulia Morace,^c Elisa Borghi^c

^aOral Sciences Research Group, University of Glasgow Dental School, School of Medicine, Dentistry and Nursing, College of Medical, Veterinary and Life Sciences, University of Glasgow, Glasgow, United Kingdom

^bDivision of Human Pathology, Department of Health Sciences, Università degli Studi di Milano, Milan, Italy

^cLaboratory of Microbiology, Department of Health Sciences, Università degli Studi di Milano, Milan, Italy

ABSTRACT Acetylcholine modulates the virulence of *Candida albicans* and regulates an appropriate immune response to infection in a *Galleria mellonella* infection model. Indeed, the evidence suggests that *C. albicans* possesses a functional cholinergic receptor that can regulate filamentous growth and biofilm formation. Furthermore, *G. mellonella* immune cell subsets possess repertoires of cholinergic receptors which regulate an effective and appropriate cellular immune response to *C. albicans* infection. This study aimed to investigate the cholinergic receptor subtype involved in regulation of filamentous growth and biofilm formation by *C. albicans* and determine the roles of cholinergic receptors in modulation of *G. mellonella* immune cell subsets. The general muscarinic receptor agonist, pilocarpine hydrochloride, inhibited *C. albicans* biofilm formation and pathogenicity, a phenomenon that could be reversed using the general muscarinic receptor antagonist, scopolamine. Pilocarpine hydrochloride protected *G. mellonella* larvae from *C. albicans* infection via inhibition of *C. albicans* filamentation and appropriate regulation of cellular immunity. However, scopolamine abrogated the capacity of pilocarpine hydrochloride to protect *G. mellonella* larvae from *C. albicans* infection. Furthermore, acetylcholine and pilocarpine hydrochloride exhibited differential modulatory capabilities on *Galleria mellonella* hemocyte responses to *C. albicans*. The data in this article demonstrate that a muscarinic receptor modulates *C. albicans* filamentation and biofilm formation. Furthermore, the results suggest that *G. mellonella* hemocyte subsets possess unique repertoires of cholinergic receptors that regulate their differentiation, activation, and function in contrasting manners. Therefore, targeting cholinergic receptors by repurposing currently licensed cholinergic drugs may offer novel therapeutic solutions for the prevention or treatment of fungal infections.

IMPORTANCE *Candida albicans* is the most common human fungal pathogen with an estimated crude mortality rate of 40%. The ability of the organism to switch from the yeast to hyphal form and produce biofilms are important virulence factors. *C. albicans* infections are combatted by the host immune system. However, *Candida* triggers a strong inflammatory response that, if not appropriately regulated, can damage host tissues. Therefore, it is important that the host immune response eliminates the fungus but limits tissue damage. This study provides evidence that targeting cholinergic receptors cannot only curb the virulence of *C. albicans* by inhibiting filamentous growth and biofilm formation but can also appropriately regulate the host immune response to induce rapid clearance with limited damage to vital tissues. This article provides evidence that repurposing licensed drugs that target cholinergic receptors may offer novel therapeutic solutions for the prevention or treatment of fungal infections.

Citation Nile C, Falleni M, Cirasola D, Alghamdi A, Anderson OF, Delaney C, Ramage G, Ottaviano E, Tosi D, Bulfamante G, Morace G, Borghi E. 2019. Repurposing pilocarpine hydrochloride for treatment of *Candida albicans* infections. mSphere 4:e00689-18. <https://doi.org/10.1128/mSphere.00689-18>.

Editor J. Andrew Alspaugh, Duke University Medical Center

Copyright © 2019 Nile et al. This is an open-access article distributed under the terms of the [Creative Commons Attribution 4.0 International license](https://creativecommons.org/licenses/by/4.0/).

Address correspondence to Christopher Nile, christopher.nile@glasgow.ac.uk.

Received 14 December 2018

Accepted 17 December 2018

Published 23 January 2019

KEYWORDS *Candida albicans*, *Galleria mellonella*, biofilm, muscarinic, pilocarpine hydrochloride, repurposing

Acetylcholine (ACh) is synthesized by almost every cell of the human body, and its functions go way beyond those of a classical neurotransmitter (1–3). ACh is known to modulate pathogen-driven immune responses, downregulating potentially damaging chronic inflammation and promoting favorable disease outcomes in selected *in vivo* models of bacterial sepsis (4–7). Furthermore, human immune cells express both nicotinic and muscarinic acetylcholine receptors (nAChRs and mAChRs). These receptors have been demonstrated to modulate cellular immunity against bacterial pathogens via cholinergic-dependent mechanisms (2, 8–10).

Evidence suggests that bacteria and fungi are capable of synthesizing ACh (11–13). However, very little is known about the cholinergic receptor repertoire of these microorganisms. Several bacterial species possess homologs of mammalian nicotinic receptors (14, 15), although the functional roles of these receptors have yet to be elucidated. To date, there are no studies that have identified or characterized fungal cholinergic receptors. However, sequencing of the *Candida albicans* genome has suggested that this organism possesses putative cholinergic receptor genes (16).

Acetylcholine has been demonstrated to promote favorable disease outcomes to *C. albicans* infection in a *Galleria mellonella* infection model (17). Acetylcholine modulates the pathogenicity of *C. albicans* by inhibiting morphogenesis, biofilm formation, and the expression of virulence factors. In addition, ACh promotes an effective cellular immune response to fungal infection, facilitating rapid clearance from infected tissues and affording protection from chronic-inflammation-induced damage of vital tissues (17).

The innate immune system plays a crucial role in protection against systemic *C. albicans* infections, as evidenced by the fact that immunocompromised, critically ill, and elderly patients show increased susceptibility. Insects lack an acquired immune system but possess a complex and effective innate immune system, which can be divided into humoral and cellular defense components. The cellular defenses are defined as hemocyte-mediated responses and involve processes such as phagocytosis and encapsulation (18). *G. mellonella* possesses at least six hemocyte subtypes. However, plasmatocytes and granulocytes are the most abundant circulating cells in *G. mellonella* hemolymph (19). These cells have similar characteristics to human neutrophils (20) and the ability to respond to ACh (17). Human immune cells, including neutrophils, possess various repertoires of nAChRs and mAChRs, and activation of specific receptors can have different consequences for immune function (21–23).

Advancements in our understanding of human cholinergic receptors and their roles in various pathologies have led to the discovery of a plethora of small-molecule agonists and antagonists with therapeutic potential. Many of these molecules have been developed for treatment of conditions whose pathology is defined by loss or gain of cholinergic function, such as neurodegenerative disorders (24). However, a variety of cholinergic drugs have been utilized to research the effects of cholinergic receptors on nonneurological pathologies, including bacterial sepsis, and investigated for their therapeutic effectiveness in inflammatory disease (25–27).

Repositioning of cholinergic drugs for the treatment of candidiasis may provide new avenues for therapeutic strategies. Hence, the aims of this study were to begin to delineate the cholinergic receptor subtype responsible for the modulation of biofilm formation by *C. albicans* and to investigate in further detail the role of cholinergic receptor subtypes on cellular immunity against *C. albicans* infection in a *G. mellonella* infection model.

RESULTS

Pilocarpine hydrochloride specifically inhibits *Candida albicans* biofilm formation and pathogenicity through interaction with a muscarinic-like receptor. Acetylcholine inhibits *C. albicans* biofilm formation (17). Therefore, the effect of a nonspe-

cific nicotinic receptor agonist, SIB1508Y maleate (SIBm), and a nonspecific muscarinic receptor agonist, pilocarpine hydrochloride (PHCl), on *C. albicans* biofilm formation was investigated to determine whether this was due to activation of a specific subtype of cholinergic receptor.

Biomass quantification assays revealed that SIBm had no effect on *C. albicans* biofilm formation *in vitro* (Fig. 1A). In contrast, PHCl caused a dose-dependent decrease in biofilm biomass, with statistically significant reductions observed with concentrations ranging between 0.39 and 50 mM (all $P < 0.001$) (Fig. 1B). The XTT metabolic assay revealed that SIBm had no effect on *C. albicans* metabolic activity (Fig. 1C). However, a slight but significant reduction in *C. albicans* metabolic activity compared to the untreated control (0 mM) was observed when treated with PHCl concentrations ranging between 3.125 and 50 mM (all $P < 0.01$) (Fig. 1D).

Reductions in metabolic activity are associated with reduced biofilm formation but can also be attributed to cell death. A planktonic MFC was performed according to the CLSI M-27A broth microdilution methodology (28) and revealed that none of concentrations of SIBm or PHCl investigated possessed fungicidal activity (data not shown). In addition, PHCl had no destabilizing effects on the *C. albicans* cell wall as observed by measuring both PI uptake (Fig. 1E) and ATP release (Fig. 1F). Microscopy was also employed to further ensure that PHCl was specifically inhibiting filamentation and not affecting cell viability. Light microscopy (LM) (Fig. 2A to E) revealed that PHCl inhibited filamentation and biofilm formation in a dose-dependent manner. Furthermore, visually, in the presence of increasing concentrations of PHCl, more *C. albicans* cells maintained a yeast morphology, suggesting that PHCl was inhibiting the yeast-to-hypha transition. Scanning electron microscopy (SEM) analysis (Fig. 2F to J) further confirmed the fact that PHCl inhibited biofilm formation due to inhibition of the yeast-to-hypha transition in a dose-dependent manner. Fluorescence microscopy (FM) (Fig. 2K to O) with CFW (blue) and PI staining (red) revealed no visible differences in cell viability between any of the concentrations of PHCl investigated and therefore confirmed that PHCl was not toxic to *C. albicans* at the concentrations used in this study.

To ensure that PHCl was specifically targeting a receptor with homology to human muscarinic receptors, biofilm biomass and metabolic activity assays were repeated in the presence of different concentrations of the nonspecific muscarinic receptor antagonist scopolamine (SCP). SCP inhibits the PHCl-induced reduction in biofilm formation in a dose-dependent manner with concentrations ranging from 64 to 128 μM , revealing no significant differences in biofilm biomass in the presence of 25 mM PHCl compared to the control (Fig. 3A). Furthermore, all concentrations of SCP abolished any PHCl-induced reductions in metabolic activity (Fig. 3B).

As hydrophobicity is a characteristic related to *C. albicans* biofilm formation (29), the effect of PHCl on *C. albicans* cell surface hydrophobicity was investigated using the microbial adhesion to hydrocarbon (MATH) assay. A statistically significant increase in cell surface hydrophobicity of *C. albicans* cells cultured as a biofilm compared to planktonic cells was observed ($P < 0.05$) (Fig. 3C). Interestingly, when *C. albicans* biofilms were cultured in the presence of 25, 12.5 (both $P < 0.01$), and 6.25 ($P < 0.05$) mM PHCl, there was a statistically significant decrease in cell surface hydrophobicity (Fig. 3C).

Pilocarpine hydrochloride specifically modulates the pathogenesis of *Candida albicans* infection in a *Galleria mellonella* model. Biofilm formation is associated with *C. albicans* pathogenicity, and ACh has previously been shown to protect *G. mellonella* larvae from *C. albicans*-induced mortality (17). Therefore, the effect of PHCl on *C. albicans* pathogenicity *in vivo* was investigated using a *G. mellonella* killing assay. PHCl alone (10.5 mM) had no adverse effects on survival of the larvae (Fig. 4A). Indeed, PHCl protects *G. mellonella* larvae from *C. albicans*-induced mortality in a dose-dependent manner compared to larvae inoculated with *C. albicans* alone observed using 10.5 and 6.25 mM PHCl ($P < 0.001$ and $P < 0.05$, respectively; as determined using the log rank test) (Fig. 4A). Furthermore, SCP (6.25 mM) alone had no adverse effects on the survival of the larvae. In fact, in the presence of PHCl and SCP, the survival of the larvae was

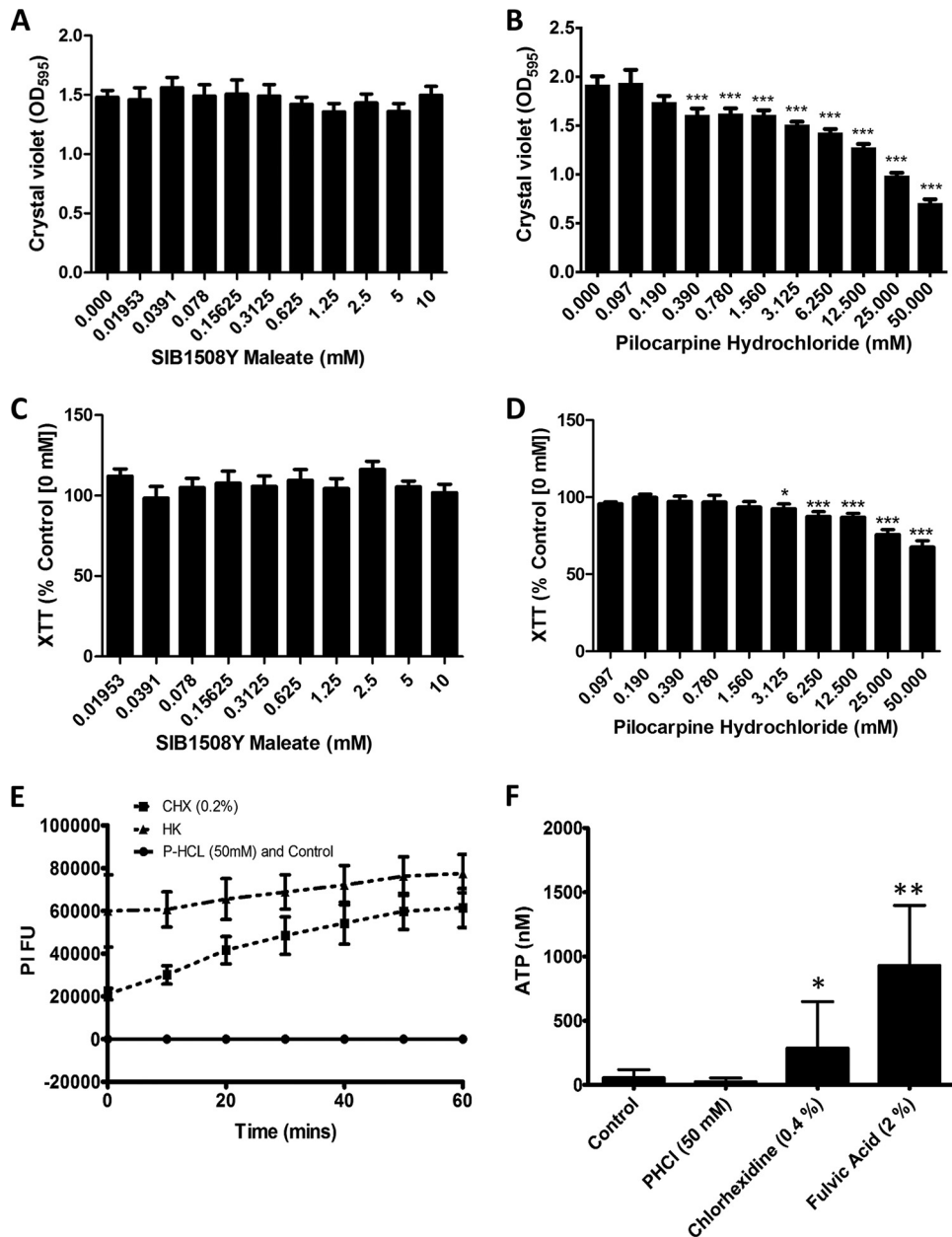


FIG 1 The general muscarinic receptor agonist pilocarpine hydrochloride inhibits *Candida albicans* biofilm formation *in vitro*. (A and B) Biofilm biomass was assessed using the crystal violet assay after *C. albicans* was cultured for 24 h in RPMI 1640 containing different concentrations of SIBm (0 to 10 mM) (A) and PHCl (0 to 50 mM) (B). Data are expressed as raw OD₅₉₅ values, and the bars represent the mean values (plus standard deviations [SD] [error bars]) from triplicate wells of six independent experiments ($n = 6$). (C and D) Biofilm metabolic activity was assessed using the XTT assay after *C. albicans* was cultured for 24 h in RPMI 1640 containing different concentrations of SIBm (0 to 10 mM) (C) and PHCl (0 to 50 mM) (D). Data are expressed as percent metabolic activity compared to untreated controls (0 mM PHCl), and the bars represent the mean values (+SD) from triplicate wells of six independent experiments ($n = 6$). For panels A to D, values that are significantly different compared to the control values (0 mM SIBm or PHCl) are indicated by asterisks as follows: *, $P < 0.05$; **, $P < 0.01$; ***, $P < 0.001$. (E and F) The effect of PHCl on the permeability of the *C. albicans* cell wall was investigated using a propidium iodide (PI) uptake (E) and ATP release assay (F). For the PI uptake assay, data are shown as fluorescence intensity units, and the bars represent the mean values (+SD) from triplicate wells of three independent experiments ($n = 3$). Heat-killed (HK) and chlorhexidine (CHX) (0.2%)-treated *C. albicans* were included as positive controls, and cells in RPMI 1640 alone were included as a negative control. For the ATP release assays, data are shown as nanomolar concentrations of ATP release, and the bars represent the mean values (+SD) from triplicate wells of three independent experiments ($n = 3$). Chlorhexidine (0.2%) and fulvic acid (2.0%)-treated *C. albicans* cells were included as positive controls, and cells in RPMI 1640 alone were included as a negative control. *, $P < 0.05$; **, $P < 0.01$ compared to the control (cells in RPMI 1640 alone).

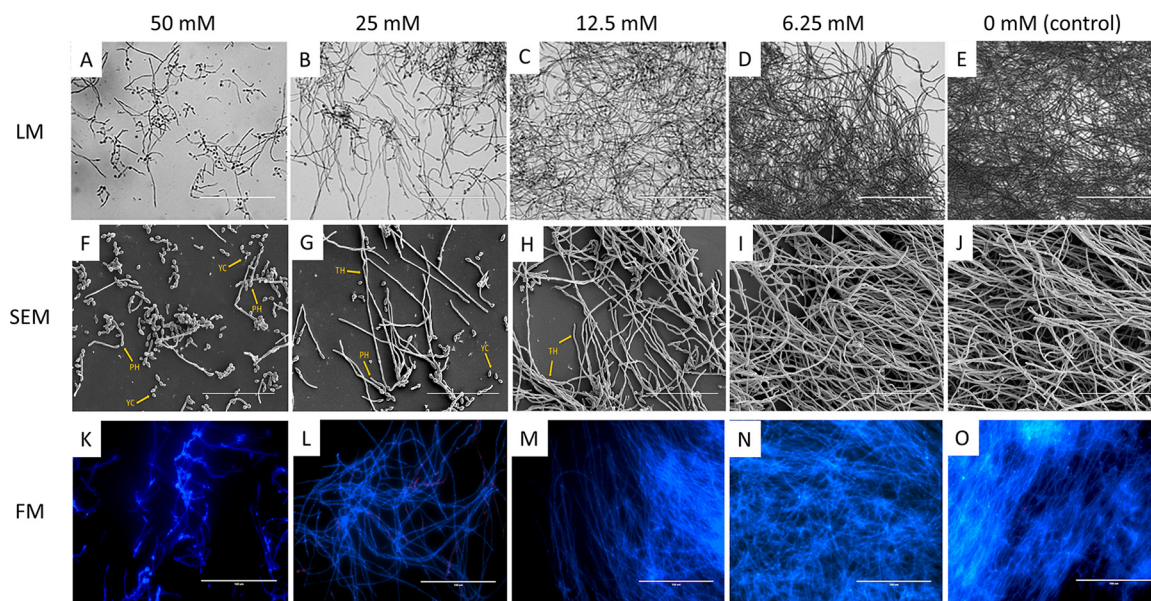


FIG 2 The general muscarinic receptor agonist pilocarpine hydrochloride inhibits filamentation and biofilm formation *in vitro* without affecting cell viability. (A to J) To assess the effects of PHCl on *C. albicans* morphology and viability, microscopy was employed. Light microscopy (LM) (A to E) and scanning electron microscopy (SEM) (F to J) was performed to visualize changes in biofilm biomass and *C. albicans* cell morphology after culture for 24 h in RPMI 1640 containing different concentrations of PHCl (0 to 50 mM). Representative images are shown from duplicate coverslips of three independent experiments. YC, yeast cells; PH, pseudohyphae; TH, true hyphae. Bars, 100 μm (A to E) and 700 μm (F to J). (K to O) Fluorescence microscopy (FM) was performed to assess cell viability. *C. albicans* was cultured for 24 h in RPMI 1640 containing different concentrations of PHCl, and viability was assessed using calcofluor white (blue) and propidium iodide (red) staining. Representative images are shown from duplicate coverslips of three independent experiments. Bars, 100 μm .

comparable to those inoculated with *C. albicans* alone, suggesting that SCP inhibited the PHCl-induced protection against *C. albicans* infection (Fig. 4B).

To visualize the effects of PHCl alone and in combination with SCP on *C. albicans* pathogenicity and *G. mellonella* hemocyte responses to infection, *in vivo* histological analysis was performed. Control sham-injected larvae after both 24 and 48 h demonstrated the presence of small hemocyte aggregates, adjacent to the gut and the tracheal system, resembling human MALT (mucosa-associated lymphoid tissue) and BALT (bronchus-associated lymphoid tissue). Furthermore, some hemocytes were also detected close to the fat body, near hemocoel cavities and distributed as a monolayer in the subcuticular areas (Fig. 4C, panels i and vi).

Twenty-four hours postinoculation, the hemocyte response in PHCl-injected larvae was characterized by uniformly dispersed small melanized nodules and an increase in circulating hemocytes (Fig. 4Cii). SCP alone resulted in poor immune activation and failed to induce melanization (data not shown). In larvae inoculated with *C. albicans* alone, the hemocyte response was characterized by melanized nodules of intermediate size, mainly located in the subcuticular area and in the fat body, with nodules found only rarely in paratracheal areas (Fig. 4Ciii). In contrast, the hemocyte response in larvae inoculated with *C. albicans* plus PHCl was characterized by the presence of single melanized hemocytes or very small aggregates of hemocytes with melanin deposition surrounding yeast cells. These aggregates were uniformly distributed in the hemolymph, close to the fat body and in peritracheal tissues. In addition, no filamentous growth was detected (Fig. 4Civ). In contrast, larvae inoculated with *C. albicans* SC5314 and treated with PHCl and SCP showed the presence of medium-sized nodules with scanty melanization and poor hemocyte recruitment into invaded tissues. Furthermore, poorly melanized yeast cells and hyphae were seldom detected in the nodules (Fig. 4Cv), similar to larvae infected with *C. albicans* alone (Fig. 4Ciii).

Forty-eight hours postinoculation, PHCl-injected larvae showed very few and small nodules with faint melanization (Fig. 4Cvii). Larvae infected with *C. albicans* alone showed increased hemocytes in the subcuticular, intestinal, and paratracheal areas with

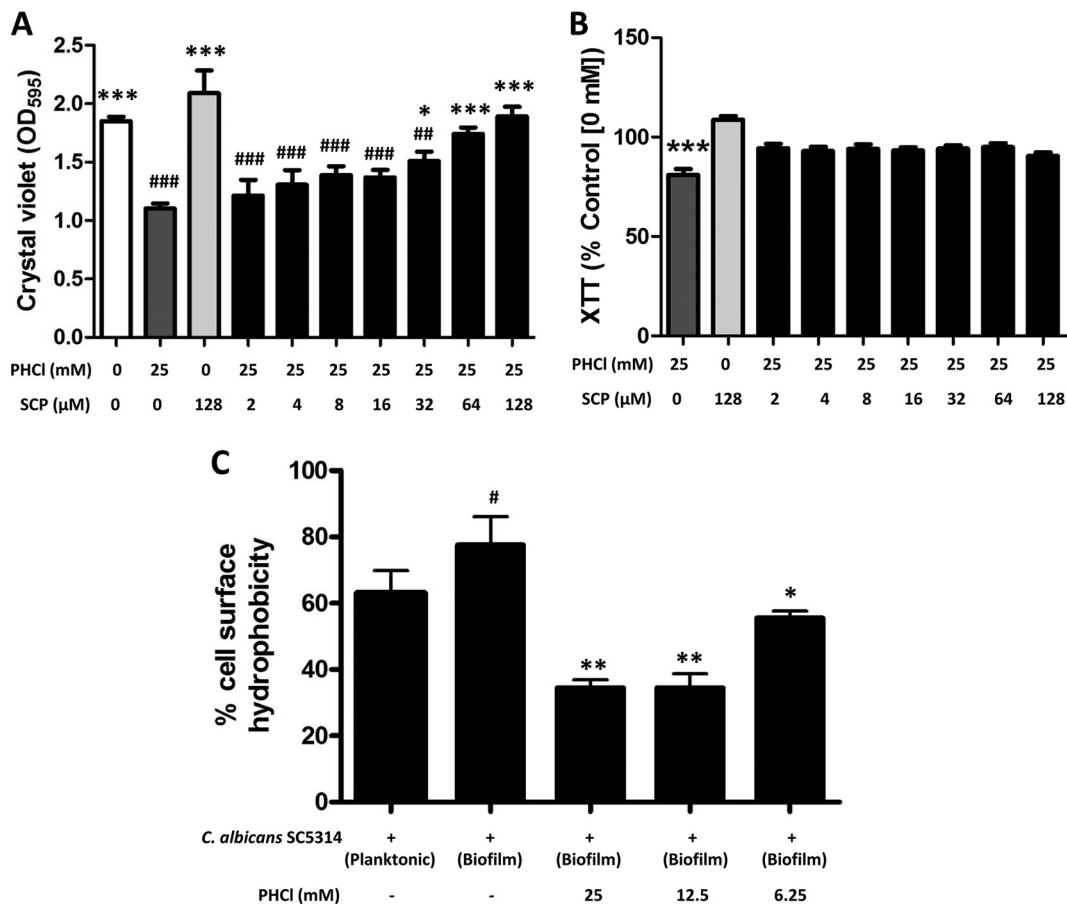


FIG 3 Pilocarpine hydrochloride acts through a specific muscarinic-like receptor to inhibit biofilm formation and modulate cell wall hydrophobicity. (A) Biofilm biomass was assessed using the crystal violet assay after *C. albicans* was cultured for 24 h in RPMI 1640 containing 25 mM PHCl and different concentrations of the nonspecific muscarinic receptor antagonist scopolamine (SCP) (0 to 128 μ M). Data are expressed as raw OD₅₉₅ values, and the bars represent the mean values (+SD) from triplicate wells of three independent experiments ($n = 3$). *Candida albicans* was cultured in the absence of any compound, in the presence of PHCl alone, and in the presence of SCP alone as controls. #, significantly different from cells cultured in the absence of any compound; *, significantly different from cells cultured in PHCl alone; * or #, $P < 0.05$; ** or ##, $P < 0.01$; *** or ###, $P < 0.001$. (B) Biofilm metabolic activity was assessed using the XTT assay after *C. albicans* was cultured for 24 h in RPMI 1640 containing 25 mM PHCl and different concentrations of the nonspecific muscarinic receptor antagonist scopolamine (SCP) (0 to 128 μ M). Data are expressed as percent metabolic activity compared to untreated controls (0 mM PHCl or SCP), and the bars represent the mean values (+SD) from triplicate wells of three independent experiments ($n = 3$). *Candida albicans* cultured in the presence of PHCl and SCP alone acted as controls. *, significantly different from cells cultured in SCP alone; ***, $P < 0.001$. (C) Cell wall hydrophobicity was assessed using the MATH assay (29). The bars represent the mean values (+SD) from duplicate samples of five independent experiments ($n = 5$). #, significantly different from cells cultured planktonically; *, significantly different from cells cultured as a biofilm in the absence of PHCl.

large nodules and multifocal melanization and heavy damage of the fat body. Hyphal invasion of the intestinal walls, and to a lesser extent, of the bronchial system was also detected (Fig. 4Cviii). In contrast, larvae infected with *C. albicans* plus PHCl exhibited decreased inflammation and less aggressive fungal infiltration of vital larval tissues, with only small melanized nodules mainly distributed in subcuticular areas. In addition, *C. albicans* hypha formation was not observed, and there was less microvacuolization of the fat body (Fig. 4Cix). When treated with both PHCl and SCP, *C. albicans* infection resulted in hyphal invasion of the intestinal walls (Fig. 4Cx), with a histological picture similar to larvae infected with *C. albicans* alone (Fig. 4Cviii).

Pilocarpine hydrochloride and acetylcholine differentially modulate hemocyte responses to *C. albicans* both *in vitro* and *in vivo*. It has previously been demonstrated that ACh promotes *G. mellonella* hemocyte function (17). Therefore, the effects of PHCl on hemocyte cellularity, subtypes, and nodule formation during the pathogen-

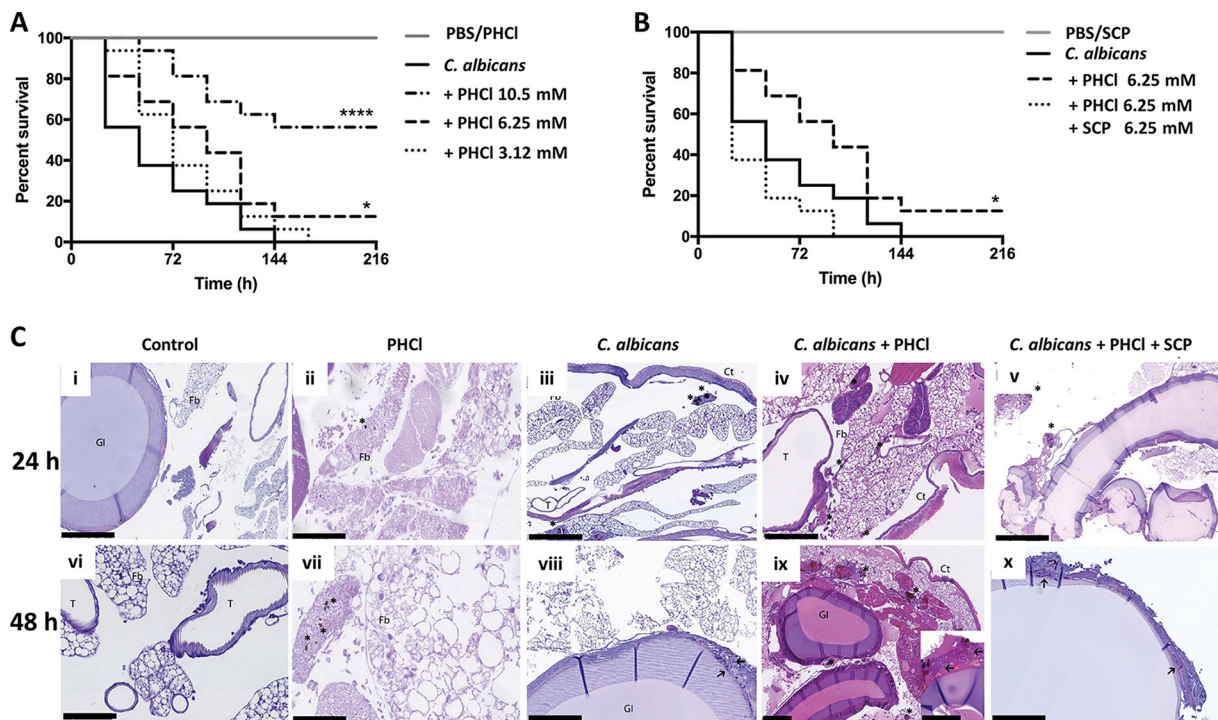


FIG 4 Pilocarpine hydrochloride acts through muscarinic-like receptors to prolong survival of *Candida albicans*-infected *Galleria mellonella* by inhibiting biofilm formation and modulating host immunity *in vivo*. The effect of PHCI on the outcome of systemic candidiasis was investigated using a *G. mellonella* infection model. (A) A Kaplan-Meier plot shows the effects of different concentrations of PHCI on the survival of *Candida albicans*-infected larvae. The data are derived from three independent experiments with groups of 16 larvae ($n = 48$). ***, $P < 0.001$; *, $P < 0.05$, as determined by the log rank test in comparison to larvae inoculated with *C. albicans* alone. PBS alone and PHCI alone-injected larvae were used as controls and had no effect on larva survival. (B) To verify specificity, *C. albicans*-infected larvae were also inoculated with PHCI and SCP in combination. The data are derived from three independent experiments with groups of 16 larvae ($n = 48$). *, $P < 0.05$, as determined by the log rank test in comparison to larvae inoculated with *C. albicans*. Larvae injected with PBS alone and SCP alone were used as controls, and PBS and SCP alone had no effect on larva survival. (C) Histological analysis of larvae was performed at 24 and 48 h postinoculation using hematoxylin and eosin (HE) and periodic acid-Schiff (PAS) staining. (i and vi; HE) (ii and vii; HE) larva inoculated with PHCI (6.25 mM) alone. (iii and viii; PAS) larvae infected with *C. albicans*. (iv and ix; HE) larvae infected with *C. albicans* in the presence of PHCI (6.25 mM). (v and x; PAS). Larvae infected with *C. albicans* in the presence of PHCI (6.25 mM) and SCP (6.25 mM). Asterisks highlight melanized nodules, whereas arrows show *C. albicans* cells and hyphae. Representative images are shown from histological analysis of two larvae for each condition from three independent experiments. Fb, fat body; Ct, cuticle; Gl, gastrointestinal tract; T, trachea; Nd, nodule. Bars, 250 μm (panels i, v, and ix) and 100 μm (panels ii, iii, iv, vi, vii, viii, and x).

esis of *C. albicans* infection were assessed and compared to the effects of ACh (Fig. 5 and Table 1).

An increase in hemocyte cellularity with a predominance of plasmatocytes, granulocytes, and spherulocytes was observed 24 h after exposure to *C. albicans* alone *in vitro*. The hemocytes formed small, mainly two-dimensional, melanized nodules. Furthermore, aggregates of yeast cells and hyphae were observed, as well as coagulation fibers similar to neutrophil extracellular traps (NETs) (Fig. 5Aii and Table 1). ACh alone induced an increase in cellularity, with a predominance of plasmatocytes and granulocytes, but no spherulocytes. Cell aggregation was more evident as well as multidimensional nodule formation with no visible melanization (Fig. 5Aiii and Table 1). Similarly, PHCI induced hemocyte aggregation, leading to multidimensional nodule formation. However, nodules were smaller and consisted mainly of plasmatocytes, a few granulocytes, and no spherulocytes (Fig. 5Aiv and Table 1). In the presence of *C. albicans* plus ACh, there was an increase in cellularity with a predominance of plasmatocytes, granulocytes, and spherulocytes. A strong induction of aggregation and multidimensional nodule formation with no melanization was also clearly visible (Fig. 5Av and Table 1). In contrast, although an increase in cellularity was also evident in *C. albicans*-plus-PHCI treated hemocytes, granulocyte and spherulocyte numbers were reduced compared with cells treated with *C. albicans* plus ACh. There was also

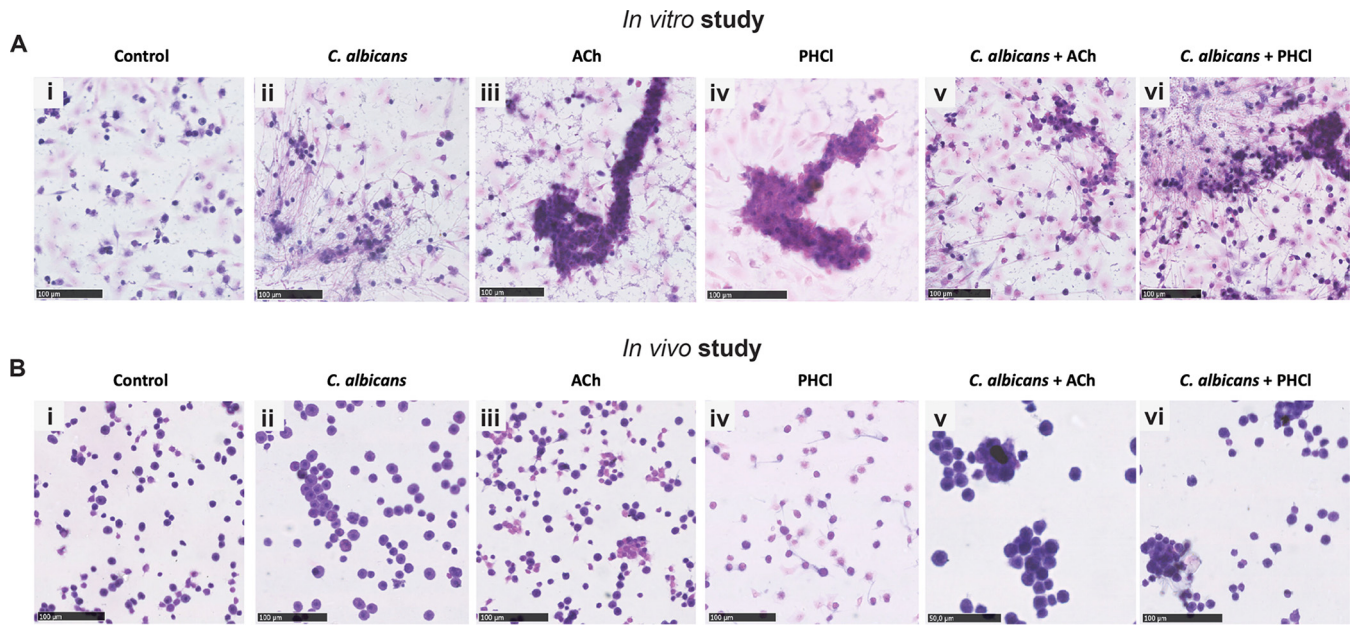


FIG 5 Effects of pilocarpine hydrochloride and acetylcholine on hemocyte responses to *C. albicans* *in vitro* and *in vivo*. (A) In the *in vitro* study, hemocytes isolated from untreated larvae were either left unstimulated (control) (i) or stimulated with *C. albicans* (ii), ACh (iii), PHCl (iv), *C. albicans* plus ACh (v), and *C. albicans* plus PHCl for 24 h. (B) In the *in vivo* study, larvae were bled 24 h after sham inoculation with PBS (control) (i) or inoculation with *C. albicans* (ii), ACh (iii), PHCl (iv), *C. albicans* plus ACh (v), and *C. albicans* plus PHCl. Representative images are shown from hematoxylin and eosin staining of hemocytes from three larvae for each condition from three independent experiments. Bars, 100 μ m.

limited cell aggregation and the formation of small two-dimensional nodules with no melanization (Fig. 5Avi and Table 1).

To determine whether the effects observed *in vitro* could be differently affected *in vivo* due to tissue secretion of regulatory molecules, the same analysis was performed on hemocytes isolated from *G. mellonella* larvae 24 h after infection with *C. albicans* in the presence and absence of ACh or PHCl. Sham-infected larvae were used as a control (Fig. 5Bi and Table 1). Comparison with the control cells *in vitro* (Fig. 5Ai and Table 1)

TABLE 1 Effects of pilocarpine hydrochloride and acetylcholine on hemocyte cellularity and subtype characteristics *in vitro* and *in vivo*

Condition and treatment ^a	Cellularity	Hemocyte subset ^b							Nodule		<i>C. albicans</i> ^c
		Pr	Gr	Pl	Co	Sp	Ad	Oe	Size	Melanization	
<i>In vitro</i>											
CTR	Low	+	+	–	–	+	+	–	–	–	–
SC5314	High	+	++	++	++	++	+	+	Medium	++	+++
ACh	High	+	++	+++	+	–	–	–	Medium	–	–
PHCl	Low	+	+	–	–	+	+	–	–	–	–
SC5314/ACh	High	+	+++	+++	++	+	+	–	Large	–	+
SC5314/PHCl	High	+	+	+++	+	+	++	+	Small	–	+
<i>In vivo</i>											
CTR	Low	+	+	–	–	+	+	–	–	–	–
SC5314	High	+	+++	++	++	++	+	+	Large	+++	+++
ACh	Intermediate	+	++	+++	+	–	–	–	Medium	–	–
PHCl	Low	+	+	+	–	+	+	–	–	–	–
SC5314/ACh	Intermediate	+	+++	+++	++	+	+	+	Large	–	+
SC5314/PHCl	Intermediate	+	++	+++	++	+	+	+	Small	–	+

^a*Galleria mellonella* larvae were inoculated with PBS (control [CTR]), *C. albicans* SC5314, acetylcholine (ACh), pilocarpine hydrochloride (PHCl), *C. albicans* plus ACh (SC5314/ACh), and *C. albicans* plus PHCl (SC5314/PHCl).

^bPr, prohemocytes; Gr, granulocytes; Pl, plasmatocytes; Co, coagulocytes; Sp, spherulocytes; Ad, adipocytes; Oe, oenocytes. Immune cell subtype quantification was scored as follows: –, absent/rare; +, 1 to 10%; ++, 11 to 30%; +++, 31 to 50%.

^c*C. albicans* presence was quantified as follows: –, absent; +, few cells; ++, multiple yeast agglomerate usually embedded in nodules; +++, abundant yeasts and/or hyphae with widespread diffusion in nodules.

revealed a greater number of cells with finely vacuolated cytoplasm, resembling spherulocytes and adipocytes. For all experimental conditions, the *in vivo* observations substantially overlapped the *in vitro* observations. However, overall cellularity was slightly reduced *in vivo* compared to *in vitro* due to tissue sequestration of hemocytes. With respect to specific treatments, hemocytes from *C. albicans*-infected larvae revealed a predominance of granulocytes and spherulocytes (Fig. 5Bii and Table 1) compared to hemocytes stimulated with *C. albicans* alone *in vitro*. In addition, the granulocytes were larger and contained large vacuoles within melanized cytoplasm compared with the small two-dimensional melanized nodules observed in the cells *in vitro* (Fig. 5Aii and Table 1). Hemocytes from larvae inoculated with ACh or PHCl alone and with *C. albicans* plus PHCl (Fig. 5Biii, iv, and vi, respectively; Table 1) showed similar cellularity and differentiation properties to hemocytes exposed to the same compound *in vitro* (Fig. 5Aiii, iv, and vi, respectively; Table 1). In contrast, hemocytes isolated from larvae infected with *C. albicans* plus ACh (Fig. 5Bv and Table 1) showed increased melanization compared to hemocytes cultured *in vitro* and infected with *C. albicans* alone (Fig. 5Av and Table 1).

DISCUSSION

Acetylcholine has previously been found to inhibit *C. albicans* virulence, both *in vitro* and *in vivo*, leading to the hypothesis that *C. albicans* possesses putative cholinergic receptors (17, 30). ACh is a general cholinergic receptor agonist with activity against both nicotinic ACh receptors (nAChR) and muscarinic ACh receptors (mAChR). In this study, the general nicotinic agonist SIB1508Y maleate had no effect on *C. albicans* biofilm formation *in vitro*. In contrast, PHCl, a nonspecific muscarinic agonist, inhibited filamentation and biofilm formation. PHCl had no fungicidal activity, and the pharmacological specificity of the response was confirmed both *in vitro* and *in vivo* using a general muscarinic receptor antagonist, scopolamine. Therefore, *C. albicans* possesses an uncharacterized cholinergic receptor involved in regulating filamentation similar in phenotype to human muscarinic receptors.

PHCl is used clinically to treat xerostomia and glaucoma (31, 32). Pharmacological studies using *in vitro* and *in vivo* models indicate that, despite being a general muscarinic agonist, PHCl has a predominance for M3 and M1 (M3<M1) muscarinic receptors in mammals (33). Muscarinic receptors are G protein-coupled receptors specialized in responding to ligands involved in cell-cell communication (34). Fungi express a number of G protein-coupled receptors that play vital roles in sensing extracellular signals (34). In *C. albicans*, G protein-coupled receptors have been shown to regulate filamentation. However, current evidence suggests that G protein-coupled receptors promote filamentation and biofilm formation (34, 35). In addition, the general muscarinic receptor antagonist dicyclomine attenuates *C. albicans* hypha formation by upregulating *tup1* expression, the master negative regulator of hypha formation (36). However, in this study, dicyclomine was found to be toxic to *C. albicans*, and the authors did not discriminate between direct fungicidal activity and specific on target effects of the compound (36).

The data herein suggest that *C. albicans* possesses a G protein-coupled receptor that can negatively regulate filamentation and biofilm formation. To date, our knowledge of fungal G protein receptors and their roles in regulation of cellular phenotype is not complete, and a number of orphan receptors have still to be functionally characterized (34). However, human studies have shown that different muscarinic receptor subtypes can have opposing functions (37, 38). It is therefore feasible that *C. albicans* possesses more than one G protein-coupled receptor that can differentially modulate filamentation, biofilm formation, and virulence. Further research is required to confirm this hypothesis.

Both M1 and M3 receptors utilize intracellular calcium as a second messenger (39). There is evidence that suggests that unrestricted calcium uptake can inhibit *C. albicans* mycelial growth, which indicates a critical role for calcium in the regulation of *C. albicans* morphogenesis (40). Calcineurin is a major player in eukaryotic calcium-

dependent signal transduction pathways. In *C. albicans*, the calcineurin pathway has been shown to be involved in tolerance to antifungal agents, cation homeostasis, and virulence. However, studies of the role of the calcineurin/calmodulin pathway in *C. albicans* hyphal growth and biofilm formation have revealed contradictory results (41). Calcineurin is a calcium-dependent serine/threonine-specific protein phosphatase, and studies have identified at least 15 novel downstream signaling targets in yeast (42). These downstream targets have been found to play roles in modulating the cell cycle, membrane structure, and cell wall integrity (42). In this study, PHCI was found to decrease *C. albicans* cell surface hydrophobicity. Cell surface hydrophobicity has been shown to be related to cell wall composition and is also a predictor of biofilm-forming capability in *Candida* species (43). Cell adhesion to host surfaces is regarded as a major virulence factor for *C. albicans* (44). Therefore, these findings suggest that cholinergic signaling inhibits *C. albicans* virulence by additional mechanisms, possibly regulated by intracellular calcium via the calcineurin/calmodulin pathway. However, further research is required to confirm this hypothesis.

C. albicans-triggered diseases represent an intriguing immunological paradigm as they result from a disrupted balance between tolerance and resistance by the immune system (45). The host immune response must eliminate the fungus while limiting collateral damage to tissues and restoring a homeostatic environment. The invasive growth of *C. albicans*, however, triggers a strong host inflammatory response that can damage infected organs (46). Acetylcholine has been found to promote rapid clearance of *C. albicans* in a *G. mellonella* infection model, while at the same time protecting against inflammation-induced tissue damage (17). The data in this article show that PHCI can also modulate host immunity to *C. albicans* infection with similar outcomes. Indeed, PHCI not only inhibited filamentation *in vivo* but could also promote rapid and effective clearance of the pathogen while limiting bystander vital tissue damage. Therefore, PHCI can also modulate the pathogenesis of *C. albicans* infection via muscarinic receptors on *G. mellonella* immune cell subsets.

Despite similarities between ACh and PHCI in terms of pathogenesis of a *C. albicans* infection in *G. mellonella*, distinct differences in the subtypes of hemocytes involved were noted. *G. mellonella* possesses at least six immune cell subsets, granulocytes, plasmatocytes, oenocytoids, spherulocytes, prohemocytes, and adipohemocytes (47). Granulocytes, the very first cells recruited to counteract pathogen invasion, were strongly activated *in vivo* in the presence of ACh, but not PHCI. Similarly, spherulocytes, whose function is still to be defined, were specifically recruited into tissues in ACh-inoculated larvae, but not in PHCI-inoculated larvae. As spherulocyte recruitment is known to be dependent on granulocyte recruitment, this finding is perhaps unsurprising. However, a direct inhibitory effect of PHCI on spherulocyte recruitment cannot be ruled out. In addition to hemocyte recruitment, PHCI was found to promote less hemocyte aggregation *in vivo* than ACh, and the resulting nodules were mainly characterized by the presence of plasmatocytes, which are usually necessary during the later phases of nodulation and encapsulation.

In this study, differences between *in vitro*- and *in vivo*-stimulated hemocytes, both in terms of morphology and quantity, were observed. In particular, under all conditions investigated, the *in vitro* spherulocyte content was reduced compared with the *in vivo* spherulocyte content, as spherulocytes do not originate from division of circulating hemocytes but are derived from the granulocyte lineage of hematopoietic organs (48). We hypothesize therefore that the biological functions of ACh and PHCI may also be modulated by larval tissue or plasma factors that are missing in cultured cells. Indeed, the fat body of *G. mellonella* plays a crucial metabolic function, producing antimicrobial peptides and proteins that are involved in dictating immune responses.

The data in this article suggest that cholinergic receptors can modulate *G. mellonella* hematopoiesis and differentiation. Interestingly, in humans, cholinergic receptors have been shown to regulate hematopoiesis (49). Platelet and megakaryocyte precursors (50), as well as myeloid and erythroid progenitors in the bone marrow (51), all express the $\alpha 7nAChR$ which is suggested to play a vital role in regulating their differentiation

and maturation. Therefore, it is interesting to speculate that similar systems operate in *G. mellonella*. However, further research using specific cholinergic receptor agonist and antagonists is required to begin to delineate the type of cholinergic receptors that regulate *G. mellonella* cellular immunity. The fact that ACh, and not PHCl, induced hemocyte recruitment and aggregation suggests that nicotinic receptors rather than muscarinic receptors may play a more important role in immune regulation in this model host.

In conclusion, the present study suggests that different cholinergic receptors may be involved in the promotion of favorable outcome to *C. albicans* systemic infection. A muscarinic-type receptor seems to modulate *C. albicans* filamentation and biofilm formation. In addition, the data suggest that hemocyte subsets of *G. mellonella* possess different repertoires of cholinergic receptors that can modulate their differentiation and function. Therefore, this article provides evidence that targeting cholinergic receptors by repurposing currently licensed cholinergic drugs may be a direct or adjunctive therapeutic strategy to prevent or treat potentially fatal fungal infections.

MATERIALS AND METHODS

Candida albicans yeast culture and biofilm formation. *C. albicans* SC5314 was subcultured and propagated as described previously (17). *C. albicans* SC5314 was then standardized to 1×10^6 cells/ml in Roswell Park Memorial Institute 1640 medium (RPMI 1640) in the presence or absence of various concentrations of pilocarpine hydrochloride (PHCl) (Tocris, UK) or SIB1508Y maleate (Tocris, UK). To determine specificity of action, experiments were also performed with PHCl in the presence or absence of various concentrations of scopolamine (SCP) (Tocris, UK). Standardized cells were allowed to form biofilms in flat-bottomed 96-well microtiter plates at 37°C for 24 h. Following incubation, metabolic activity was assessed using the 2,3-bis-(2-methoxy-4-nitro-5-sulfophenyl)-2H-tetrazolium-5-carboxanilide (XTT) assay and biofilm biomass determined using the crystal violet assay as described previously (52). Experimental conditions were run in triplicate. Results are presented as mean values from at least four independent experiments.

Propidium iodide uptake and ATP release assays. To evaluate whether any indirect antifungal activity through the disruption of the cell membrane was induced by PHCl, we used a propidium iodide (PI) uptake and ATP release assay, as previously described (29). Briefly, *C. albicans* SC5314 was standardized to 5×10^7 cells/ml in RPMI 1640 and treated with 50 mM PHCl for 60 min. After treatment, the supernatant was harvested, and the cells were washed with PBS and treated with 2 μ M PI (in PBS). After incubation at 37°C for 15 min, fluorescence was measured at excitation and emission wavelengths of 485 and 620 nm, respectively. The ATP release assay was performed according to the manufacturer's instructions on supernatants harvested after 60 min using an ATP bioluminescent assay kit (Sigma-Aldrich, UK). Experimental conditions were run in triplicate and repeated on three independent occasions.

Biofilm viability and cell morphology. Standardized *C. albicans* SC5314 (1×10^6 cells/ml) were inoculated in RPMI with or without PHCl on Thermanox coverslips (13 mm) within a 24-well tissue culture plate and then incubated for 24 h at 37°C. For light microscopy, coverslips were washed gently with PBS and stained with crystal violet (0.05% [vol/vol]). For fluorescence microscopy, the coverslips were washed gently with PBS and stained according to the manufacturers' instructions with 5 μ M calcofluor white (CFW) (Invitrogen, UK) and 20 μ M propidium iodide (PI) (Sigma, UK). For scanning electron microscopy (SEM), the specimens were prepared as previously described (53). Biofilms were visualized under a fluorescence microscope (Motic BA400 Colorview system) in normal light mode for crystal violet-stained coverslips or at Ex₃₅₀/Em₄₀₀ for calcofluor white-stained coverslips and Ex₅₄₀/Em₅₂₅ for propidium iodide-stained coverslips. For SEM, biofilms were visualized by using a JEOL JSM-6400 scanning electron microscope. Representative images from 10 fields were taken. Experiments were repeated in duplicate on at least three independent occasions, and representative images are shown.

Microbial adhesion to hydrocarbon assay. The ability of yeast cells to adhere to a hydrocarbon source (Octane; Sigma, Italy) was used to measure cell surface hydrophobicity (CSH), as previously described (43). Briefly, *C. albicans* SC5314 was cultured in YPD (planktonic cells), RPMI 1640 alone (biofilm), or RPMI 1640 with 6.25, 12.5, and 25 mM PHCl for 24 h. The cells were then standardized to 10^8 cells/ml and mixed with octane for 2 min. The aqueous and organic phases were allowed to separate for 10 min at 30°C, and the optical density of the aqueous phase was determined at OD₆₀₀. The CSH index was calculated as follows: percent CSH = $[1 - (B - A)] \times 100$ (where *A* is the initial absorbance of the aqueous phase, and *B* is the absorbance of the aqueous phase after partitioning). Samples were run in duplicate. Results are presented as mean values from five independent experiments.

Galleria mellonella killing assay. Pathogenicity of *C. albicans* SC5314 with or without PHCl was assessed using the *G. mellonella* killing assay as described previously (17). Sixteen randomly selected sixth-instar *G. mellonella* larvae (Allevamento Cirà, Como, Italy) with a body weight of between 200 to 300 mg were employed for each experimental group. Overnight YPD cultures of *C. albicans* SC5314 were standardized in PBS to the desired cell density. Larvae were inoculated into the hemocoel with 5×10^5 cells/larva with or without PHCl at different concentrations using a 10- μ l Hamilton syringe with a 26-gauge needle. In addition, larvae inoculated with PBS and PHCl alone were included for control

purposes. A group injected simultaneously with PHCl with or without SCP was further added to verify the specificity of PHCl action. The inoculated larvae were incubated at 37°C, and the number of dead larvae was scored daily. All experiments were repeated on three independent occasions.

Hemocyte characteristics. For the *in vitro* experiments, the hemolymph of five *G. mellonella* larvae was collected into ice-cold Grace's medium (Sigma-Aldrich, Italy) by lateral bleeding corresponding to the last right proleg. Hemocytes were counted and plated onto coverslips in a 24-well plate. The plates were incubated for 2 h to allow hemocytes to adhere prior to stimulation with *C. albicans* SC5314 (10^2 yeast cells/well) for 24 h in the presence and absence of PHCl or ACh. After treatment, hemocytes were fixed in 4% paraformaldehyde and stained with hematoxylin and eosin. Hemocytes incubated in media alone acted as a control.

For the *in vivo* experiments, *G. mellonella* larvae were inoculated using the same conditions described for the killing assay. Twenty-four hours after treatment, hemocytes were isolated from the larvae as described above. Hemocytes from three larvae for each experimental condition were then pooled and plated onto coverslips in a 24-well plate. The coverslips were centrifuged for 3 min at $300 \times g$ at room temperature and fixed in 4% paraformaldehyde and stained with hematoxylin and eosin.

In both *in vitro* and *in vivo* experiments, hemocyte proliferation (cellularity), subtype differentiation and nodule formation were assessed in comparison to hemocytes incubated in media only (*in vitro*) or hemocytes from sham-inoculated larvae (*in vivo*). A single trained and experienced pathologist (M. Falleni) carried out all characterization and quantification.

Larval histology. After hemolymph extraction, the same larvae were processed for histology as previously described (54). Briefly, the larvae were inoculated with buffered formalin and processed by means of transverse cut serial sections. Tissue sections were embedded in paraffin and routinely processed for conventional histopathology. Serial 4- μ m tissue sections were stained with hematoxylin and eosin (HE) or periodic acid-Schiff stain (PAS). Image acquisition was performed by the NanoZoomer-XR C12000 series (Hamamatsu Photonics). To investigate *C. albicans* filamentation and the effect on cellular immunity *in vivo*, two time points were used, 24 and 48 h. Data were confirmed in three independent experiments, and representative images are shown.

Statistical analysis. Graph production, data distribution, and statistical analysis were performed using GraphPad Prism (version 4; La Jolla, CA). Crystal violet and XTT data were found to be abnormally distributed; therefore, all concentrations were compared to the control using a Kruskal-Wallis nonparametric test with a Dunns post-test. The ATP assay data were found to be normally distributed; therefore, a Tukey's multiple-comparison test was used for statistical analysis. The *G. mellonella* survival curves were analyzed using a log rank test. Statistical significance was achieved if $P < 0.05$.

ACKNOWLEDGMENTS

This work was supported by a Wellcome Trust Strategic Award for Medical Mycology and Fungal Immunology 097377/Z/11/Z grant awarded to G.R., a Università degli Studi di Milano-Linea B grant awarded to E.B., and a BBSRC Industrial CASE Ph.D. studentship for C.D. (BB/P504567/1).

We thank Raffaella Adami for assistance with confocal microscopy and David Lappin for statistical support.

We have no conflicts of interest to report.

REFERENCES

- Wessler I, Kirkpatrick CJ. 2008. Acetylcholine beyond neurons: the non-neuronal cholinergic system in humans. *Br J Pharmacol* 154:1558–1571. <https://doi.org/10.1038/bjp.2008.185>.
- Wessler I, Kilbinger H, Bittinger F, Unger R, Kirkpatrick CJ. 2003. The non-neuronal cholinergic system in humans: expression, function and pathophysiology. *Life Sci* 72:2055–2061.
- Kawashima K, Fujii T. 2008. Basic and clinical aspects of non-neuronal acetylcholine: overview of non-neuronal cholinergic systems and their biological significance. *J Pharmacol Sci* 106:167–173.
- Fernandez-Cabezudo MJ, Lorke DE, Azimullah S, Mechkarska M, Hasan MY, Petroianu GA, Al-Ramadi BK. 2010. Cholinergic stimulation of the immune system protects against lethal infection by *Salmonella enterica* serovar Typhimurium. *Immunology* 130:388–398. <https://doi.org/10.1111/j.1365-2567.2009.03238.x>.
- Rosas-Ballina M, Tracey KJ. 2009. Cholinergic control of inflammation. *J Intern Med* 265:663–679. <https://doi.org/10.1111/j.1365-2796.2009.02098.x>.
- Song XM, Li JG, Wang YL, Hu ZF, Zhou Q, Du ZH, Jia BH. 2008. The protective effect of the cholinergic anti-inflammatory pathway against septic shock in rats. *Shock* 30:468–472. <https://doi.org/10.1097/SHK.0b013e31816d5e49>.
- Bencherif M, Lippello PM, Lucas R, Marrero MB. 2011. Alpha7 nicotinic receptors as novel therapeutic targets for inflammation-based diseases. *Cell Mol Life Sci* 68:931–949. <https://doi.org/10.1007/s00018-010-0525-1>.
- Kawashima K, Fujii T. 2004. Expression of non-neuronal acetylcholine in lymphocytes and its contribution to the regulation of immune function. *Front Biosci* 9:2063–2085.
- Hamano R, Takahashi HK, Iwagaki H, Yoshino T, Nishibori M, Tanaka N. 2006. Stimulation of alpha7 nicotinic acetylcholine receptor inhibits CD14 and the Toll-like receptor 4 expression in human monocytes. *Shock* 26:358–364. <https://doi.org/10.1097/01.shk.0000228168.86845.60>.
- Neumann S, Razen M, Habermehl P, Meyer CU, Zepp F, Kirkpatrick CJ, Wessler I. 2007. The non-neuronal cholinergic system in peripheral blood cells: effects of nicotinic and muscarinic receptor antagonists on phagocytosis, respiratory burst and migration. *Life Sci* 80:2361–2364. <https://doi.org/10.1016/j.lfs.2007.01.010>.
- Kawashima K, Misawa H, Moriwaki Y, Fujii YX, Fujii T, Horiuchi Y, Yamada T, Imanaka T, Kamekura M. 2007. Ubiquitous expression of acetylcholine and its biological functions in life forms without nervous systems. *Life Sci* 80:2206–2209. <https://doi.org/10.1016/j.lfs.2007.01.059>.
- Yamada T, Fujii T, Kanai T, Amo T, Imanaka T, Nishimasu H, Wakagi T, Shoun H, Kamekura M, Kamagata Y, Kato T, Kawashima K. 2005. Expression of acetylcholine (ACh) and ACh-synthesizing activity in Archaea. *Life Sci* 77:1935–1944. <https://doi.org/10.1016/j.lfs.2005.01.026>.

13. Horiuchi Y, Kimura R, Kato N, Fujii T, Seki M, Endo T, Kato T, Kawashima K. 2003. Evolutional study on acetylcholine expression. *Life Sci* 72: 1745–1756.
14. Bocquet N, Prado de Carvalho L, Cartaud J, Neyton J, Le Poupon C, Taly A, Grutter T, Changeux JP, Corringier PJ. 2007. A prokaryotic proton-gated ion channel from the nicotinic acetylcholine receptor family. *Nature* 445:116–119. <https://doi.org/10.1038/nature05371>.
15. Tasneem A, Iyer LM, Jakobsson E, Aravind L. 2005. Identification of the prokaryotic ligand-gated ion channels and their implications for the mechanisms and origins of animal Cys-loop ion channels. *Genome Biol* 6:R4. <https://doi.org/10.1186/gb-2004-6-1-r4>.
16. Inglis DO, Arnaud MB, Binkley J, Shah P, Skrzypek MS, Wymore F, Binkley G, Miyasato SR, Simison M, Sherlock G. 2012. The *Candida* genome database incorporates multiple *Candida* species: multispecies search and analysis tools with curated gene and protein information for *Candida albicans* and *Candida glabrata*. *Nucleic Acids Res* 40:D667–D674. <https://doi.org/10.1093/nar/gkr945>.
17. Rajendran R, Borghi E, Falleni M, Perdoni F, Tosi D, Lappin DF, O'Donnell L, Greetham D, Ramage G, Nile C. 2015. Acetylcholine protects against *Candida albicans* infection by inhibiting biofilm formation and promoting hemocyte function in a *Galleria mellonella* infection model. *Eukaryot Cell* 14:834–844. <https://doi.org/10.1128/EC.00067-15>.
18. Lavine MD, Strand MR. 2002. Insect hemocytes and their role in immunity. *Insect Biochem Mol Biol* 32:1295–1309.
19. Wu G, Liu Y, Ding Y, Yi Y. 2016. Ultrastructural and functional characterization of circulating hemocytes from *Galleria mellonella* larva: cell types and their role in the innate immunity. *Tissue Cell* 48:297–304. <https://doi.org/10.1016/j.tice.2016.06.007>.
20. Browne N, Heelan M, Kavanagh K. 2013. An analysis of the structural and functional similarities of insect hemocytes and mammalian phagocytes. *Virulence* 4:597–603. <https://doi.org/10.4161/viru.25906>.
21. Kawashima K, Fujii T, Moriwaki Y, Misawa H, Horiguchi K. 2015. Non-neuronal cholinergic system in regulation of immune function with a focus on alpha7 nAChRs. *Int Immunopharmacol* 29:127–134. <https://doi.org/10.1016/j.intimp.2015.04.015>.
22. Kistemaker LE, Bos IS, Hylkema MN, Nawijn MC, Hiemstra PS, Wess J, Meurs H, Kerstjens HA, Gossens R. 2013. Muscarinic receptor subtype-specific effects on cigarette smoke-induced inflammation in mice. *Eur Respir J* 42:1677–1688. <https://doi.org/10.1183/09031936.00112412>.
23. Su X, Matthey MA, Malik AB. 2010. Requisite role of the cholinergic alpha7 nicotinic acetylcholine receptor pathway in suppressing Gram-negative sepsis-induced acute lung inflammatory injury. *J Immunol* 184:401–410. <https://doi.org/10.4049/jimmunol.0901808>.
24. Tata AM, Velluto L, D'Angelo C, Reale M. 2014. Cholinergic system dysfunction and neurodegenerative diseases: cause or effect? *CNS Neurol Disord Drug Targets* 13:1294–1303.
25. Sales ME. 2013. Cholinergic drugs as therapeutic tools in inflammatory diseases: participation of neuronal and non-neuronal cholinergic systems. *Antiinflamm Antiallergy Agents Med Chem* 12:109–116.
26. Sales ME. 2010. Muscarinic receptors as targets for anti-inflammatory therapy. *Curr Opin Investig Drugs* 11:1239–1245.
27. Pohanka M. 2012. Alpha7 nicotinic acetylcholine receptor is a target in pharmacology and toxicology. *Int J Mol Sci* 13:2219–2238. <https://doi.org/10.3390/ijms13022219>.
28. Van Dijk P, Sjollem J, Cammue BP, Lagrou K, Berman J, d'Enfert C, Andes DR, Arendrup MC, Brakhage AA, Calderone R, Canton E, Coenye T, Cos P, Cowen LE, Edgerton M, Espinel-Ingroff A, Filler SG, Ghannoum M, Gos NAR, Haas H, Jabra-Rizk MA, Johnson EM, Lockhart SR, Lopez-Ribot JL, Maertens J, Munro CA, Nett JE, Nobile CJ, Pfaller MA, Ramage G, Sanglard D, Sanguinetti M, Spriet I, Verweij PE, Warris A, Wauters J, Yeaman MR, Zaat SAJ, Thevissen K. 2018. Methodologies for in vitro and in vivo evaluation of efficacy of antifungal and antibiofilm agents and surface coatings against fungal biofilms. *Microb Cell* 5:300–326. <https://doi.org/10.15698/mic2018.07.638>.
29. Sherry L, Jose A, Murray C, Williams C, Jones B, Millington O, Bagg J, Ramage G. 2012. Carbohydrate derived fulvic acid: an in vitro investigation of a novel membrane active antiseptic agent against *Candida albicans* biofilms. *Front Microbiol* 3:116. <https://doi.org/10.3389/fmicb.2012.00116>.
30. Borghi E, Morace G, Borgo F, Rajendran R, Sherry L, Nile C, Ramage G. 2015. New strategic insights into managing fungal biofilms. *Front Microbiol* 6:1077. <https://doi.org/10.3389/fmicb.2015.01077>.
31. Ciurtin C, Ostas A, Cojocaru VM, Walsh SB, Isenberg DA. 2015. Advances in the treatment of ocular dryness associated with Sjogrens syndrome. *Semin Arthritis Rheum* 45:321–327. <https://doi.org/10.1016/j.semarthrit.2015.06.007>.
32. Burr J, Azuara-Blanco A, Avenell A, Tuulonen A. 2012. Medical versus surgical interventions for open angle glaucoma. *Cochrane Database Syst Rev* 12:CD004399. <https://doi.org/10.1002/14651858.CD004399.pub3>.
33. Figueroa KW, Griffin MT, Ehler FJ. 2009. Selectivity of agonists for the active state of M1 to M4 muscarinic receptor subtypes. *J Pharmacol Exp Ther* 328:331–342. <https://doi.org/10.1124/jpet.108.145219>.
34. Xue C, Hsueh YP, Heitman J. 2008. Magnificent seven: roles of G protein-coupled receptors in extracellular sensing in fungi. *FEMS Microbiol Rev* 32:1010–1032. <https://doi.org/10.1111/j.1574-6976.2008.00131.x>.
35. Maitan MM, De Rop L, Serneels J, Exler S, Rupp S, Tourneau H, Thevelein JM, Van Dijck P. 2005. The G protein-coupled receptor Gpr1 and the Galpha protein Gpa2 act through the cAMP-protein kinase A pathway to induce morphogenesis in *Candida albicans*. *Mol Biol Cell* 16:1971–1986. <https://doi.org/10.1091/mbc.e04-09-0780>.
36. Ali A, Jadhav A, Jangid P, Patil R, Shelar A, Karuppaiyl SM. 2018. The human muscarinic acetylcholine receptor antagonist, dicyclomine targets signal transduction genes and inhibits the virulence factors in the human pathogen, *Candida albicans*. *J Antibiot* 71:456–466. <https://doi.org/10.1038/s41429-017-0013-z>.
37. Zhang HM, Chen SR, Matsui M, Gautam D, Wess J, Pan HL. 2006. Opposing functions of spinal M2, M3, and M4 receptor subtypes in regulation of GABAergic inputs to dorsal horn neurons revealed by muscarinic receptor knockout mice. *Mol Pharmacol* 69:1048–1055. <https://doi.org/10.1124/mol.105.018069>.
38. Zhang HM, Zhou HY, Chen SR, Gautam D, Wess J, Pan HL. 2007. Control of glycinergic input to spinal dorsal horn neurons by distinct muscarinic receptor subtypes revealed using knockout mice. *J Pharmacol Exp Ther* 323:963–971. <https://doi.org/10.1124/jpet.107.127795>.
39. Qin K, Dong C, Wu G, Lambert NA. 2011. Inactive-state preassembly of G(q)-coupled receptors and G(q) heterotrimers. *Nat Chem Biol* 7:740–747. <https://doi.org/10.1038/nchembio.642>.
40. Holmes AR, Cannon RD, Shepherd MG. 1991. Effect of calcium ion uptake on *Candida albicans* morphology. *FEMS Microbiol Lett* 61: 187–193.
41. Yu SJ, Chang YL, Chen YL. 2015. Calcineurin signaling: lessons from *Candida* species. *FEMS Yeast Res* 15:fov016. <https://doi.org/10.1093/femsyr/fov016>.
42. Goldman A, Roy J, Bodenmiller B, Wanka S, Landry CR, Aebersold R, Cyert MS. 2014. The calcineurin signaling network evolves via conserved kinase-phosphatase modules that transcend substrate identity. *Mol Cell* 55:422–435. <https://doi.org/10.1016/j.molcel.2014.05.012>.
43. Borghi E, Sciota R, Biassoni C, Cirasola D, Cappelletti L, Vizzini L, Boracchi P, Morace G. 2011. Cell surface hydrophobicity: a predictor of biofilm production in *Candida* isolates? *J Med Microbiol* 60:689–690. <https://doi.org/10.1099/jmm.0.026898-0>.
44. Mayer FL, Wilson D, Hube B. 2013. *Candida albicans* pathogenicity mechanisms. *Virulence* 4:119–128. <https://doi.org/10.4161/viru.22913>.
45. Romani L. 2011. Immunity to fungal infections. *Nat Rev Immunol* 11: 275–288. <https://doi.org/10.1038/nri2939>.
46. Lionakis MS. 2014. New insights into innate immune control of systemic candidiasis. *Med Mycol* 52:555–564. <https://doi.org/10.1093/mmy/myu029>.
47. Kavanagh K, Reeves EP. 2004. Exploiting the potential of insects for in vivo pathogenicity testing of microbial pathogens. *FEMS Microbiol Rev* 28:101–112. <https://doi.org/10.1016/j.femsre.2003.09.002>.
48. Tan J, Xu M, Zhang K, Wang X, Chen S, Li T, Xiang Z, Cui H. 2013. Characterization of hemocytes proliferation in larval silkworm, *Bombyx mori*. *J Insect Physiol* 59:595–603. <https://doi.org/10.1016/j.jinsphys.2013.03.008>.
49. Serobyan N, Jagannathan S, Orlovskaya I, Schraufstatter I, Skok M, Loring J, Khaldoyanidi S. 2007. The cholinergic system is involved in regulation of the development of the hematopoietic system. *Life Sci* 80:2352–2360. <https://doi.org/10.1016/j.lfs.2007.04.017>.
50. Thornton S, Schedel A, Besenfelder S, Kluter H, Bugert P. 2011. Cholinergic drugs inhibit in vitro megakaryopoiesis via the alpha7-nicotinic acetylcholine receptor. *Platelets* 22:390–395. <https://doi.org/10.3109/09537104.2010.551304>.
51. Koval LM, Zverkova AS, Grailhe R, Utkin YN, Tsetlin VI, Komisarenko SV, Skok MV. 2008. Nicotinic acetylcholine receptors alpha4beta2 and alpha7 regulate myelo- and erythropoiesis within the bone marrow. *Int J Biochem Cell Biol* 40:980–990. <https://doi.org/10.1016/j.biocel.2007.11.006>.

52. Jose A, Coco BJ, Milligan S, Young B, Lappin DF, Bagg J, Murray C, Ramage G. 2010. Reducing the incidence of denture stomatitis: are denture cleansers sufficient? *J Prosthodont* 19:252–257. <https://doi.org/10.1111/j.1532-849X.2009.00561.x>.
53. Erlandsen SL, Kristich CJ, Dunny GM, Wells CL. 2004. High-resolution visualization of the microbial glycocalyx with low-voltage scanning electron microscopy: dependence on cationic dyes. *J Histochem Cytochem* 52:1427–1435. <https://doi.org/10.1369/jhc.4A6428.2004>.
54. Perdoni F, Falleni M, Tosi D, Cirasola D, Romagnoli S, Braidotti P, Clementi E, Bulfamante G, Borghi E. 2014. A histological procedure to study fungal infection in the wax moth *Galleria mellonella*. *Eur J Histochem* 58:2428. <https://doi.org/10.4081/ejh.2014.2428>.

Article

Cystic Fibrosis Defective Response to Infection Involves Autophagy and Lipid Metabolism

Alessandra Mingione ^{1,†}, Emerenziana Ottaviano ^{2,†}, Matteo Barcella ², Ivan Merelli ³, Lorenzo Rosso ⁴, Tatiana Armeni ⁵, Natalia Cirilli ⁶, Riccardo Ghidoni ^{1,7}, Elisa Borghi ²  and Paola Signorelli ^{1,*} 

¹ Biochemistry and Molecular Biology Laboratory, Health Science Department, University of Milan, San Paolo Hospital, 20142 Milan, Italy; alessandra.mingione@unimi.it (A.M.); riccardo.ghidoni@unimi.it (R.G.)

² Laboratory of Clinical Microbiology, Health Science Department, University of Milan, San Paolo Hospital, 20142 Milan, Italy; emerenziana.ottaviano@unimi.it (E.O.); matteobarcella84@gmail.com (M.B.); elisa.borghi@unimi.it (E.B.)

³ National Research Council of Italy, Institute for Biomedical Technologies, Via Fratelli Cervi 93, 20090 Milan, Italy; ivan.merelli@itb.cnr.it

⁴ Health Sciences Department, University of Milan, Thoracic surgery and transplantation Unit, Fondazione IRCCS Ca Granda Ospedale Maggiore Policlinico, 20122 Milan, Italy; lorenzo.rosso@unimi.it

⁵ Department of Clinical Sciences, Section of Biochemistry, Biology and Physics, Polytechnic University of Marche, 60131 Ancona, Italy; t.armeni@staff.univpm.it

⁶ Cystic Fibrosis Referral Care Center, Mother-Child Department, United Hospitals Le Torrette, 60126 Ancona, Italy; natalia.cirilli@ospedaliriuniti.marche.it

⁷ “Aldo Ravelli” Center for Neurotechnology and Experimental Brain Therapeutics, via Antonio di Rudinì 8, 20142 Milan, Italy

* Correspondence: paola.signorelli@unimi.it

† The authors contributed equally to this work.

Received: 26 June 2020; Accepted: 4 August 2020; Published: 6 August 2020



Abstract: Cystic fibrosis (CF) is a hereditary disease, with 70% of patients developing a proteinopathy related to the deletion of phenylalanine 508. CF is associated with multiple organ dysfunction, chronic inflammation, and recurrent lung infections. CF is characterized by defective autophagy, lipid metabolism, and immune response. Intracellular lipid accumulation favors microbial infection, and autophagy deficiency impairs internalized pathogen clearance. Myriocin, an inhibitor of sphingolipid synthesis, significantly reduces inflammation, promotes microbial clearance in the lungs, and induces autophagy and lipid oxidation. RNA-seq was performed in *Aspergillus fumigatus*-infected and myriocin-treated CF patients' derived monocytes and in a CF bronchial epithelial cell line. Fungal clearance was also evaluated in CF monocytes. Myriocin enhanced CF patients' monocytes killing of *A. fumigatus*. CF patients' monocytes and cell line responded to infection with a profound transcriptional change; myriocin regulates genes that are involved in inflammation, autophagy, lipid storage, and metabolism, including histones and heat shock proteins whose activity is related to the response to infection. We conclude that the regulation of sphingolipid synthesis induces a metabolism drift by promoting autophagy and lipid consumption. This process is driven by a transcriptional program that corrects part of the differences between CF and control samples, therefore ameliorating the infection response and pathogen clearance in the CF cell line and in CF peripheral blood monocytes.

Keywords: cystic fibrosis; sphingolipids; autophagy; myriocin; *Aspergillus fumigatus*

1. Introduction

Cystic fibrosis (CF) is a hereditary disease associated with different classes of mutations in the Cystic Fibrosis Transmembrane conductance Regulator (CFTR), a chloride/carbonate channel. A deletion of phenylalanine 508 (F508) affects more than 70% of patients and results in unfolded proteins accumulation, causing a proteinopathy responsible for inflammation, impaired autophagy, and altered lipid metabolism [1–5]. CF is a multiple-organ disease characterized by life-threatening chronic inflammation and recurrent infection of the lungs, where defective immune response and altered mucus viscosity and acidity pave the way to persistent microbial colonization [6]. Indeed, CF is characterized by ineffective clearance of pathogens and reduced killing of internalized microbes, both in pulmonary airways epithelia and in macrophages [7–9]. Moreover, recurrent antibacterial therapies favor the insurgence of drug resistance and, by altering the microbiological milieu, promote colonization by opportunistic pathogens. *Aspergillus fumigatus* is the most prevalent filamentous fungus in the respiratory tract of CF patients, contributing to lung deterioration. Approximately 35% of CF patients are infected by *A. fumigatus*, and researchers are still investigating ways to prevent its colonization [10], since CFTR dysfunction itself has been directly associated with a reduced clearance ability of *A. fumigatus* conidia by CF airway epithelia [8,11].

CF cells suffer from defective autophagy, which is related to altered proteostasis and chronic inflammation [12–14]. Autophagy is a conserved cell-autonomous stress response, dedicated to the breakdown of cellular material and to cell content recycling. Apart from its homeostatic role and its crucial activity in stress conditions, autophagy is actively involved in pathogen clearance, offering the cell an extremely efficient defensive response. A specialized form of autophagy called xenophagy involves the recognition and clearance of foreign particles and pathogens. Pattern recognition receptors (PRRs), upon antigen engagement, recruit microtubule-associated protein 1B light chain-3 (LC3) and successively other components of the canonical autophagy pathway, therefore enabling the binding of foreign particles that are already contained within a single membraned phagosome or endosome and their addressing to lysosomes [15].

The ability to detoxify and/or assimilate host lipids is a crucial aspect of the infection process [16,17], particularly in fungal infection [18]. In addition, the mobilization of internal lipid stores to release growth substrates, as well as lipid-mediated cellular signaling, contribute to the pathogen invasion outcome [18]. The activation of lipid catabolism via transcriptional activity of transcription factor EB/peroxisome proliferator-activated receptor α (TFEB/PPAR α) potentiates macrophage response to infection [19].

Several studies reported an altered lipid homeostasis in blood and peripheral tissues in CF patients [1,2,20–24], and demonstrated the pathological role of the inflammatory ceramide accumulation in CF airways [4,25]. In a CF mouse model and in bronchial epithelial cells, our group previously demonstrated that hampering ceramide accumulation by the sphingolipid synthesis inhibitor myriocin (Myr) reduces inflammation and ameliorates the response against microbial infection in vivo and in vitro by promoting cell-killing ability [8,25,26]. Moreover, the inhibition of ceramide synthesis in CF cells activates TFEB, a master regulator of the stress response. Indeed, TFEB is responsible for enhancing autophagy and lipid oxidation via the activation of lipid-metabolism-related transcription factors such as PPARs and FOXO, thus reducing the overall lipid content [5].

Here we studied the myriocin modulation of gene expression profile and its effect in promoting conidial killing in CF patients' monocytes infected with *A. fumigatus*. Next, we demonstrated that *A. fumigatus* infection triggers a different expression profile in CF bronchial epithelial cells compared to healthy control cells. We further investigated the effect of Myr treatment on the expression of genes involved in inflammation and in the autophagic response to infection. Our data suggest that regulating the altered lipid metabolism could represent a possible therapeutic strategy in ameliorating CF disease.

2. Materials and Methods

2.1. Cells and Treatments

IB3-1 cells (named CF cells), an adeno-associated virus-transformed human bronchial epithelial cell line derived from a CF patient (Δ F508/W1282X) and provided by LGC Promochem (US), were grown in LHC-8 medium supplemented with 10% fetal bovine serum (FBS) and 1% penicillin/streptomycin at 37 °C and 5% CO₂. Human lung bronchial epithelial cells 16HBE14o- (named CTRL cells), originally developed by Dieter C. Gruenert, were provided by Luis J. Galiotta, (Telethon Institute of Genetics and Medicine—TIGEM, Napoli) and cultured, as recommended, in Minimum Essential Medium (MEM) Earle's salt, supplemented with 10% FBS and 1% penicillin/streptomycin at 37 °C and 5% CO₂. Myriocin (Myr) treatments were performed at a concentration of 50 µM for the indicated time lengths in 100 mm dishes plated at 1×10^5 cells/each. At least triplicate samples for each experiment were performed.

2.2. *Aspergillus Fumigatus* Culture

The reference strain *A. fumigatus* Af293 (ATCC MYA-4609, CBS 101355) was used in the study. Frozen conidia were streaked out from glycerol stocks stored at −80 °C on fresh Potato Dextrose Agar (PDA) slant and incubated at 30 °C for 72–96 h, until sporulation. Conidia were then harvested, suspended in 0.01% Tween-20, washed in phosphate-buffered saline (PBS), and counted by hemocytometer.

2.3. Cells Infection

We plated 1×10^6 cells, either CF or CTRL, in 100 mm Petri dishes and grew them overnight in 5 mL of appropriate medium. The next day, cells were pre-treated with 50 µM Myr for 1 h and then infected with *A. fumigatus* conidia with a multiplicity of infection (MOI) of 1:100 for 1 h. Cells were washed three times in PBS to eliminate non-engulfed conidia and incubated for 3 h with 5 mL medium containing or not 50 µM Myr. Cells were collected at this time, or after 12 h, for subsequent analysis.

For the killing assay, patients' monocytes were pretreated with Myr (50 µM) or medium alone for 1 h at 37 °C and then infected with *A. fumigatus* conidia (MOI 1:1). One hour after infection, cells were washed twice with PBS to remove non-internalized conidia, and incubated for a further 4 h to allow conidia killing. Cells were then harvested, counted, and lysed by osmotic shock to recover live internalized conidia. Cellular lysis was confirmed by microscopy. The supernatant was mixed vigorously, serially diluted in PBS, and plated onto Sabouraud Dextrose Agar (SAB). Plates were incubated at 37 °C, and colony forming units (CFU) were counted after 48 and 72 h of growth.

2.4. PBMC Isolation and Infection

We collected 43 blood samples from CF patients referred to the Ancona Cystic Fibrosis Centre, 22 homozygotes for the F508del mutation of the *CFTR* gene and 21 compound heterozygotes with one F508del allele (as shown in Supplementary Table S1) (United Hospital Le Torrette, Ancona, Italy, CE Regionale Marche -CERM-, protocol number 2016 0606OR).

Peripheral blood mononuclear cells (PBMCs) were freshly isolated using Leucosep protocol and stored at −80 °C until use. To avoid the influence of anti-CD14-coated microbeads selection on cytokine production, we isolated monocytes by plastic adherence [27]. Briefly, 1×10^6 PBMCs per well were seeded into 6-well plates (Corning Inc. Costar, New York, NY, USA) and allowed to adhere in a 5% CO₂ incubator at 37 °C for 2 h in 2 mL Roswell Park Memorial Institute (RPMI) 1640 medium supplemented with 10% FBS and 1% penicillin/streptomycin. Free-floating cells were then removed by washing and the adhering monocytes were used for *A. fumigatus* infection as described above for cell lines.

2.5. qRT-PCR

One microgram of purified RNA was reverse transcribed to cDNA. The amplification was performed for the following target genes: *IL-1B*, *CXCL8*, *IL-10*, *NOD2*, *TLR2*, *TLR7*, *TBK1*, *OPTN*, *TFEB*, *LAMP2a*, *TP53INP1*, *TMEM59*, *HIGD1A*. Relative mRNA expression of target genes was normalized to the endogenous *GAPDH* control gene and represented as fold change versus control, calculated by the comparative CT method ($\Delta\Delta$ CT Method). The analysis was performed by referring to control values that did not significantly differentiate (triplicate samples, and their standard deviation value divided by their mean value was <1). Supplementary Figure S1 shows the $\Delta\Delta$ CT analysis of the target genes in basal condition, with CF cells versus CTRL cells. Real-time PCR was performed by SYBR Premix Ex Taq™ II (Takara); primer sequences are available on request.

2.6. Statistical Analysis

Data are expressed as mean \pm SE, calculated from experimental replicates. Data significance was evaluated by two-way ANOVA followed by Bonferroni correction ($p < 0.05$) or Wilcoxon *t*-test (for paired samples), as specified in the figure legends. Statistical analysis was performed by GraphPad InStat software (La Jolla, CA, USA) and graph illustrations were generated by GraphPad Prism software (La Jolla, CA, USA).

2.7. RNA Extraction and Sequencing

Total RNA was isolated from harvested cells and patients' samples with the ReliaPrep™ Miniprep RNA extraction system (Promega), according to the manufacturer instructions.

Sequencing was performed on Illumina NextSeq using the SMART-Seq protocol for the preparation of the libraries, obtaining an average of 15 million single-end reads per sample. All sequences were of fixed length 75 bp, and of a high quality for a single base.

Twenty four samples were analyzed: 12 derived from a cell line of CF pulmonary epithelium, and 12 from a cell line of healthy pulmonary epithelium (CTRL). For each group, the following conditions were analyzed: (1) basal condition (CTRL or CF); (2) infection with *A. fumigatus* (Asp); (3) myriocin treatment (Myr); (4) infection and treatment (Asp-Myr). Three biological replicates were used for each condition.

RNA was also extracted from a selection of *A. fumigatus*-infected monocytes from 11 homozygous and 9 heterozygous patients. For each subject, we analyzed 2 conditions: (1) samples infected with *A. fumigatus* (untreated); (2) samples infected with *A. fumigatus* and treated with Myr (treated).

2.8. Exploratory Data Analysis

In order to evaluate samples variability, we applied principal component analysis (PCA) as a tool to make assumptions. In particular, we performed PCA starting from regularized log-transformed counts matrices created by the *rlog* function implemented in the DESeq2 package [28].

2.9. RNA-Seq Data Analysis

Raw single-end reads were aligned to the human reference genome (GRCh38) using STAR [29], and only uniquely mapping reads were considered for downstream analyses. Reads were assigned to genes with featureCounts [30], using the Gencode primary assembly v.31 gene transfer file (GTF) as reference annotation for the genomic features. Raw counts matrices were then processed with the R/Bioconductor differential gene expression analysis packages DESeq2 and EdgeR [31] following standard workflows. In particular, for the monocyte dataset we set up a paired analysis, modeling gene counts using the following design formula: \sim patient + condition. For cell lines, due to the high variability between and within cell lines, we split the dataset into specific subsets. In particular, in both CTRL and CF cells, we evaluated the effect of *A. fumigatus* (Asp) infection and of Myr with and without infection. Genes with adjusted *p*-values less than 0.01 (cell lines) and 0.05 (monocytes

dataset) were considered differentially expressed (DEGs). Downstream analyses, including gene set enrichment analysis (GSEA) and over-representation analysis (ORA), were performed with the ClusterProfiler R/Bioconductor package [32] using a list of databases including Gene Ontology (GO), KEGG, Reactome pathway, and the Molecular Signatures Database (MsigDB). Enriched terms with an adjusted p -value < 0.05 were considered statistically significant. Charts and images were produced using the ggplot2 R package.

We performed protein–protein interaction (PPI) networks functional enrichment analysis using string-db [33] web site. In particular, starting from the default setting we applied the following changes: removal of text-mining flag from active interaction sources, selection of highest confidence interaction scores, and hiding of disconnected nodes from graphical output.

3. Results

3.1. Myriocin Transcriptionally Regulates and Ameliorates the Response to *A. fumigatus* Infection in CF-Patients-Derived Monocytes

In order to study the effects of Myr on the immune response against fungal infection in CF, monocytes derived from the PBMCs of CF patients bearing homozygous or heterozygous $\Delta F508$ CFTR mutation were infected in vitro with *A. fumigatus* and either treated or not treated with Myr. Myr treatment significantly increased *A. fumigatus* killing compared with untreated infected CF monocytes (Figure 1).

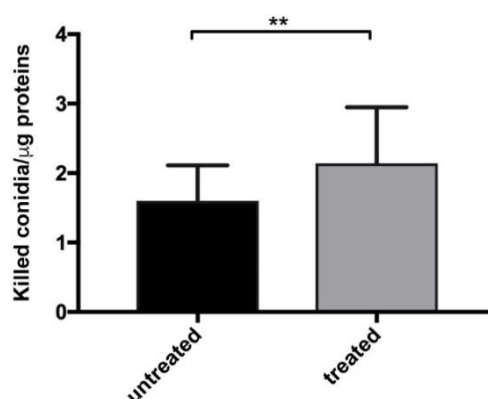


Figure 1. Myriocin (Myr) treatment improved monocyte killing ability. *Aspergillus fumigatus* conidia were added to patients' monocytes, untreated or treated with Myr, and cells incubated for 1 h to allow conidia internalization. Non-internalized conidia were then washed, and monocytes were incubated for a further 4 h before undergoing lysis. Live conidia were counted by plating cell lysate on solid medium. To normalize the results, data are expressed as killed conidia/ μg protein. Myr partially rescued cystic fibrosis (CF) monocytes' killing ability (** $p < 0.01$ Wilcoxon t -test).

Exploratory data analysis showed a patient-specific bias that we took into account by using a paired differential expression model, as described in the Methods section. After correcting for batch effect (patient), we clearly observed a separation on the second principal component (Figure 2A). Differential gene expression analysis identified 1460 DEGs between Myr-treated and untreated cells, in particular 563 upregulated and 896 downregulated genes in Myr-treated cells (Figure 2B).

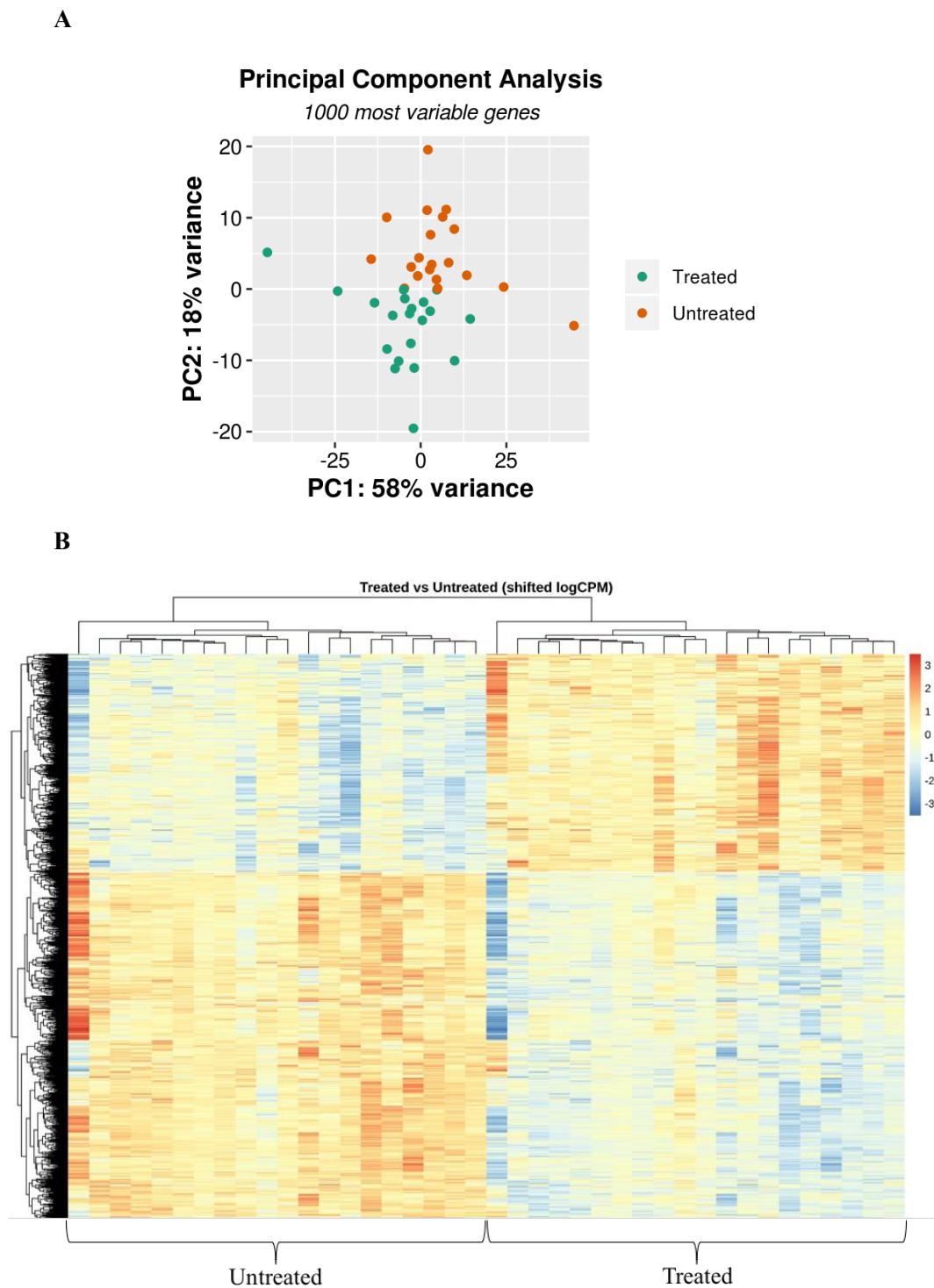
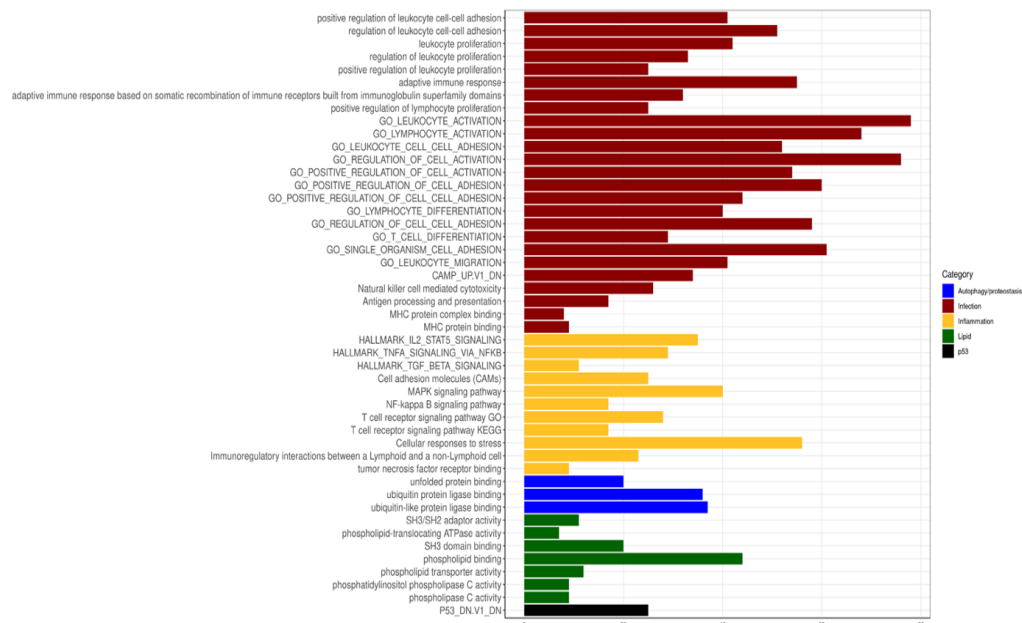


Figure 2. PCA and differential gene expression (DGE) induced by myriocin treatment in CF-patients-derived monocytes. (A) PCA was calculated considering the 1000 most variable genes across the dataset. Log-normalized counts were “shifted” for patient in order to take into account the experimental design adopted for DGE analysis. (B) Heatmap of DEGs with adjusted p -value < 0.05 resulted from the comparison between treated and untreated samples. The data used for creating this image were logCPM-corrected for patient batch and row-scaled (heatmap package).

Starting from the DEG list, we performed over-representation analysis using different gene sets, including Gene Ontology (GO), Kyoto Encyclopedia of Genes and Genomes (KEGG), and Molecular Signatures Database (MSigDB) terms, in order to identify the presence of enriched functional categories.

In particular, we observed categories related to CF disease as inflammation, autophagy, lipid metabolism, and infection (Figure 3A). We then analyzed the proportion of differentially upregulated and downregulated genes and highlighted the most significantly modulated ones. We noticed a significantly higher number of upregulated genes under Myr treatment (Figure 3B).

A



B

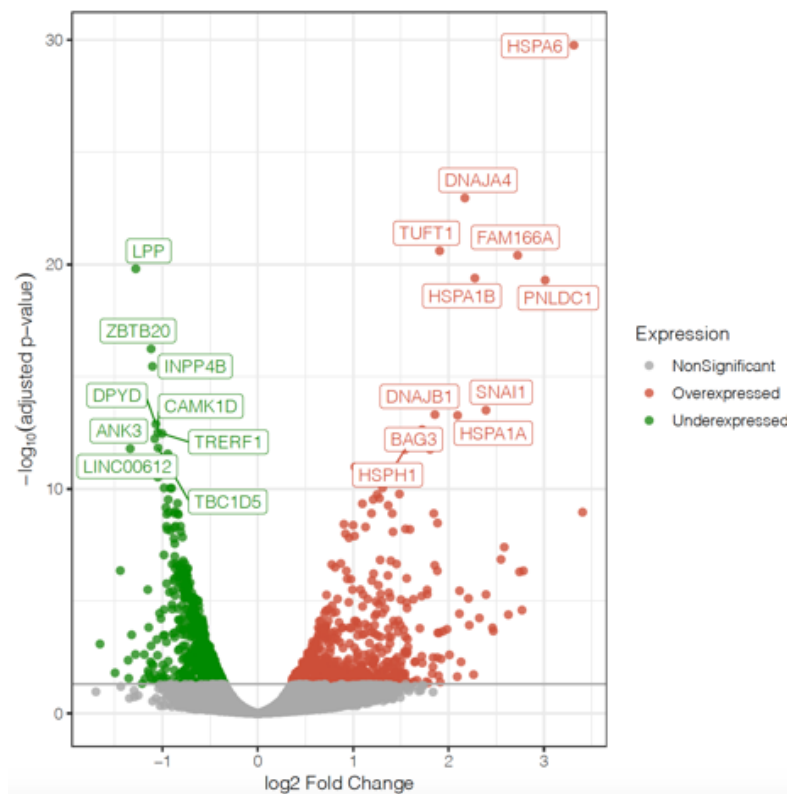


Figure 3. Cont.

Table 1. Cluster of histone protein DEGs between Myr-treated and untreated CF-patients-derived monocytes.

Symbol	Log2FoldChange	Padj	Description	Ensembl
HIST1H2BH	1.86	8.07×10^{-5}	histone cluster 1 H2B family member h	ENSG00000275713
HIST1H2BG	1.56	0.001394033	histone cluster 1 H2B family member g	ENSG00000273802
HIST1H2BO	1.54	0.021985759	histone cluster 1 H2B family member o	ENSG00000274641
HIST1H2BE	1.53	0.007600047	histone cluster 1 H2B family member e	ENSG00000274290
HIST1H2BJ	1.29	0.002758228	histone cluster 1 H2B family member j	ENSG00000124635
HIST1H2BD	1.21	0.001620018	histone cluster 1 H2B family member d	ENSG00000158373
HIST1H4C	1.14	0.004057245	histone cluster 1 H4 family member c	ENSG00000197061
H2AFX	1.04	0.009827979	H2A histone family member X	ENSG00000188486
HIST1H3A	1.02	0.05944192	histone cluster 1 H3 family member a	ENSG00000275714
HIST2H2BE	0.88	0.028428384	histone cluster 2 H2B family member e	ENSG00000184678
H2AFZ	0.63	0.044623207	H2A histone family member Z	ENSG00000164032
HIST1H3J	0.93	0.204175587	histone cluster 1 H3 family member j	ENSG00000197153
HIST1H4I	0.72	0.065534653	histone cluster 1 H4 family member i	ENSG00000276180
HIST1H2AC	0.47	0.318228769	histone cluster 1 H2A family member c	ENSG00000180573

To note that Myr also induced the upregulation of several genes encoding for heat-shock proteins: Hsp70, Hsp90, Hsp40 (DnaJ), and Hsp-interacting proteins (Table 2), as already highlighted by PPI network analysis (Figure 3C).

Table 2. Cluster of heat-shock protein DEGs between Myr-treated and untreated CF-patients-derived monocytes.

Symbol	Log2FoldChange	Padj	Description	Ensembl
HSPA6	3.41	2.65×10^{-9}	heat shock protein family A (Hsp70) member 6	ENSG00000173110
DNAJA4	2.71	2.25×10^{-16}	DnaJ heat shock protein family (Hsp40) member A4	ENSG00000140403
HSPA1B	2.71	1.19×10^{-10}	heat shock protein family A (Hsp70) member 1B	ENSG00000204388
HSPA1A	2.64	3.02×10^{-13}	heat shock protein family A (Hsp70) member 1A	ENSG00000204389
DNAJB1	2.47	8.60×10^{-13}	DnaJ heat shock protein family (Hsp40) member B1	ENSG00000132002
BAG3	2.14	1.79×10^{-11}	BCL2 associated athanogene 3	ENSG00000151929
HSPA2	2.00	1.54×10^{-5}	heat shock protein family A (Hsp70) member 2	ENSG00000126803
SERPINH1	1.94	3.78×10^{-9}	serpin family H member 1	ENSG00000149257
HSPD1	1.68	3.78×10^{-9}	heat shock protein family D (Hsp60) member 1	ENSG00000144381
ZFAND2A	1.60	1.29×10^{-9}	zinc finger AN1-type containing 2A	ENSG00000178381
HSPE1	1.40	7.08×10^{-5}	heat shock protein family E (Hsp10) member 1	ENSG00000115541
HSP90AA1	1.35	1.13×10^{-6}	heat shock protein 90 alpha family class A member 1	ENSG00000080824
DNAJB4	1.13	5.80×10^{-7}	DnaJ heat shock protein family (Hsp40) member B4	ENSG00000162616
HSPA1L	1.13	8.07×10^{-5}	heat shock protein family A (Hsp70) member 1 like	ENSG00000204390
DNAJA1	0.90	6.78×10^{-5}	DnaJ heat shock protein family (Hsp40) member A1	ENSG00000086061
HSP90AB1	0.82	0.002280106	heat shock protein 90 alpha family class B member 1	ENSG00000096384
HSPA8	0.53	0.058998158	heat shock protein family A (Hsp70) member 8	ENSG00000109971

Such proteins are directly involved in chaperone-mediated autophagy, which sustains the autophagic activity. In addition, we identified an increased transcription of the *PNPLA3* gene that codes for a lipase supporting lipid storage degradation in autophagolysosomal compartment [41].

Moreover, Myr induced the upregulation of LC3IIB (*MAP1LC3B2*), which belongs to the LC3B family, required for cargo and autophagy protein recruitment and for autophagosome nucleation [42].

3.2. CF and Control Airways Epithelial Cell Lines Exhibit a Different Transcriptional Response to Infection

Chronic inflammation contributes to defective pathogen clearance in CF airways, and epithelial cells offer the first barrier to microbial infection by exerting pathogens' uptake and killing. In order to better understand the therapeutic effect of sphingolipid synthesis inhibition in CF, we studied the transcriptomic profile of CF bronchial epithelial cells in the early phase of infection (4 h). Hence, we performed an RNA-sequencing analysis of CF and CTRL bronchial epithelial cells after infection with *A. fumigatus*.

As shown in Figure 4A, infected CF cells exhibited a stronger transcriptional response to fungal infection compared to CTRL cells, considering both fold changes and differentially expressed genes (DEGs). In response to infection, we identified 3954 DEGs in CTRL cells and 5109 DEGs in CF cells (Figure 4B).

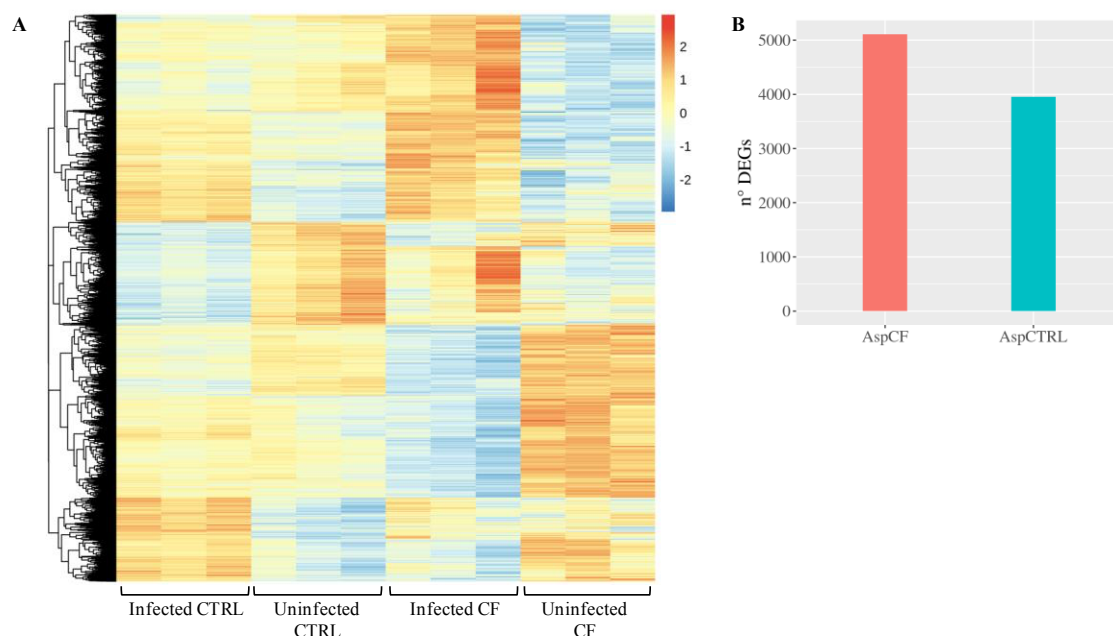


Figure 4. Transcriptional response to infection. (A) The heatmap represents the expression (rlog row-scaled) of DEGs obtained in the AspCTRL and AspCF comparisons. (B) DEGs numbers. AspCTRL: DEGs between infected and uninfected CTRL cells; AspCF: DEGs between infected and uninfected CF cells.

3.3. Myriocin Treatment Modulates CF Expression Profile under Infection

Next, we evaluated the effect of myriocin on gene expression in CF and CTRL cells, both in basal and in *A. fumigatus* infection conditions. We observed a significantly higher number of DEGs in Myr-treated CF (MyrCF, 1629 DEGs) than in CTRL cells (MyrCTRL 55 DEGs) (Figure 5A). Myr treatment in *A. fumigatus*-infected CF cells (MyrAspCF/Asp) significantly modulated only 62 DEGs versus 240 DEGs in infected CTRL cells (MyrAspCTRL/Asp) (Figure 5B). This could be related to an attenuated transcriptional effect of the compound due to the massive transcriptional change induced by *A. fumigatus* infection in CF cells (AspCF), which was significantly stronger than in CTRL cells (AspCTRL) (see above, Figure 4).

To get insight from the obtained data, we created Venn diagrams showing the common DEGs, deriving from the three different comparisons: (i) infected CTRL cells versus uninfected (AspCTRL); (ii) infected CF cells versus uninfected (AspCF); (iii) infected and Myr-treated CF cells versus uninfected and untreated (MyrAspCF).

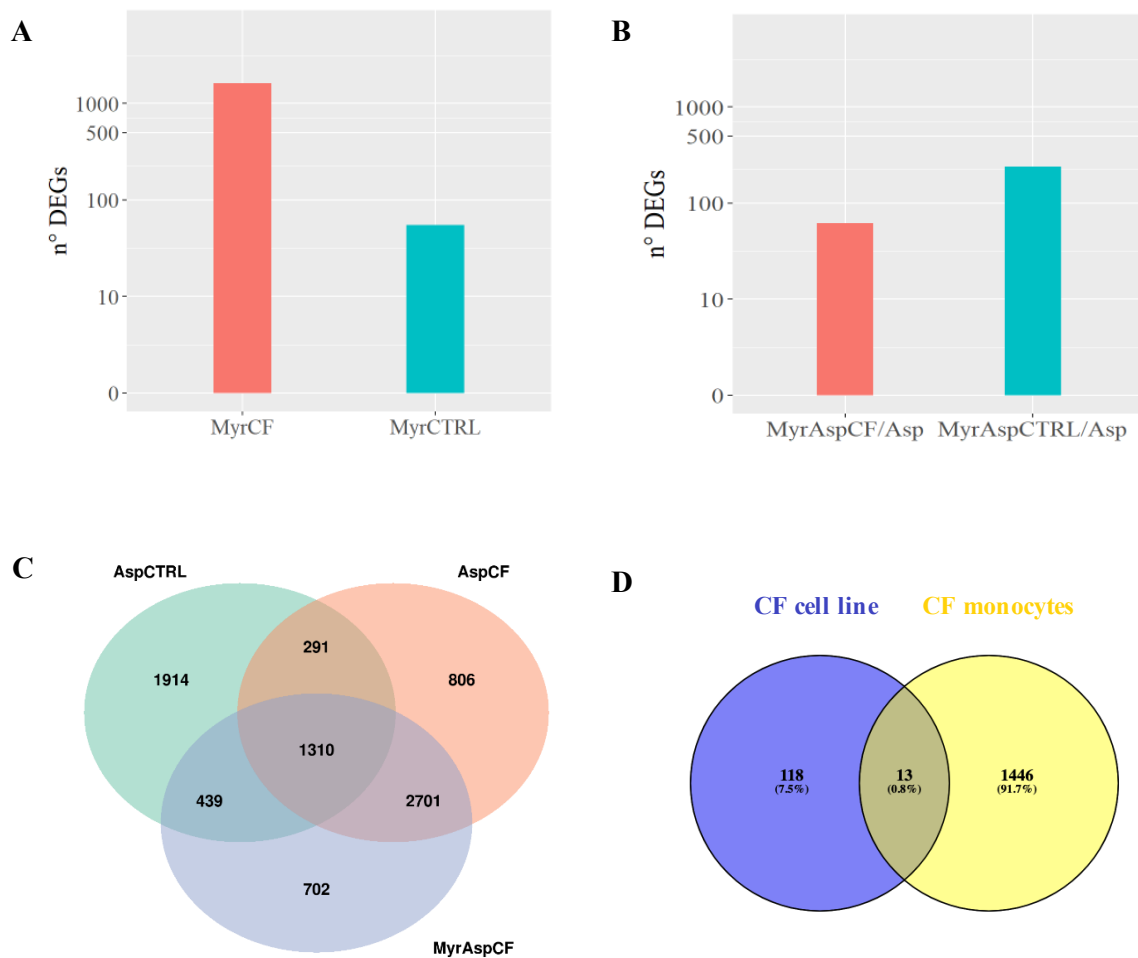


Figure 5. Effect of myriocin on CF and CTRL cells in infected and infection-free environments. (A) MyrCF indicates DEGs between Myr-treated CF cells and untreated CF cells; MyrCTRL indicates DEGs between treated CTRL cells and untreated CTRL cells; (B) MyrAspCF/Asp indicates DEGs between Myr-treated infected CF cells and untreated infected CF cells; MyrAspCTRL/Asp indicates DEGs between Myr-treated infected CTRL cells and untreated infected CTRL cells. (C) Venn diagram of CTRL and CF cells in response to infection (AspCTRL and AspCF) and infected CF cells in response to treatment (MyrAspCF). MyrAspCF: DEGs between Myr-treated infected cells and uninfected untreated CF cells. (D) Venn diagram of CF cells and CF monocytes: DEGs between Myr-treated infected CF cells and Myr-treated infected monocytes from CF patients.

We found 292 genes that were differentially expressed in both CTRL and CF cells in response to fungal infection (AspCTRL and AspCF). When CF cells were treated with Myr (MyrAspCF), the number of common regulated genes increased up to 439, indicating that Myr drives CF response to infection and partially restores the CTRL expression profile (Figure 5C). Finally, we compared the genes that found to be regulated by Myr in infected airways epithelial CF cells (MyrAspCF) and in infected CF patients' derived monocytes (treated-infected versus untreated-infected) (Figure 5D). Regardless of the different origins of the cells, we found a common upregulation of HSP90AA1 and ZFAS1, two genes belonging to heat shock and zinc fingers proteins families, involved in chaperone-mediated autophagy (previously described, Table 2, Section 3.1, [40,43,44]). In addition, the expression of another 11 genes was commonly modulated, although at minor extent in respect to the above discussed.

3.4. Myriocin Activates Gene Sets Involved in Inflammation, Infection, Autophagy/Proteostasis, and Lipid Metabolism in CF Bronchial Epithelial Infected Cells

In order to evaluate the effect of Myr on infected CF cells, we performed GSEA using logFC pre-ranked list of MyrAspCF/Asp DEGs, thus evaluating only Myr-related transcriptional activities and excluding infection-induced transcriptional modification. Results indicate that the Myr treatment modulates the expression of genes involved in autophagy/proteostasis, lipid metabolism, and in response to infection and inflammation. In particular, as highlighted in Figure 6, Myr treatment upregulated the genes involved in autophagy/proteostasis and lipid metabolism, whereas it downregulated genes related to inflammation and infection processes.

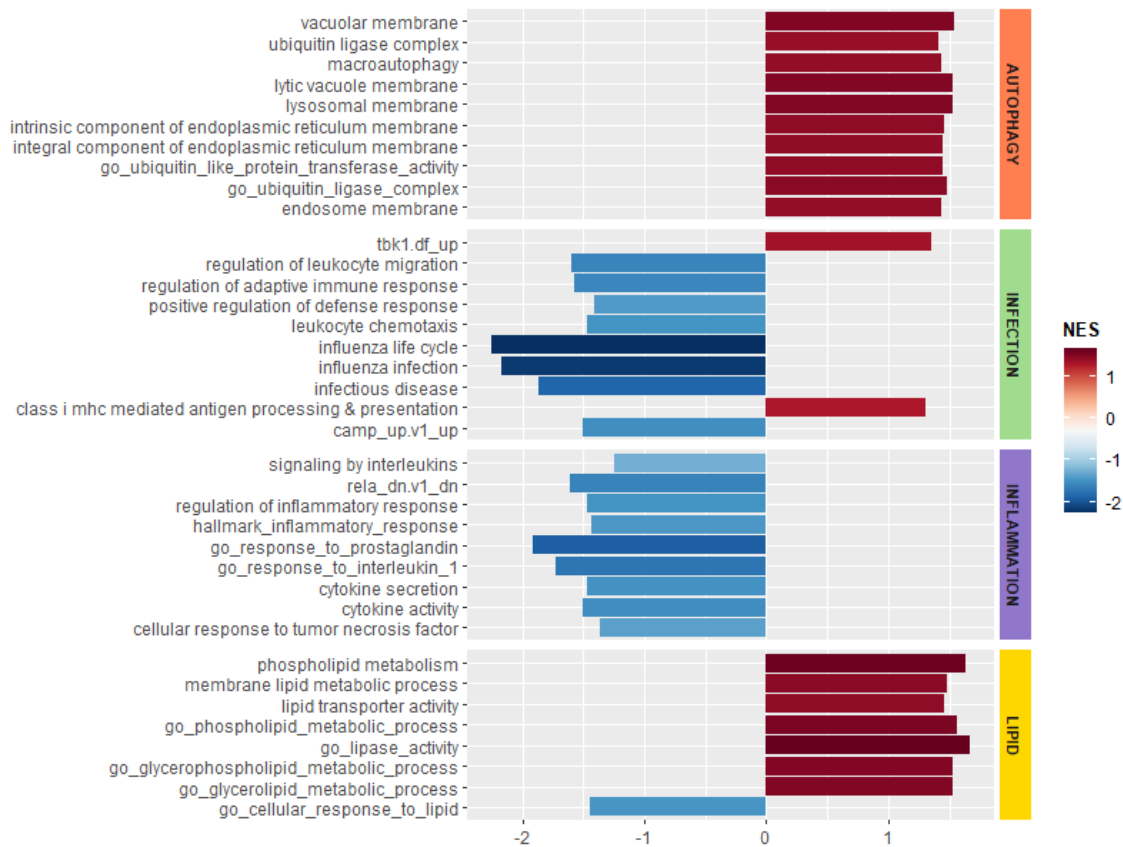


Figure 6. Enriched gene set enrichment analysis (GSEA) terms—functional categories. This chart shows the results of GSEA analysis on functional categories related to CF pathology using pre-ranked logFC list genes from MyrAsp/Asp CF analysis. In red, the terms with positive normalized enrichment score (NES), upregulated by myriocin, whereas in blue the terms with negative NES, downregulated by myriocin. GSEA terms include GO, MutSigDB, and KEGG pathway terms.

Considering a significant adjusted p -value threshold of 0.05, we observed 139 DEGs in infected CF cells in response to treatment. Among such DEGs we identified specific genes related to the molecular processes that are regulated by Myr, as evidenced by GSEA. Other than increasing IL1 β , a primary cytokine in CF disease and its defective response to infection [45,46], Myr upregulated the expression of the transmembrane protein TMEM59, which induces the LC3 labelling of endosomal vesicles, stimulating their fusion with lysosomes, in response to autophagy and xenophagy [47]. Moreover, Myr upregulated the p53-inducible protein 1 (*TP53INP1*) gene, which also promotes autophagy by interacting with autophagy-related protein family (ATG) [48]. The expression of SNX14, involved in the regulation of autophagy and lipid metabolism, was significantly increased by Myr [49,50], as well as that of hypoxia inducible gene 1 (*HIGD1A*), involved in oxidative stress and lipotoxicity protection [51]. At the same time, Myr downregulated *ACACA*, the rate-limiting enzyme regulating de novo fatty acid

synthesis, whose increased activity has been associated with inflammation and CFTR deficiency [52,53]. We next validated the upregulation of three of the above reported genes by RT-PCR and demonstrated the increase of their expression in infected and Myr-treated CF cells (Figure 7).

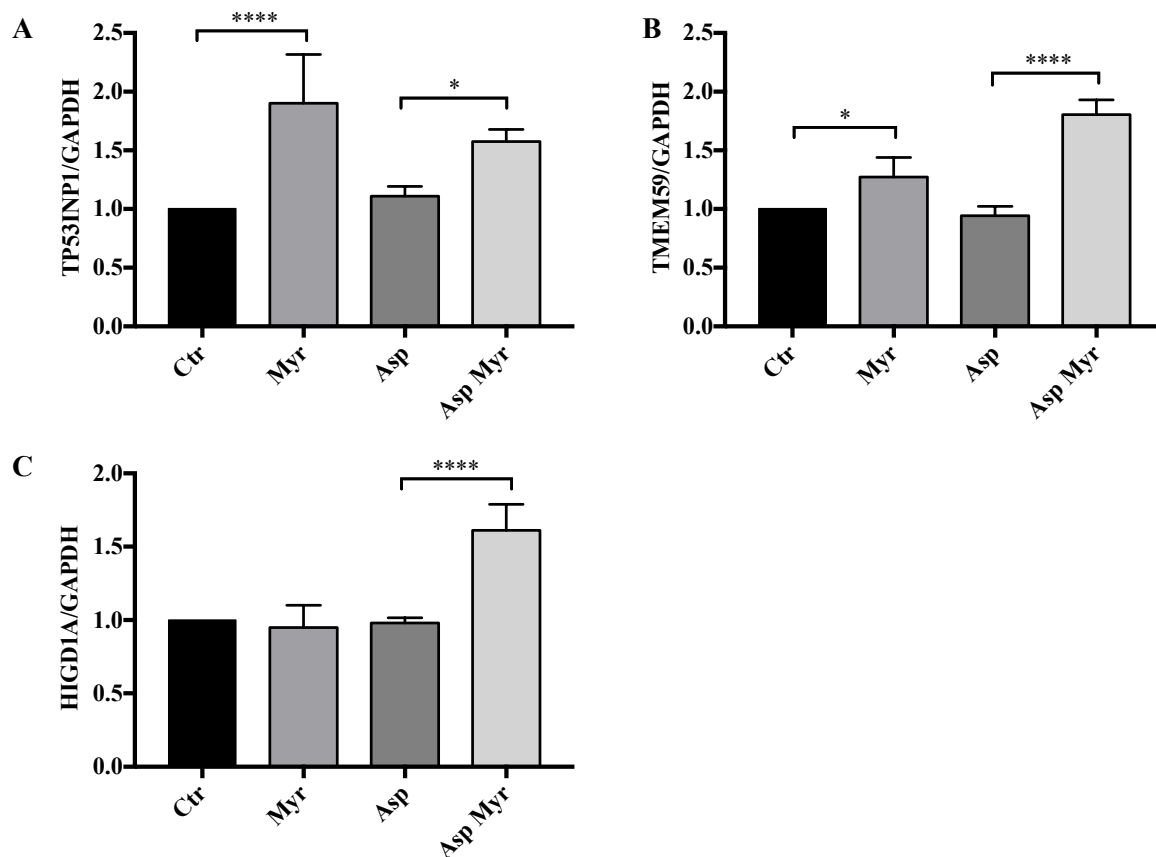


Figure 7. RNA-seq validation by RT-PCR quantification of the expression of genes involved in response to infection in CF cells: (A) transmembrane protein TMEM59; (B) p53-inducible protein 1, *TP53INP1*; (C) hypoxia inducible gene 1, *HIGD1A*. *GAPDH* was used as a housekeeping gene. Data, derived for triplicate samples, are expressed as mean \pm SE (* $p < 0.05$; **** $p < 0.0001$); two-way ANOVA followed by Bonferroni correction was used for all data.

In view of our previous results on Myr transcriptional effects in CF bronchial epithelial cells [5,8,25], we evaluated a delayed expression of specific marker genes involved in the inflammatory process and in the response against microbial infection in CF cells infected with *A. fumigatus*, treated or untreated with Myr. By real-time PCR (RT-PCR), we proved that the expression of pro-inflammatory interleukin-1 β (*IL-1 β*) and *IL-8* chemokines, known to be upregulated in CF [25], were significantly reduced by Myr, in both basal conditions and in *A. fumigatus*-infected CF cells, whereas the expression of anti-inflammatory *IL-10* was upregulated by the compound (Figure 8A–C).

Pathogen recognition receptors (PRRs) are responsible for the identification of antigens, and can mediate their lysosomal clearance. We observed that Myr treatment enhanced the expression of the *NOD2*, *TLR2*, and *TLR7* in infected CF cells (Figure 8D–F). Myr reduction of sphingolipid synthesis regulates lipid metabolism by enhancing fatty acids oxidation and reducing the overall cell amount of glycerolipids and cholesterol [5]. Myr's action on lipid-energy homeostasis is sensed as a stress that drives TFEB activation and transcriptional activities that sustain lipid consumption and autophagy induction [5]. We observed an increased expression of *TFEB* in infected CF bronchial epithelial cells treated with Myr compared to untreated infected cells (Figure 8G). TBK1 phosphorylation and interaction with optineurin (OPTN) promote autophagy-mediated pathogen clearance, namely xenophagy [54–56]. We observed that *A. fumigatus* infection reduced the expression of *TBK1* while

Myr treatment significantly rescued it (Figure 8H). Myr was also able to increase *OPTN* expression in infected CF cells (Figure 8I). Finally, Myr induced a significant increase of *Lamp2a* expression, which was reduced in *A. fumigatus*-infected CF cells, confirming the TFEB and the autophagy-related increase in lysosome formation (Figure 8L).

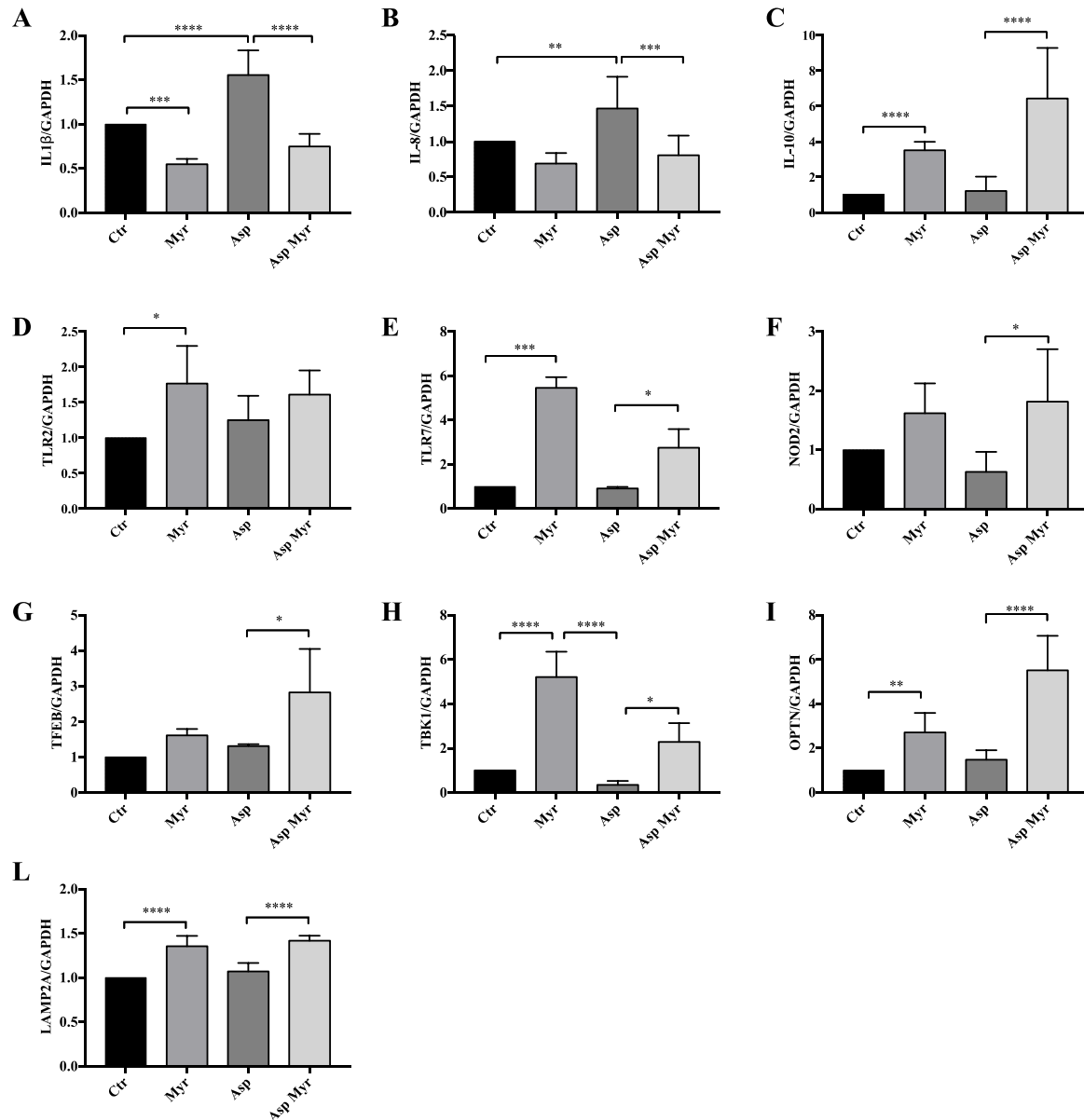


Figure 8. Quantification of the expression of genes involved in inflammation, response to infection, and autophagy: (A) pro-inflammatory *IL1β* interleukin; (B) pro-inflammatory *IL-8* chemokine; (C) anti-inflammatory *IL10* interleukin; (D–F) pathogen recognition receptors (PRRs): *NOD2*, *TLR2*, and *TLR7*; (G) *TFEB*; (H) *TBK1*; (I) *OPTN*; (L) *LAMP2a* by qRT-PCR in *A. fumigatus*-infected and uninfected CF cells, treated and untreated with Myr (12 h after infection). *GAPDH* was used as a housekeeping gene. Data, derived for triplicate samples, are expressed as mean \pm SE (* $p < 0.05$; ** $p < 0.01$; *** $p < 0.001$; **** $p < 0.0001$); two-way ANOVA followed by Bonferroni correction was used for all data.

4. Discussion

Our study demonstrates that the defective response to infection in CF is related to a dysfunction in autophagy, inflammation resolution, and lipid metabolism, which are known to be caused by

mutated CFTR [1–5]. Dyslipidemia has been associated with CF disease, and it is characterized by a reduced absorption and increased synthesis of lipids [1,2,53,57–62]. Moreover, cholesterol and the inflammatory lipid ceramide have been shown to accumulate in CF peripheral organs, in particular at the airways level [4,23,26,63–66]. Although altered lipid metabolism is a common feature of chronic inflammatory diseases, the contribution of lipids in CF pathophysiology is still to be fully elucidated. We previously demonstrated that Myr—a specific inhibitor of sphingolipid de novo synthesis—reduces the accumulation of not only ceramide but also most lipid species in CF cells [5]. By impairing sphingolipid synthesis, Myr induces the activation of a stress response that initiates with the TFEB-induced transcriptional program, sustained by PPARs and FOXOs transcription factors, aimed at increasing lipid oxidation and promoting autophagy [5]. Its modulatory action results in an overall decline of CF hyperinflammation, as a consequence of a reduced expression of pro-inflammatory cytokines, and in an ameliorated defensive response to infection, driven by the increase in xenophagy-activating PRR expression [8,25], known to be downregulated in CF [67].

Monocytes play a crucial role in pathogen eradication and CF prominent susceptibility to recurrent infections, largely relying on altered monocytes response. Therefore, we studied peripheral-blood-derived monocytes from CF patients, bearing either homozygous or compound heterozygous $\Delta F508$ mutation of CFTR, by in vitro infection with *A. fumigatus*. Myr treatment shaped a significantly different transcriptional process in infected monocytes, modulating the expression of genes involved in inflammation, response to infection, lipid metabolism, and autophagy. Among differentially expressed genes, we identified two functional clusters in terms of significant response to Myr that have not previously been associated to CF (Tables 1 and 2). Myr upregulated the expression of several proteins belonging to the histone family. Other than fundamental components of eukaryotic chromatin, histones and histone fragments display antimicrobial activities [34], either by being secreted and reacting against extracellular pathogens or by accumulating in the cytosol and binding intracellular infectious agents [38]. Cytosolic histones elude proteolysis thanks to the binding to lipid cytosolic storage [35], are released upon interaction with pathogens, and are processed to act as antimicrobial peptides against bacteria and fungi [36,37,39]. The observation that infection increases this cytosolic histone-related fraction [35] supports our hypothesis that, possibly by modulating lipid metabolism, Myr promotes histones transcription in infected cells in order to boost their cytosolic pool, which is endowed with antimicrobial activity. Moreover, Myr upregulated the expression of a number of heat-shock proteins (HSP) belonging to the 70 family (Hsp70), 90 family (Hsp90), and DnaJ family (Hsp40). HSPs take part in the response to infection by receptor-mediated activation of the innate immune response and by participation in the antigen presentation for the adaptive immune response [68,69], which is also defective in CF [6]. Hsp70 and Hsp90 play an important role in chaperone-mediated autophagy (CMA) and pathogen recognition [44,70,71]. Proteins degraded by CMA are identified in the cytosol by a chaperone complex which includes Hsp70 [72]. Upon binding to the target, Hsp70 [73] and Hsp90 [44] interact with the lysosome-associated membrane protein type 2A (LAMP-2A), which we observed to be upregulated by Myr. DnaJ proteins (Hsp40) regulate Hsp70 chaperones by stimulating ATP hydrolysis [74]. Thus, Myr's action on HSPs is aimed at sustaining innate and adaptive immunity as well as autophagy-related unfolded proteins and pathogens clearance in infected CF monocytes. Moreover, Myr increased the expression of the *PNPLA3* gene, which encodes for a lipase responsible for the mobilization of intracellular fat storage [75] and degradation in the autophagolysosomes. This process, named lipophagy, is directly promoted by TFEB activation [41]. Hence, Myr might sustain both classic autophagy, as we previously demonstrated [5], and chaperone-mediated autophagy, driving not only the autophagic pathway, but also TFEB-induced lysosome biogenesis, as revealed by increased *Lamp2a* expression. In agreement with previous data suggesting that Myr enhances killing ability in an *A. fumigatus*-infected CF bronchial epithelial cell line [8], we observed a significant increase of conidia killing in *A. fumigatus*-infected CF monocytes. This latter observation indicates that reducing inflammatory lipid accumulation and promoting autophagy is an effective therapeutic approach to

correcting proteinopathy stress, mainly related to $\Delta F508$ mutation of CFTR, and to restoring an effective response against infection.

Next, we extended our previously published data by investigating the effect of sphingolipid synthesis inhibition in the first phase of microbial infection in the airways. In order to better understand whether Myr could modulate CF response to infection, we analyzed the whole-transcriptome modification induced by *A. fumigatus* in a CF bronchial epithelial cell line and a healthy control counterpart, either treated or untreated with Myr. Our data provide clear evidence that a profound modification in gene expression, triggered by infection, differentiates CF from healthy cells, suggesting that the disease itself causes higher sensitivity to infection. Indeed, healthy cells responded to the same stimulus by engaging a smaller number of genes. This evidence is in line with CF patients' defective ability to elicit a coordinated defensive response against infection. Indeed, we observed a stronger modulation of CF cells' transcriptional activity by Myr treatment, whereas the impact on control cells was milder. These data are in agreement with our previous observation on the effects of Myr treatment on inflamed cells or organs with respect to their healthy counterparts [5,25,76]. We suggest that sphingolipid de novo synthesis is enhanced under stress conditions such as proteinopathy and inflammation. In a homeostatic state, Myr inhibition of the sphingolipid synthesis rate-limiting enzyme serine palmitoyl transferase (SPT) may be buffered by a consequent spontaneous modulation of Nogo and ORMs, two enzymes that normally control SPT activity [77,78]. When stress or inflammation upregulate the sphingolipid synthesis pathway, the effect of Myr is more pronounced and is perceived as an alarm signal that drives defense response by moving the metabolic resources via lipid mobilization and autophagy. During an infectious process, CF cells' transcriptional activities are perturbed to a higher extent than control cells. Nonetheless, Myr treatment increased the number of genes that were commonly regulated by infection in CF and healthy cells, thus driving the CF phenotype closer to that of control cells. This confirms the hypothesis that inhibition of sphingolipid synthesis activates a profound transcriptional modification aimed at inducing stress tolerance and resilience as well as pathogen resistance in CF. This concept is crucial in any chronic inflammatory disease, in which the possibility of counteracting the cellular stress is the required therapeutic effect. Our data indicate that the Myr-induced effects on infected CF cells involve genes mediating inflammation, immune response, autophagy, and lipid metabolism. Among genes whose expression was significantly affected by Myr in CF cells during infection, we identified a few that are related to the significantly regulated pathways and that may indicate novel targets for CF therapy. A specific form of LC3-associated phagocytosis can be activated by TLR signaling during the phagocytosis of fungal and bacterial pathogens: LC3 binds to the cytosolic side of the TLR-induced endosome, which evolves into autophagosomes [68]. Mediating this mechanism, TMEM59 and TMEM166 interact with ATG16L1, become incorporated into phagosomes' membranes, driving the activation and lipidation of LC3, and thus the maturation into autophagosomes [69]. Similarly, SNX14 proteins generally localize to endosomes' membranes via the PX domain, which binds to phosphoinositides (PtdIns), and this is reported to promote autophagy [49,50]. The expression of both SNX14 and TMEM59 was enhanced by Myr upon infection, suggesting that the compound drives a pathogen-clearance-related autophagy. Moreover, altered SNX14 function has been associated with reduced cholesterol esters, suggesting an alteration in neutral lipid metabolism and possibly reduced lipid delivery to droplets storage [50]. Accordingly, Myr reduced the expression of the gene encoding for acetyl-CoA carboxylase (ACACA), the rate-limiting enzyme involved in fatty acids synthesis and regulated in opposition to their oxidation. ACACA has been associated with inflammation [52] and most notably, its activity is enhanced in CFT-deficient cells [53], in line with the increased sphingolipid synthesis in CF chronic inflammation [5,25]. Myr treatment also increased the expression of hypoxia-inducible gene domain family member 1A (*HIGD1a*). Its gene product was recently reported to protect cells from hypoxia and from lipotoxicity related to fat oxidation impairment. Indeed, *HIGD1a* decreases oxygen radical production, helping to maintain a normal mitochondrial function [51]. A reduced autophagy paired with lipid accumulation because of decreased oxidation rate was already observed in CF cells and rescued by Myr [5]. Thus, Myr could possibly enhance

SNX14 to induce autophagy and lipid consumption, and it may upregulate *HIGD1a* to reduce the oxidative stress caused by proteinopathy and lipid accrual in infected CF cells. Therefore, Myr is able to directly target specific genes whose functions have not been previously associated to CF, but that sustain its pathophysiology.

In addition, lipid synthesis inhibition is a strategy to fight microbial infections that are known to take advantage of cell lipid storage, and ACACA inhibitors have been designed to develop antimicrobial strategies in infectious diseases [79].

Finally, we investigated the possibility of Myr-induced transcriptional activation of TFEB and of downstream target genes in *A. fumigatus*-infected CF bronchial epithelial cells. As expected, TFEB transcription was increased by Myr, suggesting that lipid catabolism and autophagy are enhanced even under infection conditions. A growing body of evidence highlighted that TBK1-OPTN signaling is pivotal for the initiation and resolution of the innate immune responses, and in eliciting autophagy [55,56,80]. Myr significantly increased the expression of these two proteins, both in uninfected and infected cells, thus promoting internalized pathogen clearance. To note, Myr upregulated the expression of *LAMP2A* (lysosomal-associated membrane protein 2A), encoding for a membrane glycoprotein involved in autophagy, which is directly promoted by TFEB induction of lysosomes biogenesis.

5. Strength and Limitations of the Study

The strength of the present study is that it presents data deriving from a significant number of CF patients, variable for sex and age, affected by $\Delta F508$ mutation of the *CFTR* gene (homozygous and compound heterozygous). The limitations include the fact that part of the study was conducted on epithelial cell lines, and further studies on primary epithelial cells are needed to corroborate the obtained data. Moreover, we cannot exclude that patient PBMC storage and in vitro culturing could impact the cell transcriptional response. Next, although the used *Aspergillus fumigatus* strain (Af293) is a clinical strain derived from invasive pulmonary aspergillosis, a genome-sequenced biofilm producer, the in vitro infection procedure may not completely resemble in vivo infection, and the host response may differ in terms of intensity and timing of gene expression modulation. Similarly, we cannot predict whether Myr administration would be efficient in modulating chronic infections in patients. From a technical point of view, gene expression was carried out by normalizing data with a unique housekeeping gene (*GAPDH*), whereas the use of three different housekeeping genes would ensure the highest reliability of transcriptional evaluation.

6. Conclusions

CF bronchial epithelial cells display a profound difference in the transcriptional profile compared with their normal counterpart, and infection sharpens this diversity. We demonstrated that by modulating the biosynthesis of sphingolipids by Myr, a metabolism drift occurs which is aimed at fueling energy to act against stress, and includes autophagy and lipid consumption. This is driven by a transcriptional program that significantly modifies cellular phenotype and amends part of the differences between CF and control, therefore ameliorating the response against infection and pathogens clearance in both a CF cell line [8] and monocytes. We speculate that lipid metabolism is deeply altered in CF patients, possibly due to the chronic and systemic inflammation associated with the disease. Lipids accumulation, or simply deregulation in their storage/consumption, may contribute to the defective immunity of CF patients. Literature evidence reports dyslipidemia in CF patients, measured both in blood and peripheral organs [2,81,82]. We conclude that more attention should be devoted to the alteration of lipid metabolism in CF.

Supplementary Materials: The following are available online at <http://www.mdpi.com/2073-4409/9/8/1845/s1>. Figure S1: Quantification of the expression of genes involved in inflammation, response to infection, and autophagy in CTRL and CF bronchial epithelial cells; Table S1: CF patients cohort.

Author Contributions: Conceptualization, A.M., P.S. Investigation, A.M., E.O., E.B., P.S. Formal analysis, M.B., I.M. Drafting of the manuscript, A.M., E.O. Supervision, R.G., E.B., P.S. Writing—review and editing, A.M., E.O., E.B., P.S. Resources, L.R., T.A., N.C. Funding acquisition, P.S. All authors have read and agreed to the published version of the manuscript.

Funding: This research was funded by the Italian Cystic Fibrosis Foundation, Grant FFC#11-2016.

Acknowledgments: We thank the Italian Cystic Fibrosis Foundation for their financial support of this work. E.O. was supported by the PhD program in Molecular and Translational Medicine of the Università degli Studi di Milano, Milan.

Conflicts of Interest: There are no conflict of interest.

References

1. Gelzo, M.; Sica, C.; Elce, A.; Dello Russo, A.; Iacotucci, P.; Carnovale, V.; Raia, V.; Salvatore, D.; Corso, G.; Castaldo, G. Reduced absorption and enhanced synthesis of cholesterol in patients with cystic fibrosis: A preliminary study of plasma sterols. *Clin. Chem. Lab. Med.* **2016**, *54*, 1461–1466. [[CrossRef](#)] [[PubMed](#)]
2. Figueroa, V.; Milla, C.; Parks, E.J.; Schwarzenberg, S.J.; Moran, A. Abnormal lipid concentrations in cystic fibrosis. *Am. J. Clin. Nutr.* **2002**, *75*, 1005–1011. [[CrossRef](#)] [[PubMed](#)]
3. Luciani, A.; Vilella, V.R.; Esposito, S.; Gavina, M.; Russo, I.; Silano, M.; Guido, S.; Pettoello-Mantovani, M.; Carnuccio, R.; Scholte, B.; et al. Targeting autophagy as a novel strategy for facilitating the therapeutic action of potentiators on DeltaF508 cystic fibrosis transmembrane conductance regulator. *Autophagy* **2012**, *8*, 1657–1672. [[CrossRef](#)] [[PubMed](#)]
4. Teichgraber, V.; Ulrich, M.; Endlich, N.; Riethmuller, J.; Wilker, B.; De Oliveira-Munding, C.C.; van Heeckeren, A.M.; Barr, M.L.; von Kurthy, G.; Schmid, K.W.; et al. Ceramide accumulation mediates inflammation, cell death and infection susceptibility in cystic fibrosis. *Nat. Med.* **2008**, *14*, 382–391. [[CrossRef](#)] [[PubMed](#)]
5. Mingione, A.; Dei Cas, M.; Bonezzi, F.; Caretti, A.; Piccoli, M.; Anastasia, L.; Ghidoni, R.; Paroni, R.; Signorelli, P. Inhibition of Sphingolipid Synthesis as a Phenotype-Modifying Therapy in Cystic Fibrosis. *Cell. Physiol. Biochem. Int. J. Exp. Cell. Physiol. Biochem. Pharmacol.* **2020**, *54*, 110–125.
6. Bruscia, E.M.; Bonfield, T.L. Innate and Adaptive Immunity in Cystic Fibrosis. *Clin. Chest Med.* **2016**, *37*, 17–29. [[CrossRef](#)]
7. Zhang, S.; Shrestha, C.L.; Kopp, B.T. Cystic fibrosis transmembrane conductance regulator (CFTR) modulators have differential effects on cystic fibrosis macrophage function. *Sci. Rep.* **2018**, *8*, 17066. [[CrossRef](#)]
8. Caretti, A.; Torelli, R.; Perdoni, F.; Falleni, M.; Tosi, D.; Zulueta, A.; Casas, J.; Sanguinetti, M.; Ghidoni, R.; Borghi, E.; et al. Inhibition of ceramide de novo synthesis by myriocin produces the double effect of reducing pathological inflammation and exerting antifungal activity against *A. fumigatus* airways infection. *Biochim. Biophys. Acta* **2016**, *1860*, 1089–1097. [[CrossRef](#)]
9. Leveque, M.; Le Trionnaire, S.; Del Porto, P.; Martin-Chouly, C. The impact of impaired macrophage functions in cystic fibrosis disease progression. *J. Cyst. Fibros.* **2017**, *16*, 443–453. [[CrossRef](#)]
10. Tracy, M.C.; Moss, R.B. The myriad challenges of respiratory fungal infection in cystic fibrosis. *Pediatr. Pulmonol.* **2018**, *53*, S75–S85. [[CrossRef](#)]
11. Chaudhary, N.; Datta, K.; Askin, F.B.; Staab, J.F.; Marr, K.A. Cystic fibrosis transmembrane conductance regulator regulates epithelial cell response to *Aspergillus* and resultant pulmonary inflammation. *Am. J. Respir. Crit. Care Med.* **2012**, *185*, 301–310. [[CrossRef](#)] [[PubMed](#)]
12. Bodas, M.; Vij, N. Adapting Proteostasis and Autophagy for Controlling the Pathogenesis of Cystic Fibrosis Lung Disease. *Front. Pharmacol.* **2019**, *10*, 20. [[CrossRef](#)] [[PubMed](#)]
13. Luciani, A.; Vilella, V.R.; Esposito, S.; Brunetti-Pierri, N.; Medina, D.L.; Settembre, C.; Gavina, M.; Raia, V.; Ballabio, A.; Maiuri, L. Cystic fibrosis: A disorder with defective autophagy. *Autophagy* **2011**, *7*, 104–106. [[CrossRef](#)] [[PubMed](#)]
14. Esposito, S.; Tosco, A.; Vilella, V.R.; Raia, V.; Kroemer, G.; Maiuri, L. Manipulating proteostasis to repair the F508del-CFTR defect in cystic fibrosis. *Mol. Cell. Pediatr.* **2016**, *3*, 13. [[CrossRef](#)]
15. Evans, R.J.; Sundaramurthy, V.; Frickel, E.M. The Interplay of Host Autophagy and Eukaryotic Pathogens. *Front. Cell Dev. Biol.* **2018**, *6*, 118. [[CrossRef](#)]

16. Rameshwaram, N.R.; Singh, P.; Ghosh, S.; Mukhopadhyay, S. Lipid metabolism and intracellular bacterial virulence: Key to next-generation therapeutics. *Future Microbiol.* **2018**, *13*, 1301–1328. [[CrossRef](#)]
17. Walpole, G.F.W.; Grinstein, S.; Westman, J. The role of lipids in host-pathogen interactions. *IUBMB Life* **2018**, *70*, 384–392. [[CrossRef](#)]
18. Keyhani, N.O. Lipid biology in fungal stress and virulence: Entomopathogenic fungi. *Fungal Biol.* **2018**, *122*, 420–429. [[CrossRef](#)]
19. Kim, Y.S.; Lee, H.M.; Kim, J.K.; Yang, C.S.; Kim, T.S.; Jung, M.; Jin, H.S.; Kim, S.; Jang, J.; Oh, G.T.; et al. PPAR-alpha Activation Mediates Innate Host Defense through Induction of TFEB and Lipid Catabolism. *J. Immunol.* **2017**, *198*, 3283–3295. [[CrossRef](#)]
20. Ollero, M.; Astarita, G.; Guerrero, I.C.; Sermet-Gaudelus, I.; Trudel, S.; Piomelli, D.; Edelman, A. Plasma lipidomics reveals potential prognostic signatures within a cohort of cystic fibrosis patients. *J. Lipid Res.* **2011**, *52*, 1011–1022. [[CrossRef](#)]
21. Ollero, M. Methods for the study of lipid metabolites in cystic fibrosis. *J. Cyst. Fibros. Soc.* **2004**, *3* (Suppl. 2), 97–98. [[CrossRef](#)] [[PubMed](#)]
22. Ziobro, R.; Henry, B.; Edwards, M.J.; Lentsch, A.B.; Gulbins, E. Ceramide mediates lung fibrosis in cystic fibrosis. *Biochem. Biophys. Res. Commun.* **2013**, *434*, 705–709. [[CrossRef](#)] [[PubMed](#)]
23. Fang, D.; West, R.H.; Manson, M.E.; Ruddy, J.; Jiang, D.; Previs, S.F.; Sonawane, N.D.; Burgess, J.D.; Kelley, T.J. Increased plasma membrane cholesterol in cystic fibrosis cells correlates with CFTR genotype and depends on de novo cholesterol synthesis. *Respir. Res.* **2010**, *11*, 61. [[CrossRef](#)] [[PubMed](#)]
24. Del Ciampo, I.R.; Sawamura, R.; Fernandes, M.I. Cystic fibrosis: From protein-energy malnutrition to obesity with dyslipidemia. *Iran. J. Pediatr.* **2013**, *23*, 605–606. [[PubMed](#)]
25. Caretti, A.; Bragonzi, A.; Facchini, M.; De Fino, I.; Riva, C.; Gasco, P.; Musicanti, C.; Casas, J.; Fabrias, G.; Ghidoni, R.; et al. Anti-inflammatory action of lipid nanocarrier-delivered myriocin: Therapeutic potential in cystic fibrosis. *Biochim. Biophys. Acta* **2014**, *1840*, 586–594. [[CrossRef](#)]
26. Caretti, A.; Vasso, M.; Bonezzi, F.T.; Gallina, A.; Trinchera, M.; Rossi, A.; Adami, R.; Casas, J.; Falleni, M.; Tosi, D.; et al. Myriocin treatment of CF lung infection and inflammation: Complex analyses for enigmatic lipids. *Naunyn-Schmiedeberg Arch. Pharmacol.* **2017**, *390*, 775–790. [[CrossRef](#)]
27. Elkord, E.; Williams, P.E.; Kynaston, H.; Rowbottom, A.W. Human monocyte isolation methods influence cytokine production from in vitro generated dendritic cells. *Immunology* **2005**, *114*, 204–212. [[CrossRef](#)]
28. Love, M.I.; Huber, W.; Anders, S. Moderated estimation of fold change and dispersion for RNA-seq data with DESeq2. *Genome Biol.* **2014**, *15*, 550. [[CrossRef](#)]
29. Dobin, A.; Davis, C.A.; Schlesinger, F.; Drenkow, J.; Zaleski, C.; Jha, S.; Batut, P.; Chaisson, M.; Gingeras, T.R. STAR: Ultrafast universal RNA-seq aligner. *Bioinformatics* **2013**, *29*, 15–21. [[CrossRef](#)]
30. Liao, Y.; Smyth, G.K.; Shi, W. featureCounts: An efficient general purpose program for assigning sequence reads to genomic features. *Bioinformatics* **2014**, *30*, 923–930. [[CrossRef](#)]
31. Robinson, M.D.; McCarthy, D.J.; Smyth, G.K. edgeR: A Bioconductor package for differential expression analysis of digital gene expression data. *Bioinformatics* **2010**, *26*, 139–140. [[CrossRef](#)] [[PubMed](#)]
32. Yu, G.; Wang, L.G.; Han, Y.; He, Q.Y. clusterProfiler: An R package for comparing biological themes among gene clusters. *Omics J. Integr. Biol.* **2012**, *16*, 284–287. [[CrossRef](#)] [[PubMed](#)]
33. Szklarczyk, D.; Gable, A.L.; Lyon, D.; Junge, A.; Wyder, S.; Huerta-Cepas, J.; Simonovic, M.; Doncheva, N.T.; Morris, J.H.; Bork, P.; et al. STRING v11: Protein-protein association networks with increased coverage, supporting functional discovery in genome-wide experimental datasets. *Nucleic Acids Res.* **2019**, *47*, D607–D613. [[CrossRef](#)] [[PubMed](#)]
34. Hirsch, J.G. Bactericidal action of histone. *J. Exp. Med.* **1958**, *108*, 925–944. [[CrossRef](#)]
35. Anand, P.; Cermelli, S.; Li, Z.; Kassar, A.; Bosch, M.; Sigua, R.; Huang, L.; Ouellette, A.J.; Pol, A.; Welte, M.A.; et al. A novel role for lipid droplets in the organismal antibacterial response. *Elife* **2012**, *1*, e00003. [[CrossRef](#)]
36. Kim, H.S.; Yoon, H.; Minn, I.; Park, C.B.; Lee, W.T.; Zasloff, M.; Kim, S.C. Pepsin-mediated processing of the cytoplasmic histone H2A to strong antimicrobial peptide buforin I. *J. Immunol.* **2000**, *165*, 3268–3274. [[CrossRef](#)]
37. Watson, K.; Edwards, R.J.; Shaunak, S.; Parmelee, D.C.; Sarraf, C.; Gooderham, N.J.; Davies, D.S. Extra-nuclear location of histones in activated human peripheral blood lymphocytes and cultured T-cells. *Biochem. Pharmacol.* **1995**, *50*, 299–309. [[CrossRef](#)]

38. Zlatanova, J.S.; Srebrevna, L.N.; Banchev, T.B.; Tasheva, B.T.; Tsanev, R.G. Cytoplasmic pool of histone H1 in mammalian cells. *J. Cell Sci.* **1990**, *96 Pt 3*, 461–468.
39. De Lucca, A.J.; Heden, L.O.; Ingber, B.; Bhatnagar, D. Antifungal properties of wheat histones (H1-H4) and purified wheat histone H1. *J. Agric. Food Chem.* **2011**, *59*, 6933–6939. [[CrossRef](#)]
40. Hu, B.; Zhang, Y.; Jia, L.; Wu, H.; Fan, C.; Sun, Y.; Ye, C.; Liao, M.; Zhou, J. Binding of the pathogen receptor HSP90AA1 to avibirnavirus VP2 induces autophagy by inactivating the AKT-MTOR pathway. *Autophagy* **2015**, *11*, 503–515. [[CrossRef](#)]
41. Negoita, F.; Blomdahl, J.; Wasserstrom, S.; Winberg, M.E.; Osmark, P.; Larsson, S.; Stenkula, K.G.; Ekstedt, M.; Kechagias, S.; Holm, C.; et al. PNPLA3 variant M148 causes resistance to starvation-mediated lipid droplet autophagy in human hepatocytes. *J. Cell. Biochem.* **2019**, *120*, 343–356. [[CrossRef](#)] [[PubMed](#)]
42. Tanida, I.; Ueno, T.; Kominami, E. LC3 and Autophagy. *Methods Mol. Biol.* **2008**, *445*, 77–88. [[PubMed](#)]
43. Hu, F.; Shao, L.; Zhang, J.; Zhang, H.; Wen, A.; Zhang, P. Knockdown of ZFAS1 Inhibits Hippocampal Neurons Apoptosis and Autophagy by Activating the PI3K/AKT Pathway via Up-regulating miR-421 in Epilepsy. *Neurochem. Res.* **2020**. [[CrossRef](#)] [[PubMed](#)]
44. Bandyopadhyay, U.; Kaushik, S.; Varticovski, L.; Cuervo, A.M. The chaperone-mediated autophagy receptor organizes in dynamic protein complexes at the lysosomal membrane. *Mol. Cell. Biol.* **2008**, *28*, 5747–5763. [[CrossRef](#)] [[PubMed](#)]
45. Levy, H.; Murphy, A.; Zou, F.; Gerard, C.; Klanderman, B.; Schuemann, B.; Lazarus, R.; Garcia, K.C.; Celedon, J.C.; Drumm, M.; et al. IL1B polymorphisms modulate cystic fibrosis lung disease. *Pediatr. Pulmonol.* **2009**, *44*, 580–593. [[CrossRef](#)]
46. Gillette, D.D.; Shah, P.A.; Cremer, T.; Gavrillin, M.A.; Besecker, B.Y.; Sarkar, A.; Knoell, D.L.; Cormet-Boyaka, E.; Wewers, M.D.; Butchar, J.P.; et al. Analysis of human bronchial epithelial cell proinflammatory response to Burkholderia cenocepacia infection: Inability to secrete il-1beta. *J. Biol. Chem.* **2013**, *288*, 3691–3695. [[CrossRef](#)] [[PubMed](#)]
47. Boada-Romero, E.; Letek, M.; Fleischer, A.; Pallauf, K.; Ramon-Barros, C.; Pimentel-Muinos, F.X. TMEM59 defines a novel ATG16L1-binding motif that promotes local activation of LC3. *EMBO J.* **2013**, *32*, 566–582. [[CrossRef](#)]
48. Nowak, J.; Archange, C.; Tardivel-Lacombe, J.; Pontarotti, P.; Pebusque, M.J.; Vaccaro, M.I.; Velasco, G.; Dagorn, J.C.; Iovanna, J.L. The TP53INP2 protein is required for autophagy in mammalian cells. *Mol. Biol. Cell* **2009**, *20*, 870–881. [[CrossRef](#)]
49. Akizu, N.; Cantagrel, V.; Zaki, M.S.; Al-Gazali, L.; Wang, X.; Rosti, R.O.; Dikoglu, E.; Gelot, A.B.; Rosti, B.; Vaux, K.K.; et al. Biallelic mutations in SNX14 cause a syndromic form of cerebellar atrophy and lysosome-autophagosome dysfunction. *Nat. Genet.* **2015**, *47*, 528–534. [[CrossRef](#)] [[PubMed](#)]
50. Bryant, D.; Liu, Y.; Datta, S.; Hariri, H.; Seda, M.; Anderson, G.; Peskett, E.; Demetriou, C.; Sousa, S.; Jenkins, D.; et al. SNX14 mutations affect endoplasmic reticulum-associated neutral lipid metabolism in autosomal recessive spinocerebellar ataxia 20. *Hum. Mol. Genet.* **2018**, *27*, 1927–1940. [[CrossRef](#)] [[PubMed](#)]
51. Li, T.; Xian, W.J.; Gao, Y.; Jiang, S.; Yu, Q.H.; Zheng, Q.C.; Zhang, Y. Higd1a Protects Cells from Lipotoxicity under High-Fat Exposure. *Oxid. Med. Cell. Longev.* **2019**, *2019*, 6051262. [[CrossRef](#)] [[PubMed](#)]
52. Idrovo, J.P.; Yang, W.L.; Jacob, A.; Corbo, L.; Nicastro, J.; Coppa, G.F.; Wang, P. Inhibition of lipogenesis reduces inflammation and organ injury in sepsis. *J. Surg. Res.* **2016**, *200*, 242–249. [[CrossRef](#)] [[PubMed](#)]
53. Mailhot, G.; Ravid, Z.; Barchi, S.; Moreau, A.; Rabasa-Lhoret, R.; Levy, E. CFTR knockdown stimulates lipid synthesis and transport in intestinal Caco-2/15 cells. *Am. J. Physiol. Gastrointest. Liver Physiol.* **2009**, *297*, G1239–G1249. [[CrossRef](#)]
54. Weidberg, H.; Elazar, Z. TBK1 mediates crosstalk between the innate immune response and autophagy. *Sci. Signal.* **2011**, *4*, pe39. [[CrossRef](#)] [[PubMed](#)]
55. Kuo, C.J.; Hansen, M.; Troemel, E. Autophagy and innate immunity: Insights from invertebrate model organisms. *Autophagy* **2018**, *14*, 233–242. [[CrossRef](#)]
56. Nozawa, T.; Sano, S.; Minowa-Nozawa, A.; Toh, H.; Nakajima, S.; Murase, K.; Aikawa, C.; Nakagawa, I. TBC1D9 regulates TBK1 activation through Ca²⁺ signaling in selective autophagy. *Nat. Commun.* **2020**, *11*, 770. [[CrossRef](#)]
57. Rhodes, B.; Nash, E.F.; Tullis, E.; Pencharz, P.B.; Brotherwood, M.; Dupuis, A.; Stephenson, A. Prevalence of dyslipidemia in adults with cystic fibrosis. *J. Cyst. Fibros.* **2010**, *9*, 24–28. [[CrossRef](#)]

58. Ishimo, M.C.; Belson, L.; Ziai, S.; Levy, E.; Berthiaume, Y.; Coderre, L.; Rabasa-Lhoret, R. Hypertriglyceridemia is associated with insulin levels in adult cystic fibrosis patients. *J. Cyst. Fibros.* **2013**, *12*, 271–276. [[CrossRef](#)]
59. Freedman, S.D.; Blanco, P.G.; Zaman, M.M.; Shea, J.C.; Ollero, M.; Hopper, I.K.; Weed, D.A.; Gelrud, A.; Regan, M.M.; Laposata, M.; et al. Association of cystic fibrosis with abnormalities in fatty acid metabolism. *N. Engl. J. Med.* **2004**, *350*, 560–569. [[CrossRef](#)]
60. Oliveira, G.; Dorado, A.; Oliveira, C.; Padilla, A.; Rojo-Martinez, G.; Garcia-Escobar, E.; Gaspar, I.; Gonzalo, M.; Soriguer, F. Serum phospholipid fatty acid profile and dietary intake in an adult Mediterranean population with cystic fibrosis. *Br. J. Nutr.* **2006**, *96*, 343–349. [[CrossRef](#)]
61. Peretti, N.; Roy, C.C.; Drouin, E.; Seidman, E.; Brochu, P.; Casimir, G.; Levy, E. Abnormal intracellular lipid processing contributes to fat malabsorption in cystic fibrosis patients. *Am. J. Physiol. Gastrointest. Liver Physiol.* **2006**, *290*, G609–G615. [[CrossRef](#)] [[PubMed](#)]
62. Dogliotti, E.; Vezzoli, G.; Nouvenne, A.; Meschi, T.; Terranegra, A.; Mingione, A.; Brasacchio, C.; Raspini, B.; Cusi, D.; Soldati, L. Nutrition in calcium nephrolithiasis. *J. Transl. Med.* **2013**, *11*, 109. [[CrossRef](#)] [[PubMed](#)]
63. White, N.M.; Jiang, D.; Burgess, J.D.; Bederman, I.R.; Previs, S.F.; Kelley, T.J. Altered cholesterol homeostasis in cultured and in vivo models of cystic fibrosis. *Am. J. Physiol. Lung Cell. Mol. Physiol.* **2007**, *292*, L476–L486. [[CrossRef](#)] [[PubMed](#)]
64. Desbenoit, N.; Sausseureau, E.; Bich, C.; Bourderioux, M.; Fritsch, J.; Edelman, A.; Brunelle, A.; Ollero, M. Localized lipidomics in cystic fibrosis: TOF-SIMS imaging of lungs from *Pseudomonas aeruginosa*-infected mice. *Int. J. Biochem. Cell Biol.* **2014**, *52*, 77–82. [[CrossRef](#)]
65. Gentsch, M.; Choudhury, A.; Chang, X.B.; Pagano, R.E.; Riordan, J.R. Misassembled mutant DeltaF508 CFTR in the distal secretory pathway alters cellular lipid trafficking. *J. Cell Sci.* **2007**, *120*, 447–455. [[CrossRef](#)]
66. Gentsch, M.; Chang, X.B.; Cui, L.; Wu, Y.; Ozols, V.V.; Choudhury, A.; Pagano, R.E.; Riordan, J.R. Endocytic trafficking routes of wild type and DeltaF508 cystic fibrosis transmembrane conductance regulator. *Mol. Biol. Cell* **2004**, *15*, 2684–2696. [[CrossRef](#)] [[PubMed](#)]
67. Chillappagari, S.; Venkatesan, S.; Garapati, V.; Mahavadi, P.; Munder, A.; Seubert, A.; Sarode, G.; Guenther, A.; Schmeck, B.T.; Tummeler, B.; et al. Impaired TLR4 and HIF expression in cystic fibrosis bronchial epithelial cells downregulates hemoxygenase-1 and alters iron homeostasis in vitro. *Am. J. Physiol. Lung Cell. Mol. Physiol.* **2014**, *307*, L791–L799. [[CrossRef](#)] [[PubMed](#)]
68. Bolhassani, A.; Agi, E. Heat shock proteins in infection. *Clin. Chim. Acta Int. J. Clin. Chem.* **2019**, *498*, 90–100. [[CrossRef](#)]
69. Stewart, G.R.; Young, D.B. Heat-shock proteins and the host-pathogen interaction during bacterial infection. *Curr. Opin. Immunol.* **2004**, *16*, 506–510. [[CrossRef](#)] [[PubMed](#)]
70. Osterloh, A.; Breloer, M. Heat shock proteins: Linking danger and pathogen recognition. *Med. Microbiol. Immunol.* **2008**, *197*, 1–8. [[CrossRef](#)]
71. Dokladny, K.; Myers, O.B.; Moseley, P.L. Heat shock response and autophagy—cooperation and control. *Autophagy* **2015**, *11*, 200–213. [[CrossRef](#)] [[PubMed](#)]
72. Chiang, H.L.; Terlecky, S.R.; Plant, C.P.; Dice, J.F. A role for a 70-kilodalton heat shock protein in lysosomal degradation of intracellular proteins. *Science* **1989**, *246*, 382–385. [[CrossRef](#)] [[PubMed](#)]
73. Cuervo, A.M.; Dice, J.F. A receptor for the selective uptake and degradation of proteins by lysosomes. *Science* **1996**, *273*, 501–503. [[CrossRef](#)] [[PubMed](#)]
74. Hartl, F.U.; Bracher, A.; Hayer-Hartl, M. Molecular chaperones in protein folding and proteostasis. *Nature* **2011**, *475*, 324–332. [[CrossRef](#)] [[PubMed](#)]
75. Tardelli, M.; Bruschi, F.V.; Trauner, M. The role of metabolic lipases in the pathogenesis and management of liver disease. *Hepatology* **2020**. [[CrossRef](#)] [[PubMed](#)]
76. Bonezzi, F.; Piccoli, M.; Dei Cas, M.; Paroni, R.; Mingione, A.; Monasky, M.M.; Caretti, A.; Riganti, C.; Ghidoni, R.; Pappone, C.; et al. Sphingolipid Synthesis Inhibition by Myriocin Administration Enhances Lipid Consumption and Ameliorates Lipid Response to Myocardial Ischemia Reperfusion Injury. *Front. Physiol.* **2019**, *10*, 986. [[CrossRef](#)]
77. Sasset, L.; Zhang, Y.; Dunn, T.M.; Di Lorenzo, A. Sphingolipid De Novo Biosynthesis: A Rheostat of Cardiovascular Homeostasis. *Trends Endocrinol. Metab. TEM* **2016**, *27*, 807–819. [[CrossRef](#)]
78. Cai, L.; Oyeniran, C.; Biswas, D.D.; Allegood, J.; Milstien, S.; Kordula, T.; Maceyka, M.; Spiegel, S. ORMDL proteins regulate ceramide levels during sterile inflammation. *J. Lipid Res.* **2016**, *57*, 1412–1422. [[CrossRef](#)]

79. Chen, L.; Duan, Y.; Wei, H.; Ning, H.; Bi, C.; Zhao, Y.; Qin, Y.; Li, Y. Acetyl-CoA carboxylase (ACC) as a therapeutic target for metabolic syndrome and recent developments in ACC1/2 inhibitors. *Expert Opin. Investig. Drugs* **2019**, *28*, 917–930. [[CrossRef](#)]
80. Ammanathan, V.; Mishra, P.; Chavalmane, A.K.; Muthusamy, S.; Jadhav, V.; Siddamadappa, C.; Manjithaya, R. Restriction of intracellular Salmonella replication by restoring TFEB-mediated xenophagy. *Autophagy* **2019**, 1–14. [[CrossRef](#)]
81. Khoury, T.; Asombang, A.W.; Berzin, T.M.; Cohen, J.; Pleskow, D.K.; Mizrahi, M. The Clinical Implications of Fatty Pancreas: A Concise Review. *Dig. Dis. Sci.* **2017**, *62*, 2658–2667. [[CrossRef](#)] [[PubMed](#)]
82. Tham, R.T.; Heyerman, H.G.; Falke, T.H.; Zwinderman, A.H.; Bloem, J.L.; Bakker, W.; Lamers, C.B. Cystic fibrosis: MR imaging of the pancreas. *Radiology* **1991**, *179*, 183–186. [[CrossRef](#)] [[PubMed](#)]



© 2020 by the authors. Licensee MDPI, Basel, Switzerland. This article is an open access article distributed under the terms and conditions of the Creative Commons Attribution (CC BY) license (<http://creativecommons.org/licenses/by/4.0/>).